WHERE DO I GROW FROM HERE?
THE GENETIC CONTROL OF BRANCH ORIENTATION IN *PRUNUS*

By

Andrea R Kohler

A DISSERTATION

Submitted to
Michigan State University
in partial fulfillment of the requirements
for the degree of

Plant Breeding, Genetics, and Biotechnology – Horticulture – Doctor of Philosophy

2023

ABSTRACT

Branch orientation is a crucial factor in the life of a plant, determining aspects as diverse as light interception, ability to compete with surrounding plants, and capacity to support a fruit load. Perhaps nowhere is this more true than in trees and other woody perennials, where a branch represents a long-term investment of metabolic resources which must be compensated for by new photosynthetic opportunities. To determine branch orientation, plants integrate signals from gravity and light, but each species uniquely responds to those signals in determining crotch angle and trajectory. The underlying genetics which control these responses are still largely unknown but are crucial both to plant physiology and to manipulating branch orientation in ways desirable for cultivation. In this work, I examine three genes involved in integration of gravitropic and phototropic signals for branch angle control—*WEEP*, *LAZY1*, and *TILLER ANGLE CONTROL 1* (*TAC1*)—in two commercially important tree fruit crops: peach (*Prunus persica*) and European plum (*Prunus domestica*). These three genes represent different control points in the determination of branch angle, but likely all function in the same pathway, as *LAZY1* is epistatic to *TAC1,* and *TAC1* is epistatic to *WEEP.* In the first chapter, I provide an overview of the genetic and hormonal mechanisms known to control plant architecture. In the second chapter, I investigate the function of *WEEP,* a Sterile Alpha Motif domain gene previously identified as involved in branch trajectory, as a homozygous mutation in *WEEP* causes a pendulous, downward arching branch trajectory in peach. Here, I present data that *WEEP* is crucial to the formation of an auxin gradient during gravitropism, and weeping peach branches have an inversion of that gradient in the shoot, perceiving the world "upside-down". I also present data connecting *WEEP* to set-point angle in roots. In the third chapter, I characterize the phenotype of *LAZY1*-antisense in transgenic plum. *LAZY1* is also essential to formation of the auxin gradient during gravitropism, directing the polarization of auxin efflux carriers and promoting upward branch orientation. Here, I describe phenotypes of *LAZY1*-antisense in plum, including impacts on branch angle and photosynthesis, note reproductive phenotypes observed in *LAZY1*-antisense lines, and discuss use of *LAZY1*-antisense in two planar training systems—super spindle axe and espalier. Finally, in the fourth chapter, I investigate how dosage of *TAC1* affects novel planar training in peach. While in the same gene family (IGT) as *LAZY1, TAC1* functions in light response, and promotes the opposite phenotype, directing branches outward. Using peach varieties which are homozygous wild type (Bounty, spreading habit), heterozygous (Sweet-N-UP, upright habit) or homozygous mutant

(Crimson Rocket, pillar habit) for *TAC1,* I look at implications of planar training systems for fruit quality and yield.

This dissertation is dedicated to my husband Peter.
Without you, this dissertation would not exist.

ACKNOWLEDGEMENTS

In a project of this scope, stretching through so many years, there would hardly be a hope of finishing the work's arrears—were it not for those who helped me, sped and guided on my way: standing with, around, beside me, giving courage for each day. My thanks to those who gave direction, as I learned amid stress and pain. My thanks to those whose calm reflection helped me think, and wisdom gain. My thanks to those who held and loved me, no matter how much sweat or tears. My thanks to those who sat and heard me, calmed my heart and soothed my fears.

There are so many people without whom this work would not have been possible. To my dear family, thank you so much for providing me with support and encouragement. Mom and Dad, this dissertation is the flowering of the seed you planted in my mind many years ago. I'm glad I have finally finished the 'thesis' I started when I was two. Thank you for challenging me, teaching me, and loving me. Grandma and Grandpa, thank you so much for all your advice and help. You've given me a place to go and rest during some of the most difficult times of my life. Mom K and Dad K, thank you for being supportive, showing interest in my work, asking good questions, and, incidentally, raising the most wonderful man in the world. Rachel, thank you so much for your help, with engineering, with childcare, with whatever I've needed. And thank you for the many discussions we've had about the trials of grad school. Naomi, thanks for asking me the hard questions about life, purpose, and ambitions. To my chosen sister Christabel, thank you so much for your prayers and encouragement. Charity, thank you for becoming my science sister and Roland's auntie. Thank you for helping with statistics, and lab work, and field work, and making my life so much better.

To my dear husband, you've given and sacrificed so much through the last six years. You've helped with code, fixed broken lab equipment, collected data, watered plants, and picked peaches. You've put up with broken dates, late dinners, your wife disappearing for 12 or more hours at a time, and always having your schedule rearranged around experiments. You've taken care of the house, shoved food at me at regular intervals, gotten me to buy a horse, and cared for our baby. You've supported me in every possible way, sorrowing with me in my disappointments and rejoicing in my successes. As we've always said, grad school is a lifestyle, not a job, and you've joined me in it. Thank you—this accomplishment is yours as well. I love you.

And to Roland, you've made life so much more complicated, and so much more fun. You've brought so much joy into my life! I would never have guessed it, but you provided just the encouragement and the motivation I needed to finish strong. I love you, little one.

My friends in graduate school have also had a huge impact on who I am as a scientist. Although I can never properly acknowledge all of you, I'd like to thank Dr. Joseph Hill for teaching me many lab techniques I use all the time, Sarah Lee for helping me remember there's more to life than grad school, Prabhjot Kaur for so many discussions, Kathleen Rhoades for yelling what we're all thinking down the hall, and Hannah Jeffery for dropping by with a hug and baked goods. To all my wonderful undergrads—Elise Tomaszewski, Emma Grant, Kat Rockwell, Andrew Scheil, Jack Sinnaeve, and Carla Redinger—thank you so much for your help, and everything you taught me. Alex Engelsma and Mallory St. Clair, thank you for bringing fresh energy into the lab and into my life.

Of course, this work would also never have happened without the many scientists who have mentored me over the years. From undergrad, I'd particularly like to thank Dr. Wood and Dr. Sanders for encouraging my love of research, Dr. Hartz for asking me what I would do when I failed at something, and Dr. Hill for instilling a remarkable amount of biochemistry into my brain. I'd also like to extend special thanks and appreciation to my committee, Drs. Courtney Hollender, Corny Barry, Greg Lang, and Frank Telewski. Frank, thank you for showing me the joy of anatomy and physiology, and making sure I continued my research in wood. Greg, thank you for giving me a crash course in the applied horticulture of tree fruit. Corny, I would never have gone to MSU without you. Thank you for being an excellent REU mentor, and for continuing to give me excellent guidance throughout graduate school.

Courtney, I'd like to particularly thank you for being an excellent, understanding, gracious mentor, who challenged me to continuously become a better scientist. Your heart for your students has kept me going over these last five years. Thank you for modeling what it looks like to be a kind human as well as a brilliant scientist. Thank you for sticking with me through a mental break-down, a global pandemic, and a pregnancy. Your understanding has made it possible to complete this degree, your insight has made it informative, and your creativity has made it fun.

TABLE OF CONTENTS

CHAPTER 1

Getting into Shape:

The genetic, hormonal, and environmental control of plant architecture.

Author

Andrea Kohler

Why study plant architecture?

Even the casual observer of a garden or forest is frequently struck by the wide diversity of shapes plants exhibit. This diversity is even more amazing when one considers that all those architectures are built with the same recurring phytomeric unit, which includes a node, leaf, lateral bud, and subtending internode (McSteen and Leyser, 2005). Furthermore, this is a dynamic yet controlled diversity, as each plant actively responds to light and gravity, yet retains a shape so characteristic of its species that the plant can frequently be identified by its silhouette alone (Zhu and Wagner, 2020). Finally, in addition to its aesthetic interest, plant architecture is a major contributor to crop productivity, impacting such diverse attributes such as light capture, self-shading, fruit load, susceptibility to winter damage, and pesticide application efficacy.

Control of plant architecture

Plant architecture is determined by three major factors—branch patterning (determined by meristem patterning, organ identity, and bud outgrowth), stem elongation (determined by internode length and number), and branch angle (determined by a combination of meristem location, differential cell division, and wood composition). Formal description of plant shape in the context of development can be traced back 50 years ago to Hallé, who extensively studied and categorized plant architecture according to meristematic activity (Costes et al., 2006). Hallé categorized trees based on three branch patterning traits (Hallé et al., 1978). First, he distinguished plant structure based on the life-span of the apical meristem and when and how a lateral meristem replaces it. Second, he examines phyllotaxy, or positioning of buds around a branch—particularly whether it is orthotropic (radial bud symmetry, generally seen on erect shoots) or plagiotropic (bilateral bud symmetry, generally seen on horizontal shoots). Third, he considered transition from vegetative to floral meristems. Hallé also utilized two stem elongation traits—growth rhythm and length of shoot (Hallé et al., 1978; Costes et al., 2006). Using these 5 traits, Hallé divided trees into 23 growth models (Hallé et al., 1978).

While Hallé's discussion embraces both monocots and dicots, the models and discussion below primarily apply to dicots. While many of the genetic pathways are conserved in monocots, branching differs from dicots in two main ways. First, during the vegetative state, the apical meristem remains close to the ground, beneath the leaves, rather than at the apex of the plant as in dicots (McSteen and Leyser, 2005). Second, monocots exhibit different types of branching,

including tillering, secondary vegetative branches, and multiple orders of branching in the inflorescence (McSteen and Leyser, 2005).

Molecular control of branch patterning

Branch patterning encompasses the spatial distribution of axillary meristems, which organs the axillary meristems or buds contain (flowers, leaves, stems, etc.), and when buds break dormancy. Physiologically, these three attributes are determined by axillary meristem initiation, determination, and elongation, respectively (McSteen and Leyser, 2005; Ehrenreich et al., 2007). There are two competing hypotheses concerning axillary meristem initiation. Some argue that during lateral organ formation, a few cells from the shoot apical meristem (SAM) remain undifferentiated and travel with the organ to form the basis of the axillary meristem (the 'detached meristem theory'), while others believe that axillary meristems are formed *de novo* at the base of the leaf petiole (McSteen and Leyser, 2005; Wang and Jiao, 2018). More recently, a combinatorial model has been proposed, in which cells from SAM lineage maintain expression of SHOOTMERISTEMLESS (STM), but do not express CLAVATA3 (CLV3) and WUSCHEL (WUS), a key feedback loop in meristem maintenance (Wang, 2021). In this model, an auxin

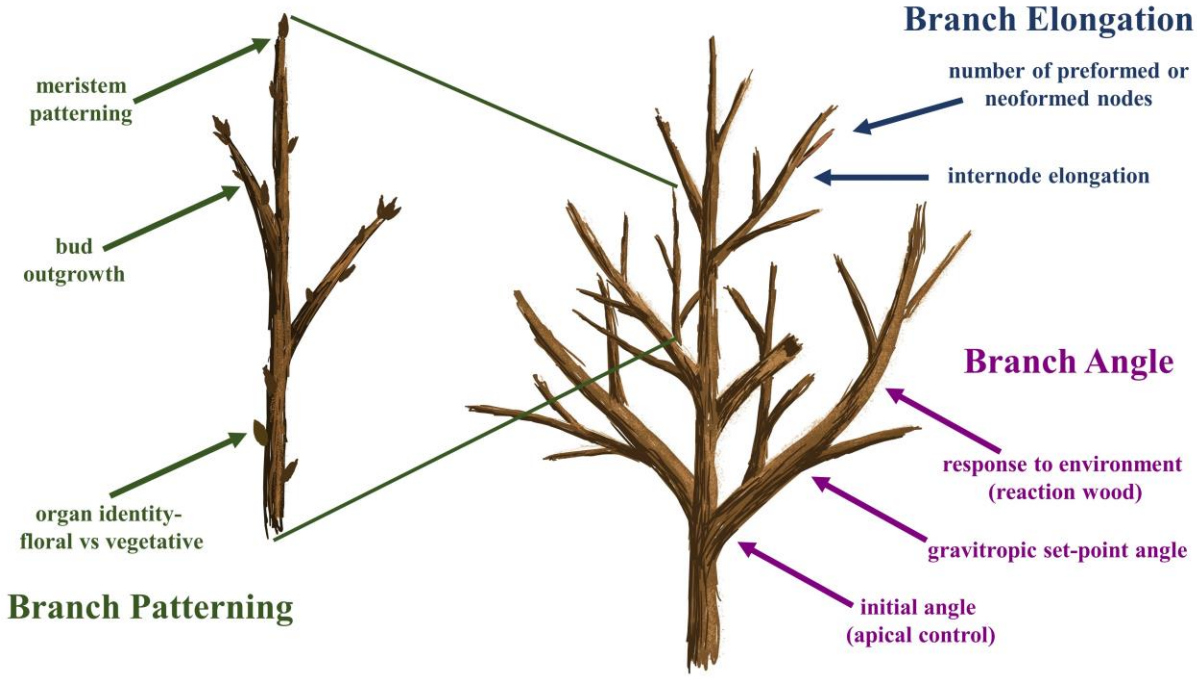

Figure 1.1: Aspects of plant architecture. Plant architecture is determined by branch patterning (including meristem patterning, bud outgrowth and organ identity), branch elongation (the number of nodes and the elongation of each internode) and branch angle (including the initial or crotch angle, the gravitropic set-point angle, and any alterations in angle due to environmental changes or release of apical control).

minimum and cytokinin pulse, and the subsequent activation of CLV and WUS expression in these cells represents the *de novo* formation of the meristem (Wang and Jiao, 2018; Cao and Jiao, 2020; Wang, 2021). Regardless of which model is correct, the spatial organization of the axillary meristems follows phyllotaxy of lateral organs (Zhu and Wagner, 2020). Thus, the spatial pattern of axillary meristems is determined by the SAM as lateral organ primordia are initiated.

Lateral primordia location depends on complex hormonal and genetic regulation within the SAM. SAM maintenance requires a dynamic equilibrium between maintenance of undifferentiated central zone stem cells, among which is the organizing center, the peripheral zone cells, where lateral organs initiate, and the rib meristem cells, which are the precursors to the xylem, phloem and pith cells of the stem below. (Shuai et al., 2002; Traas, 2018; Wang and Jiao, 2023). A whole host of opposing forces help maintain the balance between the central and peripheral zones, of which the most important is the negative feedback loop between CLV3 and WUS, with WUS promoting cell proliferation in the central zone and activating CLV3, while CLV3 represses WUS, maintaining meristem size (Cao and Jiao, 2020; Wang and Jiao, 2023). Within the peripheral zone, organ initiation is promoted by local auxin maxima, which are generated by the PIN auxin efflux carriers (Traas, 2018; Zhu and Wagner, 2020). The implications of being unable to form these auxin maxima can be clearly seen in *pin1* mutants, which are almost entirely lacking in lateral organs in the arabidopsis (*Arabidopsis thaliana*) inflorescence (Gälweiler et al., 1998). These auxin maxima activate ARF5/MONOPTEROS (MP), which in turn promotes organ identity genes (Traas, 2018). Within the organizing center, cytokinin promotes WUS expression, which represses MP (Wang and Jiao, 2023). Thus, within the meristem, auxin and cytokinin act antagonistically, with cytokinin promoting the maintenance of stems cells, and auxin promoting differentiation into lateral organs (Traas, 2018). However, PIN1 orientation around a lateral primordium is highly dynamic, switching rapidly after the organ primordium is formed to orient toward the tip, abaxial side, and tissue surrounding the organ, thus creating auxin minima on the adaxial side and organ boundary (Wang and Jiao, 2023). This asymmetric auxin transport is crucial to abaxial/adaxial patterning in lateral organs (Wang et al., 2022a). Once the lateral organ has formed, the axillary meristem can initiate.

Once the axillary meristem has initiated, it can differentiate into many different organ fates. The branching pattern depends on whether the meristem remains indeterminate, forming organs laterally as in a lateral branch, or determinate; and, if determinate, on what organ fate it

differentiates into. In arabidopsis, meristem determination and differentiation have primarily been studied in the context of its indeterminate inflorescence. Indeterminacy and vegetative branching are promoted by TERMINAL FLOWER 1 (TF1), which acts antagonistically to MADS box transcription factors that promote floral organ identity, such as LFY and AP1 (Ratcliffe et al., 1998; Ratcliffe et al., 1998; McSteen and Leyser, 2005; Teo et al., 2014). In contrast, MP promotes differentiation in floral fate by upregulating LFY and downregulating axillary meristem maintenance genes STM and BREVIPEDICELLUS (BP; Zhu and Wagner, 2020). If the shoot apical meristem continues indefinitely, the branching pattern is described as monopodial, whereas if it terminates recurrently, either through becoming determinate or dying, it is described as sympodial. Avocado (*Persea americana*) is an example of monopodial growth (Thorp and Sedgley, 1992). Tomato (*Solanum lycopersicum*) is an example of sympodial growth arising from the apical meristem gaining floral determinacy, and vegetative growth being continued by the lateral bud immediately below, while apricot is an example of sympodial growth arising from the death of the apical meristem (McSteen and Leyser, 2005; Costes et al., 2006).

The final characteristic determining branching pattern is bud dormancy. Whereas axillary meristem placement (spiral vs. dorsal, etc.) is largely constant within a species, bud dormancy is strongly influenced by external factors—such as temperature, light, gravity, and nutrients—as well as internal factors such as hormone balance (Walker and Bennett, 2018; Barbier et al., 2019; Zhu and Wagner, 2020). Axillary meristems may grow out without any intervening period of dormancy (sylleptic growth) or after a season of dormancy (proleptic growth; Hallé et al., 1978). Broadly speaking, bud dormancy can be divided into three phases: paradormancy, or dormancy due to apical dominance or other physiological signals from outside the bud; endodormancy, or dormancy due to endogenous signaling which prevents outgrowth even in the presence of favorable conditions; and ecodormancy, or dormancy due to unfavorable environmental conditions (Lang et al., 1987). While all three types of dormancy influence outgrowth of vegetative buds, paradormancy has the largest influence on branch patterning, as it represents communication within the plant on which buds will break. Perhaps the most obvious form of bud break control is apical dominance, where the shoot apical meristem prevents outgrowth of lateral buds.

Apical dominance has been associated with auxin since the 1930s experiments showing that application of auxin to a decapitated shoot tip can prevent lateral bud outgrowth (Beveridge et al., 2023). Indeed, the importance of basipetal auxin flow can be seen in mutants of AUXIN

RESISTANT1 (*axr1*) in arabidopsis, which have increased branching because fewer axillary buds remain dormant (McSteen and Leyser, 2005). However, auxin does not directly enter lateral buds, nor does it travel acropetally through xylem, yet the signal is transmitted to lateral buds, and can travel acropetally (Beveridge et al., 2023). There are two main theories concerning this signal transmission: the direct-action model and the auxin canalization model (Walker and Bennett, 2018). The direct-action model contends that auxin represses cytokinin and upregulates strigolactone, which then directly control bud dormancy through the signal integrator BRANCHED1 (BRC1; Walker and Bennett, 2018; Barbier et al., 2019; Beveridge et al., 2023). This model is supported by the observations that application of cytokinin can stimulate bud break even in the presence of an intact shoot apex, and that cytokinin and strigolactone, unlike auxin, can both impact bud dormancy when applied directly to the bud (Walker and Bennett, 2018; Barbier et al., 2019; Beveridge et al., 2023). Furthermore, grafting experiments have demonstrated that strigolactone can move acropetally from the roots (Beveridge et al., 2023). However, this model does not explain the precise patterning of bud break, as cytokinin and strigolactone ratios ought to be relatively similar in adjacent buds (Walker and Bennett, 2018). The second model of apical dominance is the canalization model. Canalization is a positive feedback loop between auxin transport and PIN localization which causes auxin flow to become progressively stronger and narrower, although the mechanism of this positive feedback is still unknown (Walker and Bennett, 2018; Hajný et al., 2022). This model argues that bud outgrowth depends on ability to actively export auxin, which is prevented by canalization of auxin transport from the apical meristem in the main stem (Walker and Bennett, 2018).

Some recent work has focused on combining the two models by dividing bud activation into two stages: release from paradormancy and bud outgrowth (Barbier et al., 2019). In this model, nutrient and energy availability are signaled by sucrose, cytokinin, and strigolactone, which set the "activation threshold" of auxin export the bud must reach to for outgrowth (Walker and Bennett, 2018). Interestingly, this idea that the growth vigor sets an activation threshold that determines response to apical dominance dates back to the 1970s (Hallé et al., 1978). While the role of sugars in signaling nutrient availability and triggering bud outgrowth was largely overlooked in the intervening time, recent work has demonstrated their importance as signaling molecules, particularly for low-concentration sugars such as trehalose 6-phosphate (Tre6P) and non-metabolizable sugars such as mannose, which indicate sucrose availability (Beveridge et al., 2023).

Application of exogenous sucrose has a similar effect to decapitating the stem, and decapitation sends a sucrose pulse which occurs before the drop in auxin levels from decapitation (Barbier et al., 2019). Furthermore, this pulse occurs at a similar timing to bud outgrowth, which also occurs before the drop in auxin levels (Chabikwa et al., 2019). This sugar surge is integrated with the other hormonal signaling pathways, as it upregulates cytokinin and may increase auxin synthesis in the bud (Barbier et al., 2019; Chabikwa et al., 2019; Beveridge et al., 2023). Inorganic nutrient availability similarly appears to promote outgrowth through cytokinin/strigolactone ratio as nitrogen and phosphorous availability stimulate cytokinin and repress strigolactone, promoting branching (Walker and Bennett, 2018; Beveridge et al., 2023) Finally, under this model, once the bud has integrated the signals from cytokinin, strigolactone, and sucrose, it is primed for growth. If the bud becomes a sufficiently strong auxin source, canalization occurs from the bud to stem, and the bud is committed to sustained growth (Walker and Bennett, 2018). This model is supported by the observation that blocking auxin export from the bud did not inhibit initial bud outgrowth, but affected continued elongation after 2-3 days (Chabikwa et al., 2019).

Molecular control of shoot elongation

Once the shoot has begun to grow, the effects of shoot elongation dominate. Shoot elongation is determined by both the number of new phytomers formed (also referred to as the number of nodes, as there is one node per phytomer) and the elongation of internodes in each phytomer (Muleo and Morini, 2008). Shoots can grow from preformed phytomers (already present in the bud) or neoformed phytomers (developed after bud-break) or a mixture of both kinds of phytomers. The number of preformed phytomers per vegetative bud stays relatively constant in a particular species, although it is influenced by location in the tree (Costes et al., 2016). Thus basitonic (longer shoots at the bottom) versus acrotonic (longer shoots at the top) growth is probably controlled by the number of neoformed phytomers (Costes et al., 2016). Literature on rate of phytomer or node formation is sparce, which is surprising given that it has long been observed that the flowering of some herbaceous plants is triggered at a fairly constant number of nodes (suggesting some method by which the plant "counts" nodes) and that this number appears to be genetically controlled (Taylor, 1953; Sachs, 1999). However, the number of nodes formed in a given amount of time can absolutely be manipulated, as demonstrated in several applied studies. For instance, interruption of night to simulate long-day conditions increased the number of nodes produced in *Dianthus,* increasing light intensity increased the number of nodes in *Cannabis,* and application of ethephon

increased nodes produced in cucumber (Park et al., 2013; Dhakal et al., 2019). Genetically, the number of nodes produced in arabidopsis is much decreased in *tfl1* mutants, and much increased in overexpressors of TFL1 (Ratcliffe et al., 1998). This was correlated with a decrease or increase, respectively, of the amount of time in the vegetative and inflorescence phase. Unfortunately, the data connecting node number and time was not reported, so it is not possible to determine the rate of node production.

Internode elongation has received much more attention than phytomer formation. Ever since the discovery in the 1930s of the role of gibberellic acid (GA) in excessively elongated rice (*Oryza sativa*) seedlings infected by the fungal pathogen *Gibberella*, discussions of elongation have centered around GA (Hedden and Sponsel, 2015). Of course, GA is part of a complex hormonal network for regulating internode elongation, in which auxin, gibberellin, brassinosteroids, and strigolactones promote elongation while ethylene, abscisic acid, and jasmonic acid inhibit elongation (de Saint Germain et al., 2013). Auxin and ethylene primarily act upstream of GA, with auxin promoting GA synthesis and ethylene inhibiting GA activity, while brassinosteroids primarily act downstream of GA (Ross et al., 2003; de Saint Germain et al., 2013; Xue et al., 2022). GA promotes elongation by triggering ubiquitination and degradation of the growth-inhibiting DELLA proteins, which normally repress BRASSINAZOLE-RESISTANT1 (BZR1), a brassinosteroid-responsive transcription factor (Xue et al., 2022). The essential role of brassinosteroids in canonical GA-dependent elongation is demonstrated by their ability to recover dwarfism in GA-insensitive mutants, while brassinosteroid-insensitive mutants cannot be recovered by GA (Xue et al., 2022).

A final aspect of branch elongation is rotational torsion, which is twisting of branch or petiole without it bending or changing trajectory. This rotation is commonly seen in petioles in order to re-orient leaves to light, but may also occur in the entire internode (Hallé et al., 1978). While this has received little attention, it dramatically affects leaf distribution and final canopy light interception. For example, in corn, where leaves are distichous (alternating on opposite sides of the stalk), upper leaves in the canopy are oriented fairly evenly in all directions, due to rotational torsion of the internode, nodes, and sheath, along with movement of the leaves themselves (Drouet and Moulia, 1997). Studies on this subject date back to the 1800s, with such fascinating observations as that the torsion could occur while the stem remained relatively straight and in either a left- or right-handed spiral as “in nature organs always twist into the correct orientation to

the stimulus by the shorter way round" (Snow, 1942). Following the discovery that similar torsions could be achieved by unilateral application of auxin, the idea occurred that torsions were connected to auxin distribution changes within the stem or petiole, and there, it seems, the observations have been left (Snow, 1950). Much more recently, a remarkable study found that that mutants of CESA INTERACTIVE PROTEIN 1 (CSI1) have their phyllotaxy altered so that the angle between lateral organs is 90˚ or 180˚, rather than the usual 137˚ (Landrein et al., 2013). Amazingly, the positions of organ primordia are not altered, rather the change in angle is due to right-handed torsion in the stem between lateral organs (Landrein et al., 2013). CSI1 is required for attachment of the CESA complex to microtubules, and cellulose microfibrils in the hypocotyls of the mutants form a left-handed spiral, rather than being oriented transversely, as in wild type hypocotyls (Landrein et al., 2013). As expansion occurs perpendicularly to microfibrils, and decreases in cellulose content were able to decrease the torsion, the authors suggest misorientation of the microfibrils causes the torsion (Landrein et al., 2013). While this does not explain the mechanism of phototropic or gravitropic torsion, it does highlight the role of torsion in altering the locations of lateral organ, and the authors suggest that torsion may play a larger role in phyllotaxy than previously believed (Landrein et al., 2013).

Molecular control of lateral organ angle

Although it is often ignored in reviews of plant architecture, the final aspect of plant architecture is the angle of lateral organs. Branch angle is a combination of three different angles: crotch angle, branch trajectory or "set-point" angle, and tip angle (Hollender and Dardick, 2015). Measuring and characterizing branch angle is complicated by the fact that each of these angles may be different. However, branch angles have major effects on plant appearance and utility and optimizing lateral organ angles in crop plants can increase planting density, light interception, yield, canopy ventilation, and pesticide distribution (Ku et al., 2011; Zhao et al., 2014; Roychoudhry and Kepinski, 2015; Xu et al., 2017; González-Arcos et al., 2019). Despite its importance, branch angle remains recalcitrant to control, despite decades of work utilizing such varied techniques as pruning, tying, and hormone application. Underlying the difficulty of manipulating branch angle is a paucity of information about the molecular mechanisms involved in determining the branch angle within the plant. Furthermore, much of the work on lateral organ angle has been performed in rice or maize (*Zea mays*) tiller angles, and it is not immediately apparent to which aspect(s) of branch angle those are physiologically analogous.

In establishing branch angle, the plant integrates environmental signals from gravity and light, positional signals of the presence or absence of apical leader and the distance of the branch from said leader, and potentially an "antigravitropic offset", although the existence and mechanism of an antigravitropic offset remain contentious. Accordingly, most of the genes involved in branch angle control can be categorized by their role in these signaling pathways.

Many of the genes which have been identified thus far as altering branch angle are part of the auxin-mediated gravitropism pathway. This pathway has been well-studied in primary shoots. Briefly, gravitropic stimulus causes the kinases MKK5 and MPK3 to phosphorylate LAZY proteins (discussed in detail below), promoting their binding to TRANSLOCON AT THE OUTER CHLOROPLAST ENVELOPE (TOC) proteins on the outer membrane of amyloplasts (Chen et al., 2023). The starch-filled amyloplasts in the endodermis then sediment to the lower side of the cell, where LAZY proteins move from the amyloplasts into the plasma membrane on the basal side of the cell (Chen et al., 2023; Nishimura et al., 2023). There, the LAZY proteins interact with RCC1-like domain (RLD) proteins to localize the auxin efflux carrier PIN3 to the bottom of the endodermal cells (Furutani et al., 2020). The PIN3 proteins promote lateral transport of auxin downward, which increases the auxin concentration on the bottom of the shoot or branch. The asymmetric auxin gradient leads to a gradient in SMALL AUXIN UPREGULATED RNAs (SAURs) which are upregulated through the canonical $SCF^{TIR1/AFB}$ signaling pathway (Ren and Gray, 2015; Du et al., 2020). SAUR proteins inhibit PP2C-D phosphatases from dephosphorylating H^+-ATPases (Spartz et al., 2014; Du et al., 2020). The phosphorylated H^+-ATPases are activated and pump protons out of the cell, hyperpolarizing the cell membrane (leading to water uptake by the cell and an increase in turgor pressure) and acidifying the apoplast (leading to activation of cell wall enzymes such as expansins, which remodel the cell wall; (Spartz et al., 2014; Marowa et al., 2016; Du et al., 2020). This mechanism leads to cell elongation on the bottom side of gravitropically stimulated shoots, bending them upward (Su and Masson, 2019).

Within the gravitropism pathway, most of the genes originally identified as controlling branch angle are involved in amyloplast sedimentation (Table 1.1). These genes may be essential for formation of the endodermis, such as *SCARECROW* (*AtSCR*) and *SHORT*-ROOT (*AtSHR*) in arabidopsis (Tasaka et al., 1999; Nakamura et al., 2019). Or, they may alter amyloplast dynamics and trafficking—by, for example, altering the endomembrane system, the actin cytoskeleton, or attachment of amyloplasts to actin—as in mutants of arabidopsis *SHOOTGRAVITROPISM*

(*AtSGR1); AtSGR2; AtSGR3*; *AtZIGZAG (AtZIG* or *AtSGR4); AtSGR6; AtSGR8; or AtSGR9* (Tasaka et al., 1999; Kato et al., 2002; Yano et al., 2003; Silady et al., 2004; Nakamura et al., 2011; Hashiguchi et al., 2014; Nakamura et al., 2019; Kawamoto and Morita, 2022). Other genes are essential for starch accumulation such as *OsAGPL1/3, OsPGM* and *AtPGM1,* or *OsLAZY2* (not an IGT gene or homologous to *OsLAZY1*) (Okamura et al., 2014; Huang et al., 2021; Wang et al., 2022b). Mutations in any of these cause defective amyloplast sedimentation and therefore wider lateral organ angles. In rice, *LOOSE PLANT ARCHITECTURE 1* (*OsLPA1*) also is needed for normal amyloplast sedimentation, though the specific mechanism is unknown, and mutants have wider branch angles, as do overexpressors of *ONAC106*, a transcription factor which represses *LPA1* in rice (Wu et al., 2013; Sakuraba et al., 2015; Sun et al., 2019; Wang et al., 2022b).

While all these genes impact lateral angles as would be expected for their functions, the rice genes OsCRCT and RICE MORPHOLOGY DETERMINANT (*OsRMD*) do not. OsCRCT promotes starch accumulation, which generally increases gravitropism, but overexpressors show wider tiller angles, while knockouts show no change in tiller angle (Morita et al., 2015). *OsRMD* impacts amyloplast dynamics by affecting actin organization, and mutants would be expected to exhibit inhibited gravitropism. As expected, mutants of *Osrmd* light-grown shoots have inhibited sedimentation and lateral angles are wider (Zhang et al., 2011; Huang et al., 2018; Song et al., 2019). However, sedimentation is not affected in *Osrmd* dark-grown shoots, and is promoted in *Osrmd* roots, which have narrower lateral root angles (Zhang et al., 2018; Song et al., 2019). It has not yet been determined why *OsRMD* has the opposite effect in roots versus shoots.

A few genes which alter lateral organ angle have been found to be involved in auxin synthesis and signaling. These all show wider angles when knocked out, and narrower angles when overexpressed. For example, *AtIDD13*, *IDD14*, and *IDD15* (also known as *AtSGR5*) and *AtYUCCA2* and *AtYUCCA6* in arabidopsis and homolog *BnaA.YUCCS6.a.* in *Brassica napus* are all involved in auxin synthesis (Cui et al., 2013; Wang et al., 2016). In rice, *OsTAC4* is believed to function in auxin synthesis and/or transport (Li et al., 2021). Other genes are part of the canonical auxin signaling pathway, as for *AtTIR1* or *AtIAA7* in arabidopsis or early auxin upregulated genes as for *OsGH3.13* in rice (Timpte et al., 1994; Nagpal et al., 2000; Zhang et al., 2009; Roychoudhry and Kepinski, 2015).

Most of the branch angle genes which have been discovered control the formation of the gravitropic auxin gradient, often by regulating expression or localization of PIN proteins. The

central gene in this regulatory network is *LAZY1,* which promotes narrowed lateral shoot and root angles and is a member of the IGT protein family, which is named for a short, conserved (GϕL(A/T)IGT) amino acid motif (Dardick *et al.*, 2013). Homologs of *LAZY1* are found throughout the plant kingdom, including in mosses and ferns, although not in green algae (Dardick et al., 2013). *LAZY* homolog mutants in many species all have wider lateral organ angles and decreased or absent gravitropic response (Godbolé et al., 1999; Li et al., 2007; Arai-Sanoh et al., 2014; Howard III et al., 2014; Ge and Chen, 2016; Taniguchi et al., 2017; Chen et al., 2020; Nakamura et al., 2019; Dougherty et al., 2023). Study of *LAZY1* is complicated by the fact that there are multiple *LAZY* paralogs in most species (6 in arabidopsis), which are partially redundant, but show distinct expression patterns (Nakamura *et al.*, 2019). Briefly, *AtLAZY1* is the primary shoot-expressed homolog, with mutants showing wider branch angles. *AtLAZY2, AtLAZY3,* and *AtLAZY4* are primarily root-expressed and control root angle, although triple mutants of *Atlazy1,2,4* do show wider branch angles compared to *Atlazy1,* pointing to a role for *AtLAZY2* and *AtLAZY4* in shoot architecture (Taniguchi *et al.*, 2017). *AtLAZY5* is believed to be a pseudogene, while *AtLAZY6* shows significant shoot expression, but does not appear to enhance the shoot phenotype of *AtLAZY1* (Waite and Dardick, 2020).

Most of the other genes that control the gravitropic auxin gradient act in relationship to *LAZY1.* In rice, two *HOX* genes (*OsHOX1*/28) repress *HEAT STRESS TRANSCRIPTION FACTOR 2D* (*HSFA2D*), which upregulates *LAZY1* (Zhang et al., 2018; Hu et al., 2020; Wang et al., 2022b). LAZY1 expression is repressed by *OsPROG1, OsARF12, OsARF17,* and *OsARF25* (Jin et al., 2008; Li et al., 2020; Wang et al., 2023). The *ARFs* are repressed by a microRNA (OsMIR167a) and activated by LAZY1, forming a negative feedback loop for *LAZY1* (Li et al., 2020). In both arabidopsis and rice, BREVIS RADIX LIKE 4 (BRXL4) protein binds LAZY1 protein in region V and sequesters it to the nucleus, repressing its function in gravitropism (Li et al., 2019; Wang et al., 2022b; Chen et al., 2023). As would be expected, the *HOX* genes, *PROG1*, and *BXRL4* all have narrower angles when mutated and wider when overexpressed. Strangely for repressors of *LAZY*, the *ARFs* have wider angles when mutated, as does an overexpressor of *OsMIR167a* (Li et al., 2020). To my knowledge, this apparent contradiction has not been resolved.

Other genes involved in auxin transport include rice *OsLPA1* which, as well as its role in amyloplast sedimentation, activates *PIN1a* expression (Sun et al., 2019). When individual PIN proteins are mutated in rice, they show opposite phenotypes, with *PIN1* mutants having wider

angles, but *PIN2* overexpressors having wider angles (Xu et al., 2005; Chen et al., 2012; Sun et al., 2019; Wang et al., 2022b). Mutants of two other rice genes (*OsFucT* and *OsPAY1*) have wider tiller angles and impaired basipetal transport, but their functions have not yet been determined (Zhao et al., 2015; Harmoko et al., 2016; Wang et al., 2022b).

Along with gravity, the plant integrates signals about the amount and quality of light as it determines branch angle. Plants respond to low light or shading by narrowing their branch angles. *TAC1* promotes outward lateral organ growth in response to light and shade, but does not appear to have a role in gravitropism, although it is in the same IGT family as the *LAZY* homologs (Hollender et al., 2020). Mutants of *tac1* and *lazy* have opposite phenotypes, with *tac1* mutants showing narrowed angles, and *lazy* mutants showing wider angles. Supporting the role of *TAC1* in light perception, wild type arabidopsis branch angles narrow in response to darkness, but *Attac1* mutant branch angles fail to narrow further in darkness (Waite and Dardick, 2018). *AtTAC1* expression is upregulated in light but dissipates in prolonged darkness (>72 hours), as well as in response to photosynthetic inhibitors, and in mutants of the light signal integrator *CONSTITUTIVE PHOTOMORPHOGENIC 1* (*cop1*; Waite and Dardick, 2018).Variation in *TAC1* expression has been correlated with lateral organ angles in rice, maize, peach (*Prunus persica*), arabidopsis, *Miscanthus sinensis,* poplar (*Populus sp.*), and tomato (*Solanum lycopersicum*;Yu et al., 2007; Ku et al., 2011; Dardick et al., 2013; Zhao et al., 2014; Xu et al., 2017; González-Arcos et al., 2019). *TAC1* function is dosage dependent, as heterozygous individuals show an intermediate angle phenotype in both peach and tomato, and overexpression of *TAC1* in rice, plum, or arabidopsis leads to wider angles (Scorza et al., 2002; Werner and Chaparro, 2005; Yu et al., 2007; Dardick et al., 2013; Hollender et al., 2018b; González-Arcos et al., 2019; Hollender et al., 2020).

Another gene involved in regulating branch angle for light response is *OsPIL15* in rice, which promotes narrower angles by enhancing gravitropism, but is repressed by light (Xie et al., 2019; He et al., 2021). Similarly, *OsPIL6* represses *OsRMD*, but is repressed by light (Song et al., 2019). Overexpressors of *OsPIL6* show the same lack of shoot gravitropism as *rmd* mutants (Song et al., 2019). On the other hand, *AtFUL* in arabidopsis, which is activated in low R:FR ratios (a sign of shading) moderates the response to shading by repressing *SAUR10* on the abaxial side, which promotes wider branches (Bemer et al., 2017). Some *LAZY* homologs may also be involved in integrating light and gravitropic response, as their expression is also light-regulated (Waite and Dardick, 2020).

However, the impacts of gravitropism and phototropism do not explain why lateral branches do not grow straight up, like the primary leader. All lateral organs are offset from the direction of the vertical leader at an angle referred to as their "set point angle". In a clinostat, which eliminates the gravitropic force, both branch and root angles widen, suggesting that at least in arabidopsis, the set point angle occurs at the balance of gravitropic forces and an outward "antigravitropic offset" (AGO) which "pushes" lateral organs wider against the "pull" of gravity (Roychoudhry and Kepinski, 2015). Remarkably the AGO, like gravitropism, appears to be regulated by auxin flow (Roychoudhry and Kepinski, 2015). If auxin transport is disrupted, either with chemical inhibitors or starchless mutant *pgm,* in mutants of multiple *LAZY* homologs (which generally have an inverted auxin gradient and upward bending roots) root direction is randomized (Ge and Chen, 2019; Kawamoto et al., 2020; Kawamoto and Morita, 2022). This suggests that the AGO and gravitropism are integrated by auxin signaling (Kawamoto and Morita, 2022).

This connection with auxin may indicate that AGO is simply another term for apical control of angle, which has been associated with auxin since the 1930s (see Thimann, 1939), although interpretation of older literature is complicated by equivocation in terms between apical dominance and apical control. Apical control describes influence the apex exerts over lateral branch angle, diameter, and elongation, as opposed to apical dominance, which is the prevention of bud outgrowth by the apex (Wilson, 2000; Hollender and Dardick, 2015). The effect of apical control on angle is most readily seen when the apex is removed, as one or more laterals will reorient to be vertical and take over as the leader (Thimann, 1939; Wilson, 2000). Reorientation of an existing branch is not seen in every species, as some species simply have a bud break and grow as the new leader (Thimann, 1939). However, almost every species has the capacity to produce a new, vertically oriented leader in some way. More subtly, lateral angles often vary depending on distance from the apex, with lateral branches closer to the apex having more acute angles than those at the bottom, indicating that apical control provides positional information to the laterals of "where in the plant" they are located (Hollender and Dardick, 2015). Interestingly, proximity to the apex can have opposite effects on elongation, either repressing growth close to the apex (described as basitonic architecture) or close to the base (described as acrotonic growth) (Wilson, 2000).

However, some authors raise concerns about crediting auxin as the signal for apical control. Some of these concerns are similar to those for auxin in apical dominance, such as the absence of a known way for auxin to travel acropetally from the main stem up a lateral branch (Cline and

Sadeski, 2002). Experiments in *Pharbitis nil* (morning glory), which exhibits strong apical control of lateral shoot length, showed that while auxin application to a decapitated dominant branch could inhibit bud outgrowth (replacing apical dominance), it did not inhibit lateral shoot growth (failed to replace apical control; Cline and Sadeski, 2002). However, a subsequent experiment in *Pseudotsuga menziesii* (Douglas fir) found that auxin application to a decapitated leader could inhibit branch angle narrowing (auxin replaced apical control) (Cline et al., 2009). An additional complication is that the effects of auxin on branch angle are dosage dependent (Blake et al., 1980). Nutrient availability also likely plays a role in apical control, as shoot elongation is largely released from apical control under high nutrient availability (Cline et al., 2009).

Other data point to ethylene as a key signal for apical control of branch angle, at least in woody species (Blake et al., 1980). Long days, high light, decapitating the leader, applying auxin to decapitated leaders, or application of gibberellic acid to soil all increased ethylene production and decreased the branch angle in *Cupressus arizonica* (Arizona cypress; Blake et al., 1980). Demonstrating that ethylene alone was sufficient to cause the more upright angles, gassing the trees with ethylene decreased the angles, while applying mercuric perchlorate to sequester the ethylene increased branch angle (Blake et al., 1980). The role of ethylene in branch angle is likely connected to formation of reaction wood.

Rection wood formation

As though branch angle control was not complicated enough in plants like arabidopsis and rice, trees can control branch trajectory and reorient branches toward the desired set-point angle not only through branch curvature during primary growth (as in arabidopsis), but also during secondary growth (when the branch can no longer elongate) through formation of reaction wood (Felten and Sundberg, 2013; Groover, 2016). In gymnosperms, reaction wood is generally compression wood, which forms on the lower side of the branch, while in angiosperms, reaction wood is generally tension wood, which forms on the top of the branch and shrinks as it matures in order to pull branches up (Groover, 2016; Aloni, 2021). In tension wood, the ratio of xylem fibers to vessels is generally increased, and the usual secondary cell wall layers of the fiber cells are often replaced by a gelatinous layer (G-layer; Andersson-Gunnerås et al., 2003; Felten and Sundberg, 2013; Groover, 2016). This G-layer is very porous and hydrated and is primarily composed of cellulose (Felten and Sundberg, 2013). The cellulose microfibrils in the G-layer are oriented parallel to the length of the fiber cell (rather than at an angle, as in a normal S2 or S3 layer) and

are four times as thick as in a typical S2 cell wall layer (Lautner et al., 2012; Felten and Sundberg, 2013; Groover, 2016). The altered structure and arrangement of these cellulose microfibrils produces tensile force as the tension wood shrinks longitudinally (Felten and Sundberg, 2013; Groover, 2016). However, the tension wood of some species (such as peach) does not produce G-fibers, although it still exerts a tensile force (Felten and Sundberg, 2013).

In addition to this change in cell wall morphology, tension wood is characterized by an increase in periclinal vascular cambium division to increase the number of xylem cell files on the upper side of the branch (Andersson-Gunnerås et al., 2003; Love et al., 2009). As with primary growth, the control of differential growth from top to bottom of the branch requires precise hormone gradients, perhaps including the gravitropic auxin gradient. Unlike in primary growth, the amyloplasts and *PIN3* expression in branches with secondary growth are not found in endodermal cells (which have been sloughed off) but in the secondary phloem, and the auxin gradient in secondary growth does not occur across the entire branch (Groover, 2016). Rather, on the upper half of the branch, auxin concentration is directed downward from the phloem toward the cambium and xylem, while on the bottom half of the branch, it is directed downward from the phloem toward the cortex (Groover, 2016). This likely contributes to the increase in xylem formation on the upper side, while the lower side has decreased xylem formation.

In addition to auxin, ethylene plays a major role in this differential division (Nelson and Hillis, 1978; Andersson-Gunnerås et al., 2003; Love et al., 2009; Felten and Sundberg, 2013). The increased cell division in tension wood is caused by a gradient of 1-aminocyclopropane-1-carboxylate (ACC) oxidase, which converts ACC into ethylene (Andersson-Gunnerås et al., 2003). High levels of ACC oxidase on the upper side of the branch increase the concentration of ethylene, which in turn stimulates cambial division (Andersson-Gunnerås et al., 2003; Love et al., 2009). Ethylene is necessary for tension wood proliferation, as ethylene-insensitive poplar does not form additional xylem layers on the tension wood side (Love et al., 2009). However, exogenous ethylene application is not sufficient for formation of normal tension wood, although it can stimulate the formation of G-fibers (Nelson and Hillis, 1978; Aloni, 2021).

Gibberellic acid (GA) also plays a role in tension wood, as exogenous application of GA can cause all three characteristics of tension wood (cell proliferation, change in cell wall morphology, and change in fiber to vessel ratio; (Felten and Sundberg, 2013). Application of GA can produce tension wood which rescues the weeping phenotype in *Prunus spachiana* (Nakamura et al., 1994; Aloni,

2021). However, no increase in endogenous GA has yet been reported in tension wood (Felten and Sundberg, 2013).

In addition to the impact of gravity, branch angle in trees is also influenced by light, mechanical loading, and the rate of secondary growth (Costes et al., 2006). These change more fluidly and locally than gravity, sometimes influencing just a single branch. Mechanical loading usually leads to bending or alteration of branch trajectory away from the force, in the same direction as the force vector. In the case of wind, branches on the upwind side of the tree curve toward the downwind side (Telewski, 2012). This is accompanied by the development of flexure wood (which increases wood flexibility) and radial thickening (which increases its resistance to force; Telewski, 2012). Unlike reaction wood and the gravitropic response, which do not occur unless a branch is displaced from its original position for a minimum amount of time (known as the presentation time), flexure wood forms in response to sway, even if the branch returns to its original position (Telewski, 2016). However, flexure wood shares many characteristic of tension wood. Flexure wood displays an asymmetric thickening in the axis of the sway, increases in cell wall thickness and decreased modulus of elasticity (Telewski, 2016). A recent study showed that the transcriptome of flexure wood in *Populus* resembles that of tension wood, and that, like tension wood, it has increased ethylene production (Urbancsok et al., 2023). There appears to be some disagreement over whether microfibril angle in flexure wood is decreased (more parallel to the length of the cell, as in tension wood) as was found by Urbancsok et al. (2023), or increased (more perpendicular to the length of the cell) as was found by Telewski (2016) and Niez et al. (2020). Given that increased microfibril angle is generally associated with greater flexibility, which was found in all studies, it seems likely that microfibril angle is, in fact, generally increased (Barnett and Bonham, 2004). Furthermore, Urbancsok et al. (2023) observed tension wood in both control trees and flexed trees, raising some concerns about whether the observed microfibril angle was truly related to the flexure.

Architecture in *Prunus*

Despite its importance, our understanding of natural tree architecture in *Prunus* is limited as *Prunus* trees are usually manipulated by pruning (Gradziel et al., 2002; Costes et al., 2006). Natural *Prunus* architectures vary widely, providing the opportunity to breed cultivars with desired architecture. Peach (*P. persica*), European plum (*P. domestica*-also known as prune), almond (*P. dulcis*), and sweet cherry (*P. avium*) are all monopodial (one central leader grows) but vary in subsequent branching (Costes et al., 2006; Costes et al., 2014). Branching in almond is generally

acrotonic (branches near the top of the canopy grow longer) but can range from long internode length to short spurs, and from a frequent branching pattern to very few branches (Gradziel et al., 2002; Costes et al., 2014). Short spurs and increased branching are preferred because they lead to greater fruit yield (Gradziel et al., 2002). Peach branching is bushy, with more basitonic growth (lower branches grow longer) than almonds, and often exhibits a "twiggy" phenotype which must be hand-pruned (Carrillo-Mendoza et al., 2010; Costes et al., 2014). This phenotype is heritable, as crosses between peaches and rarely-branching almonds decrease the undesirable branching (Carrillo-Mendoza et al., 2010). European plum is also bushy and basitonic, but with less "twiggy" branching. Sweet cherry habit may be upright or spreading, with spreading canopies improving light permeability and photosynthetic capability (Gonçalves et al., 2008). In sharp contrast to other *Prunus* species, apricots (*P. armeniaca*) are sympodial (multiple main leaders grow), with the central leader often dying and growth continuing from lateral buds (Costes et al., 2014). As these contrasting branching patterns are available in *Prunus*, the genetics underlying architecture may be expected to vary as well.

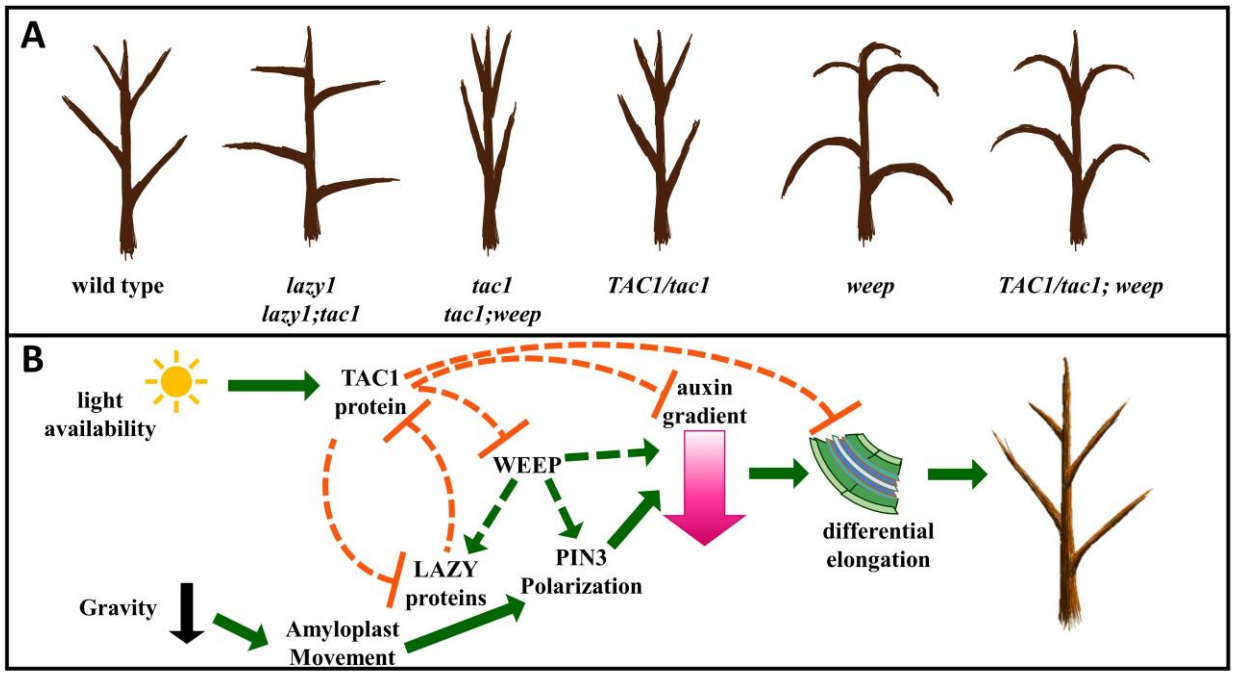

Figure 1.2: Relationships between *LAZY1*, *TAC1*, and *WEEP*. A) Epistatic relationships previously reported in Werner and Chapiro, 2005, and Hollender et al., 2020. **B)** Model of interactions between genes in establishing branch angle. Known activation relationships are shown with solid arrows, hypothetical activation is shown with a dashed arrow, and hypothetical repression with dashed T. Modified from Hill and Hollender, 2019.

In addition to this natural variation in branching pattern, some cultivars within *Prunus* species have altered branch angle or internode length. These alternative architectures are becoming increasingly common in ornamental applications and may improve training efficiency and production. For example, alternative peach growth habits include pillar, dwarf, compact, semi-dwarf, spur-type, and weeping (Scorza et al., 2006). The pillar habit in peach (caused by a homozygous mutation in *tac1*), which reduces branch angle, is associated with a higher ratio of leaf area to canopy cross section, has more efficient light interception, and requires very little pruning but can also have increased shading in the lower canopy (Bassi et al., 1994; Tworkoski and Scorza, 2001). Weeping habits are also very common in *Prunus* and often are cultivated for their beauty as ornamentals. Weeping habits are found in *P. persica, P. mume, P. subhirtella, P. spachiana,* and *P. incisa,* among others (Sebire, 1990; Yoshida et al., 1999; Dunn, 2013; Hollender et al., 2018a; Zhuo et al., 2021).

WEEP*, *LAZY1* and *TAC1* in *Prunus

In this dissertation, I investigate the molecular mechanisms underlying the weeping growth habit in peach, which is caused by a homozygous mutation in the SAM domain gene *WEEP.* Here I present evidence that *WEEP* promotes negative gravitropism in both shoots and roots and directs the gravitropic auxin gradient in shoots, which is inverted in *weep* mutants. I also present phenotypes associated with suppression of *LAZY1* expression in European plum, and consider their application for fruit production in high-density, planar training systems. Finally, I investigate the implications for fruit yield and quality of various planar training systems and peach varieties with differing dosage of TAC1.

While they all act in branch angle control, these genes promote different phenotypes. Of these three genes, *WEEP* and *LAZY1* are involved in gravitropic branch angle control, while *TAC1* is involved in light-related branch angle control. Furthermore, mutants of *LAZY1* and *WEEP* show similar phenotypes in the shoots (wider angles and weeping) but opposite phenotypes in roots, with *LAZY1* promoting wider angle and *WEEP* promoting narrower angles. From a gene family perspective, *LAZY1* and *TAC1* are both IGT family genes, while *WEEP* contains a Sterile Alpha Motif domain, but no other known functional domains.

However, epistasis between the genes suggests that all three genes are involved in the same pathway. In arabidopsis, *LAZY1* is epistatic to *TAC1,* with *lazy1;tac1* double mutants having wide branch angles as in *lazy1* (Figure 1.2A; Hollender et al., 2020). *TAC1*, in turn, is epistatic to *WEEP*

in peach, with *tac1;weep* double mutants showing a pillar phenotype (Figure 1.2A; Werner and Chaparro, 2005). Perhaps most strikingly, peach trees heterozygous for *TAC1* (*TAC1/tac1*) and homozygous for the *weep* deletion show an intermediate phenotype referred to as "archer" with upright branch angles and a weeping branch trajectory (Werner and Chaparro, 2005). In both pairs of genes demonstrating epistasis (*lazy1*;*tac1* and *tac1*;*weep)* the two genes promote opposite phenotypes, suggesting a repressor relationship between them (Figure 1.2B). In a repressor pathway, the epistatic gene is generally downstream. However, interpretation of the relationships between these architecture genes is complicated, as the interactions likely resemble a network rather than a linear pathway (Figure 1.2B). For example, it is clear that at least some functional TAC1 protein is necessary for the *weep* phenotype. It is tempting to conclude from this that TAC1 is required for auxin synthesis or transport, particularly as arabidopsis *tac1* mutant plants have decreased auxin in the shoot tip (Hollender et al. 2020). However, since functional auxin transport is required for the *lazy2;3;4* negative root gravitropism phenotype (Ge and Chen, 2019, the epistatic relation of *lazy1* to *tac1* would seem to suggest that *TAC1* functions in an auxin-independent pathway. Continuing research into the complex interplay between these genes will be essential to understanding how plants integrate light, gravity, and anti-gravitropic signals to determine branch angle.

Table 1.1: Genes known to be involved in branch angle control.

Gravity: Sensing and Amyloplasts						
Gene	**Species**	**Annotation**	**Mechanism**	**Knockout or Knockdown Phenotype**	**Overexpressor Phenotype**	**References**
AtSHORT-ROOT (SHR) aka AtSGR7	*Arabidopsis*	GRAS family transcription factor	Endodermis Formation	Wider	-	Tasaka et al., 1999; Nakamura et al., 2019
AtSCARECROW (SCR) aka AtSGR1; PnSCR	*Arabidopsis; Pharbitis nil*	GRAS family transcription factor	Endodermis Formation	Wider	-	Tasaka et al., 1999 Nakamura et al., 2019
AtSHOOTGRAVITROPISM2 (SGR2)	*Arabidopsis*	Phospholipase-like	Amyloplast Dynamics	Wider	-	Kato et al., 2002; Nakamura et al., 2019
AtSGR3 aka AtVAM3	*Arabidopsis*	Syntaxin	Amyloplast Dynamics	Wider		Yano et al., 2003; Kawamoto and Morita, 2022-Review
AtZIGZAG aka SGR4	*Arabidopsis*	Ab-SNARE	Amyloplast Dynamics	Wider	-	Kato et al., 2002; Nakamura et al., 2019
OsLPA1; AtSGR5 aka AtIDD15	*Oryza sativa, Arabidopsis*	C2H2 TF and INDETERMINATE DOMAIN TF	Amyloplast Dynamics	Wider	Narrower	Wu et al., 2013; Sun 2019
AtSGR6	*Arabidopsis*	HEAT repeat motif	Amyloplast Dynamics	Wider	-	Hashiguchi et al., 2014; Kawamoto and Morita, 2022-Review
AtSGR8, aka GRV2 aka KAM2	*Arabidopsis*	DnaJ and IWN repeat	Amyloplast Dynamics (Endocytosis related)	Wider (tip angle not affected		Silady et al., 2004; Kawamoto and Morita, 2022-Review
AtSGR9	*Arabidopsis*	RING E3 ubiquitin ligase	Amyloplast Dynamics (Actin attachment)	Wider		Nakamura et al., 2011; Kawamoto and Morita, 2022-Review
OsAGPL1 and OsAGPL3	*Oryza sativa*	ADP-Glucose pyrophosphorylase	Starch Accumulation	Wider	-	Okamura et al., 2014; Wang et al, 2022-Review
OsPHOSPHOGLUCOMUTASE DEFICIENT (PGM); AtPGM1	*Oryza sativa, Arabidopsis*	phosphoglucomutase	Starch Accumulation	Wider	-	Huang et al., 2021; Wang et al., 2022-Review
OsLAZY2	*Oryza sativa*	YbaB-like	Starch Accumulation	Wider	-	Huang et al., 2021; Wang et al., 2022-Review
OsONAC106	*Oryza sativa*	NAC TF	Represses LPA1 in Oryza sativa	-	Wider	Sakuraba et al., 2015; Wang et al., 2022-Review
OsRICE MORPHOLOGY DETERMINANT (RMD)	*Oryza sativa*	Type II Formin FH5	Amyloplast Dynamics (Actin attachment); enhances sedimentation in light-grown shoots, inhibits in roots	Wider (light-grown shoots) or Narrower (roots)	-	Zhang et al., 2011; Huang et al., 2018; Song et al., 2019; Kawamoto and Morita, 2022-Review
OsCRCT	*Oryza sativa*	CO2-Responsive CONSTANS, CONSTANS-like, and Time of Chlorophyll a/b Binding Protein1 (CCT) Protein	Promotes starch accumulation	-	Wider	Morita et al., 2015

Gravity-Generating Auxin Gradient						
Gene	**Species**	**Annotation**	**Mechanism**	**Knockout Phenotype**	**OE Phenotype**	**Papers**
OSHOX1/28	Oryza sativa	HD-ZIP II TF	Supress HSFA2D/LAZY1	Narrower	Wider	Hu et al., 2020; Wang et al., 2022-Review
OsHSFA2D	Oryza sativa	heat stress TF	Upregulates LAZY1	-	-	Zhang et al., 2018; Wang et al., 2022-Review
OsBRXL4; AtBRXL4	Oryza sativa; Arabidopsis	Brevis Radix-Like 4	Binds and surpresses LAZY1 by directing to nucleus	Narrower	Wider	Le et al., 2019; Wang et al., 2022-Review; Che et al., 2023
OsPROG1	Oryza sativa	C2H2 TF	Negative feedback loop with LAZY1	Narrower	Wider	Jin et al., 2008; Wang et al., 2023
LAZY1,2,3,4,6, aka NGR, aka LZY	Oryza sativa, Arabidopsis, Prunus persica, others	IGT	Direct PIN localization; Negatively regulates PROG1	Wider	-	Wang et al., 2022-Review
AtRLD1-4	Arabidopsis	RCC1-Like Domain	PIN localization with LAZY	Wider (but in roots)	-	Furutani et al., 2020
OsPIN1	Oryza sativa	auxin efflux carrier	Auxin export	Wider		Xu et al., 2005; Sun et al., 2019; Wang et al., 2022-Review
OsPIN2	Oryza sativa	auxin efflux carrier	Basipetal auxin transport, represses LAZY1	-	Wider	Chen et al., 2011; Wang et al., 2022-Review
OsFucT	Oryza sativa	fucosyltransferase	Basipetal auxin transport	Wider	-	Harmoko et al., 2016; Wang et al., 2022-Review
OsPAY1	Oryza sativa	trypsin family protein	Basipetal Auxin Transport	Wider	Narrower	Zhao et al., 2015; Wang et al., 2022-Review
OsMIR167a	Oryza sativa	microRNA	Represses OsARF12; OsARF17; and OsARF25	-	Wider	Li et al., 2020Wang et al., 2022-Review
OsARF12	Oryza sativa	auxin response factor	Repress basipetal transport, may be in feedback with LAZY (repress LAZY, LAZY activates them)	Wider	-	Li et al., 2020; Wang et al., 2022-Review
OsARF17	Oryza sativa	auxin response factor	Repress basipetal transport, may be in feedback with LAZY (repress LAZY, LAZY activates them)	Wider	-	Li et al., 2020; Wang et al., 2022-Review
OsARF25	Oryza sativa	auxin response factor	Repress basipetal transport, may be in feedback with LAZY (repress LAZY, LAZY activates them)	Wider	-	Li et al., 2020
PpeWEEP	Prunus persica	SAM domain protein	Direct lateral auxin gradient	Wider	-	See Chapter 2

Table 1.1 (cont'd)

Gravity-Auxin synthesis and signaling						
Gene	**Species**	**Annotation**	**Mechanism**	**Knockout or Knockdown Phenotype**	**Overexpressor Phenotype**	**References**
AtIDD13,14,15	*Arabidopsis*	INDETERMINATE DOMAIN TF	Regulation of auxin synthesis and transport	Wider		Cui et al., 2013
AtYUCCA2	*Arabidopsis*	YUCCA	Local Auxin Biosynthesis	-	Narrower	Cui et al., 2013
BnaA.YUCCA6.a; AtYUCCA6	*Brasica napus, Arabidopsis*	YUCCA	Local Auxin Biosynthesis	-	Narrower	Wang et al., 2016
AtTIR1	*Arabidopsis*	F-box	Canonical Auxin signaling	Wider	-	Roychoudhry and Kepinski, 2015
AtIAA7 aka AXR2	*Arabidopsis*	IAA family	Canonical Auxin signaling	Wider		Timpte et al., 1994; Nagpal et al., 2000
OsTAC4	*Oryza sativa*	Unknown	Basipetal auxin transport and/or auxin synthesis; not epistatic to TAC1	Wider	Narrower	Li et al., 2021; Wang et al., 2022-Review
OsGH3.13 aka OsTLD1	*Oryza sativa*	GRETCHEN HAGEN 3 (GH3)	Creation of auxin maxima	-	Wider	Zhang et al., 2009

Light						
Gene	**Species**	**Annotation**	**Mechanism**	**Knockout or Knockdown Phenotype**	**Overexpressor Phenotype**	**References**
AtFUL	*Arabidopsis*	MADS Box TF	Induced by auxin, brassinosteroids, shading/reduced R:FR light, represses AtSAUR10 (limiting shading response	Narrower	Wider	Bemer et al., 2017
OsPIL15	*Oryza sativa*	phytochrome-interacting factors-like 15	Repressed by light, enhances gravitropism	Wider	Narrower	Xie et al., 2019; He et al., 2021-Review
OsPIL6	*Oryza sativa*	phytochrome-interacting factors-like 16	Repressed by light, represses OsRMD	-	Wider	Song et al., 2019
OsRICE MORPHOLOGY DETERMINANT (RMD)	*Oryza sativa*	Actin-binding	Amyloplast Dynamics (Actin attachment); enhances sedimentation in light-grown shoots, inhibits sedimentation in roots	Wider (light-grown shoots) or Narrower (roots)	-	Zhang et al., 2011; Huang et al., 2018; Song et al., 2019; Kawamoto and Morita, 2022-Review
OsTAC1; AtTAC1; PpeTAC1	*Oryza sativa, Zea mays, Prunus persica, Arabidopsis, Miscanthus, Populus, Solanum lycopersicum*	IGT	Activated by light; response to photosynthesis	Narrower	Wider	Yu et al. 2007; Ku et al., 2011; Dardick et al., 2013; Zhao et al., 2014; Xu et al., 2017; González-Arcos et al., 2019
AtLAZY4	*Arabidopsis*	IGT	Light degrades PIFs, which activate LAZY4 in shoots			Yang et al., 2020

Brassinosteroid						
Gene	**Species**	**Annotation**	**Mechanism**	**Knockout or Knockdown Phenotype**	**Overexpressor Phenotype**	**References**
OsLIC	Oryza sativa	CCH-Type Zinc Finger TF	Negative regulation of Brassinosteroid; Epistatic to D2	Wider	-	Wang et al., 2008; He et al., 2021-Review; Wang et al., 2022-Review
OsDWARF2 (D2)	Oryza sativa	cytochrome p450	Positive regulation or signalling for brassinosteroids	Narrower	-	Dong et al., 2016; Wang et al., 2022-Review

Unknown						
Gene	**Species**	**Annotation**	**Mechanism**	**Knockout or Knockdown Phenotype**	**Overexpressor Phenotype**	**References**
OsNAC2 (Ostil1 mutant)	Oryza sativa	NAC TF	Unknown	Narrower	Wider	Mao et al., 2007
OsTIG1	Oryza sativa	TCP TF	Upregulates SAUR39, EXPA3, and EXPB5 on the upper side of tillers; Mutants have no change in gravity. Additive effect with mutations in TAC1 or PROG1	Narrower	-	Zhang et al., 2019; Wang et al., 2022-Review
OsPROG7	Oryza sativa	C2H2 TF	Unknown	Narrower	Wider	Hu et al., 2018; Wang et al., 2022-Review
OsTAC3	Oryza sativa	Unknown	Unknown	-	Wider	Dong et al., 2016
AtSAC1	Arabidopsis	SUPPRESOR OF ACTIN	Actin organization and cell wall synthesis	Wider	-	Zhong et al., 2005
OsSPL14 aka OsIDEALPLANTARCHITECTURE1	Oryza sativa	SBP binding domain TFs	Unknown	-	Narrower	Jiao et al., 2010
OsmiRNA156	Oryza sativa	miRNA	Represses SPL14	-	-	Jiao et al., 2010

REFERENCES

Aloni R (2021) Hormonal Control of Reaction Wood Formation. *In* R Aloni, ed, Vascular Differentiation and Plant Hormones. Springer International Publishing, Cham, pp 265–272

Andersson-Gunneråas S, Hellgren JM, Björklund S, Regan S, Moritz T, Sundberg B (2003) Asymmetric expression of a poplar ACC oxidase controls ethylene production during gravitational induction of tension wood. The Plant Journal **34(3)**: 339–349

Arai-Sanoh Y, Takai T, Yoshinaga S, Nakano H, Kojima M, Sakakibara H, Kondo M, Uga Y (2014) Deep rooting conferred by *DEEPER ROOTING 1* enhances rice yield in paddy fields. Scientific Reports **4**:5563

Barbier FF, Dun EA, Kerr SC, Chabikwa TG, Beveridge CA (2019) An update on the signals controlling shoot branching. Trends in Plant Science **24(3)**: 220–236

Barnett JR, Bonham VA (2004) Cellulose microfibril angle in the cell wall of wood fibres. Biological Reviews of the Cambridge Philosophical Society **79(2)**: 461–472

Bassi D, Dima A, Scorza R (1994) Tree structure and pruning response of six peach growth forms. Journal of the American Society for Horticultural Science **119(3)**: 378–382

Bemer M, van Mourik H, Muiño JM, Ferrándiz C, Kaufmann K, Angenent GC (2017) FRUITFULL controls *SAUR10* expression and regulates *Arabidopsis* growth and architecture. Journal of Experimental Botany **68(13)**: 3391–3403

Beveridge CA, Rameau C, Wijerathna-Yapa A (2023) Lessons from a century of apical dominance research. Journal of Experimental Botany **74(14)**: 3903–3922

Blake TJ, Pharis RP, Reid DM (1980) Ethylene, gibberellins, auxin and the apical control of branch angle in a conifer, *Cupressus arizonica*. Planta **148**: 64–68

Cao X, Jiao Y (2020) Control of cell fate during axillary meristem initiation. Cellular and Molecular Life Sciences **77(12)**: 2343–2354

Carrillo-Mendoza O, Sherman WB, Chaparro JX (2010) Development of a branching index for evaluation of peach seedlings using interspecific hybrids. HortScience **45(6)**: 852–856

Chabikwa TG, Brewer PB, Beveridge CA (2019) Initial bud outgrowth occurs independent of auxin flow from out of buds. Plant Physiology **179(1)**: 55–65

Chen J, Yu R, Li N, Deng Z, Zhang X, Zhao Y, Qu C, Yuan Y, Pan Z, Zhou Y, et al (2023) Amyloplast sedimentation repolarizes LAZYs to achieve gravity sensing in plants. Cell **186(22)**: 4788-4802

Chen Y, Fan X, Song W, Zhang Y, Xu G (2012) Over-expression of *OsPIN2* leads to increased tiller numbers, angle and shorter plant height through suppression of *OsLAZY1*. Plant Biotechnology Journal **10(2)**: 139–149

Chen Y, Xu S, Tian L, Liu L, Huang M, Xu X, Song G, Wu P, Sato S, Jiang H, et al (2020) *LAZY3* plays a pivotal role in positive root gravitropism in *Lotus japonicus*. Journal of Experimental Botany **71(1)**

Cline MG, Bhave N, Harrington CA (2009) The possible roles of nutrient deprivation and auxin repression in apical control. Trees **23(3)**: 489–500

Cline MG, Sadeski K (2002) Is auxin the repressor signal of branch growth in apical control? American Journal of Botany **89(11)**: 1764–1771

Costes E, Crespel L, Denoyes B, Morel P, Demene M-N, Lauri P-E, Wenden B (2014) Bud structure, position and fate generate various branching patterns along shoots of closely related Rosaceae species: a review. Frontiers in Plant Science **5**: 666

Costes E, Lauri PE, Regnard JL (2006) Analyzing fruit tree architecture: Implications for tree management and fruit production. *in* Horticultural Reviews 32 pp 1-61

Cui D, Zhao J, Jing Y, Fan M, Liu J, Wang Z, Xin W, Hu Y (2013) The *Arabidopsis* IDD14, IDD15, and IDD16 cooperatively regulate lateral organ morphogenesis and gravitropism by promoting auxin biosynthesis and transport. PLOS Genetics **9(9)**: e1003759

Dardick C, Callahan A, Horn R, Ruiz KB, Zhebentyayeva T, Hollender C, Whitaker M, Abbott A, Scorza R (2013) *PpeTAC1* promotes the horizontal growth of branches in peach trees and is a member of a functionally conserved gene family found in diverse plants species. The Plant Journal **75(4)**: 618–630

Dhakal S, Karki M, Subedi P, Gc A (2019) Effect of ethephon doses on vegetative characters, sex expression and yield of cucumber (*Cucumis sativus* cv. Bhaktapur Local) In Resunga Municipality, Gulmi, Nepal. International Journal of Applied Sciences and Biotechnology **7(3)**: 370–377

Dong H, Zhao H, Xie W, Han Z, Li G, Yao W, Bai X, Hu Y, Guo Z, Lu K, et al (2016) A novel tiller angle gene, *TAC3*, together with *TAC1* and *D2* largely determine the natural variation of tiller angle in rice cultivars. PLOS Genetics **12(11)**: e1006412

Dougherty L, Borejsza-Wysocka E, Miaule A, Wang P, Zheng D, Jansen M, Brown S, Piñeros M, Dardick C, Xu K (2023) A single amino acid substitution in *MdLAZY1A* dominantly impairs shoot gravitropism in *Malus*. Plant Physiology **193(2)**: 1142-1160

Drouet J-L, Moulia B (1997) Spatial re-orientation of maize leaves affected by initial plant orientation and density. Agricultural and Forest Meteorology **88(1-4)**: 85–100

Du M, Spalding EP, Gray WM (2020) Rapid auxin-mediated cell expansion. Annual Review of Plant Biology **71**: 379-402

Dunn N (2013) *Prunus incisa* named FPMSPL. USPP23384P2

Ehrenreich IM, Stafford PA, Purugganan MD (2007) The genetic architecture of shoot branching in *Arabidopsis thaliana*: A comparative assessment of candidate gene associations vs. quantitative trait locus mapping. Genetics **176(2)**: 1223–1236

Felten J, Sundberg B (2013) Biology, chemistry and structure of tension wood. *In* J Fromm, ed, Cellular Aspects of Wood Formation. Springer, Berlin, Heidelberg, pp 203–224

Furutani M, Hirano Y, Nishimura T, Nakamura M, Taniguchi M, Suzuki K, Oshida R, Kondo C, Sun S, Kato K, et al (2020) Polar recruitment of RLD by LAZY1-like protein during gravity signaling in root branch angle control. Nature Communications **11(76)**: 1–13

Gälweiler L, Guan C, Müller A, Wisman E, Mendgen K, Yephremov A, Palme K (1998) Regulation of polar auxin transport by AtPIN1 in *Arabidopsis* vascular tissue. Science **282(5397)**: 2226–2230

Ge L, Chen R (2016) Negative gravitropism in plant roots. Nature Plants **2**: 16155

Ge L, Chen R (2019) Negative gravitropic response of roots directs auxin flow to control root gravitropism. Plant, Cell & Environment. **42(8)**: 2372-2383

Godbolé R, Takahashi H, Hertel R (1999) The lazy mutation in rice affects a step between statoliths and gravity-induced lateral auxin transport. Plant Biology **1(4)**: 379–381

Gonçalves B, Correia CM, Silva AP, Bacelar EA, Santos A, Moutinho-Pereira JM (2008) Leaf structure and function of sweet cherry tree (*Prunus avium* L.) cultivars with open and dense canopies. Scientia Horticulturae **116(4)**: 381–387

González-Arcos M, de Noronha Fonseca ME, Zandonadi DB, Peres LEP, Arruabarrena A, Ferreira DS, Kevei Z, Mohareb F, Thompson AJ, Boiteux LS (2019) A loss-of-function allele of a *TAC1*-like gene (*SlTAC1*) located on tomato chromosome 10 is a candidate for the *Erectoid leaf* (*Erl*) mutation. Euphytica **215**: 95

Gradziel TM, Kester DE, Martin-Gomez P (2002) A development based classification for branch architecture in almond. Journal of the American Pomological Society; University Park **56(2)**: 106-112

Groover A (2016) Gravitropisms and reaction woods of forest trees – evolution, functions and mechanisms. New Phytologist **211**: 790–802

Hajný J, Tan S, Friml J (2022) Auxin canalization: From speculative models toward molecular players. Current Opinion in Plant Biology **65**: 102174

Hallé F, Oldeman RAA, Tomlinson PB (1978) Tropical Trees and Forests: An Architectural Analysis. Springer Verlag Berlin, Heidelberg

Harmoko R, Yoo JY, Ko KS, Ramasamy NK, Hwang BY, Lee EJ, Kim HS, Lee KJ, Oh D-B, Kim D-Y, et al (2016) N-glycan containing a core α1,3-fucose residue is required for basipetal auxin transport and gravitropic response in rice (*Oryza sativa*). New Phytologist **212(1)**: 108–122

Hashiguchi Y, Yano D, Nagafusa K, Kato T, Saito C, Uemura T, Ueda T, Nakano A, Tasaka M, Terao Morita M (2014) A Unique HEAT repeat-containing protein SHOOT GRAVITROPISM6 is involved in vacuolar membrane dynamics in gravity-sensing cells of *Arabidopsis* inflorescence stem. Plant and Cell Physiology **55(4)**: 811–822

He Y, Li L, Jiang D (2021) Understanding the regulatory mechanisms of rice tiller angle, then and now. Plant Molecular Biology Reporter **39**: 640–647

Hill JL, Hollender CA (2019) Branching out: New insights into the genetic regulation of shoot architecture in trees. Current Opinion in Plant Biology **47**: 73–80

Hedden P, Sponsel V (2015) A century of gibberellin research. Journal of Plant Growth Regulation **34**: 740–760

Hollender CA, Dardick C (2015) Molecular basis of angiosperm tree architecture. New Phytologist **206(2)**: 541–556

Hollender CA, Hill JL, Waite J, Dardick C (2020) Opposing influences of TAC1 and LAZY1 on Lateral Shoot Orientation in Arabidopsis. Scientific Reports **10**: 6051

Hollender CA, Pascal T, Tabb A, Hadiarto T, Srinivasan C, Wang W, Liu Z, Scorza R, Dardick C (2018a) Loss of a highly conserved sterile alpha motif domain gene (*WEEP*) results in pendulous branch growth in peach trees. The Proceedings of the National Academy of Sciences **115(20)**: E4690–E4699

Hollender CA, Waite JM, Tabb A, Raines D, Chinnithambi S, Dardick C (2018b) Alteration of *TAC1* expression in *Prunus* species leads to pleiotropic shoot phenotypes. Horticulture Research **5**: 26

Howard III TP, Hayward AP, Tordillos A, Fragoso C, Moreno MA, Tohme J, Kausch AP, Mottinger JP, Dellaporta SL (2014) Identification of the maize gravitropism gene lazy plant1 by a transposon-tagging genome resequencing strategy. PLS ONE **9(1)**: e87053

Hu M, Lv S, Wu W, Fu Y, Liu F, Wang B, Li W, Gu P, Cai H, Sun C, et al (2018) The domestication of plant architecture in African rice. The Plant Journal **94(4)**: 661–669

Hu Y, Li S, Fan X, Song S, Zhou X, Weng X, Xiao J, Li X, Xiong L, You A, et al (2020) *OsHOX1* and *OsHOX28* redundantly shape rice tiller angle by reducing *HSFA2D* expression and auxin content. Plant Physiology **184(3)**: 1424–1437

Huang G, Liang W, Sturrock CJ, Pandey BK, Giri J, Mairhofer S, Wang D, Muller L, Tan H, York LM, et al (2018) Rice actin binding protein RMD controls crown root angle in response to external phosphate. Nature Communications **9**: 2346

Huang L, Wang W, Zhang N, Cai Y, Liang Y, Meng X, Yuan Y, Li J, Wu D, Wang Y (2021) LAZY2 controls rice tiller angle through regulating starch biosynthesis in gravity-sensing cells. New Phytologist **231(3)**: 1073–1087

Jiao Y, Wang Y, Xue D, Wang J, Yan M, Liu G, Dong G, Zeng D, Lu Z, Zhu X, et al (2010) Regulation of OsSPL14 by OsmiR156 defines ideal plant architecture in rice. Nature Genetics **42(6)**: 541–544

Jin J, Huang W, Gao J-P, Yang J, Shi M, Zhu M-Z, Luo D, Lin H-X (2008) Genetic control of rice plant architecture under domestication. Nature Genetics **40(11)**: 1365–1369

Kato T, Morita MT, Fukaki H, Yamauchi Y, Uehara M, Niihama M, Tasaka M (2002) SGR2, a phospholipase-like protein, and ZIG/SGR4, a SNARE, are involved in the shoot gravitropism of *Arabidopsis*. The Plant Cell **14(1)**: 33–46

Kawamoto N, Kanbe Y, Nakamura M, Mori A, Terao Morita M (2020) Gravity-sensing tissues for gravitropism are required for "anti-gravitropic" phenotypes of *lzy* multiple mutants in *Arabidopsis*. Plants **9(5)**: 615

Kawamoto N, Morita MT (2022) Gravity sensing and responses in the coordination of the shoot gravitropic setpoint angle. New Phytologist **236(5)**: 1637–1654

Ku L, Wei X, Zhang S, Zhang J, Guo S, Chen Y (2011) Cloning and characterization of a putative *TAC1* ortholog associated with leaf angle in Maize (*Zea mays* L.). PLOS ONE **6**: e20621

Landrein B, Lathe R, Bringmann M, Vouillot C, Ivakov A, Boudaoud A, Persson S, Hamant O (2013) Impaired cellulose synthase guidance leads to stem torsion and twists phyllotactic patterns in *Arabidopsis*. Current Biology **23(10)**: 895–900

Lang GA, Early JD, Martin GC, Darnell RL (1987) Endo-, Para-, and Ecodormancy: Physiological Terminology and Classification for Dormancy Research. HortScience **22(3)**: 371–377

Lautner S, Zollfrank C, Fromm J (2012) Microfibril angle distribution of poplar tension wood. IAWA Journal **33(4)**: 431–439

Li H, Sun H, Jiang J, Sun X, Tan L, Sun C (2021) TAC4 controls tiller angle by regulating the endogenous auxin content and distribution in rice. Plant Biotechnology Journal **19(1)**: 64–73

Li P, Wang Y, Qian Q, Fu Z, Wang M, Zeng D, Li B, Wang X, Li J (2007) LAZY1 controls rice shoot gravitropism through regulating polar auxin transport. Cell Research **17(5)**: 402–410

Li Y, Li J, Chen Z, Wei Y, Qi Y, Wu C (2020) OsmiR167a-targeted auxin response factors modulate tiller angle via fine-tuning auxin distribution in rice. Plant Biotechnology Journal **18(10)**: 2015–2026

Li Z, Liang Y, Yuan Y, Wang L, Meng X, Xiong G, Zhou J, Cai Y, Han N, Hua L, et al (2019) OsBRXL4 regulates shoot gravitropism and rice tiller angle through affecting LAZY1 nuclear localization. Molecular Plant **12(8)**: 1143–1156

Love J, Bjorklund S, Vahala J, Hertzberg M, Kangasjarvi J, Sundberg B (2009) Ethylene is an endogenous stimulator of cell division in the cambial meristem of *Populus*. The Proceedings of the National Academy of Sciences **106(14)**: 5984–5989

Mao C, Ding W, Wu Y, Yu J, He X, Shou H, Wu P (2007) Overexpression of a NAC-domain protein promotes shoot branching in rice. New Phytologist **176(2)**: 288–298

Marowa P, Ding A, Kong Y (2016) Expansins: roles in plant growth and potential applications in crop improvement. Plant Cell Reports **35(5)**: 949–965

McSteen P, Leyser O (2005) Shoot branching. Annual Review of Plant Biology **56**: 353–374

Morita R, Sugino M, Hatanaka T, Misoo S, Fukayama H (2015) CO2-Responsive CONSTANS, CONSTANS-Like, and time of chlorophyll a/b binding protein Expression1 protein is a positive regulator of starch synthesis in vegetative organs of rice. Plant Physiology **167(4)**: 1321–1331

Nagpal P, Walker LM, Young JC, Sonawala A, Timpte C, Estelle M, Reed JW (2000) AXR2 encodes a member of the Aux/IAA protein family. Plant Physiology **123(2)**: 563–574

Nakamura M, Nishimura T, Morita MT (2019) Gravity sensing and signal conversion in plant gravitropism. Journal of Experimental Botany **70(14)**: 3495–3506

Nakamura M, Toyota M, Tasaka M, Morita MT (2011) An Arabidopsis E3 Ligase, SHOOT GRAVITROPISM9, modulates the interaction between statoliths and F-actin in gravity sensing. The Plant Cell **23(5)**: 1830–1848

Nakamura T, Saotome M, Ishiguro Y, Itoh R, Higurashi S, Hosono M, Ishii Y (1994) The effects of GA_3 on weeping of growing shoots of the Japanese cherry, *Prunus spachiana*. Plant and Cell Physiology **35(3)**: 523–527

Nelson ND, Hillis WE (1978) Ethylene and tension wood formation in *Eucalyptus gomphocephala*. Wood Science and Technology **12(4)**: 309–315

Niez B, Dlouha J, Gril J, Ruelle J, Toussaint E, Moulia B, Badel E (2020) Mechanical properties of "flexure wood": compressive stresses in living trees improve the mechanical resilience of wood and its resistance to damage. Annals of Forest Science **77**: 17

Nishimura T, Mori S, Shikata H, Nakamura M, Hashiguchi Y, Abe Y, Hagihara T, Yoshikawa HY, Toyota M, Higaki T, et al (2023) Cell polarity linked to gravity sensing is generated by LZY translocation from statoliths to the plasma membrane. Science **381(6661)**: 1006–1010

Okamura M, Hirose T, Hashida Y, Ohsugi R, Aoki N (2014) Suppression of starch synthesis in rice stems splays tiller angle due to gravitropic insensitivity but does not affect yield. Functional Plant Biology **42(1)**: 31–41

Park YJ, Kim YJ, Kim KS (2013) Vegetative growth and flowering of *Dianthus*, *Zinnia*, and *Pelargonium* as affected by night interruption at different timings. Horticulture, Environment, and Biotechnology **54(3)**: 236–242

Ratcliffe OJ, Amaya I, Vincent CA, Rothstein S, Carpenter R, Coen ES, Bradley DJ (1998) A common mechanism controls the life cycle and architecture of plants. Development **125(9)**: 1609–1615

Ren H, Gray WM (2015) SAUR proteins as effectors of hormonal and environmental signals in plant growth. Molecular Plant **8(8)**: 1153–1164

Ross JJ, O'Neill DP, Rathbone DA (2003) Auxin-gibberellin interactions in pea: Integrating the old with the new. Journal of Plant Growth Regulation **22**: 99–108

Roychoudhry S, Kepinski S (2015) Shoot and root branch growth angle control—the wonderfulness of lateralness. Current Opinion in Plant Biology **23(SI: Growth and Development)**: 124–131

Sachs T (1999) 'Node counting': an internal control of balanced vegetative and reproductive development. Plant, Cell & Environment **22(7)**: 757–766

de Saint Germain A, Ligerot Y, Dun EA, Pillot J-P, Ross JJ, Beveridge CA, Rameau C (2013) Strigolactones stimulate internode elongation independently of gibberellins. Plant Physiology **163(2)**: 1012–1025

Sakuraba Y, Piao W, Lim J-H, Han S-H, Kim Y-S, An G, Paek N-C (2015) Rice ONAC106 inhibits leaf senescence and increases salt tolerance and tiller angle. Plant and Cell Physiology **56(12)**: 2325–2339

Scorza R, Bassi D, Liverani A (2002) Genetic interactions of pillar (columnar), compact, and dwarf peach tree genotypes. Journal of the American Society for Horticultural Science **127(2)**: 254–261

Sebire R (1990) Weeping cherry (*Prunus subhirtella*). Variety: "Winter Sun". Application no. 90/098. Plant Varieties Journal **3(4)**: 31

Shuai B, Reynaga-Peña CG, Springer PS (2002) The lateral organ boundaries gene defines a novel, plant-specific gene family. Plant Physiology **129(2)**: 747–761

Silady RA, Kato T, Lukowitz W, Sieber P, Tasaka M, Somerville CR (2004) The *gravitropism defective* 2 Mutants of Arabidopsis Are Deficient in a Protein Implicated in Endocytosis in *Caenorhabditis elegans*. Plant Physiology **136(2)**: 3095–3103

Snow R (1942) Torsions and their analysis. The New Phytologist **41(1)**: 1–12

Snow R (1950) On the interpretation of geostrophic and auxin torsions. New Phytologist **49 (2)**: 145–154

Song Y, Li G, Nowak J, Zhang X, Xu D, Yang X, Huang G, Liang W, Yang L, Wang C, et al (2019) The rice actin-binding protein RMD regulates light-dependent shoot gravitropism. Plant Physiology **181(2)**: 630-644

Spartz AK, Ren H, Park MY, Grandt KN, Lee SH, Murphy AS, Sussman MR, Overvoorde PJ, Gray WM (2014) SAUR inhibition of PP2C-D phosphatases activates plasma membrane H+-ATPases to promote cell expansion in *Arabidopsis*. The Plant Cell **26(5)**: 2129–2142

Su S-H, Masson PH (2019) Gravitropism of plant organs undergoing primary growth. *In* S Sopory, ed, Sensory Biology of Plants. Springer, Singapore, pp 95–136

Sun Q, Li TY, Li DD, Wang ZY, Li S, Li DP, Han X, Liu JM, Xuan YH (2019) Overexpression of *Loose Plant Architecture 1* increases planting density and resistance to sheath blight disease via activation of *PIN-FORMED 1a* in rice. Plant Biotechnology Journal **17(5)**: 855–857

Taniguchi M, Furutani M, Nishimura T, Nakamura M, Fushita T, Iijima K, Baba K, Tanaka H, Toyota M, Tasaka M, et al (2017) The *Arabidopsis* LAZY1 family plays a key role in gravity signaling within statocytes and in branch angle control of roots and shoots. The Plant Cell **29(8)**: 1984–1999

Tasaka M, Kato T, Fukaki H (1999) The endodermis and shoot gravitropism. Trends in Plant Science **4(3)**: 103–107

Taylor CE (1953) The vegetative development of the potato plant. Annals of Applied Biology **40(4)**: 778–788

Telewski FW (2012) Is windswept tree growth negative thigmotropism? Plant Science **184**: 20–28

Telewski FW (2016) Chapter 5 - Flexure wood: Mechanical stress induced secondary xylem formation. *In* YS Kim, R Funada, AP Singh, eds, Secondary Xylem Biology. Academic Press, Boston, pp 73–91

Teo ZWN, Song S, Wang Y-Q, Liu J, Yu H (2014) New insights into the regulation of inflorescence architecture. Trends in Plant Science **19(3)**: 158–165

Thimann KV (1939) Auxins and the inhibition of plant growth. Biological Reviews **14(3)**: 314–337

Thorp TG, Sedgley M (1992) Shoot growth and tree architecture in a range of avocado cultivars. Proceedings of the Second World Avocado Congress pp 237–240

Timpte C, Wilson AK, Estelle M (1994) The *axr2-1* mutation of *Arabidopsis thaliana* is a gain-of-function mutation that disrupts an early step in auxin response. Genetics **138(4)**: 1239–1249

Traas J (2018) Molecular networks regulating meristem homeostasis. Molecular Plant **11(7)**: 883–885

Tworkoski T, Scorza R (2001) Root and shoot characteristics of peach trees with different growth habits. Journal of the American Society for Horticultural Science **126(6)**: 785–790

Urbancsok J, Donev EN, Sivan P, van Zalen E, Barbut FR, Derba-Maceluch M, Šimura J, Yassin Z, Gandla ML, Karady M, et al (2023) Flexure wood formation via growth reprogramming in hybrid aspen involves jasmonates and polyamines and transcriptional changes resembling tension wood development. New Phytologist **240(6)**: 2312-2334

Waite JM, Dardick C (2018) TILLER ANGLE CONTROL 1 modulates plant architecture in response to photosynthetic signals. Journal of Experimental Botany **69(20)**: 4935-4944

Waite JM, Dardick C (2020) IGT/LAZY family genes are differentially influenced by light signals and collectively required for light-induced changes to branch angle. bioRxiv 2020.07.15.205625

Walker CH, Bennett T (2018) Forbidden fruit: Dominance relationships and the control of shoot architecture. Annual Plant Reviews online **1(1)**

Wang H, Cheng H, Wang W, Liu J, Hao M, Mei D, Zhou R, Fu L, Hu Q (2016) Identification of *BnaYUCCA6* as a candidate gene for branch angle in *Brassica napus* by QTL-seq. Scientific Reports **6**: 38493

Wang J, Huang J, Bao J, Li X, Zhu L, Jin J (2023) Rice domestication-associated transcription factor PROSTRATE GROWTH 1 controls plant and panicle architecture by regulating the expression of *LAZY 1* and *OsGIGANTEA*, respectively. Molecular Plant **16(9)**: 1413–1426

Wang L, Xu Y, Zhang C, Ma Q, Joo S-H, Kim S-K, Xu Z, Chong K (2008) OsLIC, a novel CCCH-type zinc finger protein with transcription activation, mediates rice architecture via brassinosteroids signaling. PLOS ONE **3(10)**: e3521

Wang Q, Marconi M, Guan C, Wabnik K, Jiao Y (2022a) Polar auxin transport modulates early leaf flattening. The Proceedings of the National Academy of Sciences **119(50)**: e2215569119

Wang W, Gao H, Liang Y, Li J, Wang Y (2022b) Molecular basis underlying rice tiller angle: Current progress and future perspectives. Molecular Plant **15(1)**: 125–137

Wang Y (2021) Stem cell basis for fractal patterns: Axillary meristem initiation. Frontiers in Plant Science **12**: 805434

Wang Y, Jiao Y (2018) Axillary meristem initiation—a way to branch out. Current Opinion in Plant Biology **41**: 61–66

Wang Y, Jiao Y (2023) Cell signaling in the shoot apical meristem. Plant Physiology **193(1)**: 70–82

Werner DJ, Chaparro JX (2005) Genetic interactions of pillar and weeping peach genotypes. HortScience **40(1)**: 18–20

Wilson BF (2000) Apical control of branch growth and angle in woody plants. American Journal of Botany **87(5)**: 601–607

Wu X, Tang D, Li M, Wang K, Cheng Z (2013) Loose Plant Architecture1, an INDETERMINATE DOMAIN protein involved in shoot gravitropism, regulates plant architecture in rice. Plant Physiology **161(1)**: 317–329

Xie C, Zhang G, An L, Chen X, Fang R (2019) Phytochrome-interacting factor-like protein OsPIL15 integrates light and gravitropism to regulate tiller angle in rice. Planta **250(1)**: 105–114

Xu D, Qi X, Li J, Han X, Wang J, Jiang Y, Tian Y, Wang Y (2017) *PzTAC* and *PzLAZY* from a narrow-crown poplar contribute to regulation of branch angles. Plant Physiology and Biochemistry **118**: 571–578

Xu M, Zhu L, Shou H, Wu P (2005) A PIN1 family gene, OsPIN1, involved in auxin-dependent adventitious root emergence and tillering in rice. Plant and Cell Physiology **46(10)**: 1674–1681

Xue H, Gao X, He P, Xiao G (2022) Origin, evolution, and molecular function of DELLA proteins in plants. The Crop Journal **10(2)**: 287–299

Yano D, Sato M, Saito C, Sato MH, Morita MT, Tasaka M (2003) A SNARE complex containing SGR3/AtVAM3 and ZIG/VTI11 in gravity-sensing cells is important for *Arabidopsis* shoot gravitropism. The Proceedings of the National Academy of Sciences **100(14)**: 8589–8594

Yoshida M, Yamamoto H, Okuyama T, Nakamura T (1999) Negative gravitropism and growth stress in GA3-treated branches of *Prunus spachiana* Kitamura f. *spachiana* cv. *Plenarosea*. Journal of Wood Science **45**: 368–372

Yu B, Lin Z, Li H, Li X, Li J, Wang Y, Zhang X, Zhu Z, Zhai W, Wang X, et al (2007) TAC1, a major quantitative trait locus controlling tiller angle in rice. The Plant Journal **52(2)**: 891–898

Zhang N, Yu H, Yu H, Cai Y, Huang L, Xu C, Xiong G, Meng X, Wang J, Chen H, et al (2018) A core regulatory pathway controlling rice tiller angle mediated by the LAZY1-dependent asymmetric distribution of auxin. The Plant Cell **30(7)**: 1461-1475

Zhang S-W, Li C-H, Cao J, Zhang Y-C, Zhang S-Q, Xia Y-F, Sun D-Y, Sun Y (2009) Altered architecture and enhanced drought tolerance in rice via the down-regulation of indole-3-acetic acid by *TLD1/OsGH3.13* activation. Plant Physiology **151(4)**: 1889–1901

Zhang W, Tan L, Sun H, Zhao X, Liu F, Cai H, Fu Y, Sun X, Gu P, Zhu Z, et al (2019) Natural variations at TIG1 encoding a TCP transcription factor contribute to plant architecture domestication in rice. Molecular Plant **12**: 1075–1089

Zhang Z, Zhang Y, Tan H, Wang Y, Li G, Liang W, Yuan Z, Hu J, Ren H, Zhang D (2011) RICE MORPHOLOGY DETERMINANT encodes the type II formin FH5 and regulates rice morphogenesis. The Plant Cell **23(2)**: 681–700

Zhao H, Huai Z, Xiao Y, Wang X, Yu J, Ding G, Peng J (2014) Natural variation and genetic analysis of the tiller angle gene *MsTAC1* in *Miscanthus sinensis*. Planta **240(1)**: 161–175

Zhao L, Tan L, Zhu Z, Xiao L, Xie D, Sun C (2015) PAY1 improves plant architecture and enhances grain yield in rice. The Plant Journal **83(3)**: 528–536

Zhong R, Burk DH, Nairn CJ, Wood-Jones A, Morrison WH III, Ye Z-H (2005) Mutation of SAC1, an *Arabidopsis* SAC domain phosphoinositide phosphatase, causes alterations in cell morphogenesis, cell wall synthesis, and Actin Organization. The Plant Cell **17**: 1449–1466

Zhu Y, Wagner D (2020) Plant inflorescence architecture: The formation, activity, and fate of axillary meristems. Cold Spring Harbor Perspectives in Biology **12(1)**: a034652

Zhuo X, Zheng T, Li S, Zhang Z, Zhang M, Zhang Y, Ahmad S, Sun L, Wang J, Cheng T, et al (2021) Identification of the *PmWEEP* locus controlling weeping traits in *Prunus mume* through an integrated genome-wide association study and quantitative trait locus mapping. Horticulture Research **8(1)**: 131

CHAPTER 2

Defying Gravity:

WEEP promotes negative gravitropism in *Prunus persica* by establishing asymmetric auxin gradients.

The work described herein has been submitted for a peer-reviewed publication.

Anticipated authors for publication (in review):

Andrea R. Kohler[1], Andrew Scheil[1], Joseph L. Hill Jr.[1], Jeffrey R. Allen[2], Jameel M. Al-Haddad[3], Charity Z. Goeckeritz[1], Lucia C. Strader[2], Frank W. Telewski[3], Courtney A. Hollender[1,*].

[1] Department of Horticulture, Michigan State University, East Lansing, MI 48824

[2] Department of Biology, Duke University, Durham, NC 27708, USA

[3] Department of Plant Biology, Michigan State University, East Lansing, MI 48824

[*] Corresponding

Author Contributions:

ARK photographed tree phenotypes; designed and performed tree gravistimulation experiment, designed wood anatomy sectioning and analyzed data; designed and performed tension wood sectioning; analyzed data for wood biochemistry; designed and performed cell size measurements and collected and analyzed data; designed and performed biomechanical experiments, and collected and analyzed data; performed fresh sections for amyloplast sedimentation; designed and performed auxin bending response experiments; extracted RNA and analyzed data for RNAseq; performed root architecture experiments and analyzed data; performed root gravitropism experiments and collected and analyzed data; and wrote the manuscript and prepared data visualizations. AS collected data for wood anatomy sectioning and analyzed data; and collected data for root architecture experiment. JLH designed experiments for wood biochemistry and fiber cell length and collected and analyzed data. JRA designed experiments for size exclusion chromatography and collected and analyzed data. JMA-H collected and analyzed data for biomechanical experiments. CZG performed fixation and sectioning for cell size and amyloplast sedimentation. LCS designed experiments. FWT designed experiments. CAH photographed tree phenotypes; designed experiments; and wrote the manuscript. All authors contributed to editing the manuscript.

Abstract

Trees with weeping shoot architectures are valued for their beauty and serve as tremendous resources for understanding how plants regulate posture control. The *Prunus persica* (peach) weeping phenotype, which has elliptical downward arching branches, is caused by a homozygous mutation in the *WEEP* gene. Until now, little was known about the function of WEEP protein despite its high conservation throughout Plantae. Here, we present the results of anatomical, biochemical, biomechanical, physiological, and molecular experiments that provide insight into WEEP function. Our data suggest that weeping peach trees do not have defects in branch structure. Rather, transcriptomes from the adaxial (upper) and abaxial (lower) sides of standard and weeping branch shoot tips revealed flipped expression patterns for genes associated with early auxin response, tissue patterning, cell elongation, and tension wood development. This suggests that WEEP promotes polar auxin transport toward the lower side during shoot gravitropic response, leading to cell elongation and tension wood development. In addition, weeping peach trees exhibited steeper root systems and faster lateral root gravitropic response. This suggests that WEEP moderates root gravitropism and is essential to establishing the set-point angle of lateral roots from the gravity vector. Additionally, size-exclusion chromatography indicated that WEEP proteins self-oligomerize, like other SAM-domain proteins. Collectively, our results from weeping peach provide new insight into polar auxin transport mechanisms associated with gravitropism and lateral shoot and root orientation.

Introduction

Weeping trees have long been prized for their aesthetic beauty and unique shape. This pendulous growth habit, where branches bend or grow downward in the direction of gravity, exists in both gymnosperm and angiosperm lineages. The weeping trait has been mapped to single, but distinct, loci in multiple species, including Eastern redbud (*Cercis canadensis*), morning glory (*Pharbitis nil*), Japanese apricot (*Prunus mume*), and peach (*Prunus persica*) (Kitazawa et al., 2005; Hollender et al., 2018; Chen and Werner, 2021; Li et al., 2021b). Despite often being controlled by a single locus, the change to a pendulous growth habit leads to diverse alterations in plant anatomy and physiology—such as modifications in light interception, canopy density, and canopy size. Studying the genes which control weeping traits can provide insights into the molecular mechanisms by which branch orientation is regulated, many of which are still unknown. This will ultimately benefit production strategies for diverse crop species, as control of branch orientation

is crucial to aspects such as planting density, spray coverage, and yield (Ku et al., 2011; Zhao et al., 2014; Roychoudhry and Kepinski, 2015; Xu et al., 2017; González-Arcos et al., 2019).

Here, we investigate the function of *PpeWEEP,* the causative gene for a weeping peach architecture. The branches of peach trees with a homozygous *WEEP* deletion grow downwards in an elliptical trajectory beginning early in development (Figure 2.1A-D). This phenotype is visible within the first phytomer of primary shoots and branches (Figure 2.1E and F) and continues throughout their life cycle (Hollender et al., 2018). In addition, weeping peach shoots do not exhibit negative gravitropic responses. Their shoots do not reorient upward after being rotated 90° or 180° (upside-down), and growth from existing and new shoots following reorientation arches downwards (Figure 2.1G-K; Hollender et al., 2018).

The WEEP protein sequence is highly conserved throughout vascular plant clades, suggesting it plays an essential role in plant development (Hollender et al., 2018). *WEEP* codes for a small protein (125 amino acids) of unknown function that has a sterile alpha motif (SAM) domain which, at 68 amino acids, constitutes over half of the protein (Hollender et al., 2018). SAM domains are versatile interaction domains found throughout eukaryotes that can bind proteins, RNA, or lipids (Qiao and Bowie, 2005; Denay et al., 2017). SAM domains frequently function in the formation of protein homo- or hetero-oligomers or polymers (Qiao and Bowie, 2005; Denay et al., 2017). Polymerization occurs head-to-tail through association of two conserved interaction regions, the negatively charged mid-loop and the positively charged end helix (Sayou et al., 2016; Denay et al., 2017). The formation of oligomers or polymers is often essential for protein function via increasing stability, altering binding strength, or otherwise regulating protein function (Qiao and Bowie, 2005; Denay et al., 2017). In *Arabidopsis thaliana* (arabidopsis), 12 genes containing SAM domains have been identified, including the *PpeWEEP* homolog *AtWEEP* (AT3G07760*,* also known as *SAM5*; Denay et al., 2017; Hollender et al., 2018). SAM domain functions have been characterized in three arabidopsis proteins: LEAFY (LFY), TRNA IMPORT COMPONENT 1 (TRIC1), and TRIC2. TRIC1 and TRIC2 are mitochondrial tRNA importers, whose SAM domains both bind tRNA and enable homopolymerization of TRIC1 and heteropolymerization of TRIC1 and TRIC2 (Murcha et al., 2016; Denay et al., 2017). LFY is a floral identity transcription factor, whose SAM domain mediates self-oligomerization required for it to bind to low-affinity DNA binding sites and closed chromatin (Sayou et al., 2016; Denay et al., 2017). Thus, in all plant

proteins where they have been characterized, SAM domains enable protein oligomerization and are essential for protein function.

Due to the broad utility of a binding domain in proteins of highly varied cellular functions, the presence of a SAM domain provides only limited clues to WEEP function in plant physiology and development. However, studies in woody and herbaceous plants suggest the *WEEP* gene has a conserved function in regulating lateral organ orientations. Plum (*Prunus domestica*) trees with reduced *WEEP* expression have branches that wander and arch (Hollender et al., 2018). In contrast, *weep* loss-of-function mutants in arabidopsis, wheat (*Triticum aestivum*), and barley (*Hordeum vulgare*) have normal shoot architectures but steeper root systems, due to narrower seminal and lateral root angles (Hollender et al., 2018; Kirschner et al., 2021; Johnson et al., 2022). Mutations in the barley and wheat genes, named *ENHANCED GRAVITROPISM* 2 (*EGT2*), also cause accelerated root gravitropism responses (Kirschner et al., 2021; Guo et al., 2023).

Other work has suggested *WEEP* plays a role in regulating cell expansion. In melon (*Cucumis melo*), the *WEEP* homolog *DOWNWARD LEAF CURLING* (*CmDLC*) was originally identified as being upregulated during fruit expansion (Kee et al., 2009). Overexpression of *CmDLC* in arabidopsis leads to semi-dwarfism and reductions in leaf pavement cell size and number, especially on the abaxial side of the leaf (Kee et al., 2009). In arabidopsis, *AtWEEP* is upregulated in developing leaves when mature leaves are shaded, a treatment which slows the growth of developing leaves (Coupe et al., 2006). In barley roots, mutation in the *WEEP* homolog *EGT2* leads to decreased expression of *EXPANSIN* genes in the root elongation zone (Kirschner et al., 2021; Guo et al., 2023).

Transcriptomics databases show that *WEEP* is expressed throughout plant organs but is specifically upregulated in tissues consistent with a role in gravitropism, abaxial/adaxial polarity, and lateral organ development. *AtWEEP* is expressed in the hypocotyl, root, mature leaves, flowers, and seeds (Klepikova et al., 2016). Despite this ubiquitous expression, *AtWEEP* is differentially regulated in different tissues. In the shoot apex, it is upregulated in the enlarged peripheral zone of the meristem, in the organ boundary, on the adaxial side of leaf primordia, and in the epidermis (Tian et al., 2019). This localization may be related to gibberellin signaling and tissue patterning, as *AtWEEP* is transcriptionally regulated by the DELLA protein GAI, in the presence of CUP-SHAPED COTYLEDON2 (CUC2), which is essential for organ boundary

specification (Barro-Trastoy et al., 2022). In the root, *AtWEEP* is highly upregulated in the endodermis, the columella, and the stele (Ryu et al., 2019).

Thus far, protein interaction candidates identified for WEEP homologs are involved in cell wall synthesis or membrane transport. In transient heterologous expression studies, WEEP protein homologs have localized to the plasma membrane (CmDLC in onion) and the nucleus and cytoplasm (barley EGT2 in tobacco; Kee et al., 2009; Guo et al., 2023). In barley, three candidate protein interactors for EGT2 were identified with yeast-two-hybrid screening and confirmed with Bimolecular Fluorescence Complementation – GXM, OMT, and HMT (Guo et al., 2023). GXM is a glucuronoxylan methyltransferase, with sequence similarity to the three arabidopsis GXMs (GXM1,2, and 3; Guo et al., 2023). In arabidopsis, these are responsible for methylation of glucuronic acid residues in xylan (Yuan et al., 2014). OMT is a homolog of AtOMT1, an oxygen methyltransferase that methylates both 5-hydroxyconiferaldehyde and 3,4- dihydroxyphenyl compounds during the production of syringyl (S) lignin (Nakatsubo et al., 2008; Guo et al., 2023). Interestingly, increased syringyl to guaiacyl lignin ratio has been observed to cause more rapid gravitropic response in poplar (Al-Haddad et al., 2013). HMT shows homology to proteins in the heavy metal transport/detoxification superfamily (Guo et al., 2023). In addition, in arabidopsis, the AtWEEP protein was identified to interact with CPK13, a nuclear- and plasma membrane-localized kinase which acts in a calcium-independent manner to inhibit the voltage-dependent K^+ channel KAT2, which is important for light-induced stomatal opening (Jones et al., 2014; Ronzier et al., 2014; Simeunovic et al., 2016; Denay et al., 2017). CPK13 also phosphorylates the heat-shock factor AtHSfB2a (Simeunovic et al., 2016).

The pendulous habit of *weep* peaches may be due to reduced structural integrity, an impaired ability to sense or respond to gravity, or a positive gravitropic response. Lack of structural integrity leads to downward bending through self-loading, as the branch is unable to support its own weight. Supporting the structural integrity hypothesis, reduced xylem tissue width and delayed development of tension wood are associated with a weeping architecture in Japanese cherry (*Prunus spachiana*; Nakamura *et al.*, 1994; Baba *et al.*, 1995; Yoshida *et al.*, 1999). Tension wood refers to localized changes in secondary cell wall composition which occur within the upper side of angiosperm shoots in response to gravistimulation or biomechanical stress. It is associated with an increase in the proportion of crystalline cellulose, decreases in microfibril angle, and sometimes an increase in S:G ratio of lignin monomers or the formation of gelatinous fibers (Qiu et al., 2008;

Felten and Sundberg, 2013). Tension wood generates internal forces that return branches back towards their original position or "set-point angle" (Felten and Sundberg, 2013; Roychoudhry et al., 2013). Application of GA to the apical bud of *P. spachiana* rescued this weeping phenotype through increase in xylem width and earlier formation of tension wood (Nakamura et al., 1994; Taniguchi et al., 2017). This effect was not observed in weeping (*weep*) peach trees, where GA application did not alter the weeping phenotype (Hollender et al., 2018). Similar to Japanese cherry, weeping Japanese apricot (*Prunus mume*) trees have decreased xylem tissue width, and lack phloem fibers (Li et al., 2021b).

Alternatively, the weeping peach phenotype could be due to impaired shoot gravitropism, indicating a role for *WEEP* in the gravitropic signaling pathway. This pathway can be divided into five main stages. First, the gravity vector is sensed by statocytes (endodermal cells in shoots and columella cells in roots), which contain amyloplasts that serve as statoliths. Second, polarity is established through vesicle trafficking and PIN-FORMED (PIN) auxin efflux carrier localization (Nakamura et al., 2019; Zhang et al., 2020). Third, asymmetric auxin transport establishes an auxin gradient with higher auxin levels on the lower side of the shoot or root (the Cholodny-Went hypothesis; Moore, 2002; Rakusová et al., 2011). Fourth, localized expression of rapid auxin response genes such as *SMALL AUXIN UPREGULATED RNAs* (*SAURs*) leads to asymmetric growth and bending through acidification of the apoplast, leading to cell division and elongation (acid growth hypothesis; Spartz et al., 2012; Ren and Gray, 2015; Wang et al., 2020; Li et al., 2021a). Defects in any of these stages impair gravitropism, and mutants frequently exhibit weeping shoot phenotypes. Weeping shoot phenotypes have been described in mutants which affect endodermis development (*shortroot*, *scarecrow),* amyloplast sedimentation (*shoot gravitropism, zigzag*), and starchless mutants (*phosphoglucomutase deficient*; Fukaki et al., 1996; Kato et al., 2002; Kitazawa et al., 2005; Morita et al., 2007). Weeping or prostrate shoot phenotypes have also been observed for *lazy* mutants in several species, including arabidopsis*,* rice, and maize (Abe et al., 1996; Dong et al., 2013; Taniguchi et al., 2017; Yoshihara and Spalding, 2017; Chen et al., 2022; Godbolé et al.) In arabidopsis with mutations in multiple *lazy* genes, amyloplast number and sedimentation is normal, but shoots lack an auxin gradient and are agravitropic (Taniguchi et al., 2017; Yoshihara and Spalding, 2017). Similarly, in roots of these mutants, PIN3 is localized to the top of the cell, instead of the bottom, the roots have an inverted auxin gradient (higher on top), and the roots exhibit negative gravitropism (upward growth) (Ge and Chen, 2016; Taniguchi et al.,

2017; Yoshihara and Spalding, 2017). Additionally, experiments with mutations causing two amino acid changes in Domain II of the arabidopsis *LAZY1* gene (*AtLAZY1*$^{L92A/I94A}$) led to both an inverted auxin gradient in shoots and downwards growth (positive shoot gravitropism) (Yoshihara and Spalding, 2020). In sum, either the lack of an auxin gradient in lateral shoots (as in *Atlazy1,2,4*) or an inverted auxin gradient (as in *AtLAZY1*$^{L92A/I94A}$) results in a downward oriented, or weeping, lateral shoot phenotype (Taniguchi et al., 2017; Yoshihara and Spalding, 2020). Thus, removing or reversing auxin gradients in lateral shoots can result in a weeping shoot phenotype.

Finally, the weeping peach phenotype might result from positively gravitropic shoot growth. Positive shoot gravitropism could occur either through inversion of the gravitropic auxin gradient or inversion of the growth response to auxin. Inversion of the shoot auxin gradient and positive shoot gravitropism (rootward growth) have been observed in the arabidopsis *LAZY1* mutant allele AtLAZY1$^{1L92A/I94A}$, which also exhibits a pronounced weeping phenotype (Yoshihara and Spalding, 2020). Alternatively, the growth response to auxin could be inverted, with auxin inhibiting growth (as in roots) rather than promoting it (as in shoots). The mechanism for auxin inhibition of root elongation is not well understood, and it is complicated by the apparently dosage-dependent effects of auxin (Barbez et al., 2017; Du et al., 2020).

Here, we present anatomical, physiological, biomechanical, and molecular characterizations of weeping peach branches to assess the hypotheses for the cause of the weeping phenotype and identify the molecular function of PpeWEEP in branch orientation control. Our results suggest that, in peach, the WEEP protein is not required for structural integrity in branches. Rather, WEEP promotes negative gravitropism in both shoots and roots and plays a crucial role in establishing the gravitropic auxin gradient in shoots.

Results

Weeping branches have minimal differences in anatomy and wood composition.

To address the hypothesis that the weeping habit in peach was due to changes in branch structure, our early investigations into *WEEP* function focused on branch anatomy and wood composition. For this, and other comparisons, we utilized clonally propagated individuals from the previously established segregating F2 population of peaches used to identify the *weep* mutation (Hollender et al., 2018). Thus, the *weep* and 'standard' plant material come from full siblings and their main genetic difference is the absence or presence of the *weep* mutation.

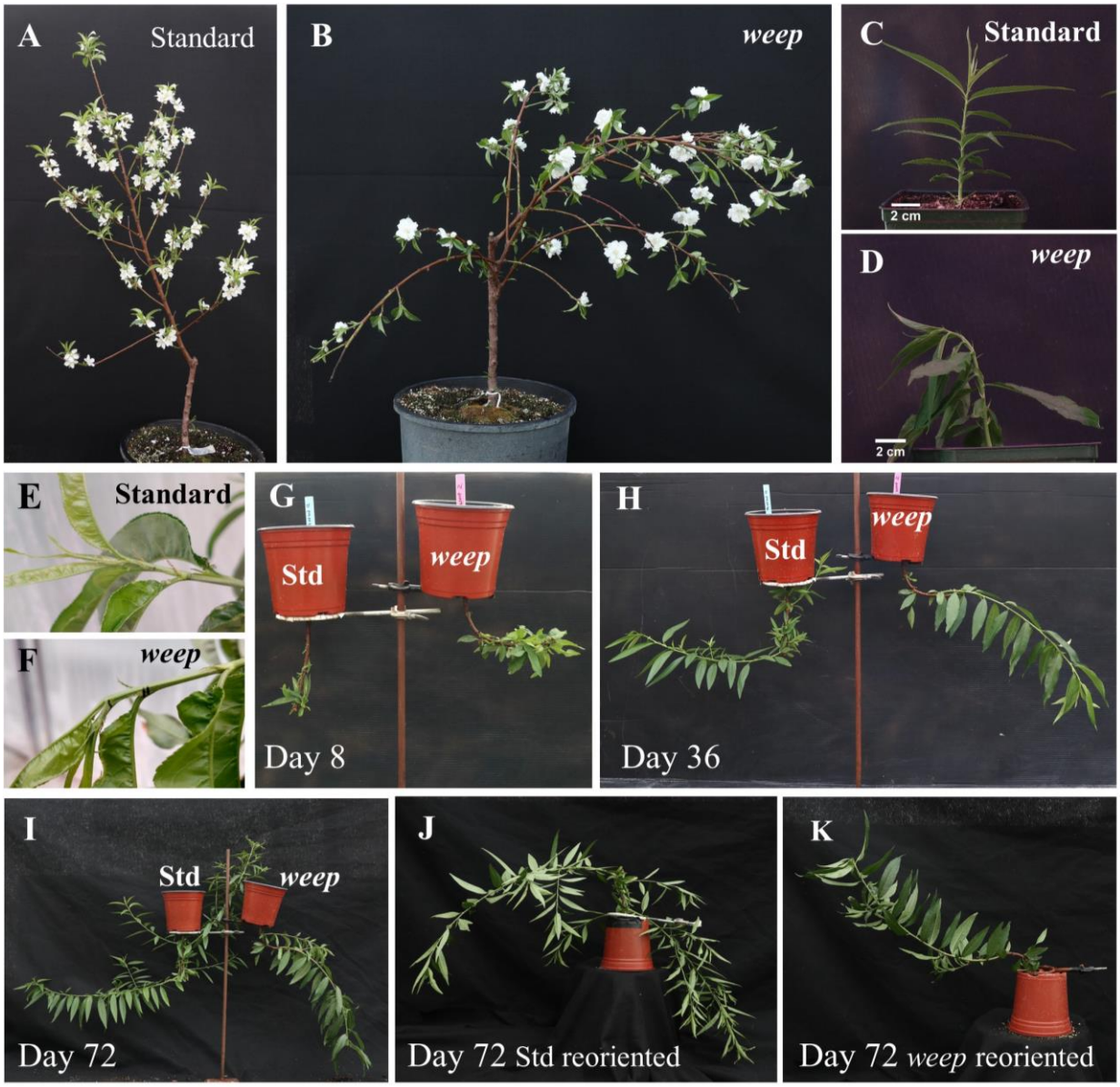

Figure 2.1: Standard and weeping peach tree phenotypes. Adult standard and weeping (weep) trees (A-B), seedling phenotypes (C-D), shoot tip phenotypes in adult trees (E-F), and the same standard (std) and weeping trees at 8, 36, and 72 days after a 180˚ reorientation (G-I) and after their return to the upright orientation on day 72 (J-K).

Not surprisingly, given the results of past 90-degree re-orientation growth observations (Hollender et al., 2018), when standard and weeping trees were reoriented 180-degrees (grown upside-down) new growth on weeping peach trees was directed downwards, while new growth on standard trees grew upwards (Figure 2.1G-I). Further, when they were reoriented to their original vertical position, the growth that occurred on upside-down weeping trees was fixed in an upward (standard)

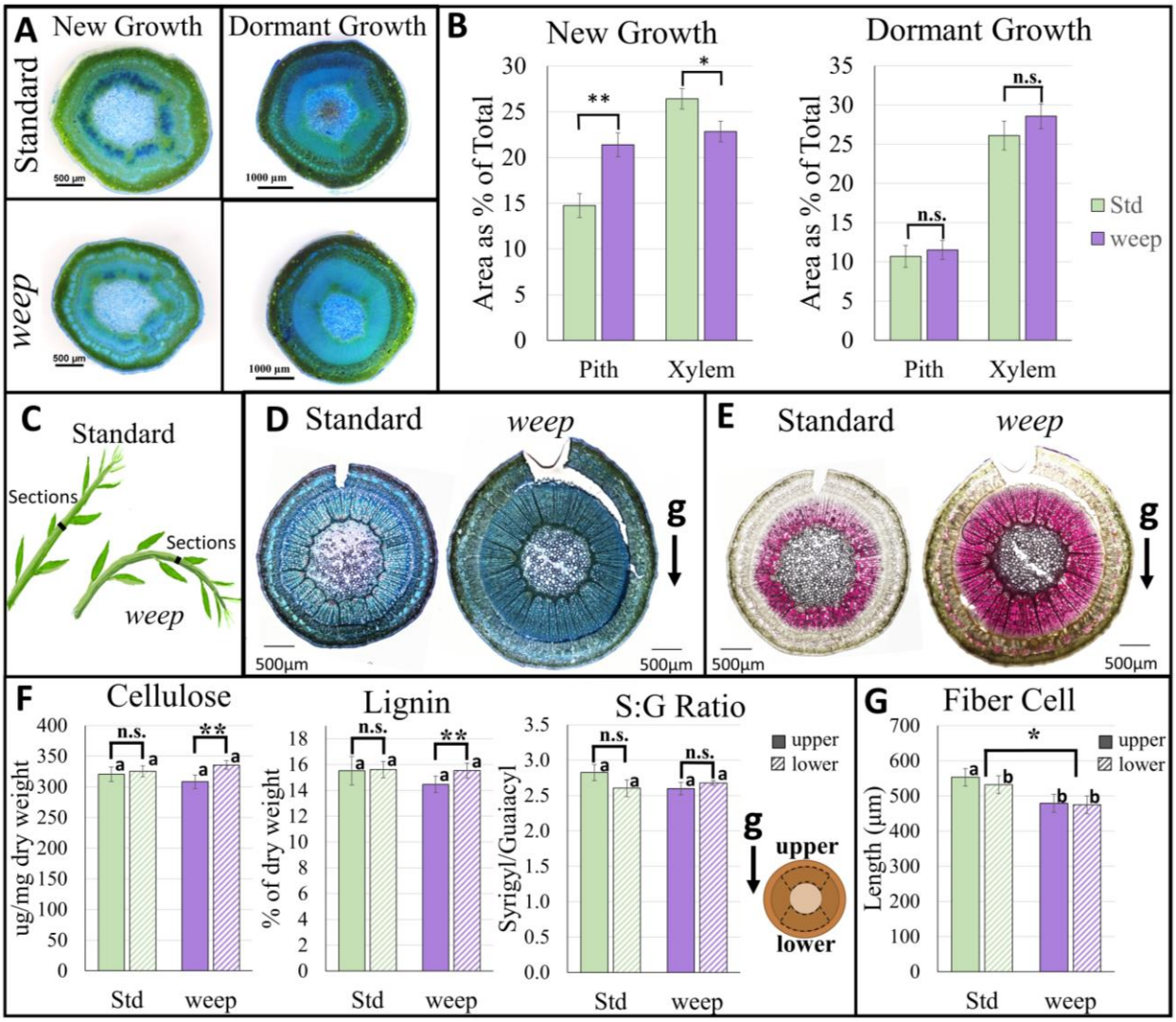

Figure 2.2: Wood anatomy and composition. New growth and dormant one-year old growth hand-sectioned and stained with toluidine (A). Area of pith and xylem relative to total cross-sectional area. Asterisks (*) above brackets indicate results of t-tests between genotypes (B). Diagram indicating the locations tissues from actively standard and weeping branches that were sectioned for tension wood formation staining analyses (C). Actively growing wood samples stained with toluidine for cellulose (D) and phloroglucinol for lignin (E). Notches indicate the upper side of the branch and the arrow below "g" indicates the relative direction of gravity. Cell wall polymers in upper and lower standard branches (F). Means with the same letter are not significantly different at α=0.05 in an all pairwise comparison of means with Tukey tests. Bracketed sets indicate the results of paired t-tests between top and bottom of each branch within a genotype. Length of fiber cells from digested wood (G); letters indicate the result of all pairwise comparisons with t-tests, and bracket indicates t-test between genotypes. Std indicates standard peach, weep indicates weeping peach. Error bars show standard error. ** indicates significantly different at α=0.05, * indicates significantly different at α=0.10, n.s. indicates not significant at the α=0.10 level.

appearance (Figure 2.1K). This suggested that a branch strength deficiency was not the cause for the weeping peach architecture. Strikingly, the standard trees, when returned to their original orientation, exhibited a weeping (downward) branch appearance (Figure 2.1J), suggesting that inverting the direction of gravity (flipping the trees upside down) is sufficient to create a weeping shoot appearance.

To assess if differences in branch anatomy contribute to architectural differences, actively growing shoot tips (new growth) and dormant 1-year old wood from weeping and standard trees were hand-sectioned. Percentages of xylem and pith tissues were calculated relative to the total cross-sectional area. Although it was not always visually obvious, the new growth of weeping branch tips had a greater percentage of pith and smaller percentage xylem relative to the total cross-sectional area of their branches, compared to standard tree branches (Figure 2.2 A and B). In contrast, no significant differences between the amounts of pith and xylem in weeping and standard branches were detected in 1-year old branches, indicating that the differences in xylem width were transient and disappeared by the end of the growing season (Figure 2.2 A and B).

To investigate wood composition and tension wood formation, lignin and cellulose content were assessed for each genotype, both visually and chemically. Tension wood is characterized by high levels of cellulose, reduced lignin, and often contains obviously visible gelatinous fibers. In contrast, the "opposite wood" on the lower (abaxial) side is enriched in lignin and does not have these specialized fiber cells. Actively growing branches from standard and *weep* trees were collected and tissues from the region where the branches were oriented upward (in standard) or downward (in *weep*) were sectioned to ascertain whether the bending was actuated by tension wood (Figure 2.2 C-E). These were stained with toluidine blue to visualize cellulose content (Figure 2.2 D), or phloroglucinol (Figure 2.2 E) to visualize lignin. No consistent differences in staining intensity or localization were detectible between the two genotypes, nor were gelatinous fibers identifiable (Figure 2.2 D and E). Biochemical analyses of upper and lower tissues from bisected weeping and standard branches were subsequently performed (Figure 2.2 F; Figure 2.13). No differences in acetyl bromide soluble lignin (ABSL) content, proportion of syringyl (S) and guaiacyl (G) lignin units, or crystalline cellulose content were detected between genotypes or tissue types (Figure 2.2 E). However, the corresponding neutral sugar analysis revealed that weeping peach tissues had lower concentrations of glucose than the standard branch tissues (Figure 2.13).

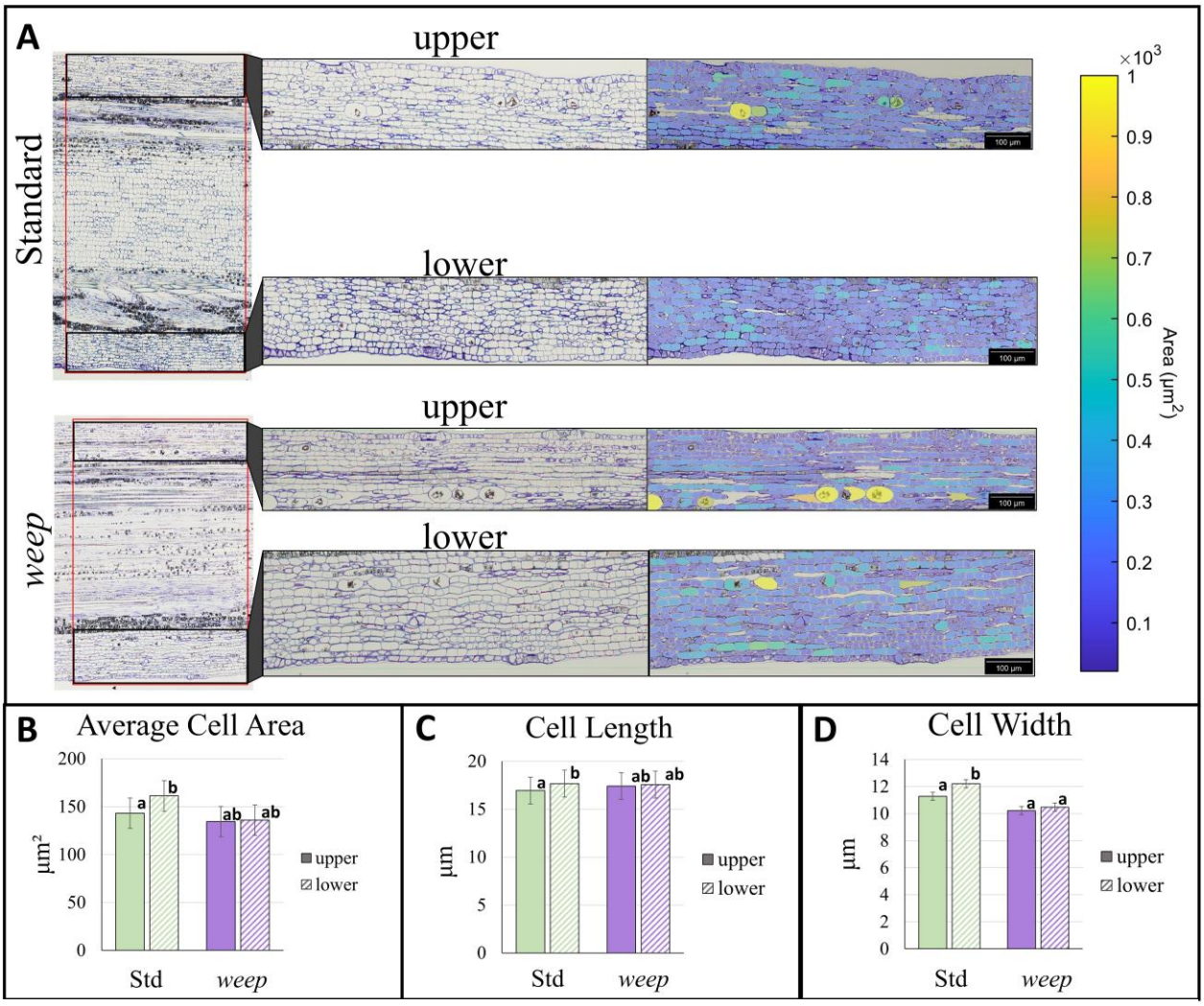

Figure 2.3: Cell size measurements of cortical cells in standard and weeping peach shoot tips. A) Illustration of regions of shoot tips used for cell size analysis, as well as analysis software output. B) Average cell area. C). Average cell length D) Average cell width. Means with the same letter are not significantly different at $\alpha = 0.05$ in an all pairwise comparison of means with Tukey's tests. Std indicates standard peach, weep indicates weeping peach. Three replicates were analyzed per genotype.

We then investigated if there were differences in cell size between the genotypes. This was initially done by measuring the length of wood fiber cells isolated from macerated tissues from upper and lower portions of bisected standard and weeping peach branches. Fiber cells from the upper tissues of standard peach branches were consistently longer than those from the underside of standard branches (Figure 2.2 F). However, no difference was detected between fiber cell lengths from upper and lower weeping branch tissues. Interestingly, when fiber cell lengths from upper and

lower tissues for each genotype were combined, the fiber cells of weeping branches were slightly, but significantly shorter than those from standard branches ($p < 0.10$; Figure 2.2 G).

Cell size differences between tissues in the upper and lower regions of standard and weeping branches were also investigated by comparing and analyzing thin longitudinal sections from resin-embedded branch tissues. Due to the direction of curvature, we hypothesized that cortical cells on the lower side of standard branches would be longer than those on the upper, and vice-versa in weeping branches. Longitudinal sections of shoot tips (about 0.5cm below apex) were used to assess cell size. Although it was not obvious by eye, cortical cells from the lower side of standard branches had a greater area, were longer (as expected), and wider than those on the upper side (Figure 2.3 A-D). In contrast, weeping shoot tips did not show a consistent difference in area, length, or width between upper and lower side (Figure 2.3 A-D). Due to differences in rates of elongation between shoot tips and the presence of vegetative lateral buds which distort the cell files and alter elongation, no definite conclusions can be drawn about the overall rate of cell expansion in weep versus standard peach. However, these results do suggest that the differential cell elongation of the lower side of the shoot tip in response to gravity is disrupted in *weep*.

Weeping shoots do not have decreased structural integrity.

To determine if weeping peach shoots curve downward because their branches are too weak to support their own weight, we assessed their biomechanical properties. We used a universal testing machine to measure shoot flexibility in the elastic region of its deformation (flexural stiffness-EI),

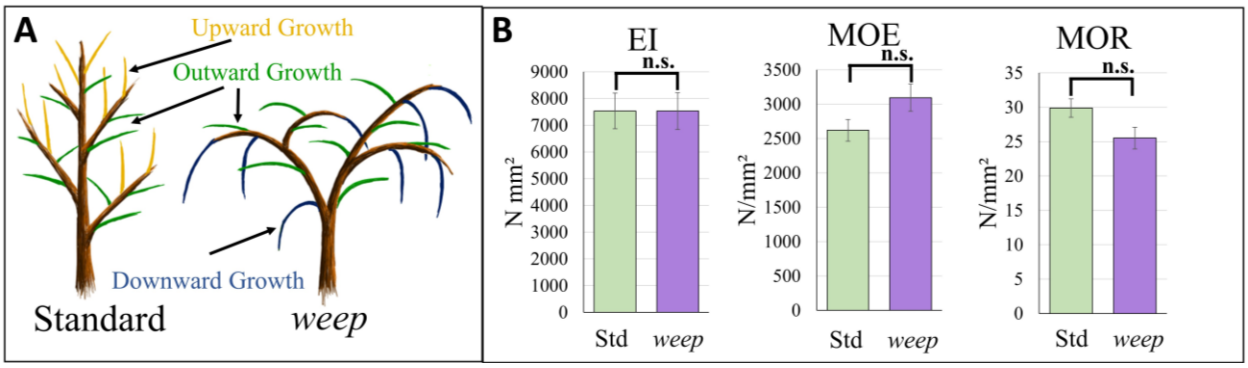

Figure 2.4: Biomechanical properties of actively growing standard and weeping peach shoots. Actively growing branches of standard (Std) and weeping (weep) peach trees were categorized into upward (gold), outward (green), or downward (blue) orientations (A). Flexural stiffness (EI), the modulus of elasticity (MOE), or the modulus of rupture (MOR) are shown for outward growing shoot tips (B). Bars represent standard error. Pairwise comparisons were done using t-test; n.s. indicates not significant at the 0.1 level.

tissue flexibility (modulus of elasticity-MOE), and tissue strength (modulus of rupture—MOR). These tests were performed on actively growing shoot tips because weeping branches already exhibit curvature at this early developmental stage (Figure 2.1 E and F). Since wood development is a dynamic process, it is impacted by shoot tip orientation as the shoot responds to gravitational forces. Thus, shoots in different orientations may exhibit different mechanical properties. For this experiment, shoots were categorized into "upward", "downward", and "outward" orientation (Figure 2.4 A). Only outward shoots were used for statistical comparison between the genotypes because standard trees have only upward and outward shoots, while weeping trees only have outward and downward shoots. No significant differences in EI, MOE, or MOR were observed between standard and *weep* in actively growing, outward-oriented shoot tips (Figure 2.3 B). These biomechanical observations indicate that the small differences in weeping peach shoot anatomy that we identified (Figures 2.2 and 2.3) do not lead to significant alterations in the shoot structural

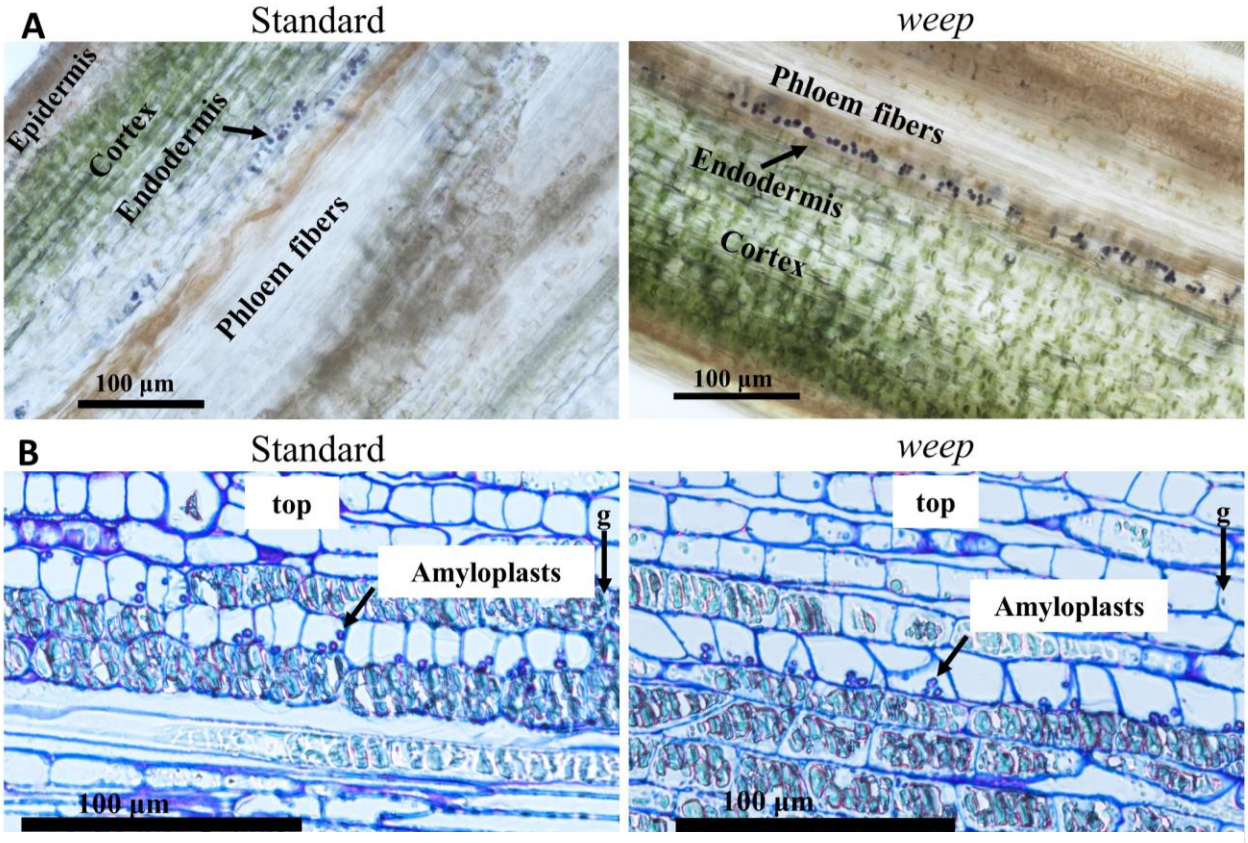

Figure 2.5: Amyloplast sedimentation. (A) Longitudinal sections of fresh standard and weeping (weep) branches 1cm below the shoot apex stained for starch with Lugol's solution. (B) Thin sections of resin-embedded standard and weep branches 0.5cm below the shoot apex reveal proper amyloplast sedimentation. Gravity vector indicated by arrow under the g.

integrity, and *weep* shoots do not bend in the direction of gravity due to changes in branch stiffness or strength.

Weeping shoot endodermis contains amyloplasts with normal sedimentation.

Given the evidence that the weeping phenotype is not due to a loss of structural integrity, coupled with the observation that weeping peach shoots do not bend upwards in response to gravistimulation, we next explored the hypothesis that the *weep* peach mutant has defects in the shoot gravitropism pathway. To first investigate gravitropic perception, we assessed if *weep* mutants had amyloplasts and normal amyloplast sedimentation. Fifty-micron thick fresh vibratome sections from actively growing shoot tips stained with Lugol's solution revealed that starch-filled

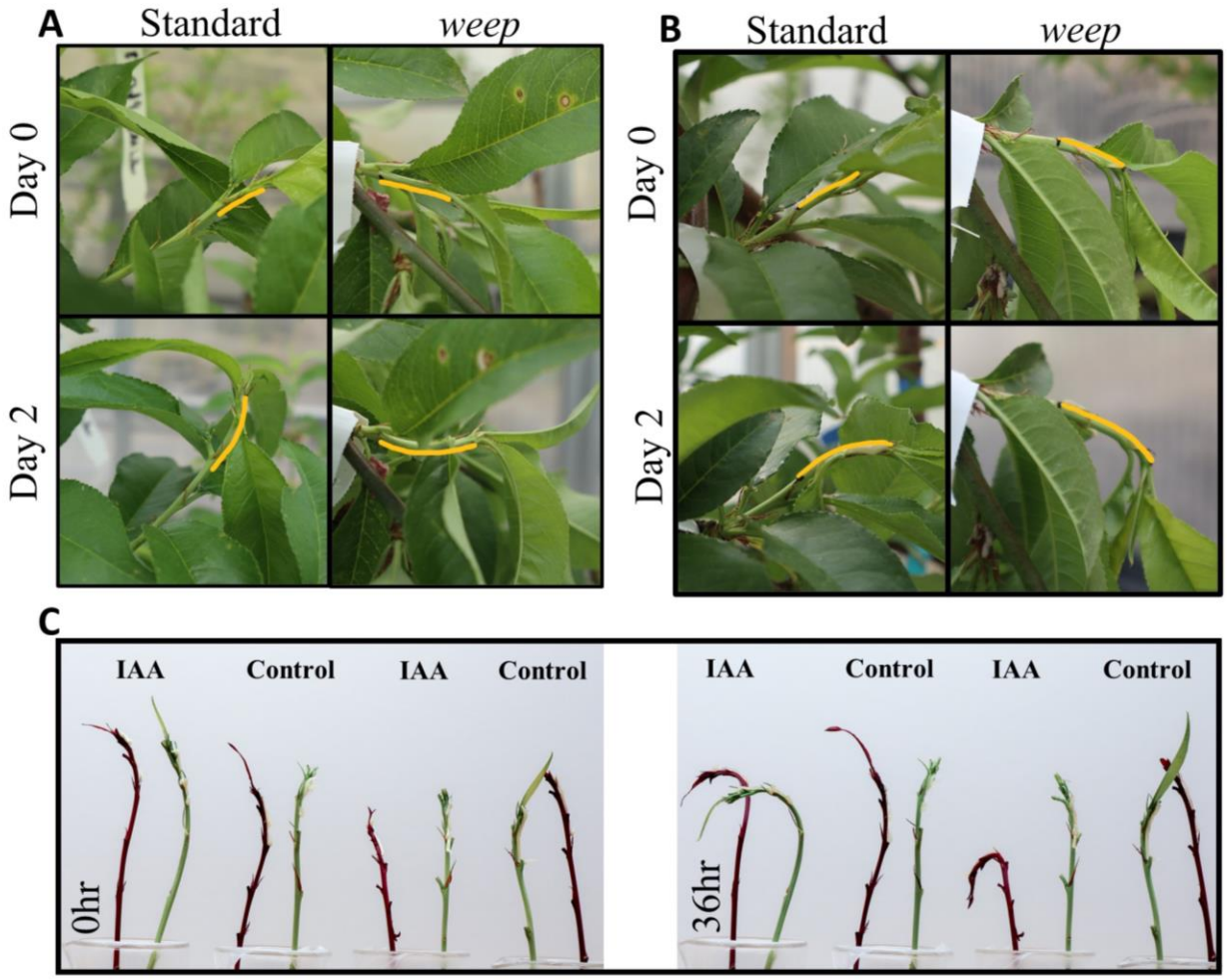

Figure 2.6: Bending response to unilateral auxin application. Application of 1% IAA in lanolin (yellow line) to the bottom (A) or the top (B) of shoot tips of standard and weeping (weep) trees in the greenhouse. (C) Application of auxin to the right side of upright, detached shoots. Red shoots are from weeping trees that also contain an unlinked anthocyanin phenotype. Green shoots are from standard trees.

amyloplasts were present in both standard and weeping branch shoot endodermis (Figure 2.5A). Additionally, 1 µm thick sections of resin-embedded shoots tips from outward-oriented branches of each genotype revealed normal amyloplast sedimentation in response to gravity within *weep* shoots. Amyloplasts were consistently found on the lower side of the endodermal cells in both weeping and standard branches (Figure 2.5B). Thus, weeping shoots contain phenotypically normal amyloplasts and amyloplast sedimentation.

Both standard and weeping shoots bend away from asymmetric exogenous auxin application.

We next assessed if weeping shoots were able to exhibit a normal elongation response and bend away from asymmetric auxin localization. Two complementary experiments were performed to simulate the asymmetric auxin concentrations that form as part of the gravitropism response pathway. First, 1% IAA in lanolin paste was applied to the upper or lower side of *weeping* and standard shoots on trees growing in our greenhouse (Figure 2.6 A and B). Second, 1% IAA was applied to one side of upright detached shoots with leaves removed (Figure 2.6 C). In both experiments, weeping and standard shoots bent away from unilateral auxin application, regardless of where it was applied (Figure 2.6). In both genotypes the degree of bending response was highly variable; however, the direction of bending was consistent across all samples from both genotypes. Therefore, weeping shoots respond normally to auxin, elongating and bending away from areas of high auxin concentration.

Transcriptome analyses reveal weeping peaches have inverted expression of auxin response and wood development genes.

Considering the ability of weeping shoot tips to respond properly to exogenous auxin, we explored the hypothesis that the auxin localization in weeping branches was flipped compared to standard branches. Specifically, we anticipated that standard branch shoot tips would have a greater concentration of auxin in the lower (abaxial) side, and the reverse would be true for weeping peach branches. To test this, RNA from tissues from the adaxial (upper) and abaxial (lower) sides of the first (IN1) and second (IN2) internodes of individual actively growing standard and weeping shoot tips (Figure 2.14) was extracted and sequenced. A principal component analysis (PCA) indicated expression profile differences between internodes when all samples were analyzed together (Figure 2.15). Within each internode, the genotypes also formed distinct clusters, particularly in IN2 (Figure 2.16). In addition, differences between upper and lower tissues of a given shoot tip

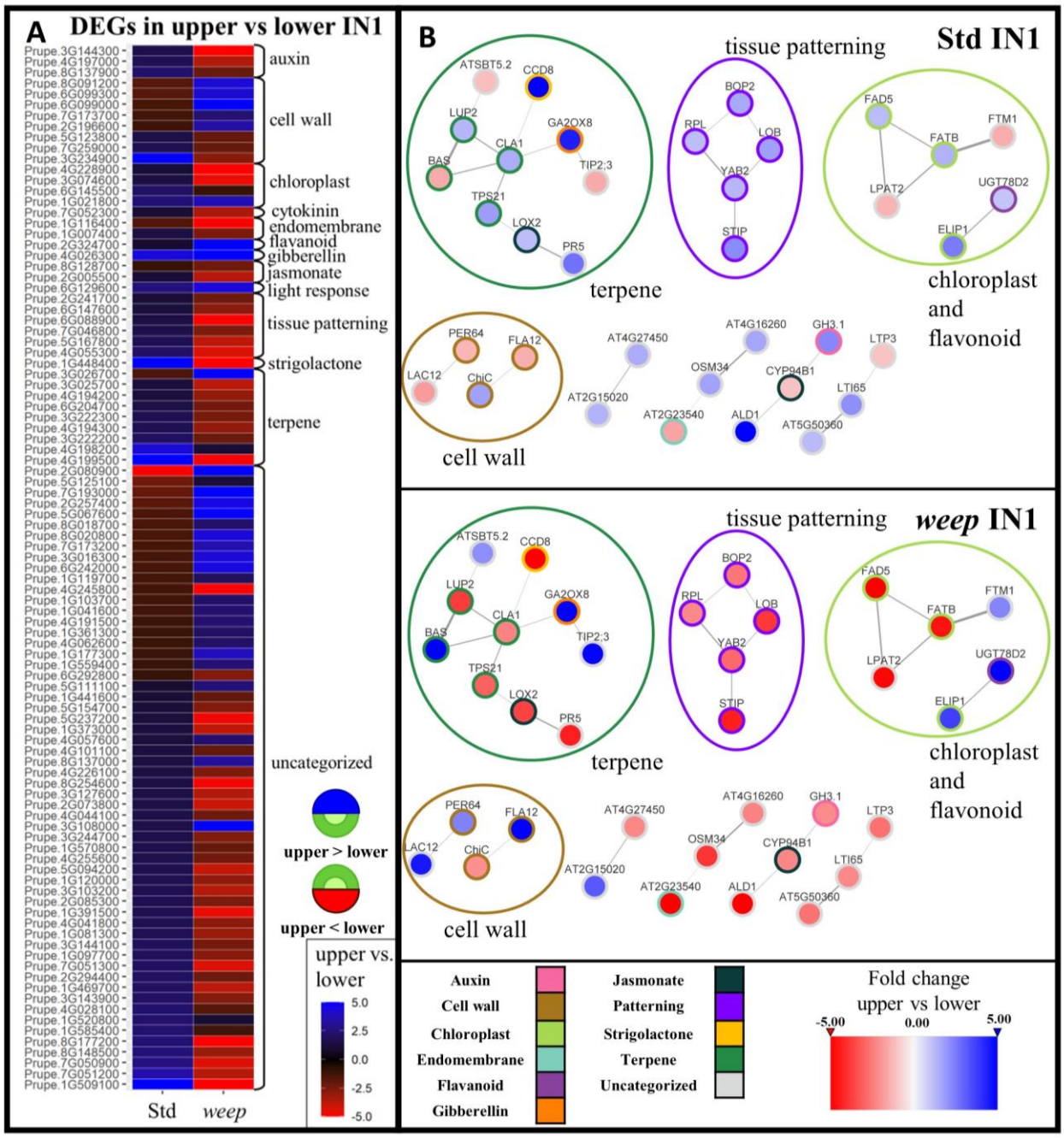

Figure 2.7: Differentially expressed genes between upper and lower tissues in the first internode (IN1). (A) Heatmap indicates fold changes between the upper and lower sides of shoots from standard and weeping (weep) trees. Red indicates that the expression is higher on the lower side, blue indicates that the expression is higher on the upper side. (B) An interaction network between the genes was created using arabidopsis homologs in STRING. Node color indicates fold change between upper and lower, edge width indicates evidence strength, and node outline indicates functional category assignment.

were much smaller than differences between individual shoot tips (Figure 2.16). Transcriptional

differences were calculated for each genotype between upper and lower tissues from the first two internodes (IN1 and IN2) of outward branch shoot tips (Supplemental Tables S2.1 and S2.2). For each internode, genes with a two-fold change in expression and a Bonferroni value < 0.01 in either genotype were selected as genes of interest (GOI). This resulted in 97 GOI for IN1 (Figure 2.7 and Supplemental Table S2.1) and 213 GOI for IN2 (Figure 2.8, Figure 2.17, and Supplemental Table S2.2). Expression differences between upper and lower branch tissues were more prevalent and stronger in the weeping branches than standard ones (more genes were differentially expressed in the *weep* mutants than in standard, and the fold change for these genes was often larger in *weep*). The greater number of differentially expressed genes (DEGs) in the IN2 samples may be due to adaxial/abaxial polarity being more strongly established further down from the meristem.

Using gene annotations and functional descriptions, the genes were also manually categorized into 10 functional groups (i.e., auxin, cell wall, chloroplast, endomembrane, flavonoid, gibberellin, jasmonate, patterning, strigolactone, and terpenes) and one uncategorized gene group (Figures 2.6 and 2.7; Supplemental Tables S2.1 and S2.2). Interestingly, most of the genes that were differentially expressed between upper and lower tissues in standard peaches were also differentially expressed in weeping peaches, but in an inverted pattern (Figures 2.7, 2.8, 2.17, and 2.18). In other words, genes that were more highly expressed in the upper branch tissues of one genotype were more highly expressed in the lower tissues of the other genotype, and vice versa. To further investigate the GOI, gene correlation networks were created using the arabidopsis homologs of each GOI (Figures 2.7 B and 2.8 B).

Of note for IN1, genes related to tissue patterning, auxin, cell wall development, and terpene biosynthesis and terpene-derived hormones were highly represented and showed inverted expression patterns in the weeping branches (Figure 2.7 B; Supplementary Table S2.1). The tissue patterning group contains genes related to meristem maintenance, adaxial/abaxial polarity, and phyllotaxy (Prupe.6G088900, homolog of *PRS*; Prupe.4G055300, homolog of *STIMPY (STIP)*; Prupe.2G241700, homolog of *REPLUMLESS (RPL)*; Prupe.6G147600, homolog of *YABBY2* (*YAB2)*; Prupe.5G167800, homolog of *LOB*; and Prupe.7G046800, homolog of *BOP2*). Interestingly, all these genes were expressed only slightly higher in the upper tissues in standard, and much more strongly in the lower tissues in weep, suggesting there might be an inversion of

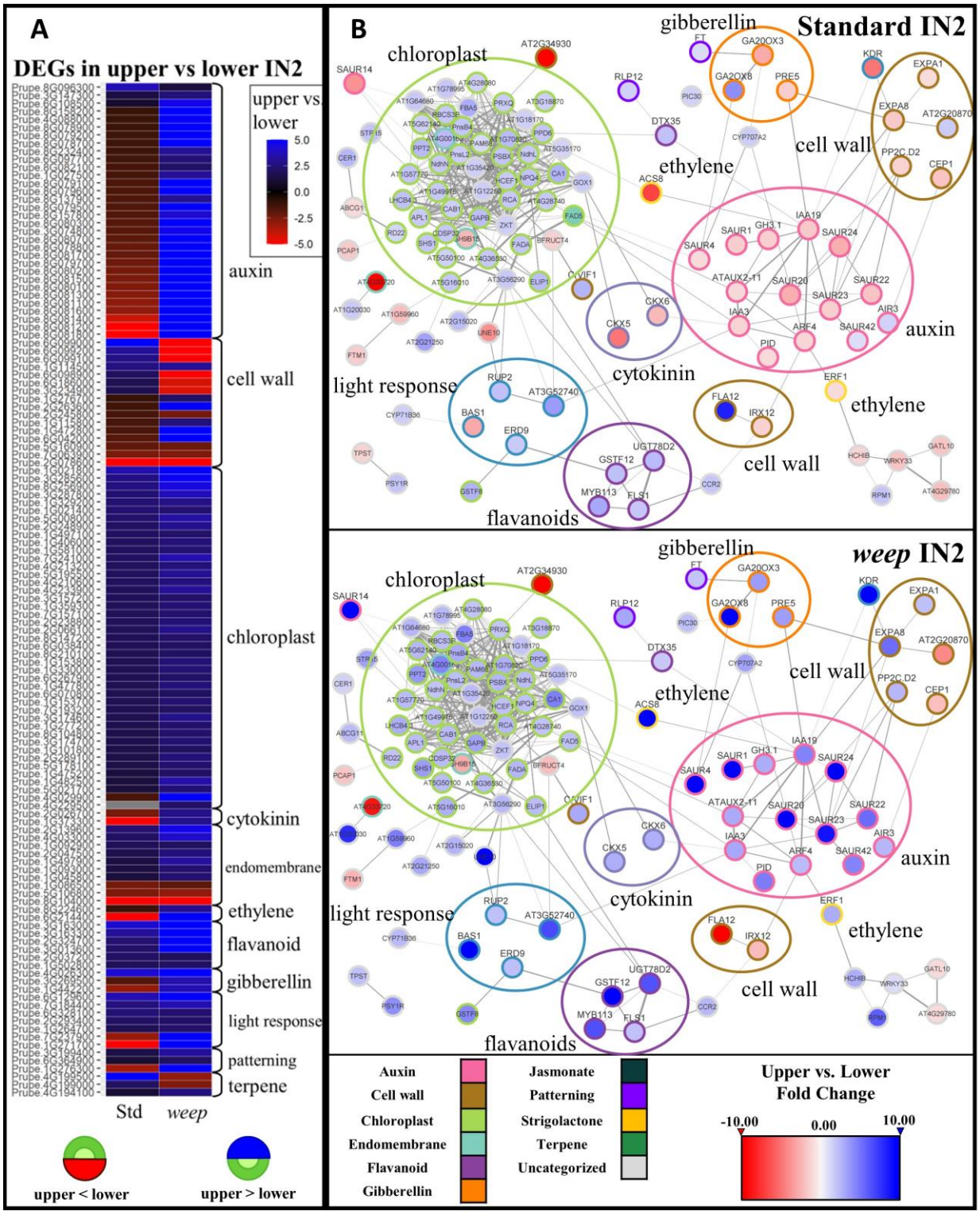

Figure 2.8: Differentially expressed genes between upper and lower tissues from the second internode (IN2). (A) Heatmap indicates fold changes between the upper and lower. (B) STRING interaction network using arabidopsis homologs. Node color indicates fold change between upper and lower, edge width indicates evidence strength, and node outline indicates functional category assignment.

abaxial/adaxial polarity in the *weep* branches. The auxin group included a putative auxin synthesis gene (Prupe.3G144300, homolog of AT4G02610) and two genes for conjugating auxin to amino acids (Prupe.4G197000, homolog of *GH3.6*, and Prupe.8G137900 homolog of *GH3.1*). These genes were also more highly expressed in the upper tissue in standard, and in the lower tissue in *weep*. The cell wall group includes genes involved in lignin metabolism (Prupe.7G173700, *PER64* homolog; Prupe.2G196600, *NST1* homolog), cellulose deposition (Prupe.6G099300 and Prupe.6G099000, *FLA12* homologs), and hemicellulose synthesis (Prupe.5G123800, *CSLG3* homolog). Finally, there was a large group of terpene biosynthesis genes and terpene-related hormones. There are nine differentially expressed terpene biosynthesis genes, including four homologs of the sesquiterpene synthase *TPS21* (Prupe.4G194200, Prupe.4G194300, Prupe.4G198200, Prupe.4G199500) and two homologs of the monoterpene synthase *TPS-CIN* (Prupe.3G222200, Prupe.3G222300). Seven of the nine differentially expressed terpene genes are more highly expressed in the upper tissues in standard, and more highly expressed in the lower tissues in *weep*. This pattern is also observed for Prupe.1G448400, a homolog of the strigolactone biosynthesis gene *CCD8* (also known as *MAX4*). In contrast, Prupe.4G026300, which is a homolog of the GA sequestering gene *GA2OX8* is more highly expressed in the upper tissues in both standard and *weep.*

Like IN1, for the IN2 comparison, chloroplast, flavonoid, and many light response genes were more highly expressed on the upper side of the shoot in both standard and *weep* (Figure 2.8A and B). This is consistent with expectations, as all of those groups would be expected to be upregulated where there is more light exposure. In contrast, several functional groups were more highly expressed on the lower side of the shoot in standard, but more highly expressed on the upper side of the shoot in *weep*. This pattern is observed in 30 auxin-related genes, including 24 *SAUR* homologs (Figure 2.8A), a homolog of *PID* (Prupe.4G088000), three homologs of *AUX-IAA* transcriptional regulators (Prupe.1G027500, Prupe.3G074800 and Prupe.8G232400), a homolog of auxin response factor 4 (Prupe.6G097700), and a homolog of GH3.1 (Prupe.8G137900). This pattern is also observed in two ethylene-related genes: a homolog of *ETHYLENE RESPONSE FACTOR 1* (Prupe.8G224600), and a homolog of ACC synthase *ACS8* (Prupe.6G214400). The *ACS8* homolog shows particularly dramatic differential regulation as it is 7-fold more highly expressed in the lower tissue in standard, and 76-fold more highly expressed in the upper in *weep*. Finally, this pattern is observed in two gibberellin-related genes (Prupe.3G269500,

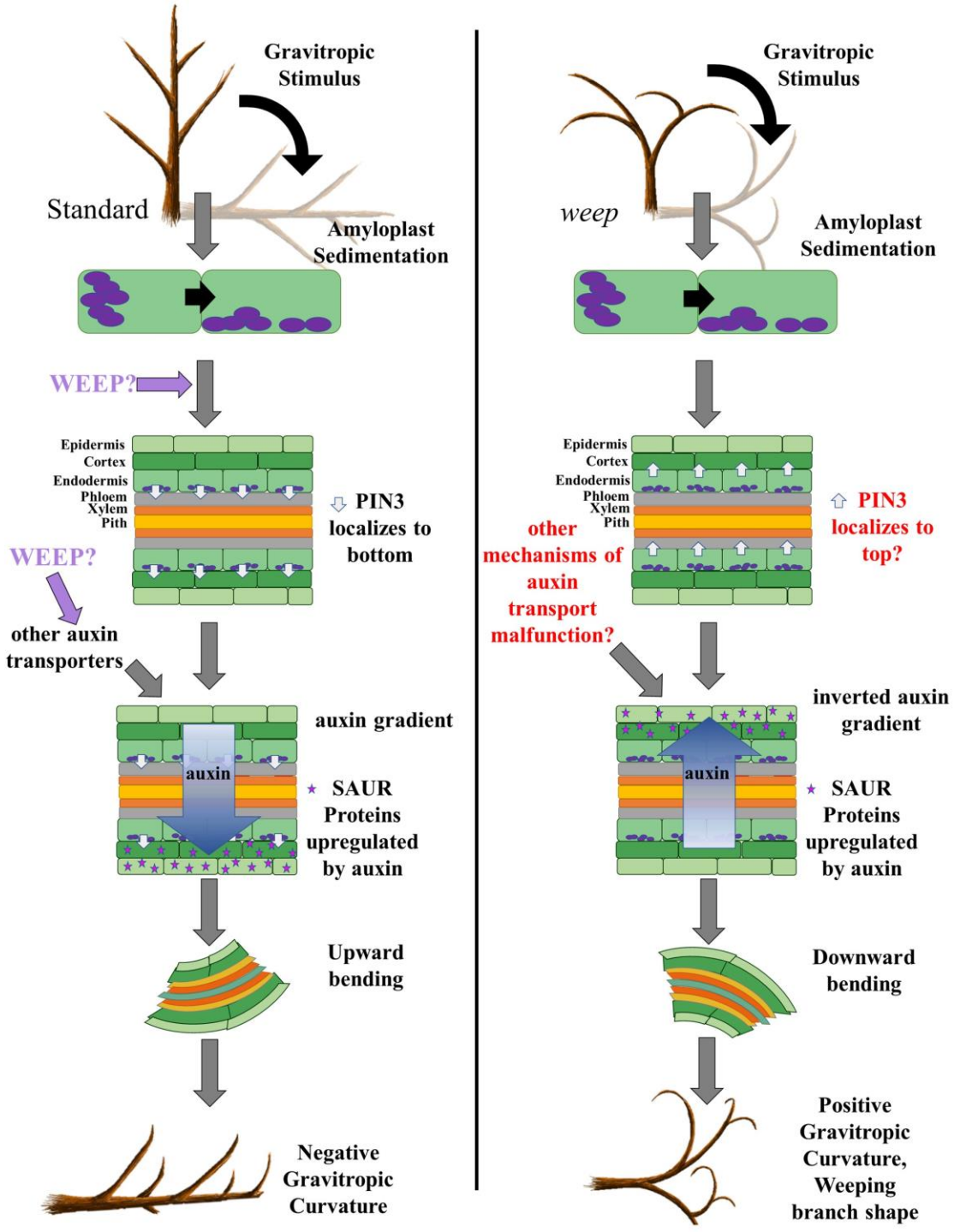

Figure 2.9: Proposed model of WEEP's role in shoot tip gravitropism. WEEP acts during gravitropic signal transduction, downstream of amyloplast sedimentation. WEEP is required for formation of the gravitropic auxin gradient, either through localization of PIN proteins or through an alternative auxin transport mechanism. The auxin gradient is required for the shoots' negative gravitropic bending response. An inverted auxin gradient in the *weep* mutant leads weeping peach shoots to exhibit positive gravitropism.

Prupe.1G442200), and three terpene synthase 21 homologs (Prupe.4G199500, Prupe.4G199000, Prupe.4G194100).

For the cell wall functional group, there are genes relating to two distinct functions, which show distinct patterns of expression. Four genes are related to cell expansion downstream of auxin, and like the auxin response genes, more highly expressed on the lower side in standard and more highly expressed on the upper side in *weep*. These include three expansins (Prupe.1G276700, Prupe.2G263600, Prupe.6G042000) and a protein phosphatase 2C (Prupe.1G115800). In contrast, four homologs of *FASCICLIN-like arabinogalactan-protein 12* (*FLA12*; Prupe.6G098900, Prupe.6G099000, Prupe.6G099100, Prupe.6G099200) which is a marker of tension wood, are more highly expressed on the upper side in standard and on the lower side in weep.

Because 24 *SAUR* homologs were differentially expressed, and *SAUR* transcript expression is known to be an early auxin response to gravitropism, we further investigated expression patterns throughout the *SAUR* family. Using KEGGORTH terms and arabidopsis homolog descriptions, 76 putative *SAUR* proteins were identified in peach, 43 of which are in a tandem array on chromosome 8. As expected, the majority (54/76) of the putative SAUR proteins in the peach genome are expressed on the lower tissue in standard IN2 (Figure 2.18, Supplemental Table S2.3). However, the majority (49/76) of the SAUR proteins in *weep* IN2 were expressed in the upper tissues (Figure 2.18), including 40 of the genes upregulated on the lower side in standard. This inverted expression trend also occurred for IN1 tissues, although the difference between expression in upper and lower tissues is more subtle (Figure 2.18). Thus, SAURs overall were more highly expressed on the lower side of the shoot in standard shoots, and on the upper side in *weep* shoots.

PpeWEEP proteins homo-oligomerize in vitro.

Oligomerization is essential for the function of some SAM domain proteins (Denay, 2017). For example, the floral meristem identity protein LFY requires head-to-tail homo-oligomerization to fully access DNA binding regions (Sayou, 2016). To test if the peach WEEP protein (PpeWEEP) homo-oligomerizes, size-exclusion chromatography (SEC) was performed. Heterologously-expressed PpeWEEP fused to 6xHis, maltose binding protein (MBP), and a Strep-Tag, with a predicted weight of 60.3 kDa, was sequentially purified via Ni-NTA and StepTactin columns prior to SEC analysis (Figure 2.10 A). The resulting elution had a prominent peak corresponding to 525 kDa, indicating an average of 8 to 10 monomers per complex, suggesting that most PpeWEEP

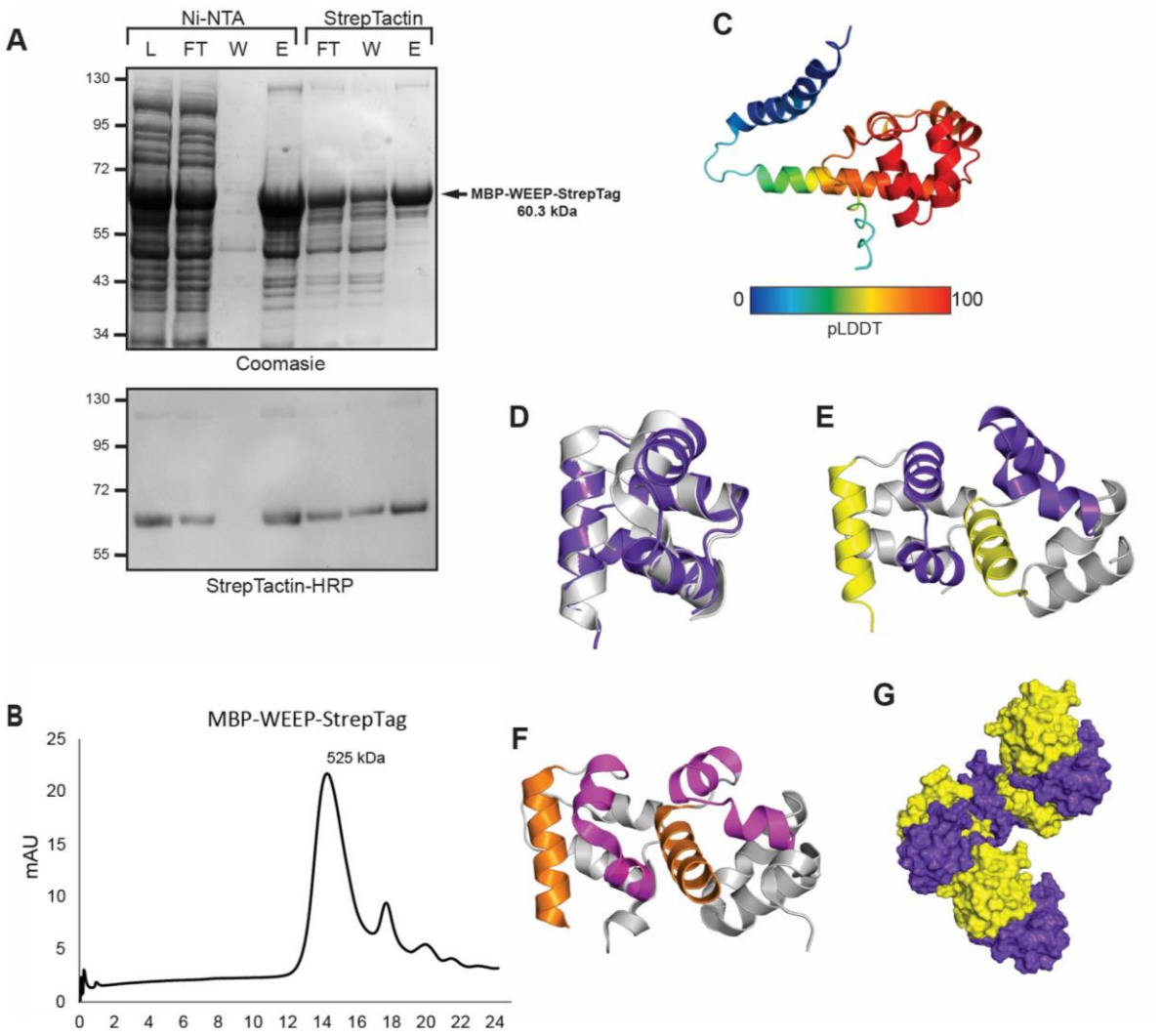

Figure 2.10: Size exclusion chromatography indicates WEEP proteins homo-oligomerize. (A) SDS-PAGE gels containing flow through (FT), wash (W), and elution (E) samples from sequential Ni-NTA and StrepTactin column purifications of a heterologously expressed 6XHis-MBP-PpeWEEP-StrepTactin fusion protein. Coomassie stained gel (left) indicates total protein. Western blot (right) indicate the presence of the 60.3 kDa fusion protein. (B) SEC chromatograph with a peak at 525 kDa, corresponding to an 8.7mer. (C) AlphaFold2 protein structure predictions for the full length PpeWEEP monomer colored by model confidence (pLDDT) (D) Overlay of WEEP over the top of scm illustrating the similarity between WEEP and scm/Ph. (E-F) AlphaFold2 protein structure prediction for a PpeWEEP SAM domain dimer (E), and the structure of the dimer between the Drosophila SAM domain proteins Polyhomeotic (F) and Sex-comb-on-midleg (Scm) (PDB: 1PK1). (G) Predicted structure of a helical PpeWEEP octomer.

protein exists as homo-oligomer in solution, similar to LFY (Figure 2.10 B, Figure 2.19; Sayou et al 2016).

To understand the structure of the PpeWEEP protein, we used AlphaFold2 to predict its structure. AlphaFold2 modeled the structure of the PpeWEEP SAM domain with high confidence, but the C-terminal region with low confidence (Figure 2.10 C; (Bryant et al., 2022). AlphaFold2 multimer modeled the structure of the PpeWEEP SAM domain as a head-to-tail dimer, structurally similar to the Drosophila SAM proteins Polyhomeotic (Ph) and Sex-comb-on-midleg (Scm), despite the low sequence homology between PpeWEEP and Ph/Scm (~20% identity; Figure 2.10 D-F; Kim et al., 2005). Lastly, PpeWEEP SAM monomers were aligned to the structure of the helical Scm polymer in PyMol to build a model for a PpeWEEP octamer (Figure 2.10 G).

Weeping peach roots have steeper gravitropic set-point angles and more rapid gravitropic response.

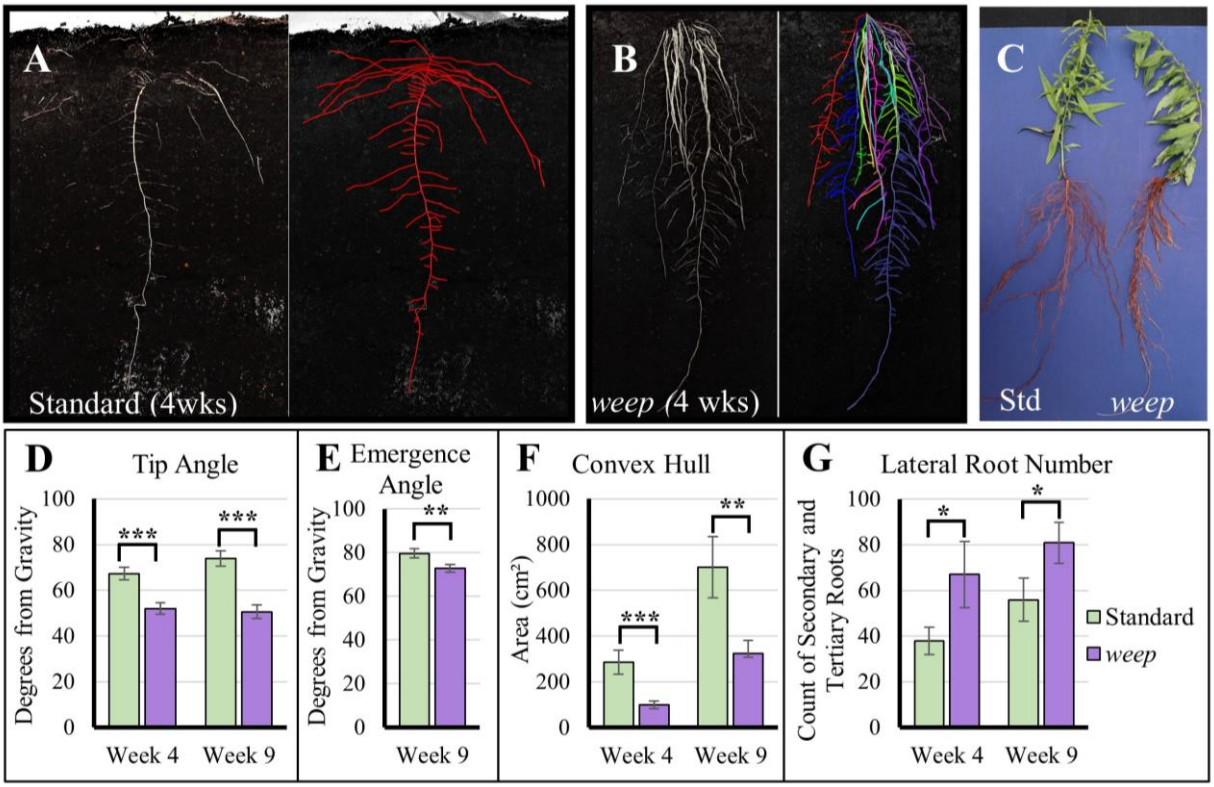

Figure 2.11: Root architecture in standard and weeping peaches. Peach seedlings were grown in rhizoboxes, imaged, and the root system was traced in RootNav (A, B). Different colors indicate separate primary roots, or secondary roots with lateral tertiary roots. RootNav was used to measure tip angle (D), emergence angle (E), convex hull (F), and lateral root number (G). At the end of the experiment, dirt was removed, and the entire root system was photographed (C). Pairwise comparisons done with t-tests. Error bars show standard error. * indicates significantly different at α=0.10; ** indicates significantly different at α=0.05; *** indicates significantly different at α=0.01.

In contras to the absence of a gravitropic response in weeping peach shoots, the roots of *weep* mutants in wheat and barley exhibit both narrower gravitropic set-point angles and a more rapid root positive gravitropic response (Kirschner et al., 2021). Therefore, we assessed weeping peach root set-point angle under normal growth conditions and performed two root gravitropism time-course experiments following 90-degree reorientations.

Freshly germinated standard and weeping peach seeds from the same population were planted in rhizotrons, and the resulting seedlings were grown for ten weeks to observe their natural root architecture. The peach *weep* mutant exhibited a dramatically different root architecture than the standard peaches (Figure 2.11 A-C). Driving this change, weeping peach roots have significantly steeper lateral root emergence and tip angles (Figure 2.11 D and E), which leads to a smaller convex hull (area of root exploration; Figure 2.11 F). In addition, the number of secondary and tertiary lateral roots was moderately increased in *weep* (Figure 2.11 G). Lastly, multiple weeping tree secondary roots grew straight downwards and were often co-dominant with the primary root (Figure 2.11 A and B). Examination of the root system at the end of the experiment after soil removal confirmed that these were true secondary roots, rather than seminal roots emerging from above the radical (Figure 2.11 C).

Next, we investigated root gravitropism for standard and weeping peach seedlings in two different ways (Figure 2.12). Five standard and nine weep peach seedlings were grown in smaller rhizoboxes (with internal dimensions of 1.5” x 7” x 11”). After 18 days of growth in the vertical position, the tip angles of the tap root and several lateral roots were measured. The seedlings were then gravistimulated by a 90-degree reorientation and roots were imaged at regular intervals over the course of eight days (Figure 2.12 A-C; Figure 2.20) to determine if the *weep* mutation led to root gravitropism differences, as it does in barley *weep* (*egt2*) mutants. Both standard and weeping peach tap and lateral roots exhibited the standard root gravitropism response by adjusting their growth to return to a downward position over time (Figure 2.12 A-C). In this experiment, however, no significant differences in root growth in response to gravistimulation were detected when we compared root tip angles (relative to their initial angle) between the genotypes at several time points (Figure 2.12 B and C). However, due to the challenges of growing tree seedlings, such as the time required for collection and vernalization and a low germination rate, the total number of roots available for this study was minimal compared to what is commonly used to detect phenotypic differences in roots, which exhibit a high degree of variability due to environmental

conditions. To address this, we assessed gravitropic response young roots from root-pruned

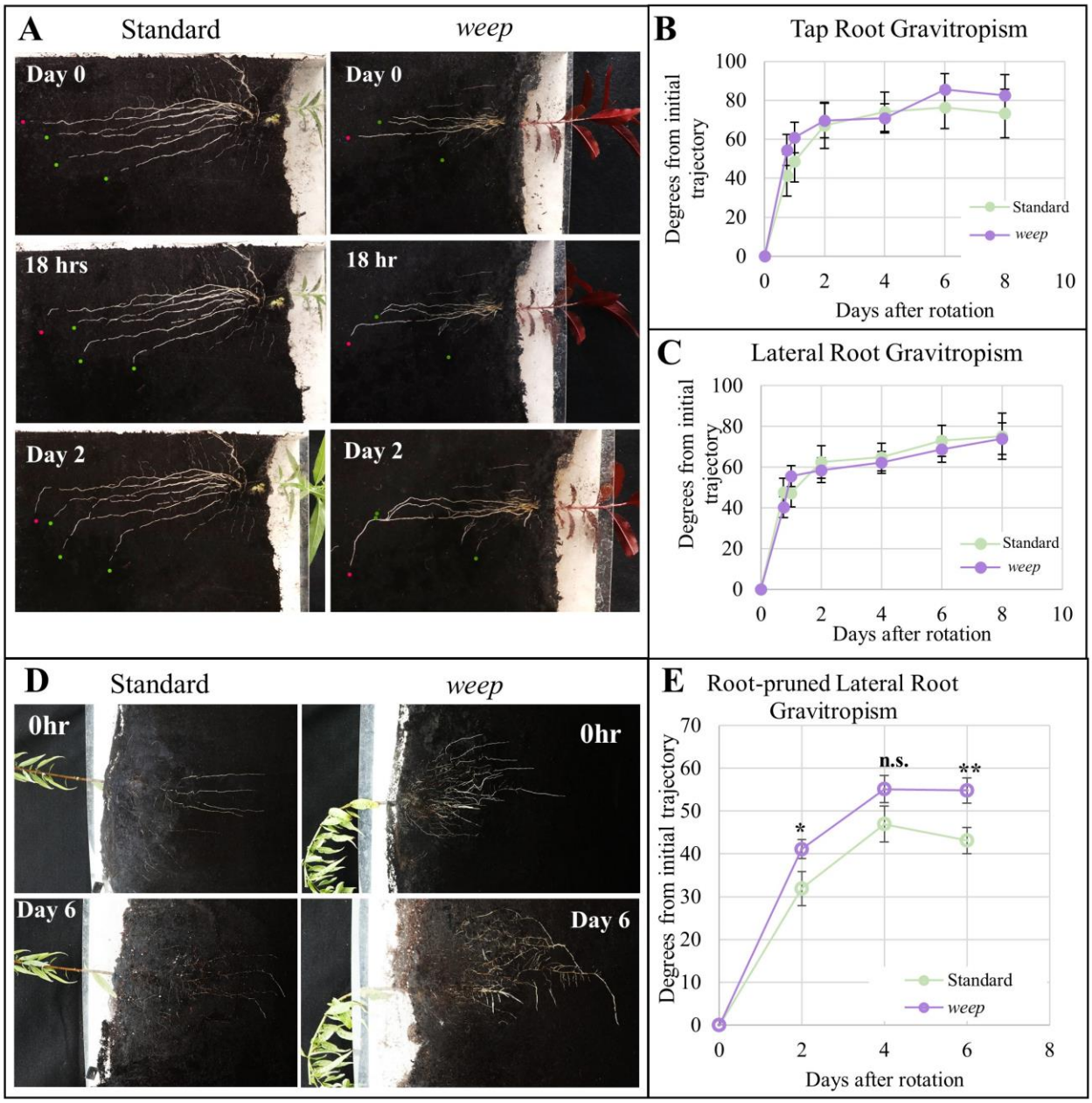

Figure 2.12: Root gravitropic responses. Standard and weep seedlings were rotated 90˚ and photographed over the course of 8 days to assess root gravitropic response (A). Roots were classified into taproot (pink dots) or lateral root (green dots), and the root tip angle of each type of root was measured from the initial trajectory (B-C). The same experiment was performed with root-pruned standard and weep seedlings (D). The root tip angle from initial trajectory was measured at 2,4, and 6 days (E). Contrast and brightness of photos adjusted for easy viewing. Pairwise comparisons done with t-tests. Error bars show standard error. * indicates significantly different at α=0.10; ** indicates significantly different at α=0.05; *** indicates significantly different at α=0.01.

seedlings (Figure 2.12 D and E). Root pruning increases root initiation and growth and enabled us to study larger numbers of roots that were uniform in age, stage of development, and size. This technique is commonly used to promote vigorous lateral root growth when transplanting fruit trees between pots, from pots to the field, or from nursery fields to commercial orchards. In total, seven root-pruned standard and seven root-pruned weeping peach seedlings were planted in our larger (1.5" x 2'x 2') rhizoboxes and grown upright for 24 days. Prior to reorientation, three to six vertically oriented secondary/lateral roots that initiated post pruning were selected for study, and root tip angle was measured from the initial trajectory of these roots. In this experiment, in response to 90-degree reorientations, weeping tree roots exhibited a faster gravitropic response than standard, having significantly greater lateral root tip angles (more vertical growth trajectories) at two and six days after reorientation (Figure 2.12 D and E). The lateral root tips angles for two genotypes were most similar at four days after rotation (Figure 2.12 E). Between four and six days, the standard root tip returned to a more horizontal trajectory, leading *weep* to once again have a significantly wider tip angle, relative to the initial trajectories of their lateral roots at six days after reorientation (Figure 2.12 E), supporting our earlier observations that *weep* peach lateral roots (Figure 2.11), as well as arabidopsis *weep* mutants (Johnson et al., 2020) have narrower set-point angles than controls.

Discussion

WEEP *directs the formation of the asymmetric auxin gradient needed for shoot gravitropism.*

Unlike other weeping *Prunus* trees, weeping peaches do not have greatly altered branch anatomy or decreases in branch stiffness. Changes in the proportion of xylem in the shoot tip are transient, disappearing by the end of the growth season (Figure 2.2 A and B). No significant differences in cellulose and lignin content or localization were detected between weeping and standard peaches (Figure 2.2 D-F). Furthermore, the flexural stiffness and other biomechanical properties of young shoots are not different between standard and *weep* (Figure 2.4). Collectively, these data suggest that weeping peach branches grow downwards and fail to reorient upwards not due to failure under self-loading, but because of an alteration in gravitropic response.

Several lines of evidence indicate that this altered shoot gravitropic response is due to an inversion of the auxin gradient in weeping peach trees shoots, which leads to positive (rootward) gravitropic shoot growth. To pinpoint the role of *WEEP* in the gravitropic pathway, we assessed gravitropic perception, gravitropic signal transduction, and gravitropic response in the *weep* peach mutant.

The normal endodermis development and amyloplast sedimentation in peach *weep* shoot tips suggest that *weep* shoots have normal gravitropic perception (Figure 2.5 A and B). This agrees with the previous finding that amyloplast sedimentation is normal in barley *egt2* mutant root columella cells (Kirschner et al., 2021). Next, we demonstrated *weep* shoots showed a normal bending response to unilateral auxin application. Notably, auxin application to the bottom of *weep* shoot tips could partially reverse the *weep* phenotype, causing them to grow upwards (Figure 2.6 A). Conversely, application of auxin to the top of standard shoots phenocopied *weep*'s downward bending of the shoot tip (Figure 2.6 B). Normal auxin response has also been observed in barley *egt2* roots, where auxin inhibits elongation and gravitropic bending in both wild type and *egt2* (Kirschner et al., 2021). Furthermore, a modest difference in cell size was detected between abaxial and adaxial cortical regions in standard branches, with larger cells on the abaxial side, but this asymmetry was not observed in weeping branches (Figure 2.3). As weeping peach trees are not impaired in either gravitropic perception or response, our results suggest the WEEP protein functions in gravitropic signal transduction upstream of the auxin gradient formation.

RNA sequencing from upper and lower shoot tip tissues from standard and weeping peach trees revealed inverted localization of early-auxin response gene expression in the *weep* mutant. Early auxin response genes provide a good marker for auxin localization, as they are rapidly upregulated by auxin (often within a few minutes). They are generally categorized in three classes: GH3s, AUX/IAAs, and SAURs, with1-amino-cyclopropane-1-carboxylate synthases (ACSs) sometimes included as a fourth class (Grossmann, 2010; Ren and Gray, 2015; Pei et al., 2019). The expression of these genes results in a highly interconnected network which immediately acts downstream of auxin to stimulate shoot elongation (Figure 2.8). Genes in all four classes were differentially regulated between upper and lower tissues in IN2 in both *weep* and standard (Figure 2.8 A and B, Supplementary Table S2.2). Specifically, they all exhibited higher expression on the lower side of standard peach shoots, but higher expression on the upper side of the weeping shoots (Figure 2.8 and Figure 2.18). The differential expression pattern in standard shoot tips suggests the mechanism behind the regulation of upward branch orientations aligns with the Cholodny-Went gravitropic response pathway: higher auxin concentrations on lower (abaxial) branch tip tissues likely promote upward growth trajectories by promoting cell elongation. Accordingly, the flipped expression pattern of the early auxin response genes in the weeping shoot tips suggests that the downward growth trajectory is due to a higher auxin concentration in the upper tissues. Similarly, the

inversion of the auxin gradient in *AtLAZY1*$^{L92A/I94A}$ branches resulted in a weeping phenotype and positively gravitropic shoots (Yoshihara and Spalding, 2020).

Of particular note is the large number of *SAURs* upregulated on the lower side of IN2 in standard and the upper side in *weep* (40 out of the 76 putative SAUR genes we identified in peach, Figure 2.18, Supplemental Table S2.3). *SAUR* genes have previously been identified as upregulated on the lower side of shoots during gravitropism in soybean (*Glycine max*) and arabidopsis (Ren and Gray, 2015; Wang et al., 2020). Most *SAURs* are very rapidly induced by auxin (often within 5 minutes) through the canonical $SCF^{TIR1/AFB}$ signaling pathway (Du et al., 2020). Auxin transport is necessary for asymmetric expression of *SAURs* during gravitropism, suggesting that this asymmetric expression is entirely generated by the auxin gradient, and there is no known alternative pathway for localization of *SAUR* expression (Du et al., 2020; Wang et al., 2020). Thus, *SAUR* expression is a reliable indicator of auxin localization. The upregulation of SAURS and representatives of all the other classes of early auxin response genes on the upper side of weep shoots leaves little doubt that the auxin gradient is inverted in *weep,* with higher levels of auxin on the top of outward-oriented *weep* stems (Figure 2.9).

Furthermore, *SAUR* expression is both necessary and sufficient for cell elongation. During shoot gravitropism responses, SAUR proteins on the lower side of shoots inhibit PP2C-D phosphatases from dephosphorylating H^+-ATPases (Spartz et al., 2014; Du et al., 2020). The phosphorylated H^+-ATPases are activated and pump protons out of the cell, hyperpolarizing the cell membrane. That hyperpolarization leads to water uptake by the cell and a resultant increase in turgor pressure, as well as apoplast acidification, which activates expansins and other cell wall remodeling enzymes (Spartz et al., 2014; Du et al., 2020). Collectively, these events lead to cell elongation on the bottom side of gravitropically stimulated shoots, reorienting the shoots upward. *SAUR* expression is necessary for auxin-mediated cell elongation as *saur* knockouts show dramatically reduced gravitropic responses and *pp2c.d2* mutants that are insensitive to *SAUR* regulation are also insensitive to auxin. *SAUR* expression is also sufficient to independently stimulate cell expansion. Plants with constitutive overexpression of *SAURs* exhibit enhanced cell expansion (Du et al., 2020; Wang et al., 2020).

In accord with the expected effects of *SAUR* expression on cell elongation, in standard peach shoot tips homologs of 60 arabidopsis cell expansion promoting genes *PACLOBUTRAZOL-RESISTANCE5* (*PRE5*), *EXPANSIN A1* (*EXPA1*), and *EXPA8* (*Prupe.3G269500*,

Prupe.1G276700, and *Prupe.2G263600*) are more highly expressed on the lower side of the shoot (Figure 2.8 A; Cosgrove, 2015; Shin et al., 2019). This correlates with the observation that standard shoot tips had slightly, yet significantly, larger cortical cells from lower (abaxial) branch tissues (Figure 2.3). In contrast, in *weep* shoot tips, the expression pattern of these genes is inverted, being more highly expressed on the upper side of the shoot. While cell size differences were not detected between cortical cells from the upper versus lower tissues of weeping branches, both increases in cell size and/or cell number on the upper side of branches could result in downward growth. A more comprehensive cell number and cell size analysis from a larger sample of branches may be needed to detect size asymmetry between the adaxial and abaxial tissues of weeping branches. The slight decrease in fiber cell size in weeping peach branches also suggests *WEEP* plays a role, direct or indirect, in cell elongation (Figure 2.2 G).

Collectively our gene expression data strongly suggest that there are increased auxin levels in the upper side of weeping branch tips as well as increased cell elongation gene activity in this region. Reduced expression of genes related to cell elongation was also observed in the root elongation zone of *egt2* mutants (Kirschner et al., 2021). Because *egt2* roots showed normal inhibition of growth when auxin was exogenously applied, Kirschner et al. concluded that *egt2* likely acted independently of auxin in control of cell elongation. Our auxin application data also show a normal auxin response in *weep* peach. However, the role of *WEEP* in controlling endogenous auxin transport within gravity stimulated tissues explains the alterations in cell elongation in upper versus lower tissues across weep shoots. Indeed, this hypothesis is more in accord with Kirschner's results than a direct role for *WEEP* in cell elongation, as *egt2* mutants in barley did not show altered root length (Kirschner et al., 2021)

In addition to the canonical effects of auxin localization on cell elongation, auxin localization is also essential for lateral organ boundaries and adaxial/abaxial patterning. Local auxin maxima are required for lateral organ initiation (Heisler and Byrne, 2020). While multiple theories have been proposed for determination of adaxial/abaxial polarity, several lines of evidence (including auxin applications, microdissections, application of polar auxin transport inhibitors, and confocal microscopy of PIN1 and auxin reporters) suggest that polar auxin transport and auxin localization is crucial to maintaining polarity (Shi et al., 2017; Heisler and Byrne, 2020; Burian et al., 2022; Wang et al., 2022). In accord with these data and the hypothesized role for WEEP in auxin localization, many tissue patterning genes showed inverted expression in *weep* IN1. Of these, five

were homologs of arabidopsis genes which formed a small gene network (Figure 2.7 B). Among these is YAB2, which is expressed on the abaxial side of lateral organs and is essential for organization of the shoot apical meristem and adaxial/abaxial differentiation (Stahle et al., 2009). Also in the group is BOP2, which is essential for proximal/distal patterning in leaves, radial patterning of flowers, promotes adaxial development, and upregulates LOB, which is essential for establishing the boundary between the meristem and lateral organs (Hepworth et al., 2005; Žádníková and Simon, 2014). Another member is *RPL,* which represses *AGAMOUS* and is involved in floral whorl differentiation and specification of phyllotaxy (Bao et al., 2004; Gish, 2013). Finally, *STIP* controls cell fate in the meristem, repressing *WUSCHEL,* promoting cell division, and preventing differentiation (Wu et al., 2005). Together, the altered localization of these genes in *weep* suggests that the mislocalization of auxin may be affecting meristem patterning.

The inversion in auxin gradient and tissue polarity may also result in a mislocalization of tension wood in weeping peaches. Although cellulose and lignin staining and extractions did not indicate the presence of tension wood in either adaxial or abaxial regions of standard or *weep* branches (Figure 2.2 C and D), our RNAseq data did show differential expression of genes associated with tension wood.

High *FLA* expression is associated with tension wood formation in *Eucalyptus,* willow (*Salix*), and poplar (*Populus*; Qiu et al., 2008; Gritsch et al., 2015; Wang et al., 2017). The arabidopsis homolog *AtFLA12* is a crucial trigger of cellulose microfibril deposition in stem vascular tissues (MacMillan et al., 2010). Double mutants of *Atfla12* and related gene *Atfla11* have even further decreases in cellulose content and higher microfibril angles (MacMillan et al., 2010). Thus, FLAs appear to induce both the higher cellulose content and lower microfibril angles, which are characteristic of tension wood. Four homologs of *AtFLA12* were upregulated on the upper side of standard peach shoots. This was consistent with the expression pattern of the eucalyptus homologs of *AtFLA12, EgrFLA1* and *EgrFLA2,* and indicates tension wood formation in the upper portion standard peach branches (Qiu et al., 2008). In contrast, all four peach homologs were upregulated on the lower side of weeping shoots. Accordingly, the downward curvature of weeping shoots may be associated with the formation of tension wood on the lower side of *weep* branches.

Further research is needed to understand how the formation of tension wood is connected to the gravitropic auxin gradient in young shoots which are undergoing both elongation and radial growth through xylem formation. Tension wood formation is associated with upregulation of auxin,

ethylene, and gibberellic acid (GA) signaling, and FLAs are upregulated by GA in poplar (Gerttula et al., 2015; Wang et al., 2017). Yet, in young shoots, such as we assessed here, genes upregulated by auxin, ethylene, and GA are all coordinately expressed on the lower side of the shoot, opposite the location of tension wood. Indeed, a homolog of the rate-limiting enzyme for ethylene biosynthesis, 1-amino-cyclopropane-1-carboxylate synthase 8 (ACS8) was upregulated 7-fold on the lower side in standard, but 76-fold on the upper side in weep. Similarly, the homolog of GA20OX3, a GA synthesis enzyme, is 3-fold upregulated on the lower side in standard and 4-fold upregulated on the upper side in *weep.* One possible solution is to look at auxin flux not at the epidermal cells (which are involved during primary growth in shoot elongation) but at the vascular cambium, where xylem formation is taking place (Gerttula et al., 2015). Under this paradigm, during gravitropism auxin is moving away from the epidermis in the upper part of the branch, but toward the vascular cambium, stimulating xylem development and tension wood formation (Gerttula et al., 2015). On the lower part of the branch, auxin is moving away from the vascular cambium, and toward the epidermis, promoting cell elongation. In *weep* the auxin flux would be toward the vascular cambium on the lower side, and toward the epidermis on the upper side, which would be consistent with the formation of tension wood on the lower side of the branch and increased cell elongation on the upper side.

WEEP *contributes to the regulation of root gravitropic set-point angle by promoting polar auxin transport.*

In agreement with studies in other species (Kirschner et al., 2021; Johnson et al., 2022), we found the weeping peach root system displays decreased lateral root angles, a narrower convex hull, a faster positive gravitropic response, and a more vertical setpoint angle. This is a strong contrast to the phenotype of plants with mutations in multiple *LAZY* family genes associated with root architecture (i.e., *AtLAZY2/DRO3, AtLAZY3/DRO2,* and *AtLAZY4/DRO1*). While the shoots of both arabidopsis *lazy1,2,4* (also known as *lzy1,2,3*) and *lazy2, 3, 4* triple mutants have a weeping phenotype, their roots are negatively gravitropic, and grow upward in the direction of the shoot (Ge and Chen, 2016; Taniguchi et al., 2017; Yoshihara and Spalding, 2017). As in shoots, auxin gradients are required for gravitropic responses in roots and auxin concentrations are higher in the lower tissues. But, in contrast to shoots, high auxin concentrations in roots inhibit cell elongation. In both types of lazy triple mutants, the gravitropic auxin gradient is inverted and the high auxin concentration at the upper side of the root inhibits growth on the upper side, causing the root to

grow upwards (Taniguchi et al., 2017; Yoshihara and Spalding, 2017; Ge and Chen, 2019). Since weeping peach roots have an enhanced positive gravitropism, it seems unlikely that the auxin gradient is inverted in their roots, although it is worth investigating. However, root response to auxin is very dosage dependent, as low levels of auxin in the upper tissues of gravistimulated roots stimulate the elongation that promotes downward growth (Du et al., 2020). Both shoot and root angles are narrower (more vertical) in mutants with higher auxin or auxin response, while mutants with lower auxin or auxin response show wider lateral angles (Roychoudhry et al., 2013).

Study of root gravitropism in dicots is also complicated by the differences between taproots and lateral roots. After all, lateral roots do not grow vertically down. Rather, as with lateral branches, lateral roots grow at a genetically-encoded angle from the gravity vector known as the gravitropic set-point angle (GSA) (Roychoudhry et al., 2013). The mechanism by which lateral organs maintain their GSA is unknown, however, GSA in roots appears to be controlled by auxin transport modulated by cytokinin (Waidmann and Kleine-Vehn, 2020),and auxin homeostasis is likely crucial to setting the balance between the two.

We hypothesize that the WEEP protein functions in both shoot and root gravitropism pathways, as well as in GSA maintenance by modifying polar auxin transport to create auxin gradients. More specifically, we suggest that the WEEP protein promotes the upward shoot growth by promoting the transport of auxin to lower tissues of gravistimulated vertical shoots and upward orientated lateral branches. In roots, we suggest that WEEP promotes the maintenance of non-vertical downward lateral root growth through a homeostasis mechanism that decreases the auxin gradient between upper and lower tissues by promoting the movement of auxin to upper side of lateral roots. Essentially, the WEEP protein may be a key player in the maintenance non-vertical growth. Further experimentation is needed to investigate the mechanism by which WEEP controls auxin homeostasis and transport during or following gravity perception. However, WEEP may directly or indirectly modify the localization of the PIN3 auxin efflux proteins in the plasma membrane of statocytes. Our rational for this is as follows. PIN protein localization is controlled by endosomal trafficking regulated by the PINOID kinase, which phosphorylates PIN proteins (Kleine-Vehn et al., 2009; Rakusová et al., 2015; Zhang et al., 2020). SAM domain proteins are known to be involved in vesicle trafficking; arabidopsis SAM1 interacts with four vesicle trafficking proteins (Wang et al., 2011), and STIM1, a human SAM protein, interacts with microtubules (Grigoriev et al., 2008). WEEP homologs are known to localize to the plasma membrane and cytoplasm (as well

as the nucleus) (Kee et al., 2009; Guo et al., 2023). Arabidopsis WEEP protein (AtSAM5) interacts with the nuclear- and plasma-membrane-localized kinase CPK13, (Denay et al., 2017). Collectively, those findings and our own suggest WEEP might regulate PIN phosphorylation at the plasma membrane. Alternatively, WEEP may act elsewhere, or additionally in the transcriptional regulation of vesicle trafficking. The mutant of the barley *WEEP* homolog, *egt2,* showed upregulation of exocyst complex component 7 (EXOCYST70A3), which is known to be involved the distribution of PIN4 and root gravitropic responses (Ogura et al., 2019; Kirschner et al., 2021). Self-oligomerization of WEEP proteins through their SAM domain may also be key to its function. Oligomerization through these domains is essential for the subcellular localization and activity of some SAM proteins (Denay et al., 2017). Oligomerization through the SAM domain is essential to the action of LFY as a transcriptional regulator (Sayou et al., 2016). Regardless of whether WEEP acts at the plasma membrane, the nucleus, or both, the absence of any known protein motifs besides the SAM domain suggests that WEEP may serve as a scaffold or structural protein regulating the formation of protein complexes.

Conclusion

Collectively, our peach shoot and root data provide exciting additions to our understanding of how plants respond to gravity and maintain non-vertical growth orientations. *WEEP* promotes negative gravitropism in both shoots and roots. In peach shoots, which are normally negatively gravitropic, a mutation in *WEEP* leads to a positively gravitropic phenotype, where the shoots grow towards the ground. Strikingly, *weep* mutant lateral roots do not lose their gravitropism, but show an enhanced positive gravitropism phenotype. Roots of peach *weep* have a narrowed set-point angle, and enhanced gravity response. This narrowed angle may useful for developing rootstocks for agricultural and ornamental applications, as deeper root systems can improve drought avoidance, nitrogen acquisition, and plant stability (Uga et al., 2013; Paez-Garcia et al., 2015; Li et al., 2016; Jiao et al., 2021). The transcriptomic evidence we present here suggests that the WEEP protein is necessary for normal establishment of a gravitropic auxin gradient in peach shoots, and that gradient is inverted in weeping peach shoot tips. Further research is needed to elucidate whether the WEEP protein plays a role in auxin localization in shoots by promoting PIN3 protein localization or whether it acts through an orthogonal mechanism. The absence of a clear shoot phenotype in barley, wheat, and arabidopsis *weep* mutants suggests the processes of lignification

and/or altered tension wood localization are necessary to “freeze” the curvature in time and produce a visible phenotype.

Materials and methods

Plant material.

Experiments used 1- to 4-year-old standard and weeping peach trees grafted on Halford rootstock, unless otherwise noted. The peach scions originated from the segregating F2 population used to map the *weep* gene (Hollender et al., 2018). Trees were grown in pots ranging in size from 1- to 15-gallons in standard greenhouse conditions, with supplemental lighting to maintain an approximately 16-hour photoperiod. Dormancy requirements were met by placing the trees once or twice a year into a 4˚C dark cold room for at least six weeks at a time.

Sectioning for pith and xylem measurements.

Actively growing shoot tips and dormant first-year branches with outward growth orientations were hand-sectioned with a double-edged razor blade. Actively growing shoot tips were sectioned at approximately 6 cm below the shoot apical meristem from three shoot-tips per tree with four trees for each genotype. Dormant branches were sectioned at about 6 cm below the tip from three shoot-tips per tree, with four trees for *weep,* and three trees for standard. Three clean sections were taken from each shoot tip. The sections were stained with 1 mg/ml Toluidine blue freshly diluted to 50% in water and photographed using a Nikon SMZ800N dissecting microscope with a Nikon DS-Fi3 camera.

Each of the three sections was measured in ImageJ using the polygon measuring tool. The pith was measured by tracing around the parenchyma cells. Xylem was measured around the outside of the rays where toluidine staining was clearly visible. The total area of the section was measured tracing around the outermost cells of the epidermis, which were clearly stained.

Data were modeled using the lme4 library in R (v. 4.2.1) with blocking by tree and by shoot tip (response= mean + Genotype + Tree:Genotype + Shoot_Tip:Tree:Genotype + error, where response is the pith area or xylem area, Genotype is the effect of genotype, Tree is the effect of the individual tree, nested within genotype, and Shoot_Tip is the effect of the shoot tip, nested within tree and genotype. The effects of tree and shoot tip were treated as random variables. Data were assessed for normality and equal variance, then pairwise comparisons between genotypes were performed using emmeans to apply two-tailed t-tests assuming equal variances.

Sectioning, staining, and imaging for tension wood.

Actively growing branches from standard and *weep* shoots were collected from the area of the branch that was outward oriented and directed or bending upward (standard) or downward (weep). The top of the shoot was identified with a nick in the cortex and a 50-100um fresh sections were taken with a vibratome. These sections were stained using toluidine blue O (0.02% in H_2O) and Phloroglucinol-HCl (1 volume HCl: 2 volumes 3% phloroglucinol in ethyl alcohol) (Mitra and Loqué, 2014). Sections were imaged with a Nikon Eclipse Ni compound microscope with a Nikon DS-Fi3 color camera and NIS-Elements BR 4.60.00 software (Nikon), using the manual real-time EDF function. Finally, images were stitched together using the pairwise stitching function in Fiji, using linear blending for fusion, with 5 check peaks, ignoring zero values when fusing, and computing overlap (Preibisch et al., 2009)

Wood composition.

Segments, approximately 1.5 cm in length, were taken from two-year-old wood from weeping and standard peach branches from the original mapping population at the USDA Appalachian Fruit Research Station (Kearneysville, WV). At collection time the 'upper' and 'lower' (adaxial and abaxial) sides of the branches with respect to gravity were marked. These segments were then bisected longitudinally, the bark and pith were removed, as well as some of the edge regions orthogonal to the gravity vector. This produced roughly trapezoidal shaped fragments of wood representing the woody growth of the top or bottom of a branch. These were cut into roughly 0.5 x 0.5 cm pieces with a sharp razor, extracted in series with 70% EtOH and 100% acetone, each overnight. Then, samples were dried and ball milled into a fine powder. The crystalline cellulose content, non-cellulosic polysaccharide content, acetyl-bromide soluble lignin content, and lignin monomer content were then assessed as described previously (Foster et al., 2010a; Foster et al., 2010b). For each measurement, three technical replicates were performed for four biological replicates per sample type.

Data were modeled using the lme4 library in R (v. 4.2.1) with blocking by sample (response= mean + Genotype + Side + Genotype*Side + sample:Genotype + error where response is the cell wall polymer, Genotype is the effect of genotype, Side is the effect of top or bottom, Genotype*Side is their interaction, and sample is a random variable nested within genotype. Data were assessed for normality and equal variance, then all pairwise comparisons were performed using emmeans to

apply Tukey tests assuming equal variances. Paired t-tests between top and bottom within a genotype were performed in Excel.

Fiber cell measurements.

Wood samples from the top and bottom of dormant two-year old branches were dissected as described for wood composition and then cut into approximately 1 x 0.2 cm 'match sticks.' Samples were then macerated by the addition of 10 mL of Franklin's solution (50% acetic acid, 4% hydrogen peroxide) and incubation at 60°C for 2-3 days, followed by heating in a boiling water bath for 10 minutes. Franklin's solution was then removed, and the samples were then washed at least three times with 10 mL H_2O. Vigorous mixing by vortex was then able to fully break apart the fiber cells (Chaffey, 2002; Franklin, 1945). Fiber cells were stained with 0.01% Safranin O in H_2O, mounted on microscope slides, and 12 pictures per sample were taken. The length of all full-length fiber cells visible in each picture were measured with NIS Elements (Nikon) and the data were exported to excel. Statistical analysis was performed as described for wood composition, except ANOVA was significant, so t-tests were used.

Wood material properties testing.

Three-point bending tests were conducted using a universal testing machine (Instron© Model 4202, Instron Corporation; Kern et al., 2005). Tests were performed on four shoot tips per tree, for three standard and four *weep* trees). Shoot tips were selected to have 2-3 mm diameter. Approximately 10 cm segments were used, starting 3 cm beneath the shoot apex, as the shoot's stiffness varied widely in the first 3 cm, but were reasonably consistent from 3 cm on down. The top of the shoot was placed downward so that the top of the shoot was under tension and bottom under compression, as it would be under self-loading. The total span length was 8cm, with the cross-head centered. The load was applied until failure using a 50 N load cell and a cross-head constant speed of 20.00 mm/min.

Modulus of rupture (MOR) was calculated as $MOR= (½F\max)(a)(R_2)/I$, where "Fmax" is the maximum force recorded by the Instron, "a" is the distance between the post and load, "R_2" is the radius of the sample perpendicular to the direction of the load, and I is the second moment of inertia. I was calculated for an elliptical cross-section as $I=(\pi)(R_1)^3 (R_2) /4$, where "R_1" is the radius in the direction of the load. Flexural stiffness (EI) was calculated using the linear (elastic) portion of the stress/strain curve. $EI=(F/V)(a^2/12)(3L-4a)$, where F/V is the slope of the

stress/strain curve, and L is the total span length. Modulus of elasticity (MOE) was calculated as MOE=EI/I.

Amyloplast staining of vibratome sectioned tissues.

An area of about 1 cm below the apex was cut into approximately 50 μm radial sections, using a Vibratome Series 1000 sectioning system. These were stained with 100% Lugol's iodine solution for several seconds, de-stained in water, and immediately observed under a Nikon ECLIPSE Ni upright microscope with a Nikon DS-Fi3 camera.

Tissue collection, fixation, and embedding for amyloplast sedimentation and cell size analysis.

Shoot tips were harvested and cut to separate apices from the 0.5 cm long stem section below them. Cuts were done so that the orientation of the 0.5 cm stem samples relative to the shoot tip could be determined, and tissues were marked with a permanent marker to denote the direction of the gravity vector. Next, they were immediately submerged in ice-cold fixative (2.5% glutaraldehyde / 2.5% formaldehyde / 0.1 M sodium cacodylate buffer, pH 7.2). Samples were vacuum infiltrated for 30 min at room temperature and then the fixative was replaced with fresh solution. This process was repeated once before storing the samples in fixative at 4°C until embedding. Prior to dehydration and embedding, drawings of each sample were done to preserve the gravity vector information (this was possible because the samples were sufficiently asymmetrical). At the start of the embedding process, fixative was removed, and samples were washed three times with 0.1 M sodium cacodylate buffer (pH 7.2) before dehydrating them with increasing concentrations of acetone (30%, 50%, 70%, 80%, 90%, 100%, 100%, 100%). Samples were vacuum infiltrated for 30 minutes at each concentration then gently shaken for 30 minutes in fresh solution, and then shaken overnight in 100% acetone. Next, tissues were gradually infiltrated with increasing concentrations of a modified low-viscosity epoxy resin (10 g ERL-4221 (vinyl cyclohexene dioxide), 6 g D.E.R. 736 (diglycidyl ether of polypropylene glycol), 26 g NSA (nonenyl succinic anhydride), and 0.2 g DMAE (dimethylaminoethanol); Spurr, 1969). Spurr:acetone solution ratios in order were 1:3, 1:3, 1:2, 1:1, 2:1, 3:1, with four 100% Spurr incubations. Each concentration was carried out for one full day. In the morning, samples were vacuum infiltrated for 1 hour in the solution for that day and then shaken in fresh solution for at least 5-12 hours. This process was repeated in the evening. At the end of the infiltration sequence, tissues were positioned in block molds with respect to the gravity vector and polymerized in Spurr resin at 60 °C for 48-72 hours.

Sectioning, staining, and imaging for amyloplast sedimentation and cell size analysis.

Tissues were sectioned with a diamond knife and an RMC PTXL ultramicrotome in the Center for Advanced Microscopy (Michigan State University, East Lansing, MI). Three samples were sectioned per genotype and tissue type (12 samples total) at 1 μm thickness. To control for location in the tissue, each sample was sectioned to the approximate center, where the pith was the widest. After adhering the plastic sections to glass slides using a hot plate, they were stained with a 25% toluidine blue and basic fuchsin solution (Electron Microscopy Sciences Cat #14950). Sections were imaged with a Nikon Eclipse Ni compound microscope with a Nikon DS-Fi3 color camera and NIS-Elements BR 4.60.00 software (Nikon).

Cell size analysis.

For cell size analysis, sections were photographed 40x magnification and a length of stem approximately 900μm long without lateral buds or flaws in the section was identified. A rectangle was drawn to identify the upper and lower cortex including which fell within this 900 μm length, and both upper and lower cortex were imaged at 100x magnification (Figure 2.3A). These images were cropped to contain only epidermis, cortex, and endodermal cell files (collectively referred to here as the cortex). Contrast was adjusted as needed, and cell debris or cells from adjacent lateral buds were hand-masked from the images if they could not be excluded by cropping. The images were then batch processed using MIPAR Image Analysis Software v4.3.0 to segment out the cells and measure cell area, cell length, and cell width. The segmentation recipe had the following steps: 1) Adjust Contrast: low 26, high level 216, gamma=1; 2) Adaptive threshold: 103 percent, window 208px, selecting bright; 3) Reject features: Aspect ratio>11; 4) Reject features: Area>13,000px; 5) Fill all holes; 6) Uniform dilation: 2px; 7) Uniform erosion: 3px; 8) Smooth features: Window size 3, Threshold 0.54; 8) Separate Features: High resolution, separation=2; 9) Reject Features: Aspect Ratio>7; 10) Fill all holes; 11)Reject Features: Area</= 200px. After this segmentation process, the following feature measurements were taken: area, cell length (length-X), and cell width (length-Y). For statistical analysis, data were modeled using the lme4 library in R (v. 4.2.1) as discussed for wood composition.

Auxin applications.

Auxin was applied to young shoots (1.5-5cm long) on greenhouse-grown trees. 1% w/w IAA in lanolin (100 μl of 100 mg/ml IAA in 1 M KOH per 1 g of lanolin) or lanolin control (100 μl 1 M KOH per 1 g of lanolin) was applied unilaterally to either the top or the bottom of the shoot. Three

replicates of each treatment (IAA top, control top, high IAA bottom, and control bottom) were performed per tree, for two trees per genotype. Shoots were photographed at the beginning of the experiment, and at 1, 2, 3, and 7 days after application.

For detached shoots, growing shoot tips were collected in the summer of 2020 from a field planting in Clarksville, MI from three-year-old trees of *weep* and the standard cultivar 'Bounty'. Three replicates were performed per treatment, and the experiment was repeated twice. After removing the leaves, twigs were placed upright in distilled water under 16-hour (first replicate) or 24-hour (second replicate) light at room temperature. The twigs were first allowed to acclimate for 12+ hours to avoid gravitropic curvature responses, then 1% auxin/lanolin paste (100 µl of 100 mg auxin/ml 1 M KOH stock solution /g lanolin) or control paste (100 µl 1 M KOH stock/g lanolin) was applied to one side of each twig. Photographs of the twigs were taken every 5 minutes for 5 days using a Canon EOS M5 camera.

RNA sequencing and read alignment.

For RNA sequencing, we selected actively growing branches with an outward orientation (roughly perpendicular to the gravity vector). Each shoot tip was collected separately. Two sections were collected: internode 1 (IN1; from the shoot apex to the base of the first elongated internode) and internode 2 (IN2; the next elongated internode). Each section was bisected into top and bottom with respect to the gravity vector, and the samples were immediately flash-frozen in liquid nitrogen. RNA was extracted using the EZNA SQ Total RNA kit followed by the Zymo RNA clean-up kit with DNA digestion.

All four sample types (IN1 top, IN1 bottom, IN2 top, and IN2 bottom) were sequenced for two shoot tips per tree, for two trees per genotype. Library preparation and sequencing were performed by the Michigan State University Genomics Core. Libraries were created using Illumina Stranded mRNA Prep and indexed with IDT for Illumina RNA UD Indexes. Quality control and quantification for the libraries were performed using a combination of Qubit dsDNA HS and Agilent 4200 TapeStation HS DNA1000 assays. A single pool, with equimolar proportions of each library, was quantified using the Kapa Biosystems Illumina Library Quantification qPCR kit. The pool was loaded onto three lanes of an Illumina HiSeq 4000 single read flow cell and single end 50 bp sequencing was performed using HiSeq 4000 SBS reagents. Base calling was performed using Illumina Real Time Analysis (RTA) v2.7.7 and the output of RTA was demultiplexed and converted to FastQ format with Illumina Bcl2fastq v2.20.0.

FastQ files were processed in CLC Genomics workbench v22. For each library, the data from all three lanes were merged into a single file prior to adapter and quality trimming. Using the trim reads tool set to remove adaptor and following sequence (3' trim), all files were trimmed for the Illumina Stranded mRNA Prep adaptor (CTGTCTCTTATACACATCT). The mismatch cost =2, gap cost=3, minimal internal match score=10, minimum end match score=4. No homopolymer trimming or filtering based on length. Following adaptor trimming, the trim reads tool was run again to perform quality trimming, with a quality score limit of 0.001 and maximum of 2 ambiguous nucleotides.

Trimmed reads were aligned to the *Prunus persica* genome v. 2.0 (Verde et al., 2017). For RNAseq alignment, CLC Genomics v22.0 the RNA-Seq Analysis (GE) tool was used with parameters as follows: reverse strand specificity, library type= no 3' bias, mismatch cost=2, insertion cost=3, deletion cost=3, length fraction=0.9, similarity fraction=0.8, with a maximum number of hits=6, expression value=RPKM.

Transcriptome analysis.

For differential expression analysis, the CLC Differential Expression for RNA-Seq tool was used to compare differential expression between upper and lower shoot tip for each genotype by internode combination, controlling for the effect of shoot tip (biological replicate). No filtering was applied prior to FDR calculation.

Heatmaps and network analysis.

Genes of interest (GOI) were selected for each internode as those genes that, in either weep or standard, had a Bonferroni of <0.01 and a 2-fold change. This identified 97 GOI for IN1, and 213 GOI for IN2. Heatmaps were created using the ggplot2 package in R. The best arabidopsis homolog of each gene was identified from the Genome Database of the Rosaceae, which uses a blastx algorithm with an expectation value cutoff of 1 e^{-6} (Jung et al., 2019). 81 arabidopsis homologs were identified for the 97 peach IN1 GOI and 164 arabidopsis homologs were identified for the 213 peach IN2 GOI.

To further assess gene interactions and identify functional groups, STRING (v. 11.5) was used to create an interaction network for the arabidopsis homologs with a medium confidence cutoff for interactions (0.4) and a FDR stringency of 5%. The IN1 network had 29 edges, with a p value of $1.79e^{-10}$. The IN2 network had 449 edges, with a p-value of <1 e^{-16}).

To visualize the network, it was imported into Cytoscape (v. 3.9.1). Since multiple peach homologs sometimes mapped to a single arabidopsis gene, the best peach homolog for each arabidopsis gene was manually selected based on the alignment score, and expression values based on the best peach homolog were assigned that arabidopsis homolog. Expression values were mapped to the node color. The protein annotations from STRING were used to manually assign each gene to a functional category, which was mapped to the node outline. Confidence scores for edges ranged from 0.4 to 1 and were mapped to a line width of 0.5 to 8.0.

Protein expression vector cloning.

The *Prunus persica* WEEP coding sequence was PCR amplified using primers JA_211 (5'-CTGTACTTCCAGATGATGATGAGGGAGATGAGCAAAGA-3')and JA_212 (5'-GTGAGACCACGCAGATGGTTCCAGCTTCAAGGA-3'). The pMal-Strep vector was linearized by PCR using primers JA_205 (5'-TCTGCGTGGTCTCACCCG-3' and JA_206 (5'-CATCTGGAAGTACAGGTTCTCCCC-3'). The resulting PCR products were assembled using Infusion cloning (Takara) to create the pMal-Strep-WEEP.

Protein expression, purification, and size exclusion chromatography.

WEEP protein was expressed with N-terminal 6xHis and maltose binding protein (MBP) tags and a C-terminal StrepTagII. WEEP protein was expressed in *E. coli* NEB Express cells (New England BioLabs). Bacterial cultures were grown at 37 ºC to an OD_{600} of ~0.6, induced with a final concentration of 1 mM isopropyl β-D-1-thiogalactopyranoside (IPTG), then grown overnight at 18 ºC. Bacterial cells were pelleted by centrifugation at 5,000 g for 10 minutes, then resuspended in lysis buffer (50 mM tris pH 8.0, 20 mM imidazole, 500 mM NaCl, 10% (v/v) glycerol, 1% Tween-20) supplemented with 1,000 units of lysozyme and 25 units of benzonase nuclease (Millipore Sigma) per ml. Cells were lysed by sonication and cell debris was pelleted by centrifugation at 10,000 g for 45 minutes at 4 ºC. The soluble cell lysate was passed through a 0.22 μm filter and then loaded onto to a Ni-NTA chromatography column. The Ni-NTA column was washed with wash buffer (50 mM tris pH 8.0, 20 mM imidazole, 500 mM NaCl, 10% (v/v) glycerol), and bound protein was eluted with elution buffer (50 mM tris pH 8.0, 250 mM imidazole, 500 mM NaCl, 10% (v/v) glycerol). To obtain higher purity full length WEEP protein, the eluted protein was next loaded onto a StrepTactin Sepharose column (IBA Life Sciences). The column was washed with buffer W (100 mM Tris pH 8.0, 150 mM NaCl, 1 mM EDTA) and the bound protein eluted with buffer E (100 mM Tris pH 8.0, 150 mM NaCl, 1 mM EDTA, 2.5 mM

desthiobiotin). The eluted protein was concentrated to 1 mg/ml using Amicon Ultra 10 kDa MWCO filters (Millipore Sigma). Size-exclusion chromatography was performed using a Superose 6 10/300 GL column (Cytiva) equilibrated with 1x phosphate buffered saline (PBS) pH 7.4. All protein quantification was done using the Qubit Protein Assay (Invitrogen).

Root architecture analysis.

Vernalized peach seeds collected from field-grown standard and weeping peach trees were planted in rhizoboxes with 1.5" x 2'x 2' internal dimensions made of opaque white plastic, with a single clear plexiglass side. These were filled with a commercial soil mix without perlite (Sta-Green Tree & Shrub Garden Soil), placed at a 45˚ angle with the plexiglass side oriented down and covered with black felt, and grown in standard greenhouse conditions. The root systems of eight standard peach trees and 10 weeping trees were imaged weekly with a Canon EOS M5 camera from 2 weeks after planting until 10 weeks after planting. Week 4 and week 9 were selected as representative weeks for image analysis for quantitative measurements.

Images were analyzed in RootNav 1.8.1 (Pound et al., 2013; https://sourceforge.net/projects/rootnav/). Some root systems had secondary roots that were co-dominant with the primary root and had tertiary roots branching from them. Because RootNav does not have a setting for tertiary roots, these large secondary roots were identified in RootNav as primary roots, and the tertiary roots off them as secondary. Lateral root number is reported as the total number of secondary and tertiary roots, calculated as (the number of "primary" roots in RootNav - 1) + (the number of "secondary" roots in RootNav). For week 4 data, the entire visible root system was traced, and used to calculate root tip angle, convex hull, and lateral root number. For week 4, primary, secondary, and tertiary roots were used to calculate root tip angle. For the week 9 data, due to the increased complexity of the root system, each image was analyzed twice. First, the entire system was traced and used to calculate convex hull and lateral root number. Second, the main primary root was traced along with a subset of secondary lateral roots which emerged between 80 and 300 mm from the start of the primary root and were visible from emergence to tip. These lateral roots were used to estimate root tip angle and emergence angle. For convex hull and lateral root number, pairwise comparisons between the genotypes were performed using t-tests in Excel, after checking whether the data were normal with equal variances in R (v. 4.1.2 and v.4.2.1). Since previous studies had shown a decrease in lateral root angle for weep mutants, t-tests for tip angle, emergence angle, and convex hull were one-tailed. Because

alterations in lateral root number had not been previously reported, tests for lateral root number were two-tailed. Each test assumed heterogenous or equal variances as appropriate to the data.

Root gravitropism study using seedlings with tap roots.

Five standard and nine weep peach seedlings were planted in small rhizoboxes, with internal dimensions of 1.5" x 7" x 11". At 18 days old they were photographed with a Canon EOS M5 camera and rotated 90˚. After rotation they were photographed at 16 hours, 1,2,4,6, and 8 days. Using the pre-rotation photograph only, one taproot was identified per tree, using the criteria that the taproot was the longest root, with the most lateral roots growing down the length of the root. If those criteria did not point to the same root, or two roots were roughly equivalent for both criteria, the root with the most vertical orientation was selected. All other roots were classified as lateral. Roots were excluded from analysis if they failed to grow or ran into another root or the edge of the box before Day 2. This left 12 standard lateral roots and 21 weep lateral roots for analysis. ImageJ was used to measure the angle between the initial root tip trajectory and the trajectory at each timepoint.

The effects of genotype and root type were modeled for each timepoint individually using the lme4 library in R (v. 4.3.1). using the equation Response= mean + Genotype+ Root_Type + Genotype*Root_Type + error, where Response is the root angle at a particular timepoint, Genotype is the effect of genotype, and Root_Type is the effect of the type of root. Due to the low number of roots per seedling, including the random effect of tree led to a singularity error, so the effect of tree was not included. Data were assessed for normality and equal variance and gated with ANOVA, then pairwise comparisons between each Genotype and Root_Type combination were performed using emmeans to apply two-tailed Tukey's tests.

Root gravitropism study using root-pruned trees.

Seven standard and seven *weep* peach seedlings approximately six months old had their roots pruned to a total length of about 10 cm,, lateral roots were thinned into a single plane, and the shoot was pruned to approximately 30 cm. Seedlings were transplanted into our large (1.5" x 2'x 2') rhizoboxes (constructed as previously described) and allowed to grow for 24 days, until the seedlings had about 15-30 cm of visible new root growth. Boxes were then photographed with a Canon EOS M5 camera and rotated 90˚. After rotation they were photographed at 3, 6, and 9 hours, 1-6 days, and again at 16 days.

3-6 roots per plant which were vertically oriented prior to rotation were selected for measurements. Root angle was assessed at 2 days, 4 days, and 6 days. Each root was then assessed for whether they grew and responded to gravity. After excluding roots that failed to grow or were otherwise un-measurable, 50 roots remained for analysis. ImageJ was used to measure the angle between the initial root growth trajectory and the root tip angle trajectory.

Because there were interaction effects between the genotype and the timepoint, the effect of genotype was modeled slicing by timepoint using the lme4 library in R (v. 4.2.1) with blocking by tree (Response= mean + Genotype + Tree:Genotype + error, where Response is the root angle at a particular timepoint, Genotype is the effect of genotype, and Tree is the effect of the individual tree, nested within genotype. The effect of tree was treated as a random variable. Data were assessed for normality and equal variance, then pairwise comparisons between genotypes were performed using emmeans to apply two-tailed t-tests assuming equal variances.

Acknowledgements

The authors acknowledge Kat Rockwell and Emma Grant for assistance with tree care and imaging, Peter Kohler for assistance with data formatting and statistical analysis, and Dr. Miranda Haus for guidance on root analyses.

Funding

This work was funded by United States Department of Agriculture National Institute of Food and Agriculture grant #2018-67013-27457 (to CAH and FWT), the United States Department of Agriculture National Institute of Food and Agriculture HATCH project 1013242 (to CAH), and the National Institutes of Health R35GM136338 (to L.C.S.).

Conflict of interest statement

The authors declare that they have no conflict of interest.

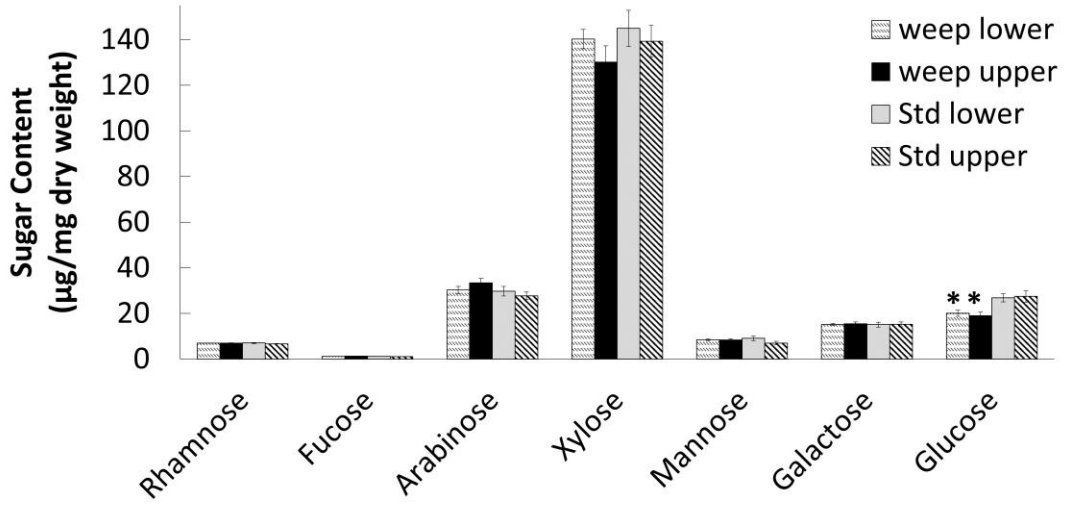

Figure 2.13: **Neutral sugar content of hand dissected standard (Std) and weeping (weep) tissues from upper and lower regions of each branch.** Glucose levels were significantly lower in weeping branch tissues compared to standard branch tissues ($p < 0.5$). There were no statistically significant differences between tissues or genotypes for all other sugars. Bars represent standard error and $n = 4$ for each tissue type.

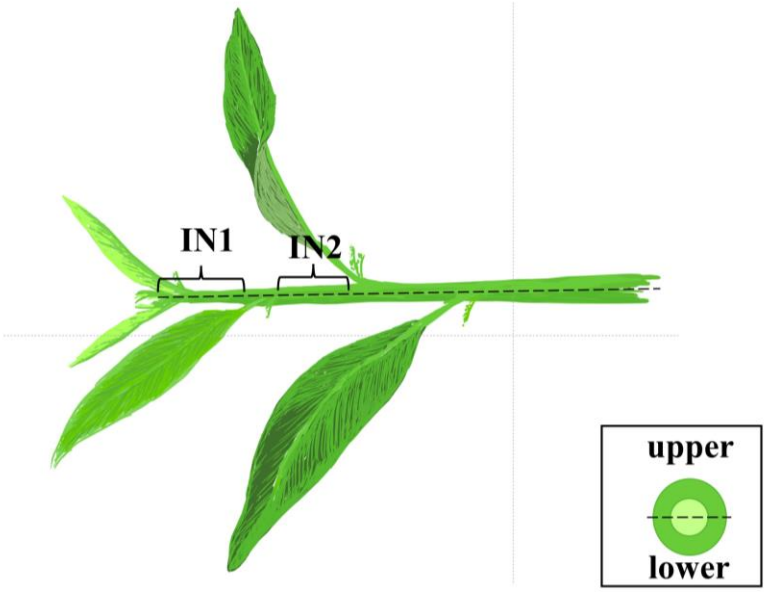

Figure 2.14: Diagram illustrating the location of the shoot tip tissues that were harvested for RNAseq. Tissues were divided into internodes 1 and 2 (IN1 and IN2), and each internode was bisected into top and bottom. Boxed diagram shows a cross-section view of the dissection.

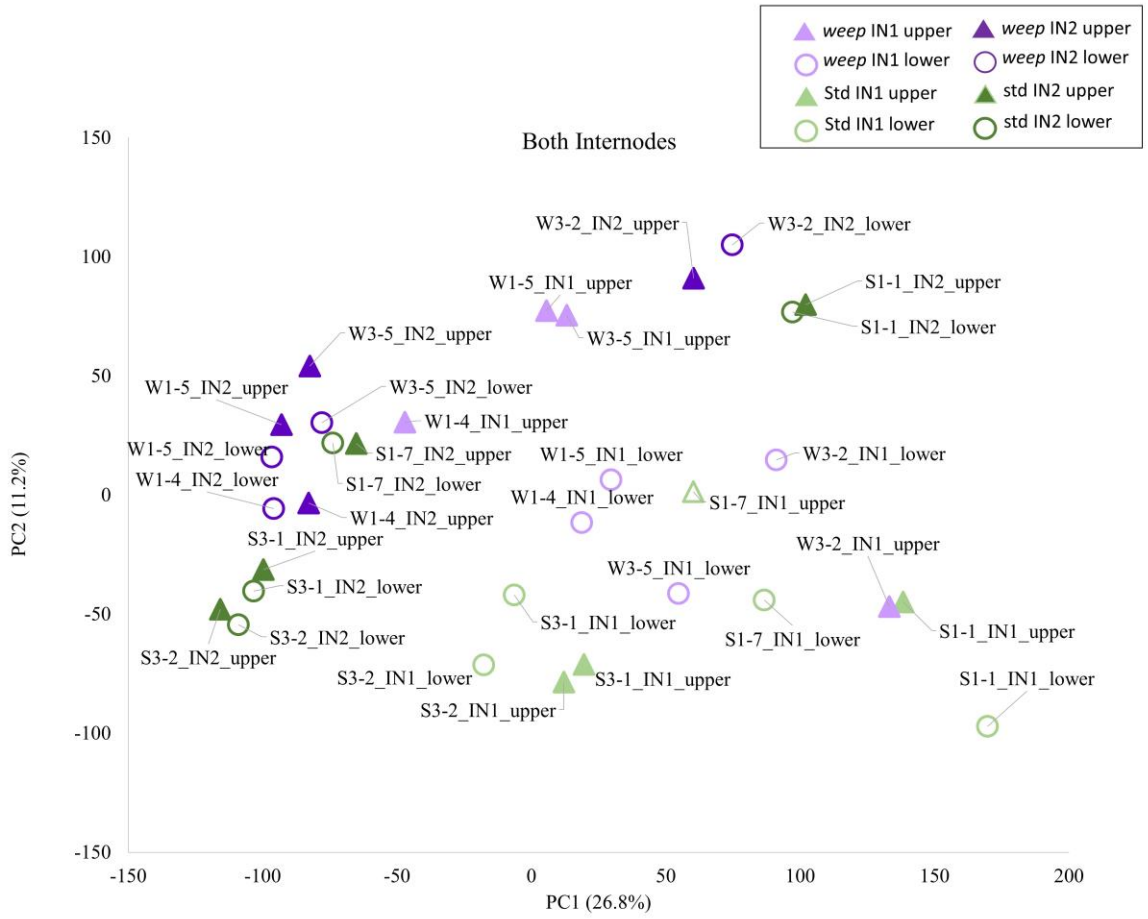

Figure 2.15: Principal component analysis for RNAseq data. Data from and lower shoot tissues of internodes (IN) 1 and 2 from both standard (S) and weeping (W) peach branches. Sample naming system indicates genotype (S or W), followed by tree identification number (e.g., 3-2), followed by internode (e.g. IN2 for internode 2), followed by tissue type (i.e., upper or lower).

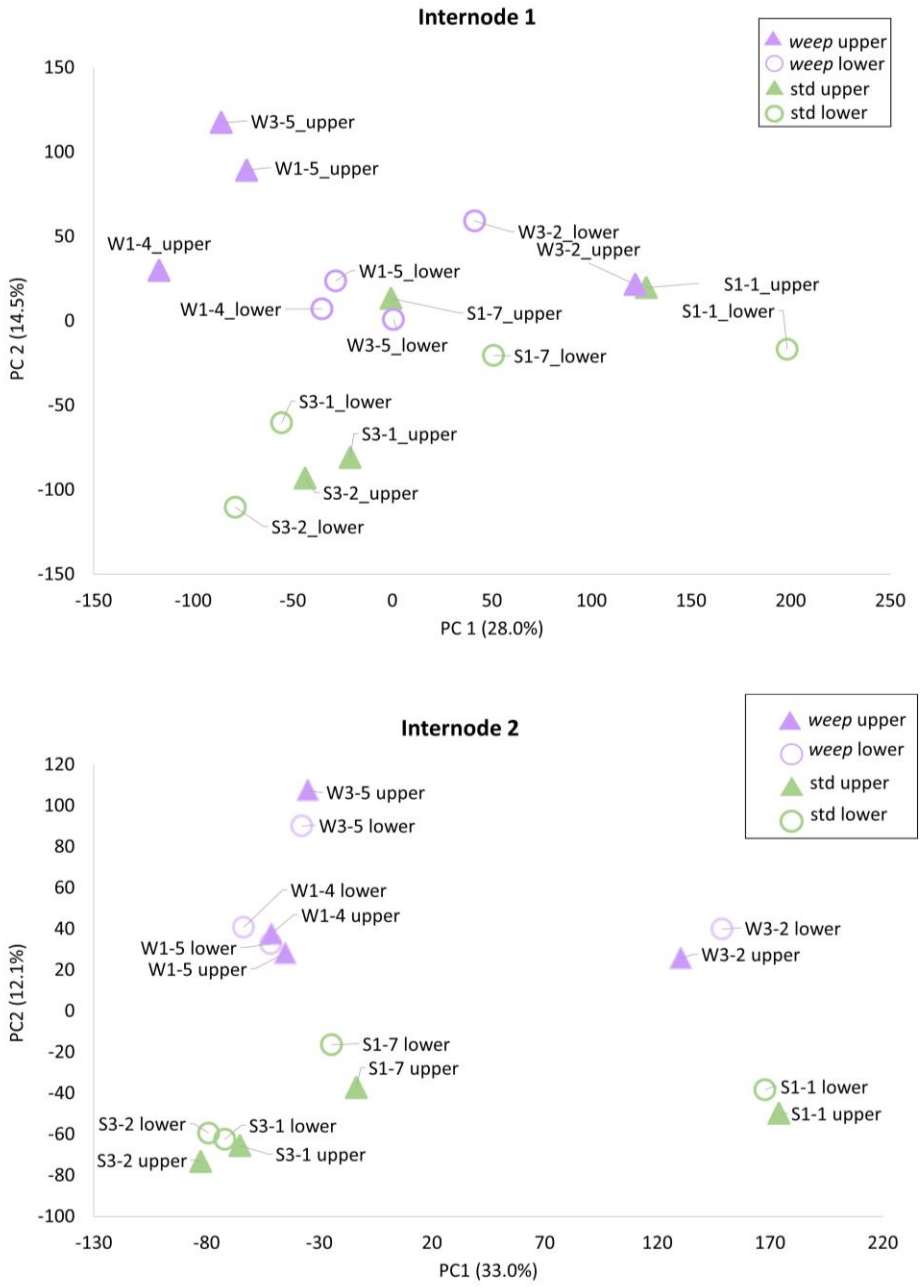

Figure 2.16: Principal component analysis for RNAseq data. Upper and lower shoot tissues from internode 1 (Top graph) and internode 2 (Bottom graph) from both standard (S) and weeping (W) peach branches. Sample naming system indicates genotype (S or W), followed by tree identification number (e.g., 3-2), followed by tissue type (i.e., upper or lower).

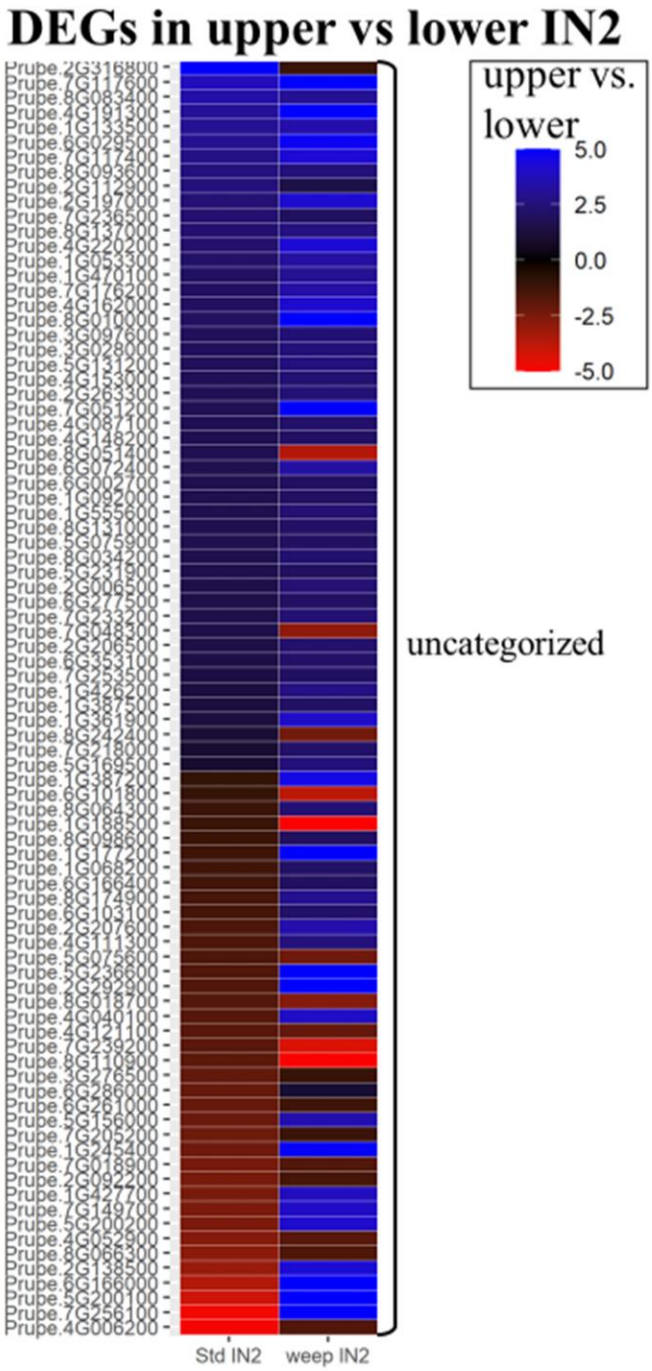

Figure 2.17: Uncategorized differentially expressed genes in IN2. Heatmap indicates fold changes between the upper and lower sides of shoots from standard and weeping (weep) trees. Red indicates that the expression is higher on the lower side, blue indicates that the expression is higher on the upper side.

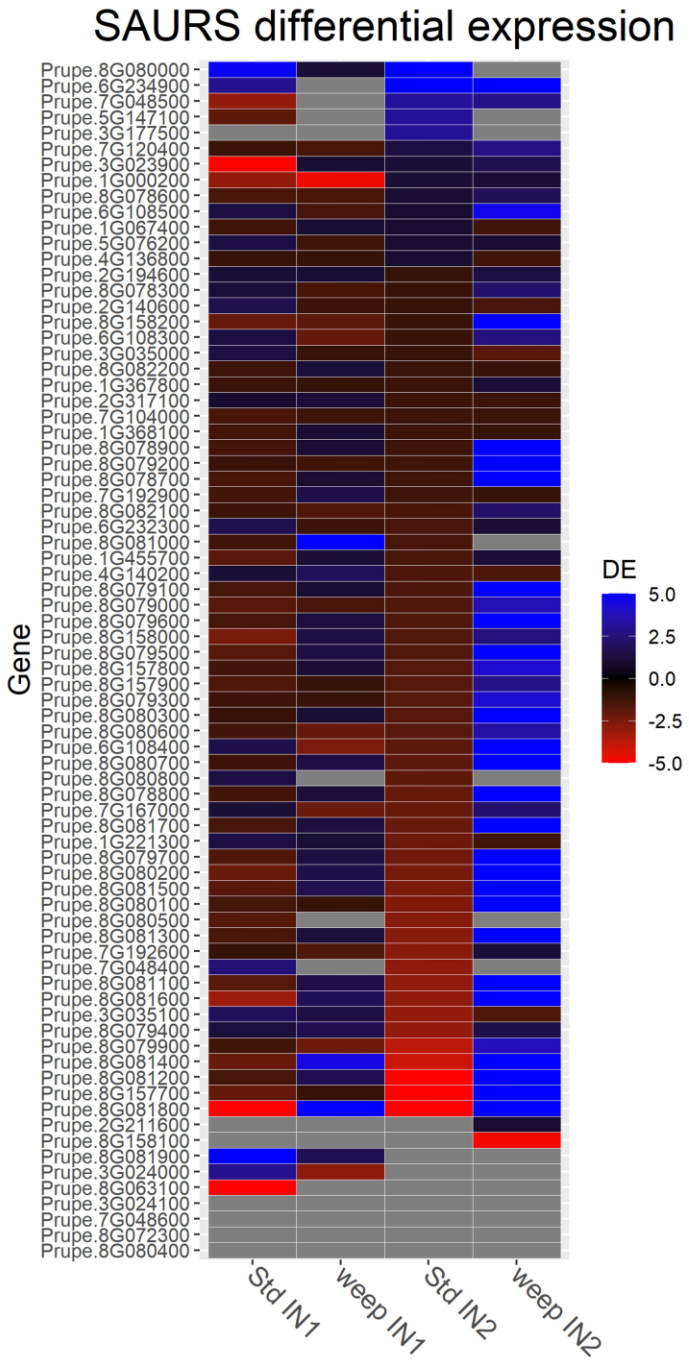

Figure 2.18: Differential expression of *SAUR* genes. Heatmap indicates fold changes between the upper and lower sides of shoots from standard and weeping (weep) trees. Red indicates that the expression is higher on the lower side, blue indicates that the expression is higher on the upper side. Grey indicates expression was not detected in that tissue.

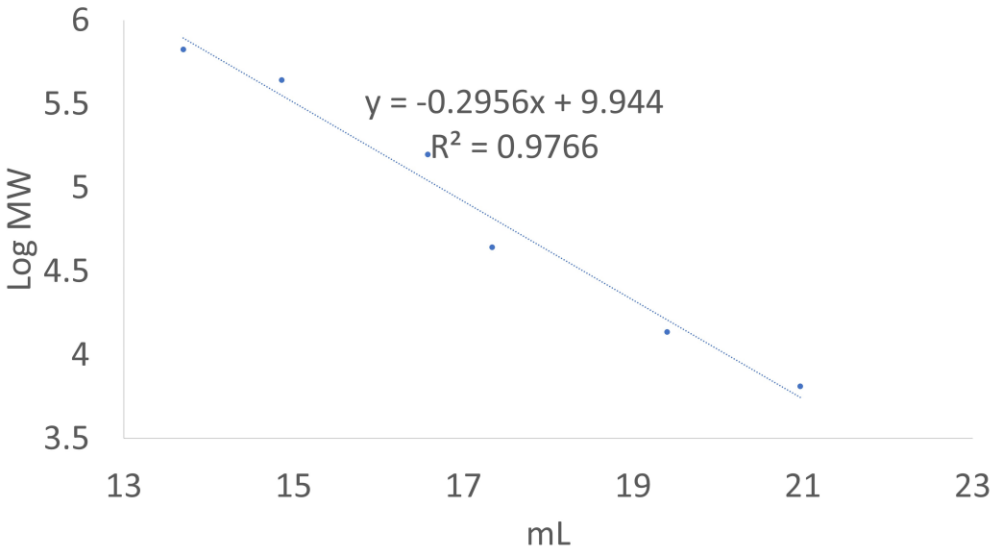

Standard	Ve	LogMW	MW
Aprotinin	20.97	3.81291336	6500
Ribonuclease A	19.4	4.13672057	13700
Ovalbumin	17.34	4.64345268	44000
Aldolase	16.58	5.19865709	158000
Ferritin	14.86	5.64345268	440000
Thyroglobulin	13.7	5.82542612	669000

Figure 2.19: Calibration curve for SEC flow cytometer and corresponding protein standard information.

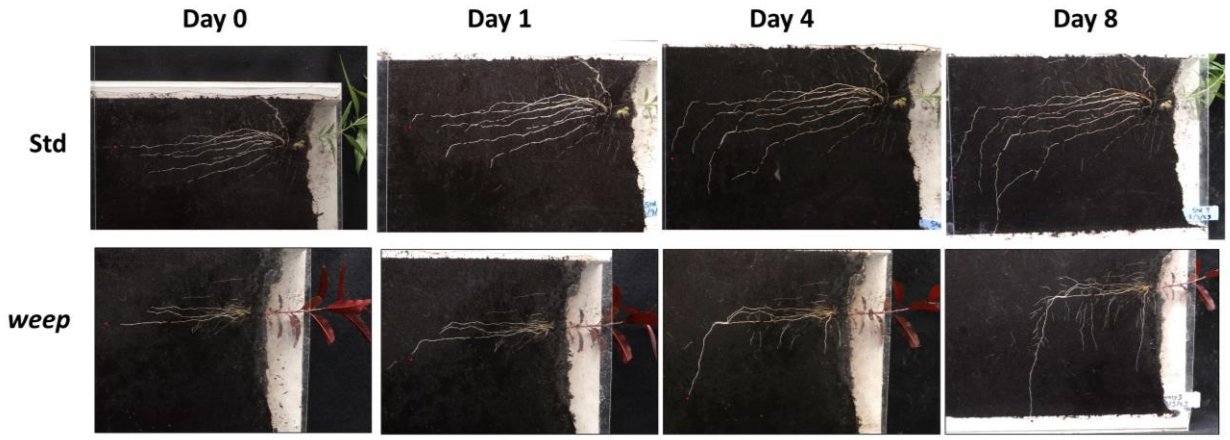

Figure 2.20: Standard and weeping peach seedlings growing in rhizoboxes after a 90-degree reorientation. Red dot indicates tap root.

REFERENCES

Al-Haddad JM, Kang K-Y, Mansfield SD, Telewski FW (2013) Chemical responses to modified lignin composition in tension wood of hybrid poplar (*Populus tremula* x *Populus alba*). Tree Physiology **33(4)**: 365–373

Bao X, Franks RG, Levin JZ, Liu Z (2004) Repression of *AGAMOUS* by *BELLRINGER* in floral and inflorescence meristems. The Plant Cell **16(6)**: 1478–1489

Barbez E, Dünser K, Gaidora A, Lendl T, Busch W (2017) Auxin steers root cell expansion via apoplastic pH regulation in *Arabidopsis thaliana*. The Proceedings of the National Academy of Sciences **114(24)**: E4884–E4893

Barro-Trastoy D, Gomez MD, Blanco-Touriñán N, Tornero P, Perez-Amador MA (2022) Gibberellins regulate ovule number through a DELLA–CUC2 complex in *Arabidopsis*. The Plant Journal **110(1)**: 43–57

Bryant P, Pozzati G, Elofsson A (2022) Improved prediction of protein-protein interactions using AlphaFold2. Nature Communications **13**: 1265

Burian A, Paszkiewicz G, Nguyen KT, Meda S, Raczyńska-Szajgin M, Timmermans MCP (2022) Specification of leaf dorsiventrality via a prepatterned binary readout of a uniform auxin input. Nature Plants **8**: 269–280

Chen H, Werner DJ (2021) Inheritance of compact growth habit, and investigation of linkage to weeping architecture and purple leaf color in Eastern redbud (*Cercis canadensis* L.). HortScience **56(12)**: 1513–1515

Cosgrove DJ (2015) Plant expansins: diversity and interactions with plant cell walls. Current Opinion in Plant Biology **25**: 162–172

Coupe SA, Palmer BG, Lake JA, Overy SA, Oxborough K, Woodward FI, Gray JE, Quick WP (2006) Systemic signalling of environmental cues in *Arabidopsis* leaves. Journal of Experimental Botany **57(2)**: 329–341

Denay G, Vachon G, Dumas R, Zubieta C, Parcy F (2017) Plant SAM-domain proteins start to reveal their roles. Trends in Plant Science **22(8)**: 718–725

Du M, Spalding EP, Gray WM (2020) Rapid auxin-mediated cell expansion. Annual Review of Plant Biology **71**: 379-402

Felten J, Sundberg B (2013) Biology, chemistry and structure of tension wood. *In* J Fromm, ed, Cellular Aspects of Wood Formation. Springer, Berlin, Heidelberg, pp 203–224

Foster CE, Martin TM, Pauly M (2010a) Comprehensive compositional analysis of plant cell walls (lignocellulosic biomass) Part I: Lignin. Journal of Visualized Experiments **(37)**: e1745

Foster CE, Martin TM, Pauly M (2010b) Comprehensive compositional analysis of plant cell walls (lignocellulosic biomass) Part II: Carbohydrates. Journal of Visualized Experiments **(37)**: 1837

Fukaki H, Fujisawa H, Tasaka M (1996) *SGR1*, *SGR2*, and *SGR3*: Novel genetic loci involved in shoot gravitropism in *Arabidopsis thaliana*. Plant Physiology **110(3)**: 945–955

Ge L and Chen R (2016) Negative gravitropism in plant roots. Nature Plants **2(11)**: 16155

Ge L and Chen R (2019) Negative gravitropic response of roots directs auxin flow to control root gravitropism. Plant, Cell & Environment **42(8)**: 2372–83

Gerttula S, Zinkgraf M, Muday GK, Lewis DR, Ibatullin FM, Brumer H, Hart F, Mansfield SD, Filkov V, Groover A (2015) Transcriptional and hormonal regulation of gravitropism of woody stems in *Populus*. The Plant Cell **27(10)**: 2800–2813

Gish LA (2013) Identification of components controlling meristem homeostasis. Ph.D. University of Michigan, United States -- Michigan

González-Arcos M, de Noronha Fonseca ME, Zandonadi DB, Peres LEP, Arruabarrena A, Ferreira DS, Kevei Z, Mohareb F, Thompson AJ, Boiteux LS (2019) A loss-of-function allele of a *TAC1*-like gene (*SlTAC1*) located on tomato chromosome 10 is a candidate for the *Erectoid leaf* (*Erl*) mutation. Euphytica **215**: 95

Grigoriev I, Gouveia SM, Vaart B van der, Demmers J, Smyth JT, Honnappa S, Splinter D, Steinmetz MO, Putney JW, Hoogenraad CC, et al (2008) STIM1 is a MT-plus-end-tracking protein involved in remodeling of the ER. Current Biology **18(3)**: 177–182

Gritsch C, Wan Y, Mitchell RAC, Shewry PR, Hanley SJ, Karp A (2015) G-fibre cell wall development in willow stems during tension wood induction. Journal of Experimental Botany **66(20)**: 6447–6459

Grossmann K (2010) Auxin herbicides: current status of mechanism and mode of action. Pest Management Science **66(2)**: 113–120

Guo L, Klaus A, Baer M, Kirschner GK, Salvi S, Hochholdinger F (2023) ENHANCED GRAVITROPISM 2 coordinates molecular adaptations to gravistimulation in the elongation zone of barley roots. New Phytologist **237(6)**: 2196–2209

Heisler MG, Byrne ME (2020) Progress in understanding the role of auxin in lateral organ development in plants. Current Opinion in Plant Biology **53(SI: Growth and Development)**: 73–79

Hepworth SR, Zhang Y, McKim S, Li X, Haughn GW (2005) BLADE-ON-PETIOLE–dependent signaling controls leaf and floral patterning in *Arabidopsis*. The Plant Cell **17(5)**: 1434–1448

Hollender CA, Pascal T, Tabb A, Hadiarto T, Srinivasan C, Wang W, Liu Z, Scorza R, Dardick C (2018) Loss of a highly conserved sterile alpha motif domain gene (*WEEP*) results in pendulous branch growth in peach trees. The Proceedings of the National Academy of Sciences **115**: E4690–E4699

Johnson JM, Kohler AR, Haus MJ, Hollender CA (2022) *Arabidopsis weep* mutants exhibit narrow root angles. MicroPublication Biol **2022:** 10.17912/micropub.biology.000584

Jones AM, Xuan Y, Xu M, Wang R-S, Ho C-H, Lalonde S, You CH, Sardi MI, Parsa SA, Smith-Valle E, et al (2014) Border control—A membrane-linked interactome of *Arabidopsis*. Science **344(6185)**: 711–716

Jung S, Lee T, Cheng C-H, Buble K, Zheng P, Yu J, Humann J, Ficklin SP, Gasic K, Scott K, et al (2019) 15 years of GDR: New data and functionality in the Genome Database for Rosaceae. Nucleic Acids Research **47(D1)**: D1137–D1145

Kato T, Morita MT, Fukaki H, Yamauchi Y, Uehara M, Niihama M, Tasaka M (2002) SGR2, a phospholipase-like protein, and ZIG/SGR4, a SNARE, are involved in the shoot gravitropism of *Arabidopsis*. The Plant Cell **14(1)**: 33–46

Kee J-J, Sang EJ, Baek S-A, Lee T-S, Cho MR, Hwang H-S, Lee S-C, Kim J, Kim G-T, Im K-H (2009) Overexpression of the *downward leaf curling* (*DLC*) gene from melon changes leaf morphology by controlling cell size and shape in *Arabidopsis* leaves. Molecules and Cells **28(2)**: 93–98

Kern KA, Ewers FW, Telewski FW, Koehler L (2005) Mechanical perturbation affects conductivity, mechanical properties and aboveground biomass of hybrid poplars. Tree Physiology **25(10)**: 1243–1251

Kim CA, Sawaya MR, Cascio D, Kim W, Bowie JU (2005) Structural organization of a Sex-comb-on-midleg/polyhomeotic copolymer. Journal of Biological Chemistry **280(30)**: 27769–27775

Kirschner GK, Rosignoli S, Guo L, Vardanega I, Imani J, Altmüller J, Milner SG, Balzano R, Nagel KA, Pflugfelder D, et al (2021) *ENHANCED GRAVITROPISM 2* encodes a STERILE ALPHA MOTIF–containing protein that controls root growth angle in barley and wheat. The Proceedings of the National Academy of Sciences **118(35)**: e2101526118

Kitazawa D, Hatakeda Y, Kamada M, Fujii N, Miyazawa Y, Hoshino A, Iida S, Fukaki H, Morita MT, Tasaka M, et al (2005) Shoot circumnutation and winding movements require gravisensing cells. The Proceedings of the National Academy of Sciences **102(51)**: 18742–18747

Kleine-Vehn J, Huang F, Naramoto S, Zhang J, Michniewicz M, Offringa R, Friml J (2009) PIN auxin efflux carrier polarity is regulated by PINOID kinase-mediated recruitment into GNOM-independent trafficking in *Arabidopsis*. T**he** Plant Cell **21(12)**: 3839–3849

Klepikova AV, Kasianov AS, Gerasimov ES, Logacheva MD, Penin AA (2016) A high resolution map of the *Arabidopsis thaliana* developmental transcriptome based on RNA-seq profiling. Plant J **88(6)**: 1058–1070

Ku L, Wei X, Zhang S, Zhang J, Guo S, Chen Y (2011) Cloning and characterization of a putative *TAC1* ortholog associated with leaf angle in maize (*Zea mays* L.). PLOS ONE **6(6)**: e20621

Li L, Gallei M, Friml J (2021a) Bending to auxin: fast acid growth for tropisms. Trends in Plant Science **27(5)**:440-449

Li L, Zhang Y, Zheng T, Zhuo X, Li P, Qiu L, Liu W, Wang J, Cheng T, Zhang Q (2021b) Comparative gene expression analysis reveals that multiple mechanisms regulate the weeping trait in *Prunus mume*. Scientific Reports **11**: 2675

MacMillan CP, Mansfield SD, Stachurski ZH, Evans R, Southerton SG (2010) Fasciclin-like arabinogalactan proteins: specialization for stem biomechanics and cell wall architecture in Arabidopsis and Eucalyptus. Plant J **62**: 689–703

Moore I (2002) Gravitropism: Lateral Thinking in Auxin Transport. Current Biology **12**: R452–R454

Morita MT, Saito C, Nakano A, Tasaka M (2007) endodermal-amyloplast less 1 is a novel allele of SHORT-ROOT. Adv Space Res **39**: 1127–1133

Murcha MW, Kubiszewski-Jakubiak S, Teixeira PF, Gügel IL, Kmiec B, Narsai R, Ivanova A, Megel C, Schock A, Kraus S, et al (2016) Plant-Specific Preprotein and Amino Acid Transporter Proteins Are Required for tRNA Import into Mitochondria. Plant Physiol **172**: 2471–2490

Nakamura M, Nishimura T, Morita MT (2019) Bridging the gap between amyloplasts and directional auxin transport in plant gravitropism. Current Opinion in Plant Biology **52**: 54–60

Nakamura T, Saotome M, Ishiguro Y, Itoh R, Higurashi S, Hosono M, Ishii Y (1994) The effects of GA_3 on weeping of growing shoots of the Japanese cherry, *Prunus spachiana*. Plant and Cell Physiology **35(3)**: 523–527

Nakatsubo T, Kitamura Y, Sakakibara N, Mizutani M, Hattori T, Sakurai N, Shibata D, Suzuki S, Umezawa T (2008) At5g54160 gene encodes *Arabidopsis thaliana* 5-hydroxyconiferaldehyde *O*-methyltransferase. Journal of Wood Science **54**: 312–317

Ogura T, Goeschl C, Filiault D, Mirea M, Slovak R, Wolhrab B, Satbhai SB, Busch W (2019) Root system depth in Arabidopsis is shaped by EXOCYST70A3 via the dynamic modulation of auxin transport. Cell **178(2)**: 400-412.e16

Pei M, Gu C, Zhang S (2019) Genome-wide identification and expression analysis of genes associated with peach (*Prunus persica*) fruit ripening. Scientia Horticulturae **246**: 317–327

Pound MP, French AP, Atkinson JA, Wells DM, Bennett MJ, Pridmore T (2013) RootNav: Navigating images of complex root architectures. Plant Physiology **162(4)**: 1802–1814

Preibisch S, Saalfeld S, Tomancak P (2009) Globally optimal stitching of tiled 3D microscopic image acquisitions. Bioinformatics **25**: 1463–1465

Qiao F, Bowie JU (2005) The many faces of SAM. Science's STKE **2005(286)**: re7

Qiu D, Wilson IW, Gan S, Washusen R, Moran GF, Southerton SG (2008) Gene expression in *Eucalyptus* branch wood with marked variation in cellulose microfibril orientation and lacking G-layers. New Phytologist **179(1)**: 94–103

Rakusová H, Fendrych M, Friml J (2015) Intracellular trafficking and PIN-mediated cell polarity during tropic responses in plants. Current Opinion in Plant Biology **23**: 116–123

Rakusová H, Gallego-Bartolomé J, Vanstraelen M, Robert HS, Alabadí D, Blázquez MA, Benková E, Friml J (2011) Polarization of PIN3-dependent auxin transport for hypocotyl gravitropic response in *Arabidopsis thaliana*. The Plant Journal **67(5)**: 817–826

Ren H, Gray WM (2015) SAUR proteins as effectors of hormonal and environmental signals in plant growth. Molecular Plant **8(8)**: 1153–1164

Ronzier E, Corratgé-Faillie C, Sanchez F, Prado K, Brière C, Leonhardt N, Thibaud J-B, Xiong TC (2014) CPK13, a noncanonical Ca2+-dependent protein kinase, specifically inhibits KAT2 and KAT1 Shaker K+ channels and reduces stomatal opening. Plant Physiology **166(1)**: 314–326

Roychoudhry S, Del Bianco M, Kieffer M, Kepinski S (2013) Auxin controls gravitropic setpoint angle in higher plant lateral branches. Current Biology **23(15)**: 1497–1504

Roychoudhry S, Kepinski S (2015) Shoot and root branch growth angle control—the wonderfulness of lateralness. Current Opinion in Plant Biology **23(SI: Growth and Development)**: 124–131

Ryu KH, Huang L, Kang HM, Schiefelbein J (2019) Single-cell RNA sequencing resolves molecular relationships among individual plant cells. Plant Physiology **179(4)**: 1444–1456

Sayou C, Nanao MH, Jamin M, Posé D, Thévenon E, Grégoire L, Tichtinsky G, Denay G, Ott F, Peirats Llobet M, et al (2016) A SAM oligomerization domain shapes the genomic binding landscape of the LEAFY transcription factor. Nature Communications **7**: 11222

Shi J, Dong J, Xue J, Wang H, Yang Z, Jiao Y, Xu L, Huang H (2017) Model for the role of auxin polar transport in patterning of the leaf adaxial–abaxial axis. The Plant Journal **92(3)**: 469–480

Shin K, Lee I, Kim E, Park SK, Soh M-S, Lee S (2019) *PACLOBUTRAZOL-RESISTANCE* gene family regulates floral organ growth with unequal genetic redundancy in *Arabidopsis thaliana*. International Journal of Molecular Sciences **20(4)**: 869

Simeunovic A, Mair A, Wurzinger B, Teige M (2016) Know where your clients are: Subcellular localization and targets of calcium-dependent protein kinases. Journal of Experimental Botany **67(13)**: 3855–3872

Spartz AK, Lee SH, Wenger JP, Gonzalez N, Itoh H, Inzé D, Peer WA, Murphy AS, Overvoorde PJ, Gray WM (2012) The *SAUR19* subfamily of *SMALL AUXIN UP RNA* genes promote cell expansion. The Plant Journal **70(6)**: 978–990

Spartz AK, Ren H, Park MY, Grandt KN, Lee SH, Murphy AS, Sussman MR, Overvoorde PJ, Gray WM (2014) SAUR inhibition of PP2C-D phosphatases activates plasma membrane H+-ATPases to promote cell expansion in *Arabidopsis*. The Plant Cell **26(5)**: 2129–2142

Spurr AR (1969) A low-viscosity epoxy resin embedding medium for electron microscopy. Journal of Ultrastructure Research **26(1-2)**: 31–43

Stahle MI, Kuehlich J, Staron L, von Arnim AG, Golz JF (2009) YABBYs and the transcriptional corepressors LEUNIG and LEUNIG_HOMOLOG maintain leaf polarity and meristem activity in *Arabidopsis*. The Plant Cell **21(10)**: 3105–3118

Taniguchi M, Furutani M, Nishimura T, Nakamura M, Fushita T, Iijima K, Baba K, Tanaka H, Toyota M, Tasaka M, et al (2017) The *Arabidopsis* LAZY1 family plays a key role in gravity signaling within statocytes and in branch angle control of roots and shoots. The Plant Cell **29(8)**: 1984–1999

Tian C, Wang Y, Yu H, He J, Wang J, Shi B, Du Q, Provart NJ, Meyerowitz EM, Jiao Y (2019) A gene expression map of shoot domains reveals regulatory mechanisms. Nature Communications **10**: 141

Verde I, Jenkins J, Dondini L, Micali S, Pagliarani G, Vendramin E, Paris R, Aramini V, Gazza L, Rossini L, et al (2017) The Peach v2.0 release: high-resolution linkage mapping and deep resequencing improve chromosome-scale assembly and contiguity. BMC Genomics **18**: 225

Waidmann S Kleine-Vehn J. (2020) Asymmetric cytokinin signaling opposes gravitropism in roots. Journal of Integrative Plant Biology **62(7)**:882-886

Wang H, Jin Y, Wang C, Li B, Jiang C, Sun Z, Zhang Z, Kong F, Zhang H (2017) Fasciclin-like arabinogalactan proteins, PtFLAs, play important roles in GA-mediated tension wood formation in *Populus*. Scientific Reports **7**: 6182

Wang P, Hummel E, Osterrieder A, Meyer AJ, Frigerio L, Sparkes I, Hawes C (2011) KMS1 and KMS2, two plant endoplasmic reticulum proteins involved in the early secretory pathway. The Plant Journal **66(4)**: 613–628

Wang Q, Marconi M, Guan C, Wabnik K, Jiao Y (2022) Polar auxin transport modulates early leaf flattening. The Proceedings of the National Academy of Sciences **119**: e2215569119

Wang X, Yu R, Wang J, Lin Z, Han X, Deng Z, Fan L, He H, Deng XW, Chen H (2020) The asymmetric expression of *SAUR* genes mediated by ARF7/19 promotes the gravitropism and phototropism of plant hypocotyls. Cell Reports **31(3)**: 107529

Wu X, Dabi T, Weigel D (2005) Requirement of homeobox gene *STIMPY/WOX9* for *Arabidopsis* meristem growth and maintenance. Current Biology **15(5)**: 436–440

Xu D, Qi X, Li J, Han X, Wang J, Jiang Y, Tian Y, Wang Y (2017) *PzTAC* and *PzLAZY* from a narrow-crown poplar contribute to regulation of branch angles. Plant Physiology and Biochemistry **118**: 571–578

Yoshihara T, Spalding EP (2017) *LAZY* genes mediate the effects of gravity on auxin gradients and plant architecture. Plant Physiology **175(2)**: 959-969

Yoshihara T, Spalding EP (2020) Switching the direction of stem gravitropism by altering two amino acids in AtLAZY1. Plant Physiology **182(2)**: 1039-1051

Yuan Y, Teng Q, Lee C, Zhong R, Ye Z-H (2014) Modification of the degree of 4-O-methylation of secondary wall glucuronoxylan. Plant Science **219–220**: 42–50

Žádníková P, Simon R (2014) How boundaries control plant development. Current Opinion in Plant Biology **17(SI: Growth and development)**: 116–125

Zhang X, Adamowski M, Marhava P, Tan S, Zhang Y, Rodriguez L, Zwiewka M, Pukyšová V, Sánchez AS, Raxwal VK, et al (2020) *Arabidopsis* flippases cooperate with ARF GTPase exchange factors to regulate the trafficking and polarity of PIN auxin transporters. The Plant Cell **32(5)**: 1644–1664

Zhao H, Huai Z, Xiao Y, Wang X, Yu J, Ding G, Peng J (2014) Natural variation and genetic analysis of the tiller angle gene *MsTAC1* in *Miscanthus sinensis*. Planta **240(1)**: 161–175

CHAPTER 3

Onward and Outward:

Reduction of *LAZY1* expression leads to altered branch angles and orientations in *Prunus domestica* (European plum).

The work described herein is being prepared for a peer-reviewed publication.

Anticipated authors for publication (in preparation)

Andrea R Kohler[1], Courtney A Hollender[1,*], Doug Raines[2], Chris Dardick[2*]

[1] Michigan State University Department of Horticulture, East Lansing MI 48824

[2] USDA Agricultural Research Service Appalachian Fruit Research Station, Kearneysville WV

[*]Co-Corresponding

Author Contributions

CAH and CD conceived project idea. CAH, ARK, and CD planned experiments. Experiments were performed and data were analyzed by CAH, DR and ARK. CAH performed initial expression analysis, angle measurements, and grafting. ARK performed biomechanical analysis, net photosynthesis measurements, quantification of flower and fruit phenotypes, and training experiments. ARK wrote the manuscript with input from other authors. CAH and CD edited the manuscript.

Abstract

One of the central challenges in tree fruit production is control of branch orientation, as it affects light interception and crop load management. However, the many management practices which have been tried, such as tying or growth regulator application, have proved either ineffective or costly. In contrast, altering the expression of genes which control the natural angle of the branch provides an alternative that can permanently optimize tree architecture with minimal interventions. One of the essential genes for controlling branch orientation is *LAZY1,* which promotes upward growth by acting in the gravitropism pathway to polarize PIN3 auxin efflux carriers. Here, we use an antisense vector to silence *LAZY1* in plum (*Prunus domestica*). We demonstrate that *LAZY1*-silenced (*LAZY1*-sil) lines have significantly increased branch and petiole angles, and lack a central leader, releasing apical dominance. We also examine pleiotropic effects observed in *LAZY1-sil* trees*,* including alterations in wood biomechanical properties and a chlorotic leaf phenotype. Finally, we consider the implications of these phenotypes for planar tree fruit production and ornamental use, using examples from *LAZY1*-sil trees trained into two planar orchard systems: super spindle axe (a common commercial system), and espalier (a commercial or ornamental system ideal for small spaces).

Introduction

Controlling the orientation of lateral organs is crucial to a plant's ability to survive in a changing environment and compete with other plants. In a horticultural or agricultural context, lateral organ angle impacts essential traits such as light interception (through positioning of lateral branches), drought tolerance (through positioning of lateral roots), and harvest mechanisms (through positioning of the inflorescence). In perennial species, such as fruit trees, growers often expend considerable labor trying to control the position of branches through pruning, tying or growth regulator application (Quinlan and Tobutt, 1990). However, the angle of lateral organs is largely determined by genetics, often rendering these attempts futile. In contrast, using selective breeding or gene editing to manipulate genes which control lateral organ orientation provides a permanent solution to both branch and root angle control throughout the lifetime of the plant (Quinlan and Tobutt, 1990).

One of the primary gene families known to control lateral organ angle is the IGT family (Zhang et al., 2022). The family includes *LAZY* homologs, which promote narrowed lateral organ orientation, and *TAC1* homologs, which promote outward lateral organ orientation (Waite and Dardick, 2021).

Most species have multiple paralogs of *LAZY,* which can be divided into three clades: *LAZY1-like, DRO1-like,* and *LAZY5-like* (Zhang et al., 2022). *LAZY* paralogs are partially redundant in controlling shoot and root angles, but show distinct expression patterns (Nakamura et al., 2019). The IGT protein family is named for a short, conserved (GϕL(A/T)IGT) amino acid motif and is characterized by a set of 5 conserved regions (Dardick et al., 2013; Zhang et al., 2022). In arabidopsis (*Arabidopsis thaliana*) AtLAZY1, region I is necessary but not sufficient for localization to the plasma membrane (Yoshihara and Spalding, 2020; Chen et al., 2022). Region II contains the IGT motif and is essential for LAZY's role in auxin transport (Yoshihara and Spalding, 2020; Zhang et al., 2022). Regions III contains a transmembrane domain, and an amino acid substitution in *Malus domestica* homolog MdLAZY1disrupted function (Dougherty et al., 2023). The LAZY protein also has a nuclear localization signal between Region III and Region IV (Yoshihara et al., 2013; Li et al., 2019; Yoshihara and Spalding, 2020). Region V contains an Ethylene-responsive element binding factor-associated Amphiphilic Repression motif (EAR motif; Dardick et al., 2013; Yoshihara and Spalding, 2020; Dougherty et al., 2023).

LAZY proteins promote narrowed lateral shoot and root angles by integrating signals from light and gravity. *LAZY* homolog mutants in many species have wider lateral organ angles (Li et al., 2007; Arai-Sanoh et al., 2014; Howard III et al., 2014; Ge and Chen, 2016; Taniguchi et al., 2017; Chen et al., 2020; Nakamura et al., 2019; Dougherty et al., 2023). Mutants of *LAZY* homologs also show a slowed or absent gravitropic response, sometimes to the point that shoots grow prostrate on the ground (as in *Oryza sativa*, *Zea mays*, and the arabidopsis *lazy1,2,4* mutant) or roots are negatively gravitropic, as in *Medicago truncatula, Lotus japonicus,* and arabidopsis *lazy2,3,4* mutants (Godbolé et al., 1999; Howard III et al., 2014; Ge and Chen, 2016; Taniguchi et al., 2017; Chen et al., 2020). In contrast, overexpression of *LAZY* homologs leads to narrower branch and root angles and enhanced gravitropism (Li et al., 2021; Xia et al., 2021; Loarce et al., 2022).

During gravitropism, LAZY proteins are essential to correct polarization of PIN3 auxin proteins. In gravistimulated arabidopsis *lazy1;lazy2;lazy4* triple mutants, the auxin efflux carrier PIN3, which carries auxin laterally in a stem or root, is mis-localized to the upper side of the cell instead of the lower side (Taniguchi et al., 2017). This causes an inverted auxin gradient in arabidopsis *lazy1,2,4* mutants (Yoshihara and Spalding, 2017). Inverse auxin gradients were also observed in *Lotus japonicus lazy* mutants (*Ljlazy3*) and in the arabidopsis mutant allele AtLAZY1$^{1L92A/I94A}$,

which has an amino acid substitution in region II (Chen et al., 2020; Yoshihara and Spalding, 2020).

The mechanism by which LAZY proteins determine PIN3 localization has been the subject of several recent studies. Using LAZY proteins in arabidopsis root columella cells as a model system, it was possible to observe that LAZY proteins localize to the lower side of gravistimulated cells (Furutani et al., 2020; Chen et al., 2023). Upon gravistimulation, LAZY is phosphorylated by the kinases MKK5 and MPK3, which promotes LAZY binding to TRANSLOCON AT THE OUTER CHLOROPLAST ENVELOPE (TOC) proteins on amyloplasts (Chen et al., 2023). As a result, LAZY proteins follow the sedimentation of the amyloplast to the new lower side of the cell, which is believed to enrich them in the plasma membrane there (Chen et al., 2023; Nishimura et al., 2023). Once polarized to the lower side of the cell, LAZY proteins recruit the PIN proteins there, likely through interactions with RLD, a protein family that controls polar auxin transport during gravitropism and development (Furutani et al., 2020). LAZY proteins are required to recruit RLD proteins to the plasma membrane and to localize them to the lower side of gravistimulated cells, and both LAZY and RLD proteins are required to localize PIN3 to the lower side (Furutani et al., 2020).

Some work has also connected *LAZY* homologs to light response. Maize *ZmLAZY1* expression is higher in the dark (Dong et al., 2013). In arabidopsis, the *LAZY* homologs show differing responses to light, with *AtLAZY1* showing no response, *AtLAZY4* and *AtLAZY6* showing decreased expression in darkness, and *AtLAZY3* showing increased expression in darkness (Waite and Dardick, 2020). These differences in responses may be due to the unique organ-specific roles of each gene, as the *AtLAZY4* gene was recently found to be downregulated by light in the hypocotyl through degradation of the PHYTOCHROME INTERACTING FACTORs (PIFs) which activate *AtLAZY4,* but upregulated by light in the root through stabilization of HY5, which also activates *AtLAZY4* (Yang et al., 2020). Thus, *LAZY* homologs may be important integrators of light and gravity signaling during the establishment of the default lateral organ angle or "set-point angle" (Yang et al., 2020; Dougherty et al., 2023).

Wide branch angles are generally considered desirable in tree fruit production, particularly in high-density or planar training systems (Warner, 1991). Some species, such as European plum, naturally tend toward a highly vigorous, upright phenotype that is not highly branched, which causes problems implementing these systems (Quinlan and Tobutt, 1990). Generally, European plum is

grown in low-density plantings. Some moderate density plantings are used, both in palmette training, a planar canopy architecture with a central leader and lateral branches growing upwards at structured angles, and slender spindle training (a central leader system; Corelli-Grappadelli, 2000; Milosevic et al., 2008; Sottile et al., 2010; Lammerich et al., 2020). High-density plantings have the potential to improve yield and return on investment; however, they require high initial investment due to the cost of trees and of the extensive labor required to prune and shape the tree canopy (Milosevic et al., 2008). These authors found the cost of labor for training European plum at high density (1,250 trees/ha) was 4.3X the cost of low density (333 trees/ha), even though tree density was increased less than four-fold (Milosevic et al., 2008). However, many of the challenges for growing European plum at high density could be addressed with plum trees which had more branching and wider crotch angles. Two training systems that could be of particular interest are espalier and super spindle axe (SSA). Espalier is moderate- to high-density planar system (planted at 2.4m in-row spacing in our orchard or ~1,120 trees/hectare assuming 3.7m rows). Espalier is similar to palmette, but has lateral branches trained horizontally and is suitable for both commercial production and ornamental applications. SSA is a high-density central leader system (planted at 0.9m in-row spacing or ~2,990 trees/hectare).

Here, we present the results of a long-term field study of transgenic European plum (*Prunus domestica*) lines with silencing of the lateral organ control gene *LAZY1*. We report control of branch orientation in both own-root and grafted lines, and discuss pleiotropic phenotypes that may impact production. Finally, we present some work on applications of *LAZY1* silenced (*LAZY1*-sil) plums in various orchard systems.

Results

LAZY *genes in plum.*

European plum is an allohexaploid likely arising from *P. cerasifera* (2x) and *P. spinosa* (4x; Zhebentyayeva et al., 2019). As *P. spinosa* may itself be an allotetraploid, there may be up to three distinct subgenomes in *P. domestica* (Zhebentyayeva et al., 2019). Depending on how heterozygous each subgenome is, there could be as many as six distinct homologs for each *LAZY* gene identified in peach. BlastP identified 20 *LAZY* homologs in plum, with 4-6 homologs per peach *LAZY* gene (Figures 3.1 and 3.10). Of the six homologs which clustered with peach *LAZY1* (*PpeLAZY1*), 4 homologs had an identical amino acid sequence to *PpeLAZY1*, 1 homolog had a

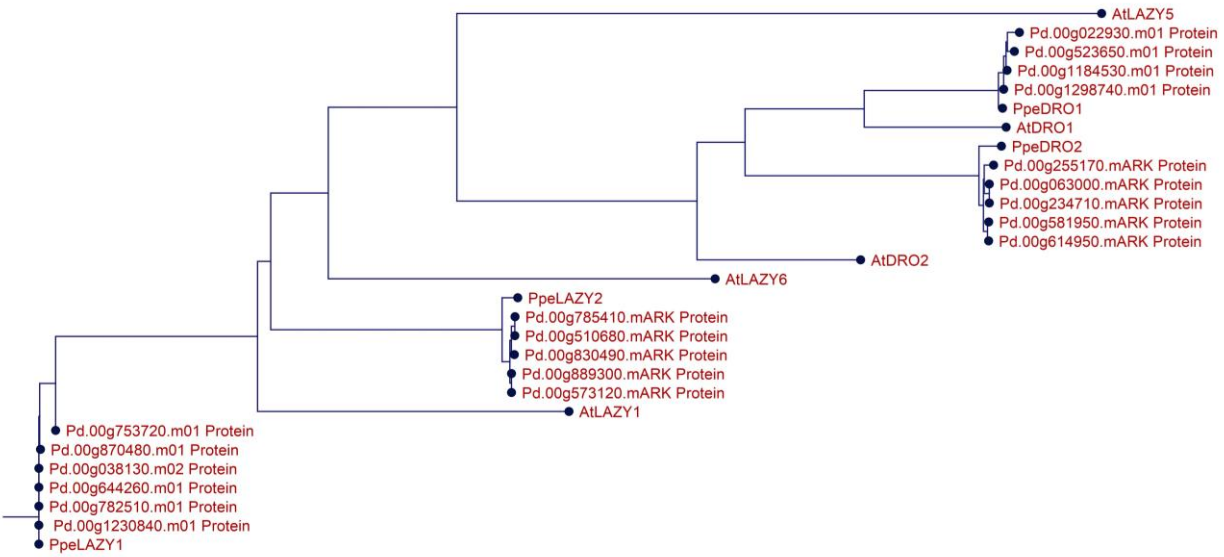

Figure 3.1: *LAZY* genes in *Prunus domestica.* (A) Phylogenetic tree of *LAZY* genes in plum (*P. domestica,* Pd), with peach (*P. persica*, Ppe) and arabidopsis (*A. thaliana,* At) homologs for reference.

single amino acid substitution at the 48th a.a, and 1 homolog was either mis-sequenced, mis-annotated, or truncated, starting at a.a 288 of *PpeLAZY1* (Figure 3.10).

LAZY1-silenced lines exhibit increased lateral organ angles and undirected lateral branch growth.

A hairpin construct using pHellsgate 8.0 was designed using *PpeLAZY1* to silence plum *LAZY1* homologs and transformed into plum. The construct used for transformation had single insert in the reverse orientation behind the 35S promoter within pHellsgate 8.0 (Figure 3.11), serving as an anti-sense vector for *LAZY1*. To identify which homologs this construct would probably target, the gene sequence of all plum *LAZY* homologs was aligned to that of *PpeLAZY1* (Figure 3.12). As anticipated, the *PdoLAZY1* homologs had highly similar sequences, with limited point mutations, except for the truncated homolog which was missing this sequence altogether. Other *PdoLAZY* homologs (related to *PpeLAZY2* or *PpeDRO* genes), did not show high sequence similarity in this region (Figure 3.12).

The expression of the *LAZY1* homologs targeted in these plum lines (*LAZY1*-sil) was quantified using qPCR and primers which aligned to all five targeted homologs (Figure 3.13). Expression of *LAZY1* was significantly reduced in 6 out of 7 independent *LAZY1*-sil lines (Figure 3.2 A). *LAZY1*-sil lines exhibited an increase in lateral organ angles, with both petioles and branch angles

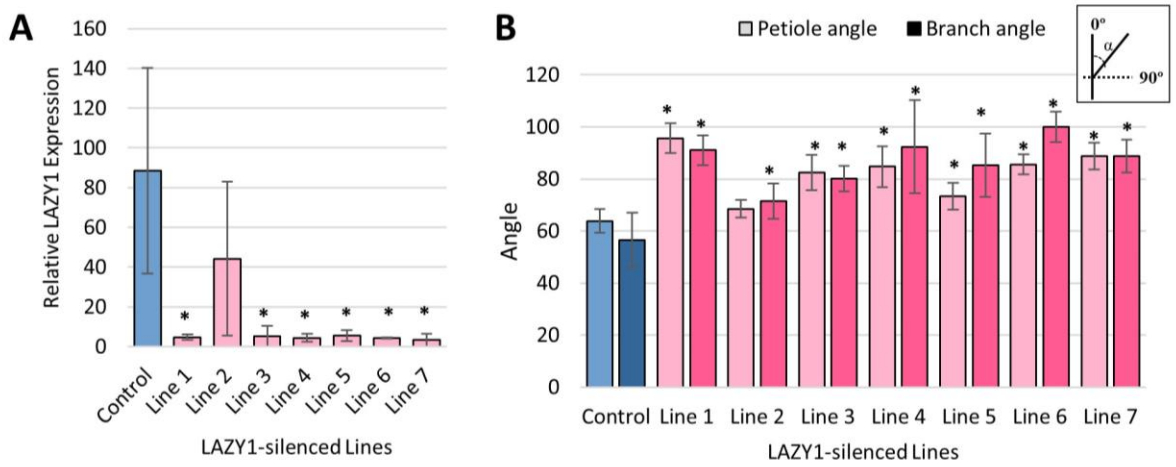

Figure 3.2: *Prunus domestica* plum trees transformed with a *LAZY1* antisense construct exhibited reduced expression of *LAZY1* along with wider petiole and branch angles. (A) *LAZY1* gene expression in control and *LAZY1*-silenced lines. Expression was determined by qPCR on at least three biological replicates (trees) per line, each with three technical replicates. Values are in relation to a standard curve of known RNA from control plants. (B) Average branch and petiole angles for LAZY1-sil and control lines. Both petiole and branch angles represent the average from at least three trees per line. Diagram in the upper right indicates that angles reported are those between the branch or petiole and the apex of the corresponding shoot and a measurement of 45º represents a branch or petiole that is perpendicular to the shoot. Bars represent standard deviation and * indicates a significant difference between the control plants and a *LAZY*1-sil line ($p < 0.05$) according to a Student's t-test. For both figures, control trees were plum seedlings from the same cultivar that do not contain the *LAZY1-silenced* vector.

becoming significantly wider (Figure 3.2 B, Figure 3.3 A). The alteration to branch angle both increased the initial crotch angle and oriented the growth trajectory horizontally (Figure 3.3 A). Mature trees in both field and greenhouse displayed a wandering branch phenotype, alternately arching up and down, but generally maintaining roughly horizontal growth (Figure 3.3 B, C). The branches appeared undirected by light or gravity and were neither oriented upward, nor fully weeping (Figure 3.3 B). Furthermore, the initial leader eventually ceased upright growth and began growing horizontally (Figure 3.3 A, B).

Horizontal shoot growth in LAZY1-silenced trees cannot be rescued by grafting, and trees lack gravitropic response and apical dominance/control.

Since *LAZY1*-sil lines have an increase in initial crotch angle of lateral branches, we tested to see whether this phenotype could be rescued by grafting. *LAZY1*-sil vegetative buds were grafted onto Myrobalan plum rootstock. After bud break, the resultant shoot grew horizontally, just as on the

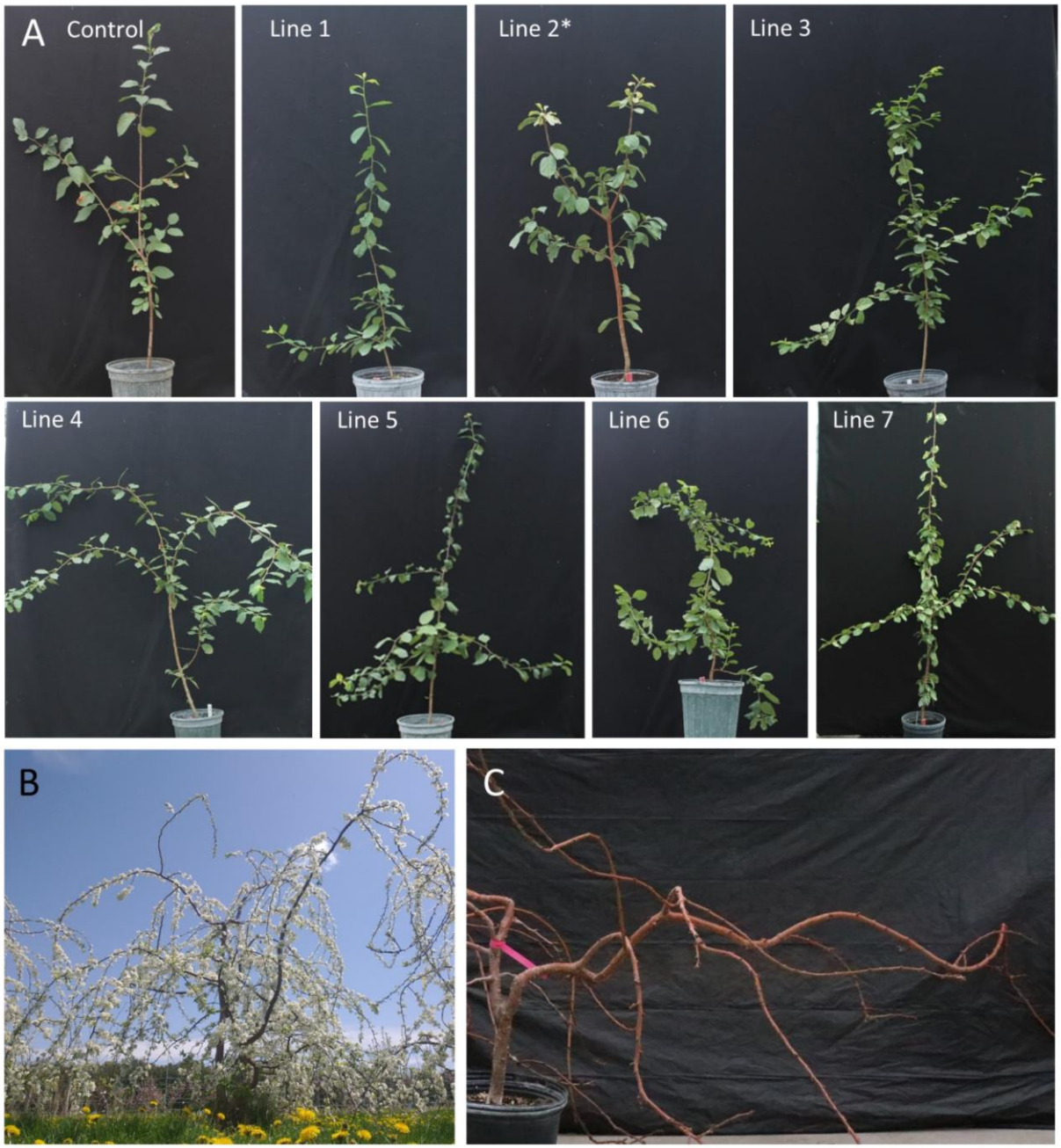

Figure 3.3: LAZY1-silenced plums exhibit altered leaf and branch orientations. A) Representative control and *LAZY1-silenced* trees from each transgenic line growing in the greenhouse. Images were taken in 2014 when they were approximately 18 months old. *LAZY1 expression was not significantly reduced in Line 2. B) A mature *LAZY1-silenced* Line 6 tree growing in Clarksville, MI. C) A *LAZY1-silenced* Line 6 tree growing the greenhouse, demonstrating the wandering growth trajectory.

LAZY1-sil trees (Figure 3.4 A, see also Figure 3.14). This suggests that the horizontal shoot phenotype is pre-programmed in the vegetative bud. Furthermore, heading the rootstock

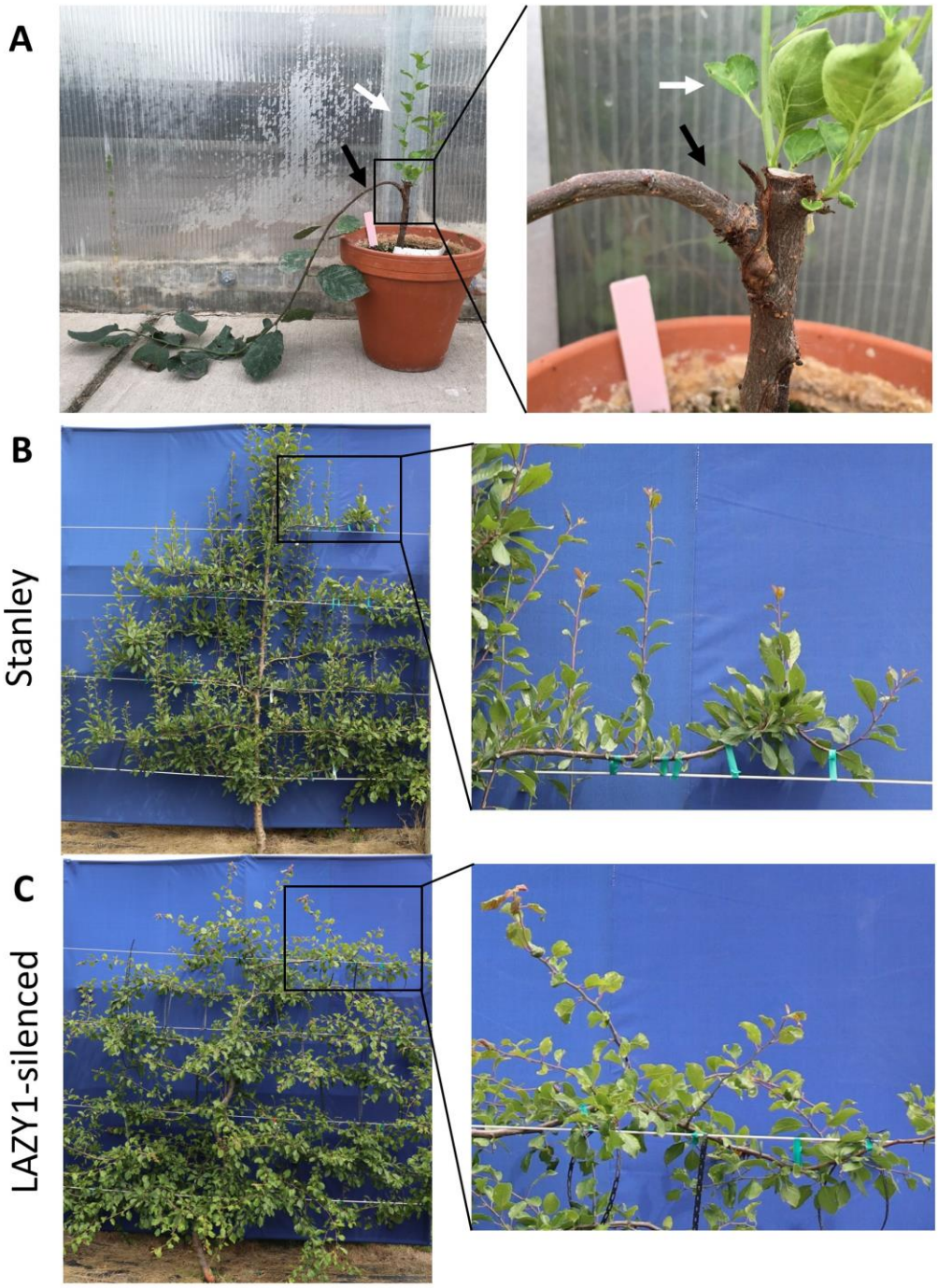

Figure 3.4: The *LAZY1*-silenced shoots lack apical dominance, even when grafted on standard rootstock. A) Representative plum tree with a *LAZY1*-sil branch (black arrow) growing from a bud that was grafted onto a standard 'Myrobalan' plum rootstock, with shoots emerging from dormant rootstock buds (white arrow). B) When Stanley branches are tied horizontal, they continue trying to re-orient upwards, and buds break from the top of the branch. C) In contrast, *LAZY1*-sil branches tied horizontal do not reorient, and buds break from all sides of the branch.

above the graft union did not lead to upward-reorientation of the *LAZY1*-sil shoot to take over apical dominance. Rather, rootstock buds broke and produced upward-oriented shoots above the *LAZY1*-sil shoot (Figure 3.4 A).

Both Stanley control and *LAZY1*-sil line 4 trees grafted on Myrobalan rootstock were grown in a field near Clarksville, MI. The main leader of each tree was tied to a stake or trellis wire to maintain vertical orientation. The main leader of Stanley trees grew straight upward, whereas the main leader of the *LAZY1*-sil line 4 trees continued to wander and arch downward after each point where it was tied. When lateral branches were tied to horizontal trellis wire, Stanley branches attempted to reorient upward (Figure 3.4 B), whereas *LAZY1*-sil branches did not show directed growth (Figure 3.4 C). Furthermore, as expected, reorienting the Stanley branches broke apical dominance and lateral buds broke dormancy and grew primarily from the upper side of the branch, and new shoots were oriented straight up (Figure 3.4 B). In contrast, tied *LAZY1*-sil branches had lateral buds break on every side of the branch, and new shoots were oriented in every direction (Figure 3.4 C).

LAZY1-silenced branches do not have reduced stiffness or strength, but show altered material properties.

Since the LAZY1 protein is known to direct polar auxin transport through PIN3 localization, and polar auxin transport has been implicated in xylem differentiation and development, we investigated the biomechanical properties of *LAZY1*-sil wood by conducting materials testing on new growth and one-year-old branches (Johnson et al., 2018; Furutani et al., 2020). Neither flexural stiffness (the ability of the branch to resist bending) nor the Fmax (maximum force the branch can resist) is decreased in *LAZY1*-sil branches (Figure 3.5 B, E). Thus, the wandering phenotype of the branches is not due to floppiness, or an inability to hold themselves upright.

Interestingly, the modulus of elasticity (a material property independent of branch diameter which reflects the ability of the wood to resist bending) and the modulus of rupture (a material property which reflects the wood's resistance to breaking) are both significantly reduced in one-year branches (Figure 3.5 C, F). This means that the wood is more flexible and less strong, even though flexibility and strength of the branches themselves is not affected. This is possible through an increase in average diameter in one-year branches (Figure 3.5 D).

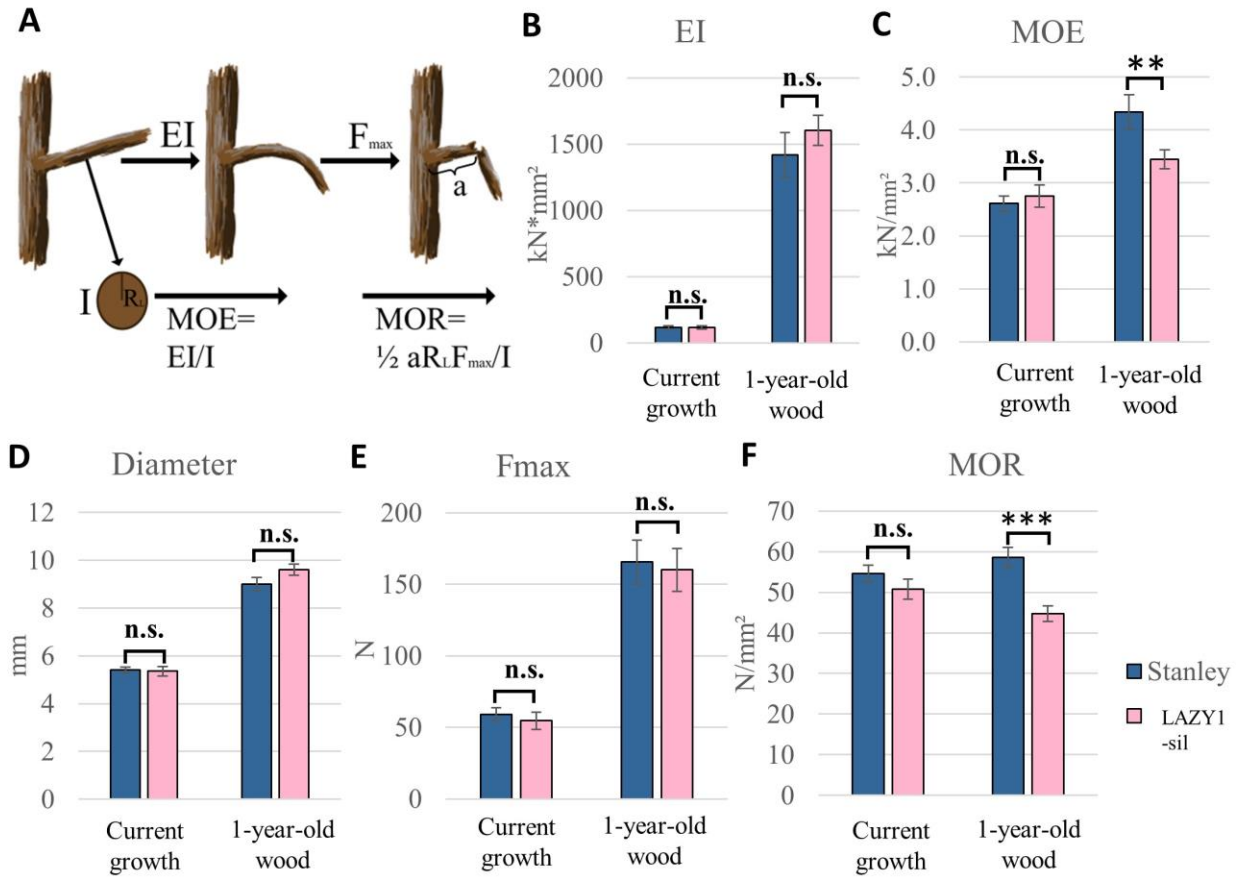

Figure 3.5: Biomechanical properties of *LAZY1*-silenced current year growth and one-year-old branches. A) Diagram illustrating biomechanical properties, including flexural stiffness (the resistance of the branch to bending, EI), area moment of inertia (a measure of how the cross-sectional area is distributed, I), radius in direction of loading (RL), modulus of elasticity (a measure of how the material resists bending in the elastic region, MOE), maximum force the branch can withstand (Fmax), distance from support to load (a), and modulus of rupture (a measure of how much force the material can withstand-MOR). Note that the formula shown for MOR is for a four-point bending test, as was performed on our branches. B-F) Biomechanical properties of LAZY1-silenced branches compared to Stanley: EI (B), MOE (C), diameter (D), Fmax (E), and the MOR (F). Bars represent standard error. Branches taken from 4 trees per genotype. N=30 per genotype for new growth, N=13 for Stanley 1st year, and N=14 for LAZY1-sil 1st year. Comparisons between genotypes done with pairwise t-tests. * indicates significantly different at α=0.10, ** indicates significant at α=0.05, *** indicates significant at α=0.01, n.s. indicates not significant at α=0.10.

LAZY1-silenced leaves are chlorotic, with reduced chlorophyll and altered photosynthesis.

All six transgenic lines on their own roots were planted in the field near Kearneysville, WV, while line 4 grafted on Myrobalan and line 6 on its own roots were also planted in the field near

Clarksville, MI. Toward the end of each growing season, some field-grown *LAZY1*-sil lines in both locations exhibited leaf chlorosis (Figure 3.6 B-D). To quantify this chlorosis, relative chlorophyll content was measured across all lines in West Virgina in 2021 (Figure 3.6 A). The phenotype was somewhat variable, with lines 1,5,6, and 7 showing reduced chlorophyll content, while lines 2,3, and 4 did not. However, additional data on lines 1-4 from 2018 showed significantly reduced chlorophyll in lines 1, 2, and 3 (Figure 3.15). This is consistent with our observations that the extent and timing of chlorosis varies depending on line, year, and location, indicating G x E interaction in this phenotype.

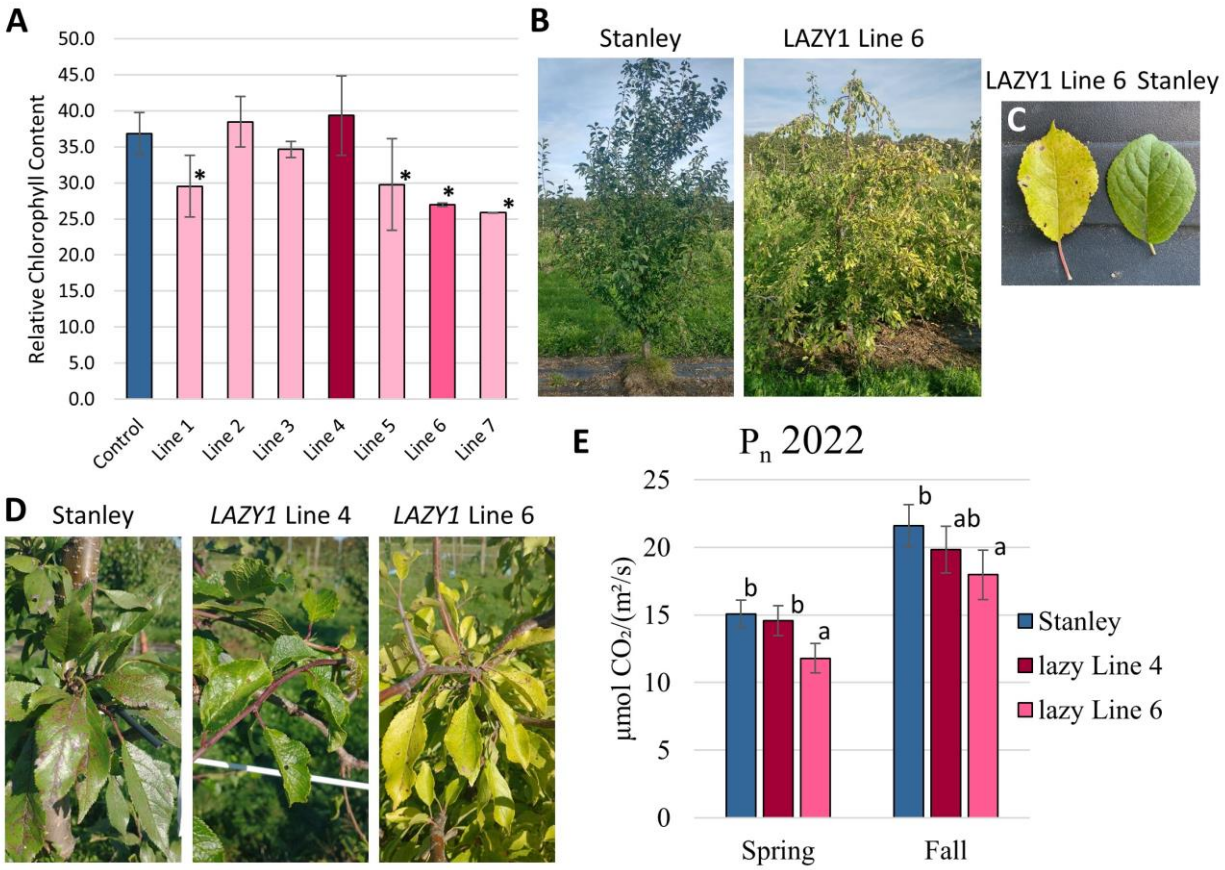

Figure 3.6: Photosynthetic phenotype of *LAZY1*-silenced lines. A) Chlorophyll content of *LAZY1*-sil lines in West Virginia. B) *LAZY1*-sil line 6 and Stanley control grown in Michigan. C) Leaf chlorosis comparison for Stanley and line 6 in West Virginia. D) Leaf photos taken Fall 2021 in Michigan. E) Net photosynthesis in spring vs fall for the 2022 growing season in Michigan. Means within the same timepoint with the same letter are not significantly different at α=0.05. 30 or more measurements were taken for each Genotype*Timepoint combination.

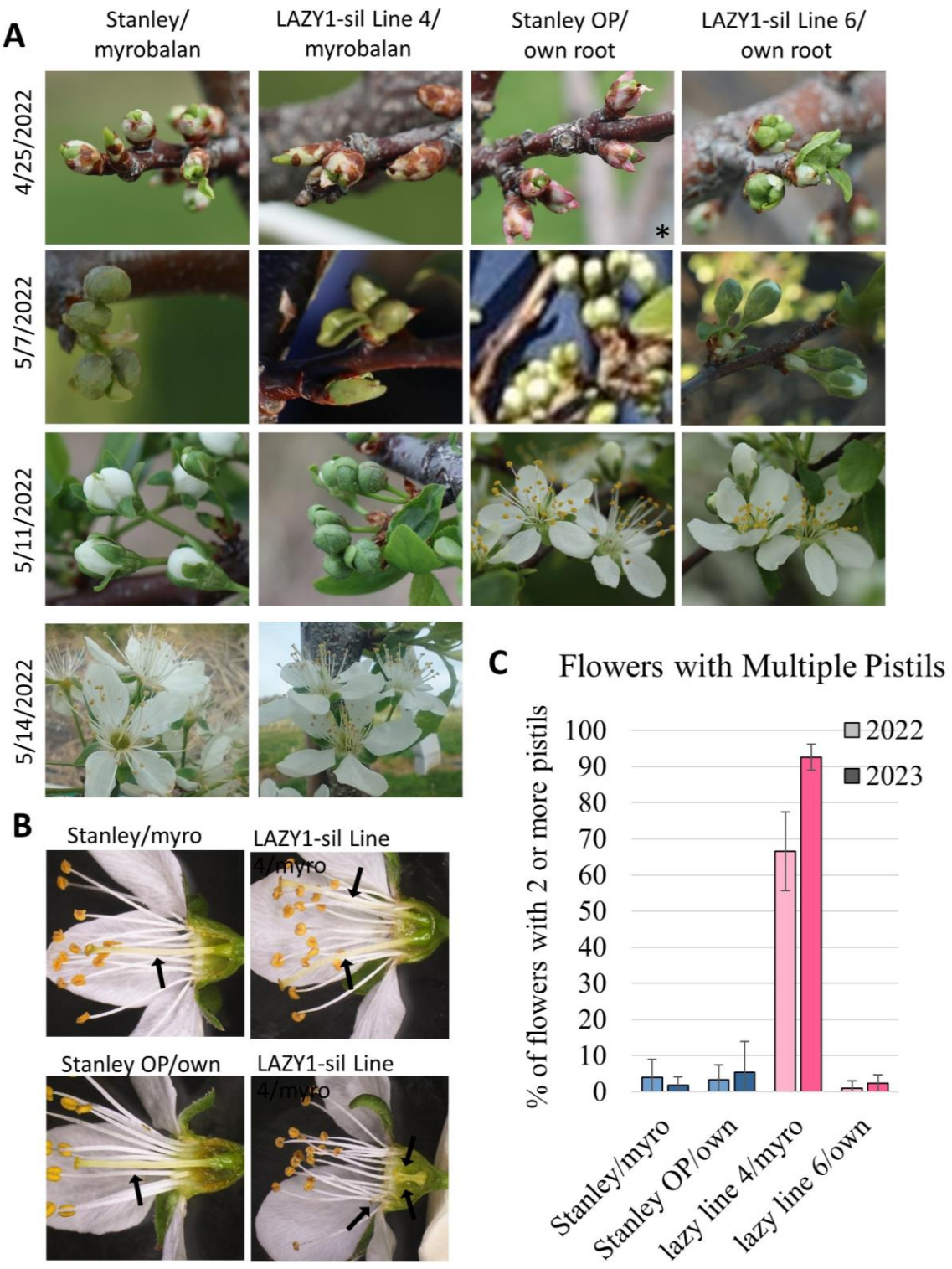

Figure 3.7: Flower phenotypes in *LAZY1*-silenced lines. A) Bloom time phenotypes in LAZY1-sil on myrobalan rootstock and own roots. *Note that the photo for Stanley OP own root for 4/25/22 is a photo of Stanley OP transgenic control for a different gene, on own root. B) Double pistil phenotype in Line 4/myro C) Quantification of the double pistil phenotype.

To further investigate the potential causes and effects of this chlorosis, we measured net photosynthesis for the consistently non-chlorotic line 4 and the consistently chlorotic line 6, during spring and fall 2022 in the Michigan trees. Consistent with the chlorophyll measurements, photosynthesis was reduced in Line 6, but not in Line 4 (Figure 3.6 E). Interestingly, Line 6 had decreased photosynthesis at both timepoints, even though leaves were not yet chlorotic at the spring timepoint.

LAZY1-silenced lines show some aberrant reproductive phenotypes.

LAZY1-sil trees in Michigan demonstrated alterations in bloom time, which were affected by whether the trees were own-root or grafted onto myrobalan. Line 6 on own roots bloomed earlier than Stanley OP on own root. In contrast, line 4 on myrobalan bloomed slightly later than Stanley on myrobalan (Figure 3.7 A).

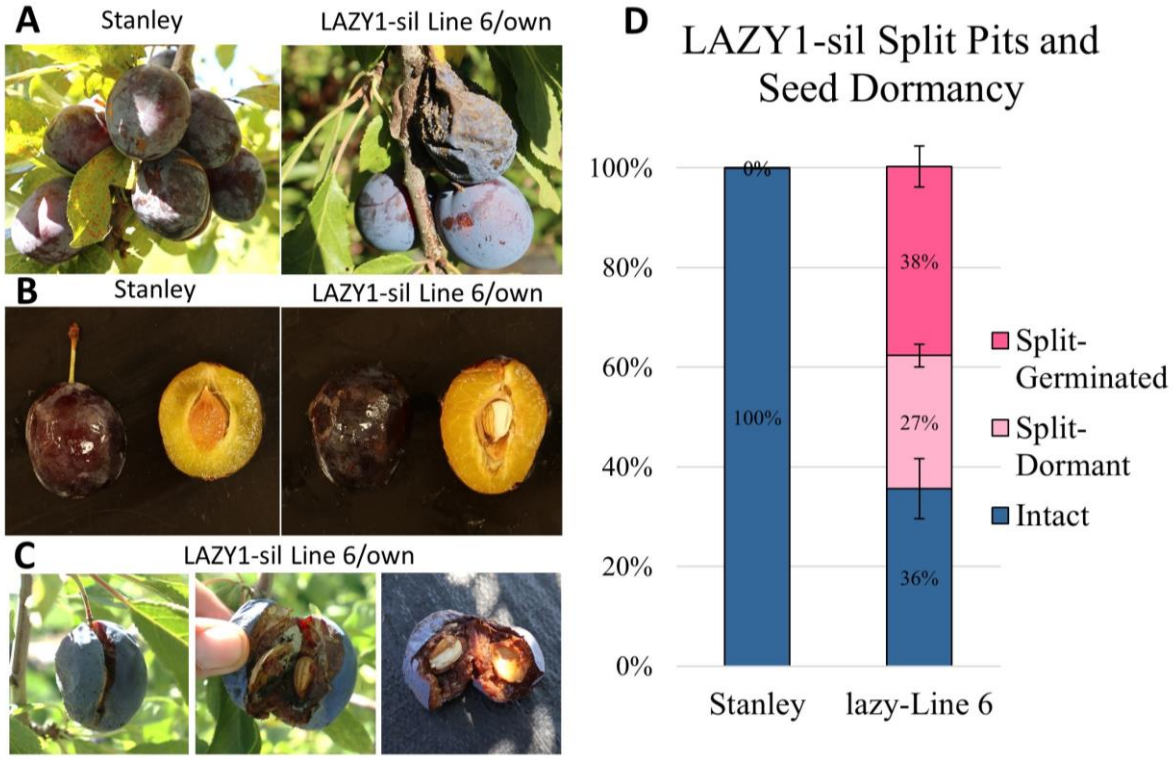

Figure 3.8: Fruit and germination phenotypes in *LAZY1*-silenced Line 6. A) Uneven ripening in LAZY1-sil Line 6 as compared to Stanley. B) Normal fruit from Stanley, and split pit with germinating seed from Line 6. C) Example of split pit in a split fruit on Line 6 and of a seed germinating in the field without any chilling. D) Quantification of split pits and number germinated. N fruit=896 for Stanley OP, and 420 for lazy Line 6.

Once the trees had reached reproductive age in the field in West Virginia, LAZY1-sil lines 4 and 5 were observed to have a double pistil phenotype, which was not observed in line 1 or in Stanley or Stanley OP controls. This phenotype was subsequently quantified in lines 4 and 6 in Michigan in 2022 and 2023. For line 4 grafted on myrobalan rootstock, 67-93% of flowers had two or more pistils, compared 2-5% for Stanley on myrobalan or Stanley OP on own roots (Figure 3.7 C). Interestingly, lazy line 6 on own roots did not have a significant number of double pistils either year. Dissection of the *LAZY1*-sil flowers revealed some flowers with three pistils, which was not observed in Stanley (Figure 3.7 B). Some of these pistils were growing out of the top of the hypanthium, among the stamen, indicating a localized homeotic transformation in the third floral whorl (Figure 3.7 B). *LAZY1*-sil line 4 on myrobalan and some Stanley on myrobalan trees did not set fruit. For the line 4 trees, this is likely related to the double pistil phenotype. *LAZY1*-sil line 6 on own root set fruit, which ripened very unevenly in comparison to Stanley, with some fruit over-ripe and desiccated immediately next to fruit that was just barely ripe or slightly green (Figure 3.8 A). Further, *LAZY1*-sil line 6 had a dramatic "exploding fruit" phenotype in which many of the fruits split along the suture line to reveal a split pit, and the seed dropped out of the fruit onto the ground (Figure 3.8 C). Split pits were observed at low frequency in open-pollinated Stanley, but about 65% of fruit in line 6 had a split pit (Figure 3.8 D). Other phenotypes observed rarely in *LAZY1*-sil Line 6 which suggest disturbance in carpel development included pits which were not split, but had a segment of the pit missing (forming a "window" into the pit), presence of double pits in a single fruit, and presence of two seeds in a single pit. Finally, *LAZY1*-sil Line 6 exhibited vivipary, with many of the seeds germinating in the fruit on the tree, without vernalization (Figure 3.8 B, C). Subsequent analysis found that 58% of seeds in split pits were germinating (Figure 3.8 D).

Discussion

In this work, we have demonstrated that manipulation of *LAZY1* expression can effectively alter branch angle in a tree fruit crop. Branch angle in *LAZY1*-silenced lines was increased throughout the life of the plant, from the seedling stage through maturity. Furthermore, the phenotype was stable even when grafted onto rootstock. These wider branch angles have the potential to facilitate a movement in tree fruit production toward planar training systems, which have been shown to be more efficient and more economical than traditional three-dimensional systems (DeJong et al., 1997). As an illustration of the potential of trees with reduced *LAZY1* expression in planar training,

line 4 trees grafted onto Myrobalan were trialed in planar systems. The two training systems trialed were super spindle axe (SSA), a commonly used system for commercial tree fruit production (Figure 3.9 B), and espalier, an ornamental production system with applications for home growers, especially in areas with limited space (Figure 3.9 A). As anticipated, the wider angles in *LAZY1*-sil lines resulted in a more open canopy, which particularly facilitated SSA training. More open canopies are beneficial to production systems because they improve light penetration, increasing fruit quality and flower bud development (Tustin et al., 1988). The wider crotch angle, horizontal orientation, and lack of gravitropic response also simplified obtaining horizontal branches in the espalier training.

A more unexpected benefit to planar training from manipulating *LAZY1* expression came from the lack of apical dominance and the failure of the main trunk to grow upright. As described, mature *LAZY1*-silenced trees tend to have a bush-like growth habit, with no clear leader, and more growth horizontally than vertically (Figure 3.9 B). This unexpectedly solved one of the central problems in planar systems, which is keeping the trees at or below the height of the trellis without stimulating excessive vegetative vigor by heading the tree. For example, Stanley generally sends up a single leader with limited lateral branches, which rapidly grows above the trellis (Figure 3.9 B). Heading this leader provokes a strong flush of growth that must be thinned. Because *LAZY1*-sil trunks must be staked upright for vertical growth, they will never grow significantly taller than the trellis (Figure 3.9 B). Further, because of the alterations in apical dominance/control, this does not provoke a flush of vegetative growth at the top of the tree.

The undirected growth of *LAZY1*-sil branches does present unique challenges for training. For Stanley espalier, horizontal branches can be trained between wires through counteracting gravitropism by tying the branches to the wire below. Since *LAZY1*-sil trees do not have gravitropic responses, it is extremely difficult to train branches between wires, as they have to be tied both up and down (Figure 3.9). From a training perspective, the problem can be solved by placing a wire at each interval where horizontal growth is desired, and tying the branch directly to it. The phenotype may also be of value in an ornamental context, where wandering branches, as in corkscrew willows, often are prized for adding winter interest to landscaping. Interestingly, the wandering branch trajectory in *LAZY1* knockdowns or mutants has not been previously reported, to our knowledge, even in woody species such as apple (Dougherty et al., 2023). This may indicate that the wandering phenotype is sensitive to dosage of *LAZY* genes and levels of expression from

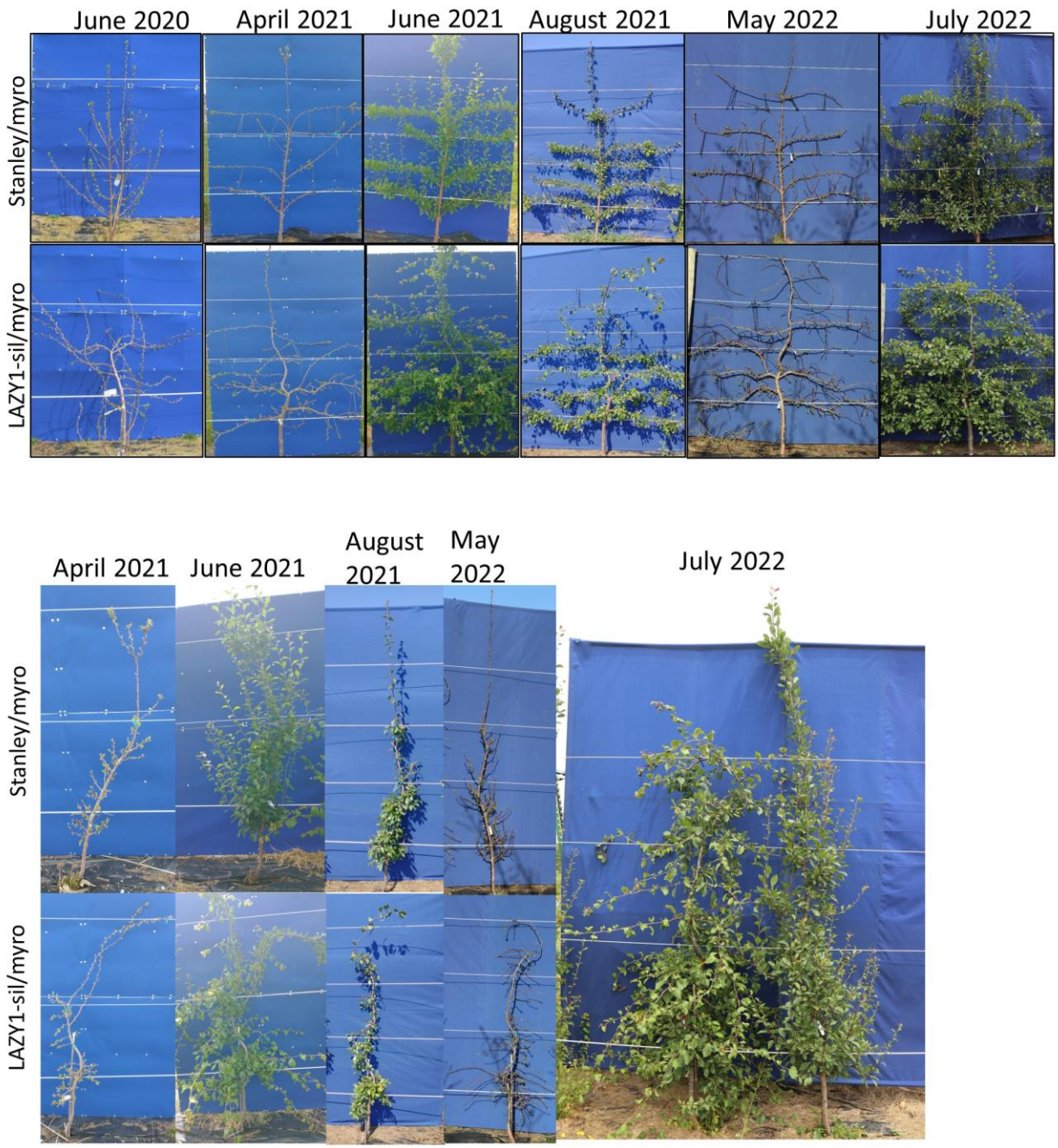

Figure 3.9: Examples of Stanley and *LAZY1*-silenced Line 4 on myrobalan rootstock trained into planar systems A) Espalier training. B) SSA training. Note how by August 2021, Stanley in Espalier is way above the top (fourth) trellis wire, while LAZY1-sil is growing along it and down.

the various homologs. Alternatively, it may be a phenotype which is unique to plum due to differences in wood composition and natural growth habit.

Crucially, modification of *LAZY1* expression did not reduce the strength or stiffness of branches on *LAZY1*-sil trees, and these more horizontal branches are capable of supporting a crop load. The decrease in MOE and MOR and the concomitant increase in diameter is consistent with flexure wood, such as is formed under wind stress (Telewski, 2012). In flexure wood, MOE and MOR are reduced while diameter in the direction of the wind increases, allowing the branch to simultaneously resist bending better, while absorbing more of the energy (Telewski, 2012). The decrease in MOE in flexure wood is driven by an increase in xylem wall microfibril angle, which is also seen in reaction wood (wood that forms when branches are displaced to return them to their setpoint angle; Telewski, 2012). Thus, the alterations seen in *LAZY1*-sil branches are consistent with known responses in horizontal limbs. Therefore, a parsimonious explanation for these changes is that they are byproducts of the unique *LAZY1*-sil branch orientation, with branches forming reaction wood and/or flexure wood in response to their horizontal orientation.

In addition to the architecture phenotypes, we observed a number of pleiotropic phenotypes. Particularly notable is the chlorotic leaves and associated reduction in chlorophyll and photosynthesis. Leaf chlorosis was observed in six out of seven *LAZY1*-sil lines in at least one of the seasons when chlorophyll content was measured. This phenotype has not been previously reported for *lazy1* mutants. That may be because most studies are short-term experiments in growth chambers, whereas the chlorotic phenotype becomes apparent midway through the growing season in the strong light of the greenhouse or field. Given recent revelations about the presence of LAZY1 protein in the plastid membrane (Chen et al., 2023; Nishimura et al., 2023), this chlorosis may indicate a role for LAZY1 in the response of photosynthesis to light-related signaling, the absence of which results in damage. This hypothesis is strengthened by the observation that photosynthesis is reduced in the spring in the chlorotic line 6, prior to any observable leaf chlorosis. Obviously, this chlorotic phenotype is a problem for production systems, although it may be considered a desirable trait in ornamentals. The variance of the phenotype among lines and seasons suggests that the phenotype may not have 100% penetrance, which may assist with overcoming this challenge.

The various reproductive phenotypes observed in *LAZY1*-sil lines relate to problems with meristem and organ-boundary formation (double carpels) or dormancy (flowering time and vivipary). Defects in inflorescence organization have been reported previously for *lazy1* mutants in maize, which had disrupted ear and tassel development, with disorganized placement of floral axillary

meristems (Dong et al., 2013). This is consistent with the expression of LAZY homologs in floral organs (as in maize, camellia, and arabidopsis; Dong et al., 2013; Hollender et al., 2020; Xia et al., 2021), and the known role of polar auxin transport in floral meristem development (Dong et al., 2013). Dormancy and chilling requirements of flower buds and seeds are known to be correlated in apple and peach, sharing common regulatory pathways (Mehlenbacher and Voordeckers, 1991; Fu et al., 2014). The earlier bloom time and vivipary in Line 6 are consistent with this known correlation. Unintended impacts on bloom time, flower and fruit morphology, or seed dormancy may all present additional challenges for utilizing trees with reduced *LAZY1* expression in commercial production. Further research is needed on the consistency and penetrance of these phenotypes, both in plum and other tree fruit species.

Materials and methods

LAZY gene identification and phylogeny.

LAZY genes in *P. domestica* were identified using BLASTp of the previously identified peach LAZY proteins (Waite and Dardick, 2021) against predicted proteins from the *Prunus domestica* draft genome v1.0 (Callahan et al., 2021). Due to a highly unusual exon-intron structure, *LAZY* genes are often mis-annotated (Zhang et al., 2022). This structure is conserved across species, with each gene containing five exons, with the first exon including just two codons (often an "ATGAAG") and the last exon containing only ~20 bases (Zhang et al., 2022). To identify and correct errors in annotation, the DNA sequences of plum genes identified as *LAZY* homologs were aligned to the homologous peach and arabidopsis sequences. Using that alignment, the plum and peach genes were re-annotated with particular attention to identifying a gene model that fit the conserved gene structure. Following re-annotation, the protein sequences were predicted, and the resulting protein sequences were used for subsequent alignments.

Alignments and phylogenetic trees were produced in CLC Genomics Workbench v22.0. Alignments were performed using a gap open cost of 10.0 and a gap extension cost of 1.0, the alignment set to "Very accurate." The protein phylogenetic tree was constructed using the Neighbor Joining method with Jukes-Cantor as the protein distance measure, and 100 bootstrap replicates.

Cloning.

To generate *LAZY1* silenced plum lines, a 306bp fragment corresponding to the peach LAZY1 gene (peach genome version 1.0 ID ppa007017, now named Prupe.1G222800 in genome version

2) was amplified using primers PpLazy-1 1F (5' AAG CCA AAC TGT GGC ACA AAG C) and PpLazy-1 2R (5'AGC TGC CAG GAC TTT CTC CAA T), cloned into the pENTR-D TOPO vector (Invitrogen, Carlsbad, CA), and then into the pHellsgate 8.0 vector (Helliwell et al., 2002) using LR Clonase (Invitrogen, Carlsbad, CA). While the intended construct would have had two copies of the 306bp fragment as a hairpin, the construct used for transformation was later discovered to only have a single insert in the reverse orientation behind the 35S promoter within pHellsgate 8.0, creating an anti-sense vector for *LAZY1* rather than an RNAi construct (Figure 3.11).

Plum transformation.

The pHELLSGATE 8.0 plasmid containing the peach *LAZY1* gene fragment was transformed into Agrobacterium tumefaciens strain GV3101. The gene construct was engineered into European plum (*Prunus domestica* L) following the protocol of Petri et al., 2012. Cold (4˚C) stored seeds of 'Stanley' plum were used for transformation. Briefly, the seeds were first cracked to remove the stony endocarp, surface sterilized with 15% commercial bleach for 15 min., washed three times with sterile water, and the hypocotyl slices were excised from the zygotic embryos under a laminar flow hood using a stereomicroscope. After incubating for 20 min. in an Agrobacterium suspension, the transformed hypocotyl sections were cultured for 3 days in co-cultivation medium. Finally, the hypocotyl sections were plated in antibiotic (80 mg/l kanamycin) selection medium to produce transgenic shoots. The kanamycin resistant transgenic shoots were multiplied in plum shoot multiplication medium, rooted, acclimatized in the growth chamber and planted in 15-23cm pots in a temperature-controlled greenhouse to evaluate growth and development.

Plant material.

Greenhouse-grown *LAZY1-sil* and control lines were used for quantifying gene expression and for branch and petiole angle analysis. Trees were 1-2 years old when gene expression was quantified and petiole angles were measured, and 2-3 years when branch angles were measured.

The controls for lazy expression were transformed plum seedlings from open-pollinated plum cultivar 'Stanley' (Stanley OP) that did not contain the *LAZY1-sil* vector. These plums instead contained the pSUC/PSUL vector, which does not impact branch angle (Collum et al., 2020).

LAZY1-sil plum trees and controls for the *Prunus domestica* background 'Stanley' were also planted at the USDA ARS Appalachian Fruit Research Station (AFRS) research field near Kearneysville, WV and at the Michigan State University Clarksville Research Center (CRC) near

Clarksville, MI. The trees at AFRS were planted at ~2.4 m spacing in October 2014. The *LAZY1-sil* plums were planted in two blocks of three trees. Control plums were planted between groupings of *LAZY1-sil* trees. The trees at CRC were generated in 2017 and 2018 from budwood from AFRS, and were planted in September 2018. *LAZY1*-sil Line 4 trees and open-pollinated Stanley trees, grafted onto Myrobalan rootstock, were used for training studies. The trees were planted at ~2.4m spacings for espalier training and ~0.9m spacing for SSA training. The trees were trained to a trellis with ~46 cm spacing between wires. The CRC planting also contains the *LAZY1-sil* Line 6 trees on their own roots.

RNA extraction and gene expression analysis.

Total RNA was extracted from frozen tissue samples using E.Z.N.A SQ Total RNA Kit (Omega Bio-tek, Inc., USA), according to the manufacturer's instructions. Leaf tissue was used for extraction and for expression analysis in transgenic plums. Resulting RNA samples were then treated with DNase I to remove contaminating genomic DNA. To determine gene expression levels, qPCR reactions were carried out using the gene specific primers PpLAZY-qPCR-5F (5' ATGCTTTATGCTTCTTCTCG) and PpLAZY-qPCR-5R (5' TTGCTCAGCAGATGAGGT), and the SuperScript III Platinum SYBR Green One-Step qRT-PCR Kit with ROX (Invitrogen Corp., USA). The qPCR was run using an ABI 7900DNA Sequence detector (Applied Biosystems) according to the following parameters: cDNA synthesis step at 50 ˚C for 5 min, followed by PCR reactions at 95 ˚C for 5 min and 40 cycles of 95 ˚C for 15s, 60 ˚C for 30s, and a final cycle of 40 ˚C for 1 min. The qPCR was performed on RNA from three to four independent biological replicates (trees) for each transgenic line, as well as on five control trees. Each biological replicate had three technical replicates for the reactions. Relative expression values were determined using a standard curve (generated from serial dilutions of RNA from a tree that did not have the *LAZY1* vector), which was run at the same time.

Petiole and branch angle measurements.

Petiole angles for up to ten leaves growing from the trunk of young (<1-year old) trees that had not yet initiated lateral shoots were measured in 2013 using a protractor. For the control and lines 3 through 7, five trees were measured. Ten trees were measured for line 1, and three trees for line 2. Crotch (branch) angles for six branches from three to ten trees per genotype growing at AFRS were measured in 2021 using a protractor. Angles represent the angle between the branch and the

shoot from which it emerged. When the branch angles were measured, the trees were approximately 9-years-old and had been growing in the field for six years.

For both petiole and branch angle statistical analyses, the average angle per tree was considered a biological replicate, and standard deviations are based on those averages. Significant differences between the *LAZY1-sil* lines and control trees were determined by a p-value < 0.05 from Student's t-test.

Biomechanics measurements.

Branches were taken from clonal trees generated from budwood from a single Stanley tree and a single *LAZY1*-sil Line 4 tree grafted onto Myrobalan rootstock, grown at CRC and trained as Espalier. Horizontally oriented new growth and 1st year wood (branches initiated the previous season) were collected July 9, 2023. Four to five branches per tree were collected from four trees per genotype for new growth, for a total of 20 'Stanley' OP and 19 *LAZY1*-sil samples. Three to five branches per tree were collected from three trees per genotype for 1st year samples, for a total of 13 'Stanley' OP and 14 *LAZY1*-sil samples.

Four-point bending tests were conducted on an Instron Universal Testing Machine (Model 4202, Instron Corporation, Canton, MA) using a 500N load cell. The span of the outer supports was set to 90mm, while the two posts of the actuator were set to 30mm. Leaves and lateral branches were removed from a section of wood ~10 cm long, and the section was oriented so that the upper side of the branch was positioned down on the Instron, so that force was exerted in the same direction as gravitropic force acted on the branch in its original position. The force versus displacement curve was measured until a maximum force was reached.

Flexural stiffness (EI) was calculated using the equation $EI=(F/V)(a^2/12)(3L-4a)$, where (F/V) is the slope of the linear section of the force/displacement curve, a is the post to load distance and L is the total length of the span. Flexural stiffness was used to calculate the modulus of elasticity (MOE), using the equation MOE=EI/I where I is the area moment of inertia. For a branch with an elliptical cross section, $I= (\pi/4) (R_P)(R_L^3)$, where R_L is the radius in the direction of loading and R_P is the radius perpendicular to loading. The modulus of rupture (MOR) was calculated using the equation $MOR=(1/2\ Fmax)(a)(R_L)/I$, where Fmax is the maximum force withstood by the branch. To test for statistically significant differences between the genotypes, a Student's t-test was performed using the T.TEST function in Excel, assuming a homoscedastic two-tailed distribution.

Chlorophyll and photosynthesis measurements.

Chlorophyll measurements were taken in triplicate from field-grown trees at the AFRS using a SPAD 502 Chlorophyll Meter (Konica Minolta, Inc., Tokyo, Japan).

Photosynthetic parameters were measured in late spring (June 9th and June 23rd, 2022) and early fall (October 5, 2022) using a CI-340 infrared gas analyzer (CID Bio-science, Camas, WA). Measurements were taken with an open system in differential mode, with 6.25 cm² of leaf area in the chamber, and a flow rate of 0.3 l/min. Measurements were taken from trees at CRC, including control trees ('Stanley' OP on myrobalan rootstock and on own root), *LAZY1*-sil line 4 on myrobalan, and *LAZY1-sil* line 6 trees on their own roots. At each time point, three to five measurements were taken per leaf, on three to five leaves per tree, with two to six trees per genotype.

Statistical analysis was performed in R v4.3.1. To control for the environmental variability of the field conditions, net photosynthesis (Pn) for all genotypes from two seasons (2021 and 2022) was modeled as a response to photosynthetically active radiation (PAR), carbon dioxide concentration at intake (CO2in), air temperature (Tair), air pressure (Pressure), and water vapor pressure (H2Oin) at intake. Externally studentized residuals were used to identify influential outliers, and observations with a studentized residual greater than |2| were dropped (10 in total). Studentized residuals and the criterion Cooks Distance for point>3(mean Cooks distance) was used to identify outliers. Outliers were then manually checked. Outliers for which there were two or more outliers per leaf were retained as reflecting true biological variability, while single outliers were omitted. The model was then re-checked without outliers. Variance inflation factor (VIF) was used to check for collinearity of the environmental variables. Added variable plots were used to check for linearity and the contribution of each additional variable. Variables with the least contribution or the highest VIF were sequentially dropped until VIF<3 for all variables, and all variables had a clear contribution to the model. Finally, variables for genotype and for accounting for the repeated measures were added to the model and each year was modeled separately.

The resultant model for photosynthesis was Pn = μ + Genotype + Timepoint + Genotype*Timepoint + (1|Genotype:Tree) +(1|Genotype:Tree:Leaf) + PAR+ CO2 + Tair+ Pressure+error where μ indicates the grand mean, "Genotype" is a variable for the control or RNAi line, "Timepoint" accounts for the effects spring versus fall, "Genotype*Timepoint" accounts for the interaction between genotype and timepoint, (1|Genotype:Tree) controls for the effects of tree,

which is a random variable nested within genotype, (1|Genotype:Tree:Leaf) controls for leaf to leaf variation, and is nested in tree, and "PAR", "CO2in" and "Tair" are continuous variables controlling for their respective environmental factor. This model was gated with ANOVA, and normality and equal variances of the residuals were checked. Since interaction between genotype and timepoint was significant, all pairwise comparisons were performed for genotype slicing by timepoint using t-tests at α=0.05.

Reproductive phenotypes.

Flowering time was observed at CRC across the 2021-2023 seasons. The double pistil phenotype was initially observed in spring 2022 at AFRS in lines 4 and 5 ('Stanley', 'Stanley' OP, and lines 1,4, and 5 on own root were assessed). Subsequently, the percentage of flowers with two or more pistils was quantified in 'Stanley' OP on myrobalan and own roots, line 4/myrobalan, and line 6 on own roots at CRC in spring 2022 and 2023. In spring 2022, pistil number was counted for approximately 50 flowers per tree, for three or four trees per genotype. In spring 2023, pistil number was counted for approximately 100 flowers per tree, for three trees per genotype.

The split pit and seed dormancy phenotypes were observed in line 6 trees in the field at CRC in fall 2022 and fall 2023. It was quantified in fall 2023 using three Stanley OP and three line 6 trees, all on their own roots. Approximately 200-300 fruit per tree (or all the fruit from a tree if there were fewer than 200) were harvested for quantifying number of split pits and seed dormancy. Fruit was harvested September 1, 2023 and stored at 4C until the fruit could be pitted (two to five weeks). To minimize any effects of storage prior to pitting, one Stanley and one line 6 tree were assessed on each date that fruit was pitted.

Acknowledgments

The authors would like to acknowledge our funding sources: Michigan State University, The United States Department of Agriculture National Institute of Food and Agriculture HATCH project 1013242 (to CAH) and MSU AgBioResearch Project GREEEN grant GR18-031 (to CAH). We would also like to acknowledge Srinivasan Chinnithambi and Ralph Scorza for performing plant transformations, Elizabeth Lutton for cloning the constructs, Frank Telewski's lab for allowing us to use their Instron and assistance with it, Peter Kohler for assistance with data formatting and statistical analysis, and Joy Johnson and Andrew Scheil for assistance with photosynthesis measurements and imaging at MSU Clarksville Research Station.

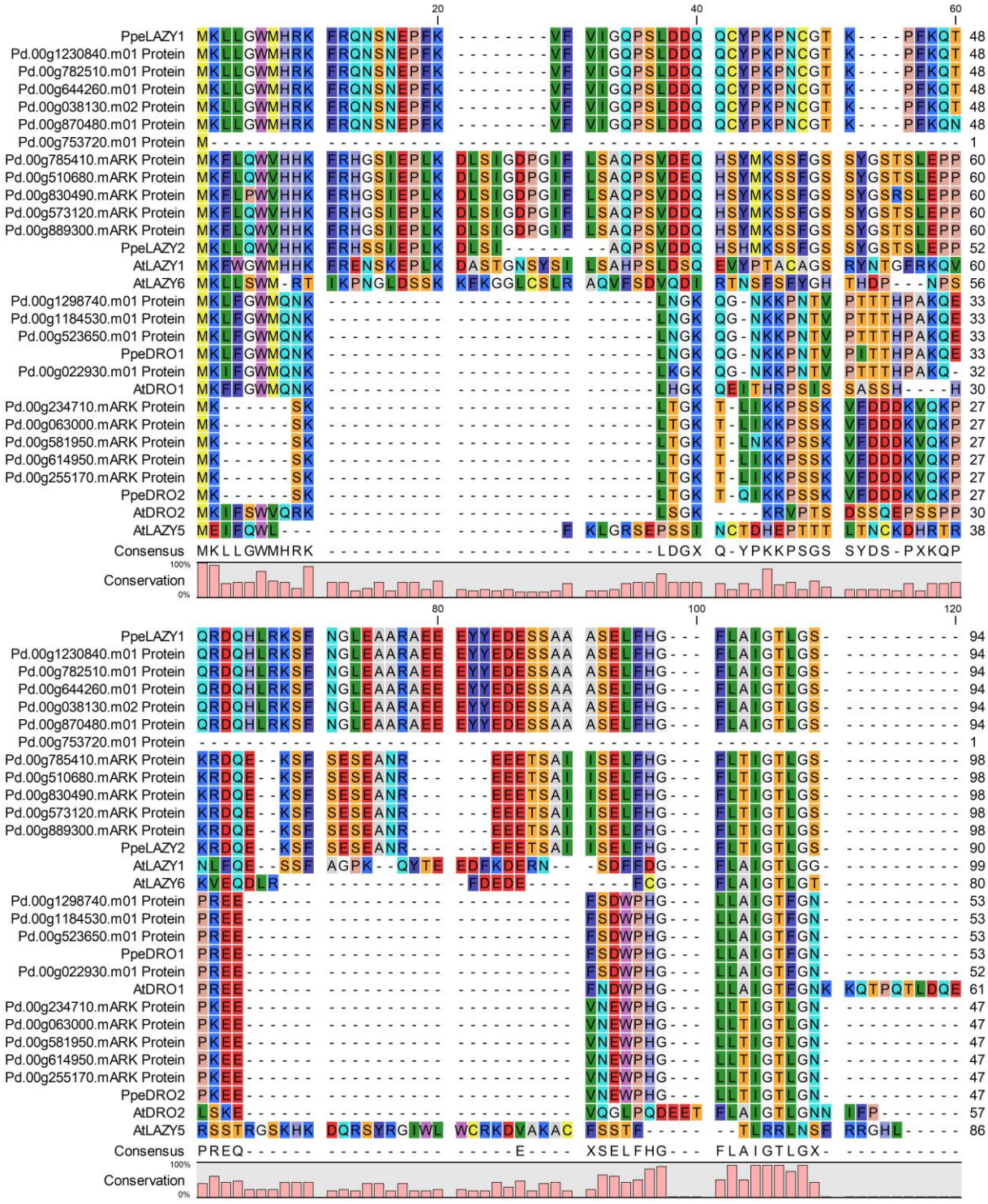

Figure 3.10: LAZY protein alignment. Pd=*Prunus domestica;* Ppe=*Prunus persica*; At= *Arabidopsis thaliana.*

Figure 3.10 (cont'd)

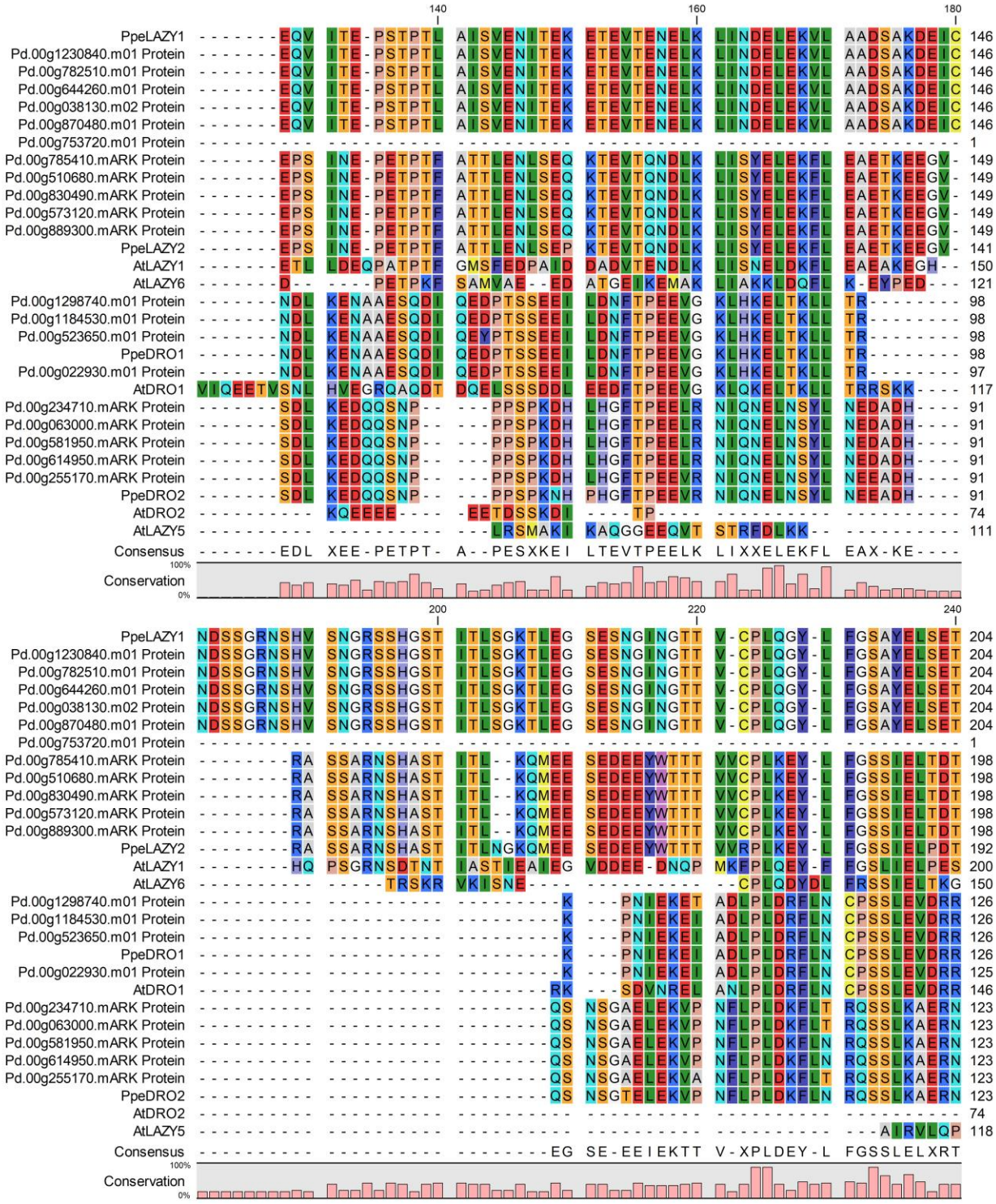

Figure 3.10 (cont'd)

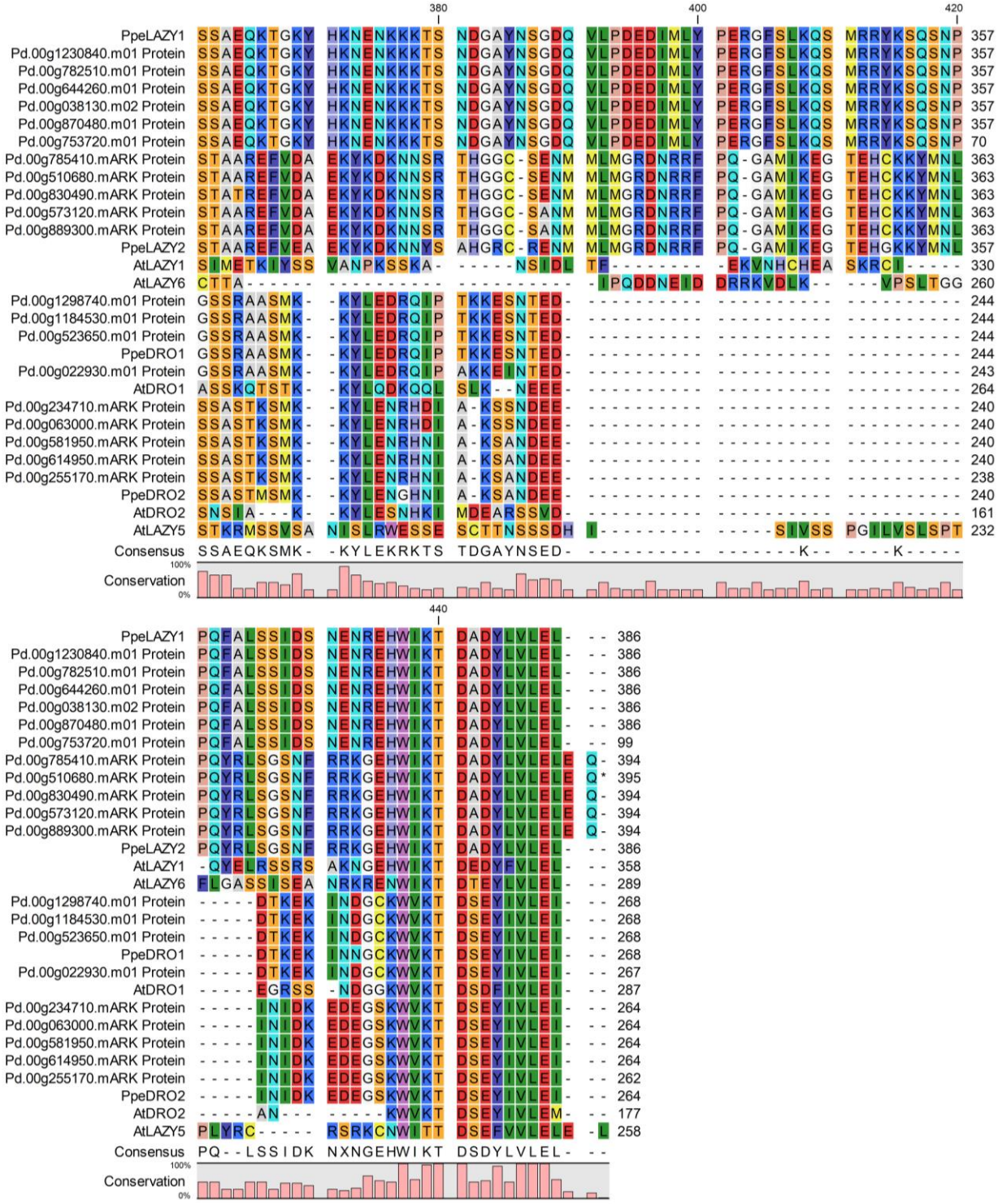

Figure 3.10 (cont'd)

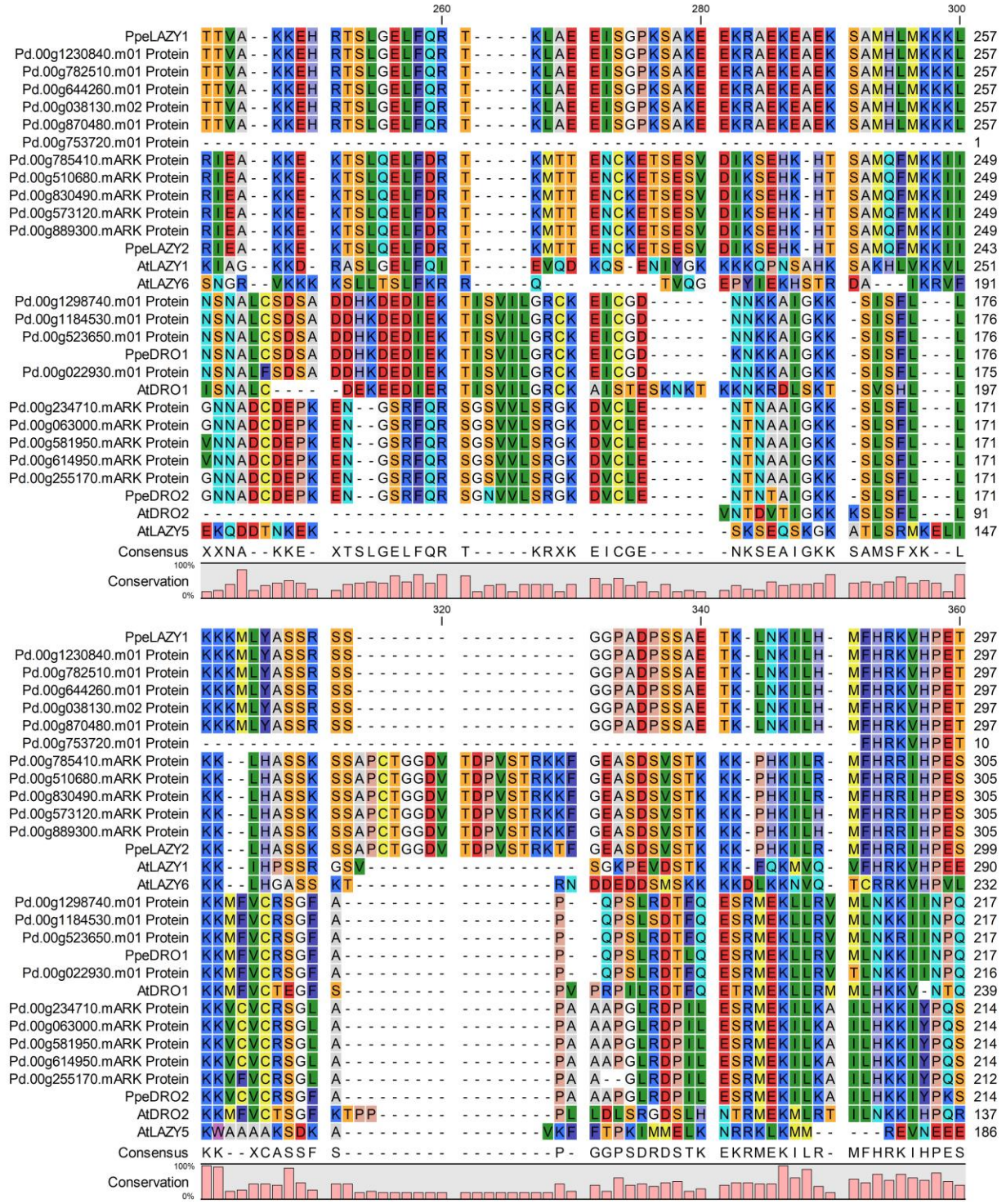

>PpeLAZY1 mRNA

ATGCCAATGTTGCAGTTACTAGGTTGGATGCATCGTAAGTTTCGGCAGAATAGCAACG
AGCCATTTAAAGTTTTTGTCATTGGGCAGCCATCTCTCGATGATCAACAATGCTATCCT
AAGCCAAACTGTGGCACAAAGCCCTTTAAACAAACCCAGAGAGACCAGCACCTTCG
GAAGTCTTTCAACGGTCTAGAGGCAGCCAGGGCAGAAGAAGAATACTATGAAGATGA
ATCATCTGCTGCAGCATCTGAGCTCTTCCATGGCTTCCTTGCAATTGGTACCCTTGGCT
CAGAGCAAGTCATCACGGAACCATCAACTCCAACACTTGCCATCTCTGTGGAGAACA
TAACTGAAAAAGAGACTGAGGTCACAGAGAATGAATTGAAGCTCATCAATGATGAAT
TGGAGAAAGTCCTGGCAGCTGATTCAGCTAAAGATGAGATTTGCAATGATTCATCTGG
AAGAAACAGCCATGTTAGCAATGGAAGAAGTAGCCATGGTAGCACCATCACACTAAG
TGGCAAGACACTGGAAGGCTCAGAGAGCAATGGGATTAATGGAACCACAGTGTGCC
CACTCCAGGGATATCTTTTTGGGTCAGCATATGAATTGTCAGAAACAACAACAGTGGC
AAAGAAGGAACACAGGACATCTCTTGGCGAGCTGTTTCAGAGGACTAAATTGGCAG
AGGAGATTTCTGGACCGAAATCGGCCAAGGAGGAGAAGCGAGCAGAGAAGGAAGC
TGAAAAGTCCGCCATGCACTTGATGAAAAAGAAGCTCAAGAAAAAAATGCTTTATGC
TTCTTCTCGCAGCTCTGGTGGACCTGCAGATCCTTCCTCAGCGGAAACAAAACTGAA
TAAGATCCTTCACATGTTCCACAGAAAAGTTCACCCTGAAACCTCATCTGCTGAGCAA
AAAACTGGTAAGTACCATAAGAACGAAAACAAGAAGAAAACAAGCAATGATGGGGC
TTACAACAGTGGAGATCAGGTGCTTCCAGATGAAGACATCATGCTATATCCTGAACGA
GGCTTCTCCTTGAAGCAGAGCATGCGGCGCTACAAGAGTCAATCAAACCCACCGCAA
TTCGCGCTTAGCAGCATTGATTCAAATGAGAACAGGGAGCACTGGATCAAAACAGAT
GCAGACTACTTAGTCTTGGAGCTGTGA

Figure 3.11: PpeLAZY1 mRNA sequence. Cloning primers highlighted in yellow and the remaining insert sequence in gray highlighting.

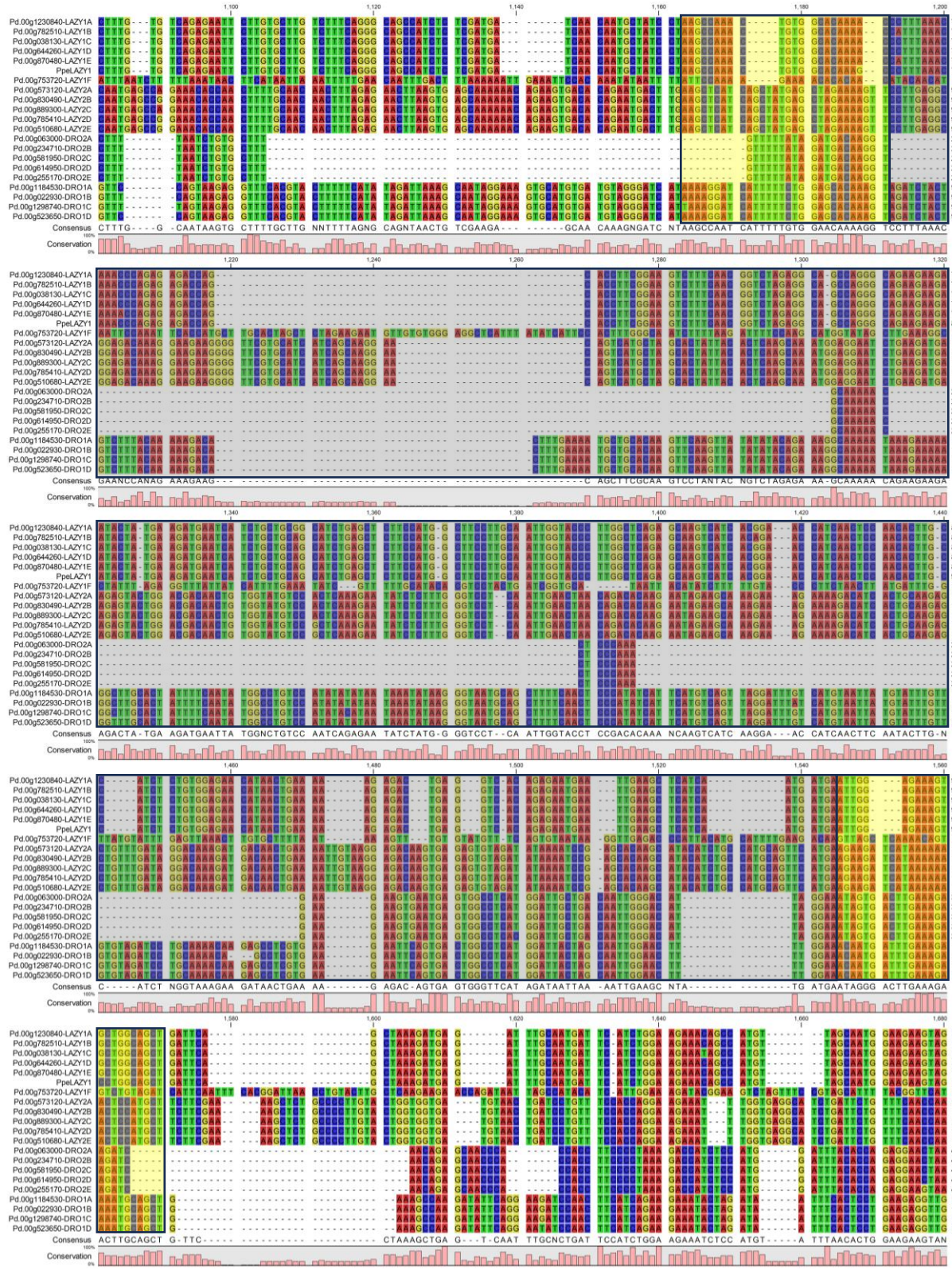

Figure 3.12: Plum *LAZY* gene alignment to the insert sequence from *PpeLAZY1*. Cloning primers highlighted in yellow and the remaining insert sequence in gray.

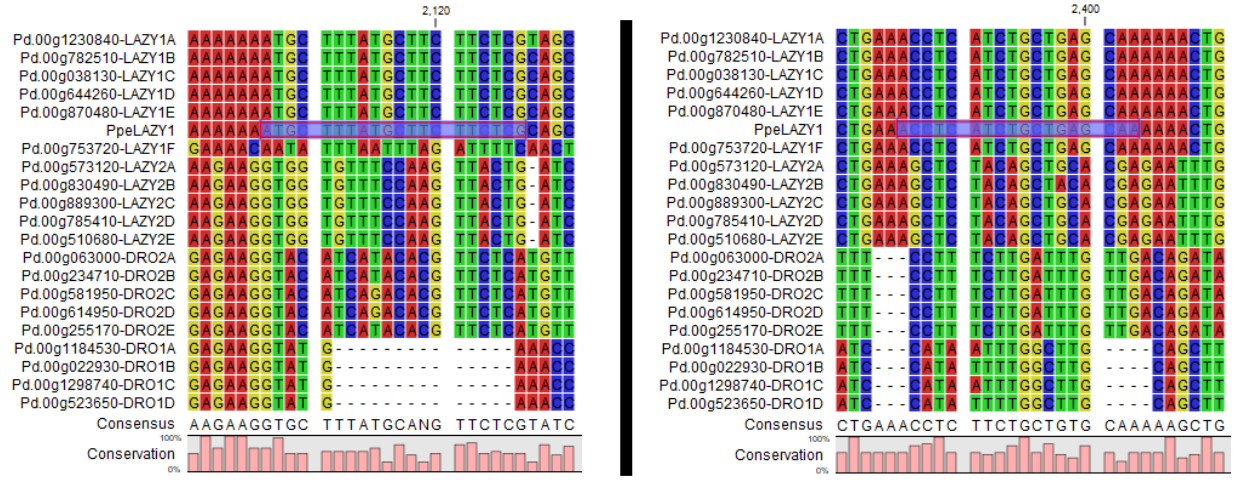

Figure 3.13: Sequence alignment for sequence used for gene expression primers.

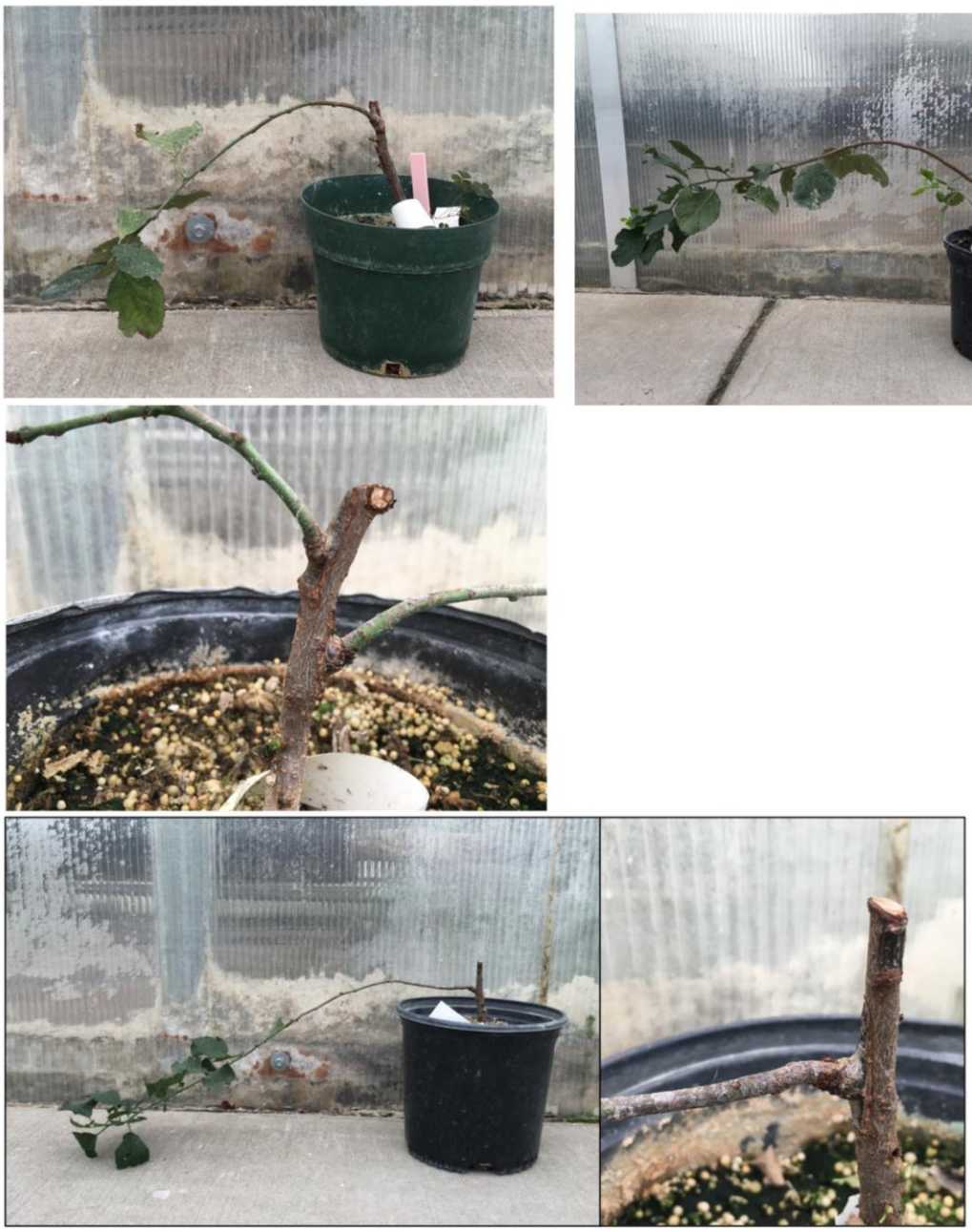

Figure 3.14: Additional trees with *LAZY1*-silenced buds grafted onto Myrobalan rootstock.

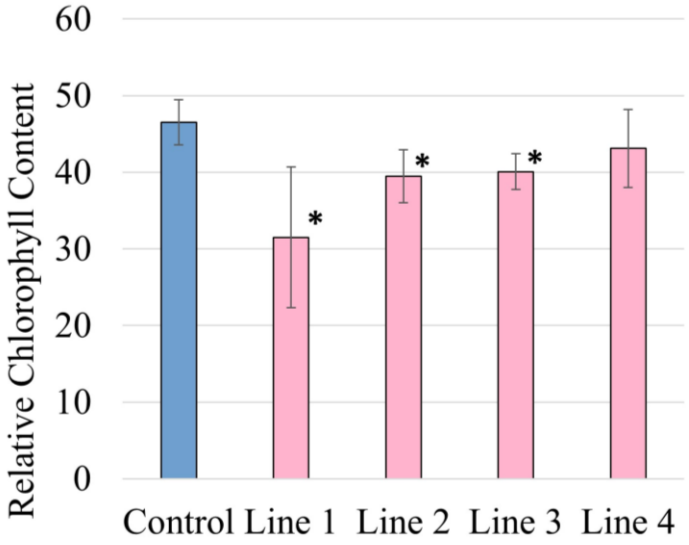

Figure 3.15: Chlorophyll content for AFRS trees in 2018.

REFERENCES

Arai-Sanoh Y, Takai T, Yoshinaga S, Nakano H, Kojima M, Sakakibara H, Kondo M, Uga Y (2014) Deep rooting conferred by *DEEPER ROOTING 1* enhances rice yield in paddy fields. Scientific Reports **4**: 5563

Callahan AM, Zhebentyayeva TN, Humann JL, Saski CA, Galimba KD, Georgi LL, Scorza R, Main D, Dardick CD (2021) Defining the 'HoneySweet' insertion event utilizing NextGen sequencing and a de novo genome assembly of plum (*Prunus domestica*). Horticulture Research **8(1)**: 8

Che X, Splitt BL, Eckholm MT, Miller ND, Spalding EP (2023) BRXL4-LAZY1 interaction at the plasma membrane controls *Arabidopsis* branch angle and gravitropism. The Plant Journal **113(2)**: 211–224

Chen J, Yu R, Li N, Deng Z, Zhang X, Zhao Y, Qu C, Yuan Y, Pan Z, Zhou Y, et al (2023) Amyloplast sedimentation repolarizes LAZYs to achieve gravity sensing in plants. Cell **186(22)**: 4788-4802

Chen S, Huang Y, Han J, Zhang S, Yang Q, Li Z, Zhang Y, Mao R, Fan L, Liu Y, et al (2022) Blocking rice shoot gravitropism by altering one amino acid in LAZY1. International Journal of Molecular Sciences **23(16)**: 9452

Chen Y, Xu S, Tian L, Liu L, Huang M, Xu X, Song G, Wu P, Sato S, Jiang H, et al (2019) The *LjLAZY3* gene plays a distinct role in the positive root gravitropism in *Lotus japonicus*. Journal of Experimental Botany **71(1)**: 168-177

Corelli-Grappadelli L (2000) The palmette training system. Acta Horticulturae **513**: 329–336

Dardick C, Callahan A, Horn R, Ruiz KB, Zhebentyayeva T, Hollender C, Whitaker M, Abbott A, Scorza R (2013) *PpeTAC1* promotes the horizontal growth of branches in peach trees and is a member of a functionally conserved gene family found in diverse plants species. The Plant Journal **75(4)**: 618–630

DeJong TM, Tsuji W, Doyle JF, Grossman YL (1997) Do high density systems really pay? - Evaluation of high density systems for cling peaches. Acta Horticulturae **451**: 599-604

Dong Z, Jiang C, Chen X, Zhang T, Ding L, Song W, Luo H, Lai J, Chen H, Liu R, et al (2013) Maize LAZY1 mediates shoot gravitropism and inflorescence development through regulating auxin transport, auxin signaling, and light response. Plant Physiology **163(3)**: 1306–1322

Dougherty L, Borejsza-Wysocka E, Miaule A, Wang P, Zheng D, Jansen M, Brown S, Piñeros M, Dardick C, Xu K (2023) A single amino acid substitution in MdLAZY1A dominantly impairs shoot gravitropism in *Malus*. **193(2)**: 1142-1160

Fu XL, Xiao W, Wang DL, Chen M, Tan QP, Li L, Chen XD, Gao DS (2014) Roles of enedoplasmic reticulum stress and unfolded protein response associated genes in seed stratification and bud endodormancy during chilling accumulation in *Prunus persica*. PLOS ONE **9(7)**: e101808

Furutani M, Hirano Y, Nishimura T, Nakamura M, Taniguchi M, Suzuki K, Oshida R, Kondo C, Sun S, Kato K, et al (2020) Polar recruitment of RLD by LAZY1-like protein during gravity signaling in root branch angle control. Nature Communications **11**: 76

Ge L, Chen R (2016) Negative gravitropism in plant roots. Nature Plants **2**: 16155

Godbolé R, Takahashi H, Hertel R (1999) The *lazy* mutation in rice affects a step between statoliths and gravity-induced lateral auxin transport. Plant Biology **1(4)**: 379–381

Guseman JM, Webb K, Srinivasan C, Dardick C (2017) DRO1 influences root system architecture in *Arabidopsis* and *Prunus* species. The Plant Journal **89(6)**: 1093–1105

Hollender CA, Hill JL, Waite J, Dardick C (2020) Opposing influences of *TAC1* and *LAZY1* on Lateral Shoot Orientation in *Arabidopsis*. Scientific Reports **10**: 6051

Howard III TP, Hayward AP, Tordillos A, Fragoso C, Moreno MA, Tohme J, Kausch AP, Mottinger JP, Dellaporta SL (2014) Identification of the maize gravitropism gene lazy plant1 by a transposon-tagging genome resequencing strategy. PLOS ONE **9(1)**: e87053

Johnson D, Eckart P, Alsamadisi N, Noble H, Martin C, Spicer R (2018) Polar auxin transport is implicated in vessel differentiation and spatial patterning during secondary growth in *Populus*. American Journal of Botany **105(2)**: 186–196

Lammerich S, Kunz A, Damerow L, Blanke M (2020) Mechanical crop load management (CLM) improves fruit quality and reduces fruit drop and alternate bearing in European plum (*Prunus domestica* L.). Horticulturae **6(3)**: 52

Li D, Zhao M, Yu X, Zhao L, Xu Z, Han X (2021) Over-Expression of rose *RrLAZY1* negatively regulates the branch angle of transgenic *Arabidopsis* inflorescence. International Journal of Molecular Sciences **22(24)**: 13664

Li P, Wang Y, Qian Q, Fu Z, Wang M, Zeng D, Li B, Wang X, Li J (2007) LAZY1 controls rice shoot gravitropism through regulating polar auxin transport. Cell Research **17(5)**: 402–410

Li Z, Liang Y, Yuan Y, Wang L, Meng X, Xiong G, Zhou J, Cai Y, Han N, Hua L, et al (2019) OsBRXL4 regulates shoot gravitropism and rice tiller angle through affecting LAZY1 nuclear localization. Molecular Plant **12(8)**: 1143–1156

Loarce Y, Cabeza A, Cañas R, González JM (2022) Isolation and molecular characterisation of *TtDro1A* and *TtDro1B* genes from *Triticum turgidum* subspecies *durum* and *turgidum*, study of their influences on Seedling Root Angles. Plants **11**: 821

Mehlenbacher SA, Voordeckers AM (1991) Relationship of flowering time, rate of seed germination, and time of leaf budbreak and usefulness in selecting for late-flowering apples. Journal of the American Society for Horticultural Science **116(3)**: 565–568

Milosevic T, Zornic B, Glisic I (2008) A comparison of low-density and high-density plum plantings for differences in establishment and management costs, and in returns over the first three growing seasons – a mini-review. Journal of Horticultural Science & Biotechnology **83**: 539–542

Nakamura M, Nishimura T, Morita MT (2019) Bridging the gap between amyloplasts and directional auxin transport in plant gravitropism. Current Opinion in Plant Biology **52**: 54–60

Nishimura T, Mori S, Shikata H, Nakamura M, Hashiguchi Y, Abe Y, Hagihara T, Yoshikawa HY, Toyota M, Higaki T, et al (2023) Cell polarity linked to gravity

sensing is generated by LZY translocation from statoliths to the plasma membrane. Science **381(6661)**: 1006–1010

Quinlan JD, Tobutt KR (1990) Manipulating fruit tree structure chemically and genetically for improved performance. HortScience **25(1)**: 60–64

Sottile F, Bellini E, Nencetti V, Cristiana P, Palara U, Pirazzini P, Mezzetti B, Capocasa F, Mennone C, Catalano L (2010) Plum production in Italy: State of the art and perspectives. Acta Horticulturae **874**: 25–34

Taniguchi M, Furutani M, Nishimura T, Nakamura M, Fushita T, Iijima K, Baba K, Tanaka H, Toyota M, Tasaka M, et al (2017) The *Arabidopsis* LAZY1 family plays a key role in gravity signaling within statocytes and in branch angle control of roots and shoots. The Plant Cell **29(8)**: 1984–1999

Telewski FW (2012) Is windswept tree growth negative thigmotropism? Plant Science **184**: 20–28

Tustin DS, Hirst PM, Warrington IJ (1988) Influence of orientation and position of fruiting laterals on canopy light penetration, yield, and fruit quality of 'Granny Smith' apple. Journal of the American Society for Horticultural Science **113(5)**: 693–699

Waite JM, Dardick C (2021) The roles of the IGT gene family in plant architecture: past, present, and future. Current Opinion in Plant Biology **59**: 101983

Warner J (1991) Rootstock affects primary scaffold branch crotch angle of apple trees. HortScience **26**: 1266–1267

Xia X, Mi X, Jin L, Guo R, Zhu J, Xie H, Liu L, An Y, Zhang C, Wei C, et al (2021) CsLAZY1 mediates shoot gravitropism and branch angle in tea plants (*Camellia sinensis*). BMC Plant Biology **21(1)**: 243

Yang P, Wen Q, Yu R, Han X, Deng XW, Chen H (2020) Light modulates the gravitropic responses through organ-specific PIFs and HY5 regulation of *LAZY4* expression in *Arabidopsis*. PNAS **117(31)**: 18840–18848

Yoshihara T, Spalding EP (2020) Switching the direction of stem gravitropism by altering two amino acids in *AtLAZY1*. Plant Physiology **182(2)**: 1039-1051

Yoshihara T, Spalding EP (2017) *LAZY* genes mediate the effects of gravity on auxin gradients and plant architecture. Plant Physiology **175(2)**: 959-969

Yoshihara T, Spalding EP, Iino M (2013) AtLAZY1 is a signaling component required for gravitropism of the *Arabidopsis thaliana* inflorescence. The Plant Journal **74(2)**: 267–279

Zhang H, Wafula EK, Eilers J, Harkess AE, Ralph PE, Timilsena PR, dePamphilis CW, Waite JM, Honaas LA (2022) Building a foundation for gene family analysis in Rosaceae genomes with a novel workflow: A case study in *Pyrus* architecture genes. Frontiers in Plant Science 13: 975942

Zhebentyayeva T, Shankar V, Scorza R, Callahan A, Ravelonandro M, Castro S, DeJong T, Saski CA, Dardick C (2019) Genetic characterization of worldwide *Prunus domestica* (plum) germplasm using sequence-based genotyping. Horticulture Research **6(1)**: 1–13

CHAPTER 4

The Way is Planar:

Exploring how planar training systems and variation in natural branch angle impact fruit quality and early yield in peach.

Authors:

Andrea R Kohler[1], Greg Lang[1], Bill Shane[2], Courtney Hollender[1]*

[1]Department of Horticulture, Michigan State University;

[2]Extension Agriculture and Agribusiness Institute, Michigan State University

*Corresponding

CH and GL conceived project and obtained funding. All authors designed experiments. ARK and CH performed experiments. ARK collected and analyzed data. ARK wrote the manuscript. All authors contributed to and reviewed the manuscript.

Abstract

Planar training systems, which constrain the canopy to two dimensions, have dramatically improved yield per hectare, fruit quality, and cost of labor for commercial tree fruit production. However, implementing planar systems in peach (*Prunus persica*) has been inhibited by the high vegetative vigor of peach, and the associated costs of implementing planar systems. Here, we begin to tackle those challenges. First, we used the commercial cultivar Bounty to investigate three planar systems—super spindle axe (SSA), dual SSA (DSSA), and upright fruiting offshoots (UFO)—and compared them to a three-dimensional system—quad SSA (QSSA). Second, we trialed varieties with different dosages of the *TAC1* gene, which controls outward branch growth. We tested Bounty (*TAC1/TAC1*, spreading), Sweet-N-UP (*TAC1/tac1*, upright), and Crimson Rocket (*tac1/tac1*, pillar) in several planar systems. Here we present preliminary yield and fruit quality data from the earliest harvests. For Bounty during 4^{th}-6^{th} leaf, yield/ha for SSA, significantly outperformed the three-dimensional QSSA. These higher yields could also be achieved by increasing the number of leaders per acre while holding tree density constant, as observed in UFO. We did not observe any consistent differences among training styles in average fruit weight, soluble solids content (SSC), or dry weight. For Bounty, Sweet-N-Up and Crimson Rocket trained as SSA and UFO during 4^{th}-6^{th} leaf, we observed significant differences between varieties in yield (Sweet-N-UP exhibited precocious yield and Crimson Rocket struggled to produce) and quality (Crimson Rocket had decreased quality), but these differences were largely unaltered by training system. For all three varieties in DSSA and DUFO during the 3^{rd} and 4^{th} leaf, we once again observed precocious yield from Sweet-N-UP, which led to higher yields per tree and per hectare, but the training system did not significantly alter yield or quality per variety.

Introduction

Over the last 50 to 60 years, fruit-growing regions around the world have seen a revolution in apple orchard production systems from low-density plantings in which each tree has a unique, three-dimensional architecture, to high-density plantings with the canopy simplified and constrained to a planar architecture or "fruiting wall" (Robinson et al., 2013). These changes have been motivated by improved yield and profitability, which are driven by the increase in tree density, and improved fruit quality and ease of management, driven by planar training (Parker et al., 1998; Robinson et al., 2013). Over the past 25 years alone, apple (*Malus domestica*) production efficiency has increased approximately 30% per hectare (Lang, 2023). Despite the success of this transition in

apple, and the occasional publication of research on high-density peach since the 1970s (e.g. Phillips and Weaver, 1975; Giulivo et al., 1984; DeJong et al., 1997; Iglesias and Echeverria, 2022), peach is generally still grown in low-density, three-dimensional systems and production efficiency per hectare has not increased over the past 25 years (Lang, 2023). The primary barrier to adopting planar, high-density orchard systems in peach is high vegetative vigor due to the lack of commercially-viable dwarfing rootstocks, which makes training difficult and increases labor costs (Phillips and Weaver, 1975; DeJong et al., 1997; Loreti and Massai, 2002; Anthony and Minas, 2021; Iglesias et al., 2023).

The advances made with high-density plantings in apple provide useful data, but questions remain about how to apply that data to peach. Increasing apple tree density dramatically increasse yield per land area under many different training systems and in many geographical areas (Cahn and Goedegebure, 1992; Hampson et al., 2004; Eccher and Granelli, 2006; Platon, 2007; Robinson et al., 2013). Underlying this yield increase is the physiology of how the trees respond to crowding. As density is increased, each tree has a smaller area available for growth. In apple, as the area per tree decreases, yield per tree decreases, but by a smaller proportion than the decrease in area, so the overall yield is increased (Hampson et al., 2004; Eccher and Granelli, 2006; Platon, 2007). In high-density peach plantings, some studies have shown a similar response to apple (Phillips and Weaver, 1975; DeJong et al., 1997), while others have found that the decrease in yield per tree is high enough that overall yield is decreased at higher densities (Giulivo et al., 1984). One potential problem for peach trees, which are highly vigorous, is that extremely high densities or excessively vigorous trees lead to shading, negatively effecting both fruit quality and yield (Hampson et al., 2004; Eccher and Granelli, 2006; Anthony and Minas, 2021). In fact, Giulivo et al. (1984) report decreased flower bud density, a common result of excessive shading, in higher density plantings.

A further complication for selecting planting density is that incremental gains in yield diminish as density increases, so maximizing profit requires identifying the balance point between reducing initial investment and increasing production (Hampson et al., 2004; Eccher and Granelli, 2006; Robinson et al., 2013). Optimum density is dependent on factors that are highly variable, such as variety, climate, soil type, and training system. As a result, estimates of optimum density vary widely, and may be unique for different cultivars.

Precocity is one of the most important benefits of high-density apple orchards. Increasing early yield is essential for profitability, because it decreases time to break-even return on investment

(Robinson et al., 2013). Several studies in apple have reported that the largest difference in yield between high-density and low-density planting occurs in the earliest years of production (Cahn and Goedegebure, 1992; Hampson et al., 2004).

Planar training is increasingly being combined with high-density planting because together they can increase early light interception and improve light distribution, leading to greater photosynthetic potential and improved fruit quality (Grossman and DeJong, 1998; Sharma et al., 2018; Sharma et al., 2018; Tustin et al., 2018; Anthony and Minas, 2021). This is even more essential in peach than apple, as peach requires particularly good light distribution for fruit color and flower bud formation (Sharma et al., 2018). Planar systems also facilitate improved pest control. Planar systems allow more even pesticide application and increase the light and wind penetration of the canopy, which can decrease pest and pathogen frequency (Lauri et al., 2009). Finally, planar systems have a more consistent and accessible canopy, making them more suitable for mechanization of fruit thinning, summer pruning and harvest, potentially addressing labor costs (Iglesias and Echeverria, 2022; Iglesias et al., 2023).

Within high-density planar training, many different training strategies can be utilized, each providing unique advantages and disadvantages. In apple, the dominant commercial training systems are variants of single-leader systems, such a slender spindle, tall spindle, and super spindle (Robinson et al., 2013). These systems generally have exceptional early yield, and are preferred by growers due to their simplicity (Robinson et al., 2013; Iglesias and Echeverria, 2022). However, controlling vigor in a single-leader system is highly dependent on dwarfing rootstocks, low soil quality, or heavy pruning (Iglesias et al., 2023). Single leader systems have been trialed in peach, sometimes with success (Phillips and Weaver, 1975; Iglesias and Echeverria, 2022), and sometimes not (Giulivo et al., 1984). Using training systems with multiple leaders provides significant advantages for vigor diffusion, but at the cost of greater complexity in canopy structure and training decisions (Anthony and Minas, 2021). In current commercial plantings, peach is often grown in open vase, a three-dimension system which generally has 3-5 leaders (Anthony and Minas, 2021). Multileader training strategies for peach include two leader systems such as bi-axis (DeJong et al., 1997), three leader systems such as tri-axis, four leader systems such as Quad-V (a free standing three-dimensional system quite similar to open vase; Anthony and Minas, 2021), or variable leader systems, such as upright fruiting offshoots (UFO, also known as cordon or Guyot training), in which one or two main scaffolds are bent nearly horizontal along a bottom trellis wire

to form a “cordon” from which grow many upright leaders tied to upper wires at the desired spacing (Lang, 2023). For multi-leader systems to achieve the same yield as high-density single leader systems, a high density of *leaders* per hectare is required, which does not necessarily equate to a high number of *trees* (Iglesias et al., 2023).

Amid peach training studies, little attention has been paid to cultivar growth habits, yet this can have a major impact on fruit placement, pruning techniques, and canopy porosity to light (Iglesias et al., 2023). One architecture trait with the potential for particular impact is branch angle. Past breeding efforts that decreased lateral organ angle in field crops has been a crucial means of improving agronomic efficiency. For example, decreasing the expression of *TILLER ANGLE CONTROL 1* (*TAC1*), which promotes outward orientation, was essential to the domestication of japonica rice (Yu et al., 2007). While peach germplasm includes diverse growth habits, most commercial cultivars exhibit a spreading habit with wide branch angles (Scorza et al., 1999). One growth habit with potential for high-density, planar training systems is the columnar or pillar trait, which results from narrowed branch angles (Scorza et al., 1999). The pillar trait has been mapped to a deletion in *TAC1,* with homozygous wild-type individuals showing a spreading architecture, heterozygous individuals showing an intermediate upright architecture, and individuals homozygous for the deletion showing a columnar architecture (Dardick et al., 2013). Pillar peaches have been tested in medium-, high-, and ultra-high-density plantings and showed increased yield at increasing densities (Scorza et al., 1999). However, this trial was performed with unimproved germplasm, rather than improved cultivars, and no particular training system was attempted (Scorza et al., 1999). The *tac1* deletion has since been bred into commercial-quality cultivars showing upright (‘Sweet-N-Up’, *TAC1*/*tac1*) and pillar architectures (‘Crimson Rocket’, *tac1*/*tac1*; Figure 4.1 C; Scorza, 2004a; Scorza, 2004b).

Here we examine early yields and fruit quality in two peach trials which combine Crimson Rocket (pillar), Sweet-N-Up (upright), and Bounty (spreading) varieties in planar training systems—including single, dual, and multiple leader systems.

Materials and methods

Plant material and cultivation.

To compare the effects of differing leader numbers and planting densities for novel planar training systems, we used a 2018 planting (Clarksville, MI) of Bounty peaches on Lovell rootstock. These were trained into three planar systems —upright fruiting offshoots (UFO) at 2.4 m x 3.7 m spacing,

super slender axe (SSA) at 0.9 m x 3.7 m spacing, and dual SSA (DSSA) at 1.8 m x 3.7 m spacing —and a three-dimensional system, quad SSA (QSSA) at 2.4 m x 3.7 m spacing (Figure 4.1 A). 12 to 36 trees were planted per training type, with one row per training type. Irrigation and pesticides were applied as needed. Weeds were controlled in the row with weed cloth, and mowed grass in between rows. Data were collected for three growing seasons, 2021- 2023 (4^{th}-6^{th} leaf).

To compare the effects of varieties with differing branch angle in different planar training systems, we utilized 2018 and 2020 plantings in Clarksville, MI of Bounty (spreading branch angle), Sweet-N-UP (upright branch angle) and Crimson Rocket (narrow branch angle; Figure 4.1 C). The 2018 planting was trained in UFO or SSA. The UFO was planted at 2.4 m x 3.7 m spacing with 12 trees each of Bounty on Lovell, Sweet-N-UP on Halford with Early Red Haven (ERH) interstock, and Crimson Rocket/ERH/ Halford in a randomized block design. The SSA was planted at 0.9 m by 3.7 m spacing with 25 trees of Bounty/Lovell and 9 of Sweet-N-UP/ERH/Halford in a randomized block design. The planting was managed as described above, and data were collected in 2021-2023.

The 2020 planting included Bounty, Sweet-N-UP, and Crimson Rocket, all on Bailey rootstock (Figure 4.1 C). All three varieties were trained as DSSA at 1.8 m x 3.7 m spacing or Drapeau-UFO (DUFO) at 2.4 m x 3.7 m spacing (Figure 4.1 A, B). Trees were planted in a randomized block design with three trees per block, and four blocks per training system, with each training system in a single row. Irrigation and pesticides were applied as needed, weeds were controlled in the row with herbicide applications between rows with mowed grass. Data for the 2020 planting were collected for the first and second harvest in 2022-2023 (3^{rd} and 4^{th} leaf).

Pruning, thinning, and harvest methods.

Trees were generally hand-pruned one or two times a year, with an initial hand-pruning during bloom and a second hand-pruning if needed during fruit thinning. Summer hedging was performed in the 2018 planting a few weeks before harvest. In 2021, SSA, DSSA, and QSSA were hedged, while in 2022 only SSA and DSSA were hedged. No treatments were hedged in 2023.

Thinning was performed after initial hand-pruning during bloom but prior to pit-hardening. In 2021, due to a spring frost during bloom which reduced fruit set to under commercial load, no further thinning was performed. In 2022, the 2018 planting was hand-thinned according to the number of linear row space occupied by each tree, with a target of 65-82 fruit per meter in the row. So, for QSSA with 2.4 m in-row spacing, target was 160-200 fruit per tree, while for SSA with 0.9

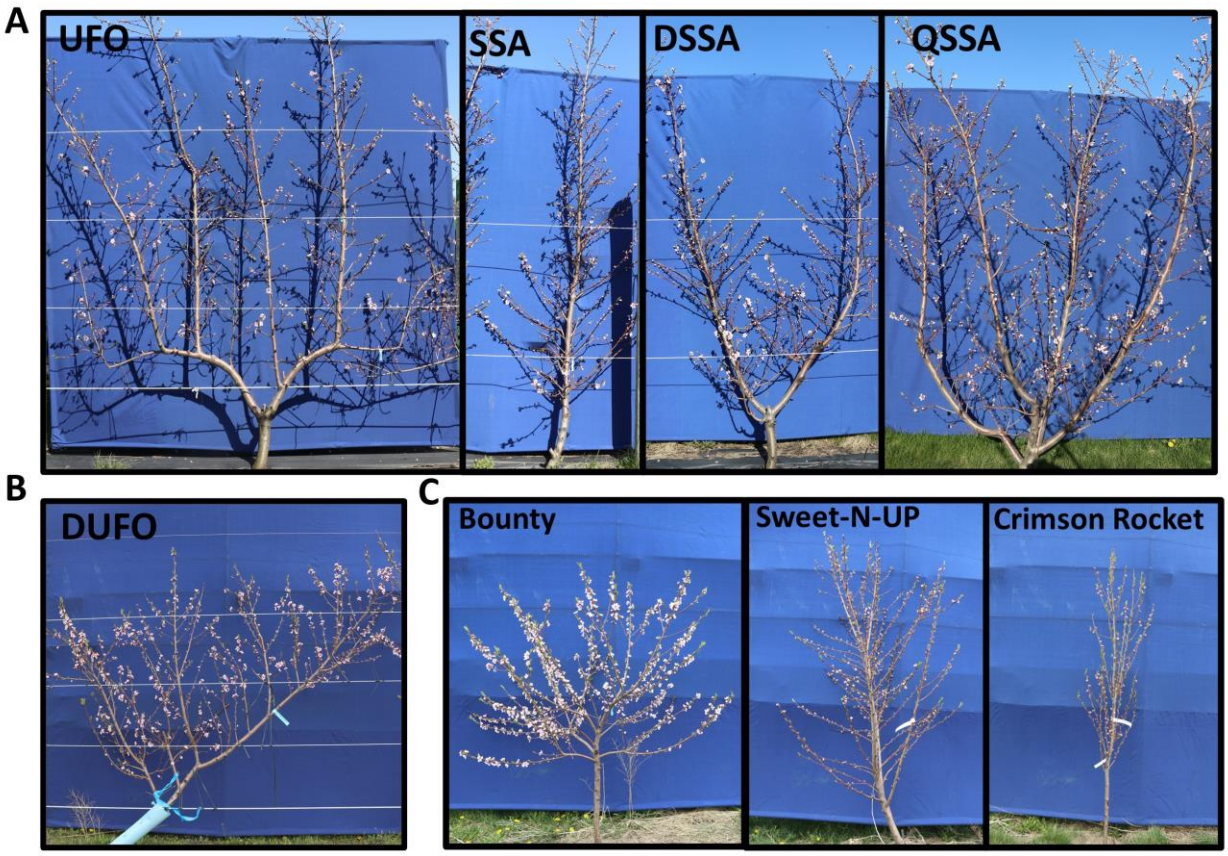

Figure 4.1: Training systems and varieties used in this study. A) Training strategies for the 2018 planting, shown with Bounty. B) Additional training strategy for the 2020 planting, which also included DSSA , shown with Bounty. C) Varieties used had different genetic architectures, including spreading (Bounty), upright (Sweet-N-UP), and pillar (Crimson Rocket); UFO, Upright Fruiting Offshoots, SSA (super spindle axe), DSSA (dual-SSA), QSSA (quad-SSA), and DUFO (Drapeau-UFO).

m in-row spacing it was 60-75, etc. The 2020 planting was in its initial year of production, and so was primarily thinned to space out clusters of fruit. In 2023, the 2018 planting was thinned to a target of 115 fruit per meter in the row. This averaged approximately 1-2 fruit per stubbed branch. The 2020 planting was thinned to a target of 43 per meter in the row, although Crimson Rocket fruit-set was less than that target.

Fruit was harvested at approximately “farm-market ripe”. At this stage, fruit has no ridge at the suture, a yellow background color, and a firmness of approximately 4.2-5.7kg/cm² (Shane, 2011). The three varieties have slightly different ripening times, Crimson Rocket is earlier than Bounty, and Sweet-N-UP is later than Bounty. Sweet-N-UP generally also ripened over a narrower window than Crimson Rocket or Bounty. Number of picks during the harvest season varied from one to

three, depending on ripening rate and number of fruit on the tree. The final harvest of the season, the trees were picked clean.

Yield and efficiency measurements.

To estimate excess vegetative growth, fresh weight of branches pruned throughout the season was measured. For yield, fresh weight of fruit per tree (excluding rotten or badly damaged fruit) was measured immediately. Average yield per tree was multiplied by land area per tree to get estimated kg per hectare. To estimate efficiency of production, yield per excess vegetative growth was calculated as the ratio of fruit fresh weight to the fresh weight of branches pruned.

Fruit quality measurements.

To evaluate the effects of each system or variety on fruit quality and uniformity, we measured fruit weight, fruit firmness, dry weight, SSC, and percent blush. Quality was measured on five randomly selected trees per treatment, with 10 (2021), 6-8 (2022), or 4 (2023) peaches randomly selected per tree. Due to the light harvest in 2022 for the 2020 planting, seven trees were randomly selected and four fruit were randomly sampled per tree.

Fruit weight was measured using a digital lab scale. Fruit firmness was measured using the mechanical fruit hardness tester GY-3, with the 8mm probe. For dry weight, an approximately 15g slice of peach with the skin attached was measured for fresh weight, dried at 65˚ for several days, and measured again for dry weight. ºBrix were determined using juice squeezed through a nylon filter and measured with an ATAGO pocket digital refractometer (ATAGO USA, Inc., Bellevue, WA).

Statistical analysis.

Statistical analysis was performed in R v4.3.1, using the lme4 library for modeling and emmeans, multcomp, and lmertest for multiple comparisons. Models were gated with ANOVA (α=0.05), and residuals were examined for equal variance and normality. For multiple comparisons, t-tests were used if ANOVA was significant, otherwise Tukey's tests were used.

Bounty yield and quality in 2018 planting.

For Bounty training systems, yield, yield per hectare, pruning weight, and yield per pruning weight were modeled as a completely randomized design, with Yield=mean + Training+ error, where Yield is the yield measure of interest, mean is the grand mean, Training is the effect of the training system, and error is the residual.

Bounty fruit quality attributes were modeled as a randomized block design. In 2021, the model chosen was Quality=mean + Harvest + Training + (Training:Tree) +error, where Quality is the quality attribute of interest, Harvest is the effect of harvest date, and (Training:Tree) is a random variable to account for the effect of tree, nested within the training system. This model was chosen for 2021 because significant interactions effects between Harvest and Training were not observed for any of the quality attributes reported. In 2022 and 2023, significant interactions were observed, so the model was Quality=mean + Harvest + Training + Harvest*Training + (Training:Tree) +error, where Harvest*Training was the interaction between harvest date and training system. Interaction effects were investigated using the phia library. Since our question of interest related to the effect of training on quality across the season multiple comparisons for training were performed across harvest dates.

Variety yield and quality in 2018 planting.

Variety yield, yield per hectare, and pruning weight in the 2018 planting was modeled as Quality =mean + Treatment +error where Treatment is the effect of each combination of genotype and training system. Because we were missing one combination (Crimson Rocket in SSA) we were not able to calculate marginal means for genotype and training system separately.

Variety quality in the 2018 planting was modeled as Quality =mean + Treatment + (Treatment:Tree) + error, where (Treatment:Tree) is a random variable to account for effect of tree, nested within the treatment. Due to the differences in harvest window among the varieties, harvest date was not considered a useful variable.

Variety yield and quality in 2020 planting.

Variety yield in the 2020 planting was modeled as Quality = mean + Genotype + Training + Genotype*Training + e, where Genotype is the effect of genotype and Genotype*Training is the effect of the interaction between Genotype and Training.

Variety quality in the 2020 planting was modeled as Quality = mean + Genotype + Training + Genotype*Training + (Genotype*Training:Tree) + e, where (Genotype*Training:Tree) is a random variable to account for the effect of tree, nested in both Genotype and Training.

Results

Bounty early yield was increased for planar training systems, while fruit quality was unaffected.

For the first year of cropping (2021, 4th leaf), yield was not strongly correlated with the tree spacing (Figure 4.2 A) However, yield per tree was highly correlated in subsequent years (Figure 4.2A).

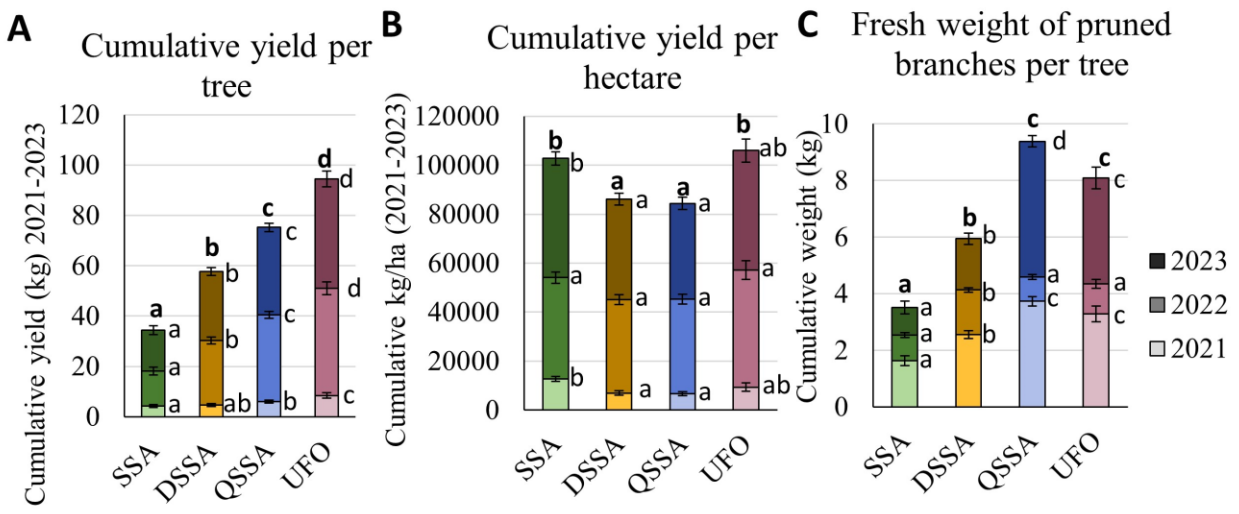

Figure 4.2: Yield and production efficiency of Bounty. A) Yield per tree for Bounty in each training system B) Estimated yield per hectare for Bounty. C) Weight of fresh branches pruned for Bounty in each training system. Error bars indicate standard error for each year's measurement. Means with the same letter were not significantly different at α=0.05 from other means within that year. Bold letters indicate significance for cumulative totals.

This may reflect low crop levels in the first year due to a spring freeze, and thinning relative to the tree spacing in subsequent years. However, in all three years, UFO had the highest yield per tree, despite being planted at the same spacing as the QSSA (Figure 4.2 A). For yield per hectare, SSA and UFO were highest over the three years (Figure 4.2 B). These two were the planar training systems with the highest tree density (SSA, 0.9 m x 3.7 m) and lowest tree density (UFO, 2.4 mx 3.7 m), suggesting that tree density alone was not a primary determiner of yield per hectare. Instead, using a low tree density but spacing UFO-trained leaders only 0.45 m to 0.6 apart equaled the yield of SSA. Cumulative pruning weight per tree correlated surprisingly well with the in-row spacing, with ~3.3 kg/meter in the row, although QSSA dramatically exceeded that average (Figure 4.2 C).

Average fruit weight and soluble solids content were measured for all three years. No differences were observed among training systems, aside from transient differences in SSC which varied from year to year (Figure 4.3 A, B, D, E, G, H). Dry weight was measured in 2021 and 2022. As with SSC, only transient differences were observed. In accordance with what has been reported in literature (Anthony and Minas, 2021) a high correlation was observed between SSC and dry weight in both 2021 and 2022, and that correlation did not appear to be altered by training system. As a result, dry weight was not measured in 2023.

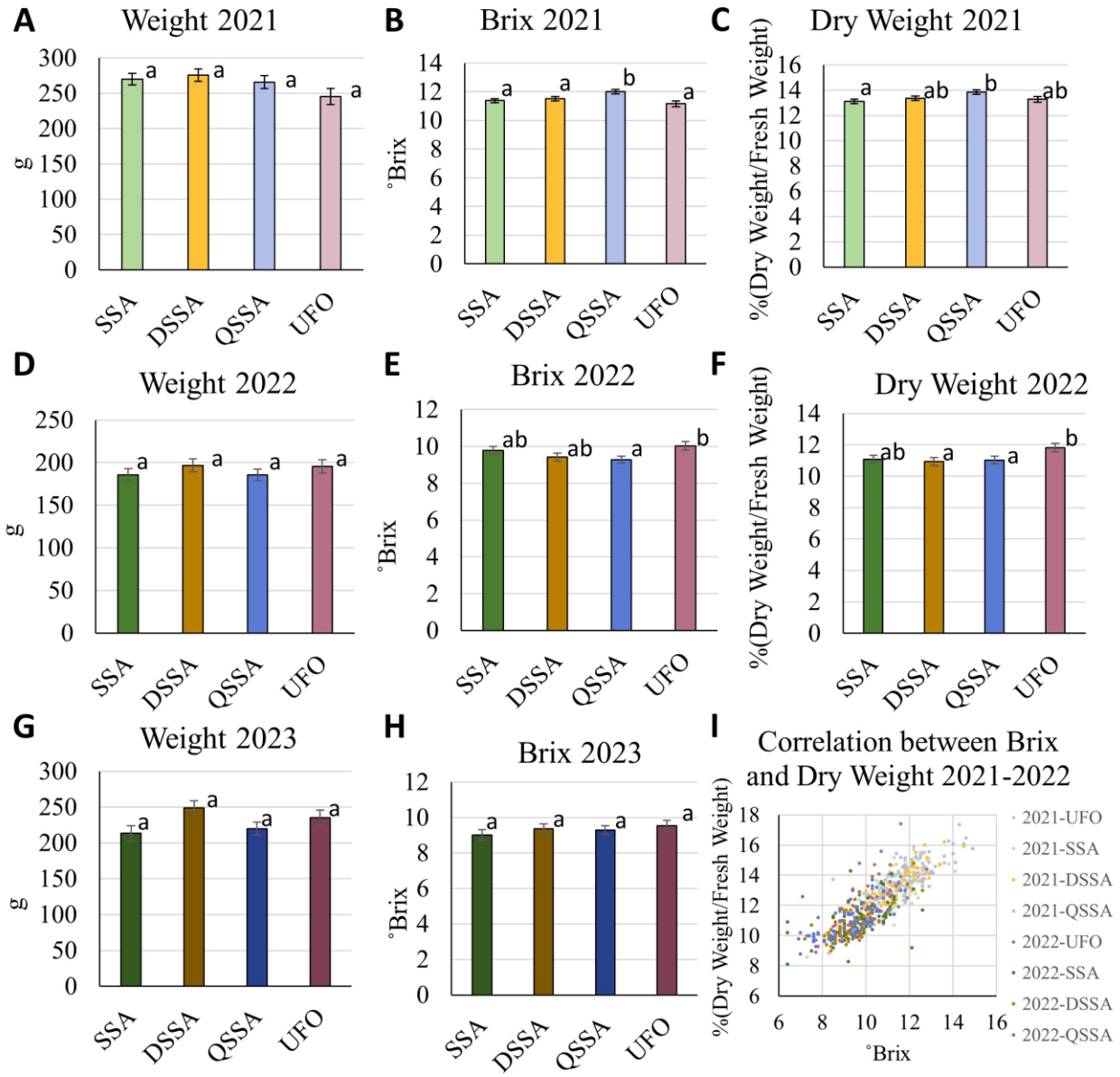

Figure 4.3: Fruit quality measures for Bounty. Fruit quality measures across training systems for 2021 (A-C), 2022 (D-F), and 2023 (G-H) harvests. Correlation between soluble solids content (SSC) and dry weight (I). Error bars indicate standard error for each year's measurement. Means with the same letter were not significantly different at α=0.05 from other means within that year.

In the 2018 planting, Sweet-N-UP early yield was similar to Bounty with SSA training, but lower with UFO training.

For yield per tree and yield per hectare, Sweet-N-UP performed similarly to Bounty in SSA, but significantly worse than Bounty in UFO (Figure 4.4 A-B). This was true even though Sweet-N-UP performed significantly better than Bounty in both SSA and UFO in 2021 (Figure 4.4 A). However,

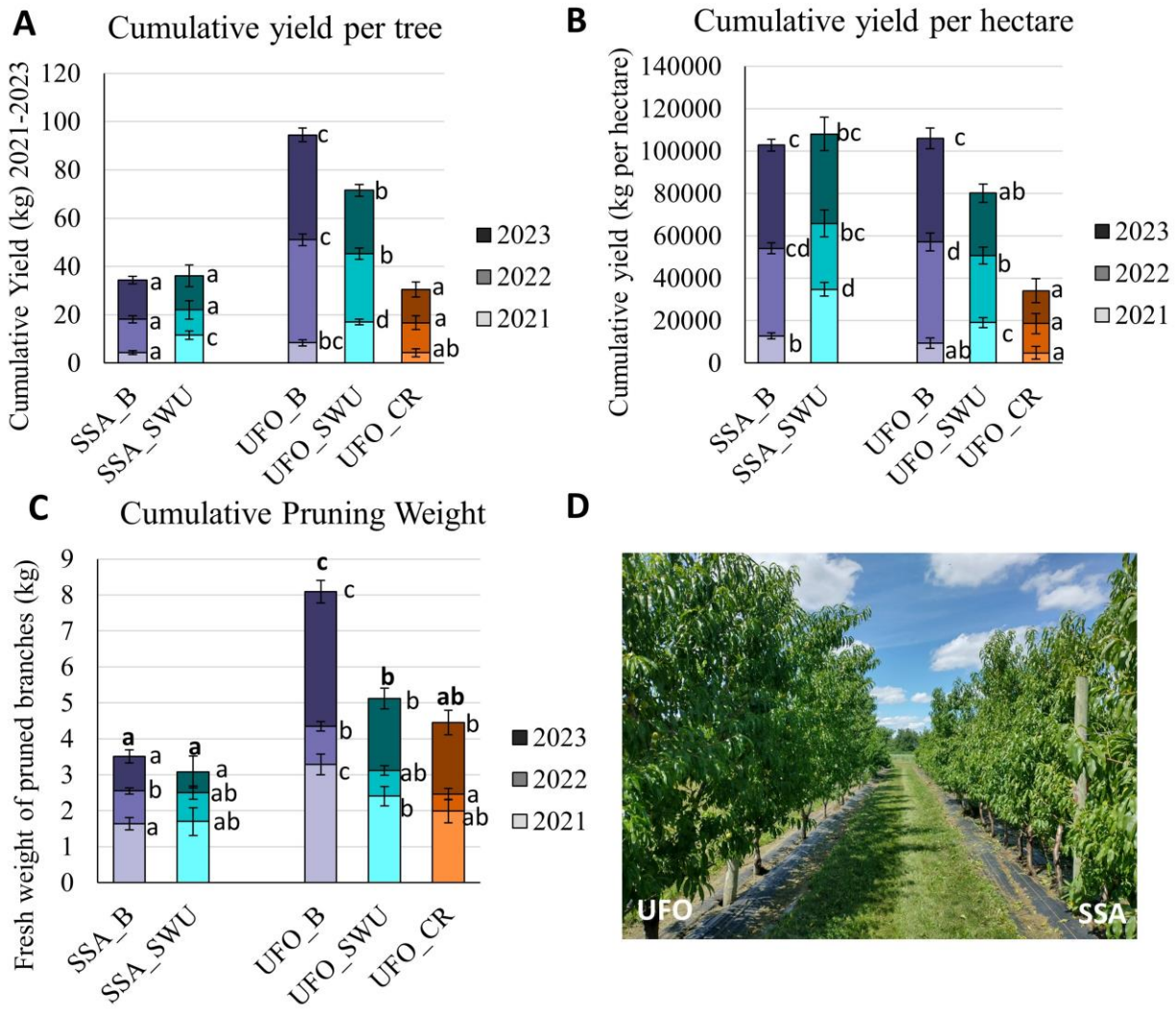

Figure 4.4: Yield and production efficiency by variety--2018 planting. A) Cumulative yield per tree 2021-2023 B) Estimated cumulative yield per hectare based on yield per tree and area per tree for each training system. C) Cumulative fresh weight of pruned branches 2021-2023. D) SSA and UFO trees in July 2022, when summer pruning was performed for SSA, but not UFO. SSA= Super Spindle Axe, UFO=Upright Fruiting Offshoots, B=Bounty, SWU=Sweet-N-UP, CR=Crimson Rocket. Error bars indicate standard error for each year's measurement. Means with the same letter were not significantly different at α=0.05 from other means within that year. Bold letters indicate significance for cumulative totals.

the data for these years may be skewed by the severe bacterial gummosis which affected Sweet-N-UP, which reduced the replication number for Sweet-N-UP. Furthermore, SSA trees infected with gummosis generally died entirely, as there was only one scaffold, whereas UFO trees often had gummosis in only one horizontal cordon, and the tree could recover (see Figure 4.5 F, I). Thus, yield data from Sweet-N-UP trained as SSA only include the strongest trees, whereas in UFO some

of the trees providing data were missing part of their canopy. Strikingly, while the SSA-trained SWU outperformed Bounty slightly for yield, it had slightly decreased pruning weight, and the reduction in pruning weight for UFO-trained SWU was greater than the reduction of yield (Figure

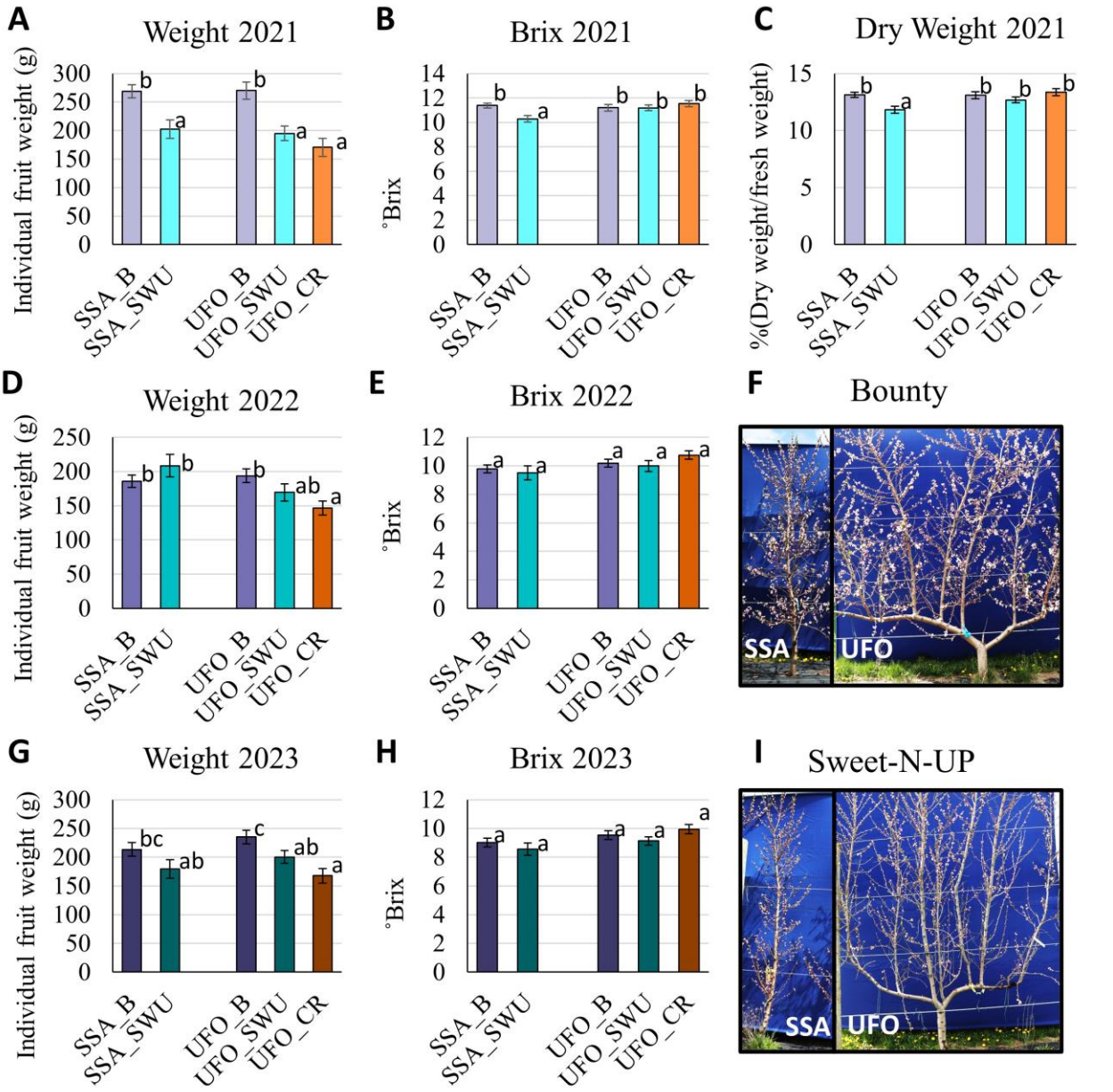

Figure 4.5: Quality by variety and training system--2018 planting. Quality measures for each variety and training treatment in 2021 (A-C), 2022 (D,E), and 2023 (G, H). Bounty in SSA and UFO (F) and Sweet-N-UP in SSA and UFO (I) SSA= Super Spindle Axe, UFO=Upright Fruiting Offshoots, B=Bounty, SWU=Sweet-N-UP, CR=Crimson Rocket. Error bars indicate standard error for each year's measurement. Means with the same letter were not significantly different at α=0.05 from other means within that year.

4.4 A and C). This suggests good efficiency of production as compared to excess vegetative growth. Crimson Rocket performed poorly in UFO trials, as the canopy failed to fill the space available, and yields were low, although it is unclear to what extent bacterial gummosis impacted performance, as Crimson Rocket was very severely infected (Figure 4.4 A-B).

Average fruit weight was higher for Bounty than Sweet-N-UP in both training systems in 2021, and for UFO in 2023, while Crimson Rocket consistently had the smallest fruit size (Figure 4.5 A, D, G). No consistent differences were observed for SSC, although Sweet-N-UP in SSA was slightly lower in 2021, and dry weight also reflected that difference (Figure 4.5 C, E, H).

In the 2020 planting, Sweet-N-UP showed superior early yields in both DSSA and DUFO.

For the 2020 planting in both 2021 and 2022, Sweet-N-UP outperformed both Bounty and Crimson Rocket in both training systems, with almost double the cumulative yield of Bounty (Figure 4.6 A). For Bounty and Sweet-N-UP, as in the 2018 planting, the training system with wider spacing (DUFO—2.4 m x 3.7 m) had slightly superior yields per tree than the system with narrower spacing (DSSA—1.8 m x 3.7 m). However, in contrast to the 2018 planting, this increase was not observed in yield per hectare, with Bounty yields being almost identical for both training systems, and Sweet-N-UP having slightly (though not significantly) greater yields with DSSA (Figure 4.6 B). This difference may reflect the difference in space-filling of the two varieties: Bounty trees had mostly filled their space by 2023 for both training systems, whereas Sweet-N-UP trained as DUFO had not. As in the 2018 planting, Crimson Rocket performed poorly in both training systems. Even though bacterial gummosis damage was low, the tree canopy failed to fill the space available, remaining overly compact.

For fruit quality, differences were observed between genotypes, but no differences were observed between training systems for any of the genotypes. Crimson Rocket had smaller fruit size than Bounty and Sweet-N-UP, while Sweet-N-UP fruit had lower dry weight for DUFO in 2022. No differences were observed in SSC (Figure 4.6 C-G).

Discussion

Multileader planar training systems show promise for improving early peach yield.

In accordance with what has been observed in apple and some previous studies in peach, yield per tree decreased with area of the tree (Eccher and Granelli, 2006). However, yield per hectare in the highest density planting, SSA (0.9 m x 3.7 m), was higher than in the traditional three-dimensional planting, as the reduction in yield is proportionally smaller than the reduction in tree area. Perhaps

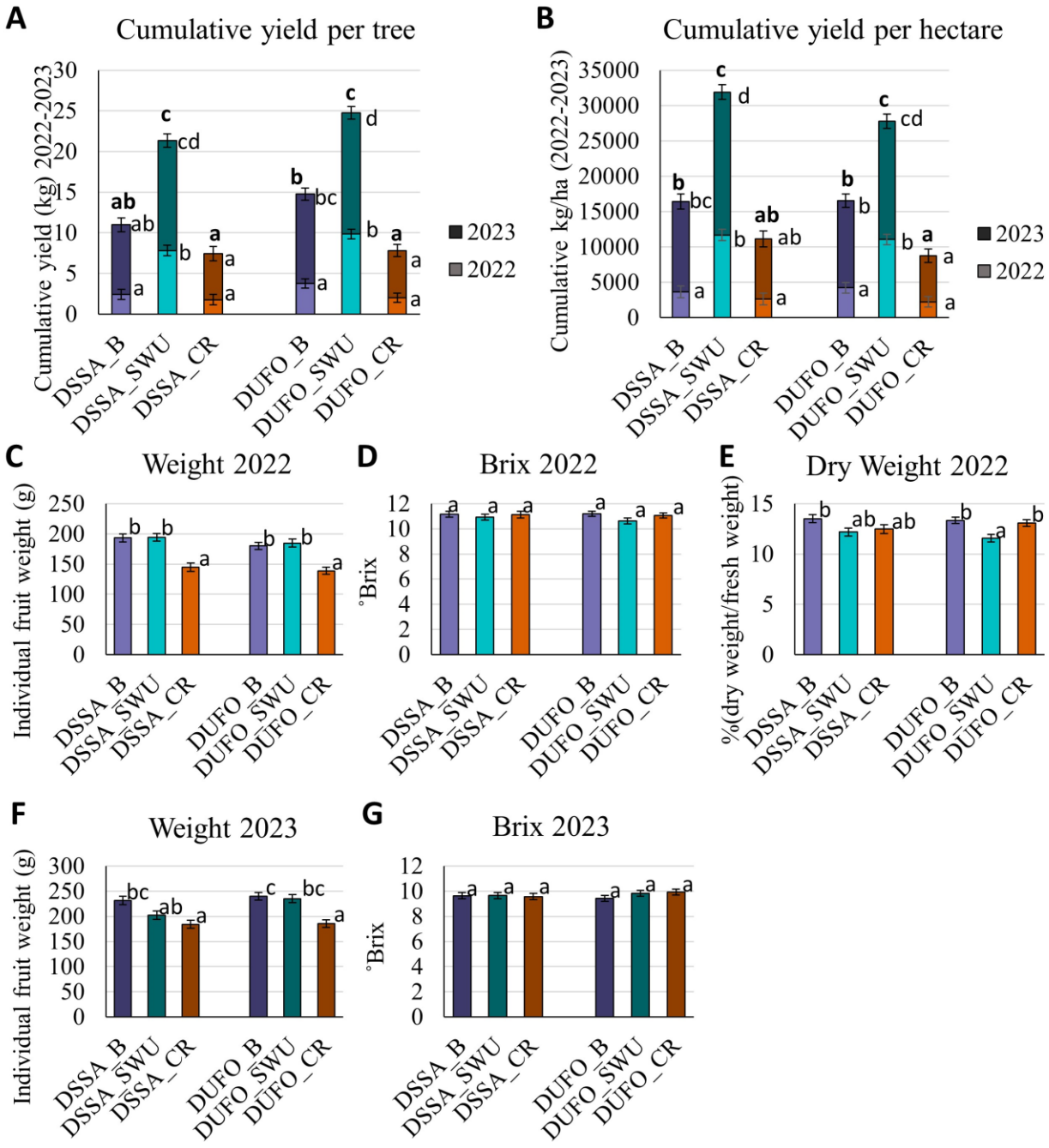

Figure 4.6: Yield, production efficiency, and quality by training style and genotype--2020 planting. Cumulative yield per tree (A) and estimated yield per hectare (B) from the 2022 and 2023 harvests. Quality measures for 2022 (C-E) and 2023 (F-G). DSSA= Dual SSA, DUFO=Drapeau-UFO, B=Bounty, SWU=Sweet-N-UP, CR=Crimson Rocket. Error bars indicate standard error for each year's measurement. Means with the same letter were not significantly different at α=0.05 from other means within that year. Bold letters indicate significance for cumulative totals.

the most exciting observation, however, is that with trees trained in UFO and spaced at 2.4 m we were able to achieve the same yield as SSA, potentially decreasing input costs by lowering the density of trees. Furthermore, when considered in terms of the area occupied per tree, both DSSA and UFO required less pruning than QSSA, suggesting that implementing multileader systems in planar training can reduce pruning by diffusing vigor among the leaders. Reducing pruning decreases the stimulation of excess vegetative growth and decreases labor costs (Dejong et al., 2012). While three-dimensional multileader orchard systems have long been used to diffuse vigor in both peach and sweet cherry (*Prunus avium*), multileader planar orchard systems in sweet cherry have only been developed over the past ~20 years, and have proven successful at increasing yield while decreasing excessive vegetative growth (Lang, 2023).

Although we are projecting training system yields from a relatively small sample and yields are cultivar dependent, our yield data are in line with commercial production. Yields for SSA- and UFO- trained orchards in the 2018 planting in 5th and 6th leaf (39-49 ton/ha) are slightly below yields previously reported for single row central leader training in nectarine (Anthony and Minas, 2021). Furthermore, for the cumulative yield over the first three harvests, the difference between the best yielding UFO (108 ton/ha) and our three-dimensional QSSA (85 ton/ha) is an estimated 23 ton/ha, or almost an additional season's worth of fruit. Anthony and Minas (2021) found significant improvements in yield per hectare for central leader trees through planting in double rows, and a similar intensification either through narrowing all row spacing or utilizing double rows could similarly improve yields of the planar systems in this trial.

Previous studies showed that the improved light characteristics of some planar training systems improve fruit quality in peach (Sharma et al., 2018; Anthony and Minas, 2021). In our study, fruit quality was not improved in planar training systems. However, quality was maintained despite the increased yield in the planar systems, and the quality was in line with industry standards. Consumers generally desire soluble solids content (SSC) of 10-12 ºBrix, and our average SSC ranged from 9-12 ºBrix (Anthony and Minas, 2021). The United States Department of Agriculture does not have size classifications for peaches, however, according to Standard FFV-26 for quality control of peach and nectarine, our average peach size would be class A to class AAA, depending on the year (United Nations, 2008).

Upright architectures show promise for high-density, planar training.

Differences among the varieties in pathogen resistance and fruit size complicated comparisons between the different architectures trialed. However, the narrow branch angles of the pillar variety, Crimson Rocket, made it surprisingly difficult to train. Crimson Rocket did not fill the allotted orchard space in UFO, DUFO, or DSSA, largely because the growth was very densely centered immediately above the trunk, and the trees responded to thinning cuts with further growth at the base. In contrast, Bounty trees trained as UFO, DUFO, and QSSA very rapidly filled the allotted space. However, due to its spreading habit and the tendency to produce blind wood at the base of new growth, it was difficult to constrain the canopy and set fruit close to the scaffolds, which proved problematic in the UFO and DUFO where upright fruiting offshoots (or leaders) were spaced around 0.3-0.45 m. In the SSA and DSSA trials of Bounty, adequate fruit set could be obtained while keeping the canopy to about a 0.6 m width around the scaffold, so the trees did not fully occupy the 0.9 m available per scaffold. Our observations suggest that ~0.6 m may be the ideal distance for uprights in planar training of a peach genotype with spreading habit, which is toward the lower end of previous recommendations for uprights in nectarine (.62-.75 m; (Lang, 2023).

In all training systems except UFO, Sweet-N-UP equaled or outperformed Bounty for cumulative yield per hectare, although some of this effect may be explained by precocity of Sweet-N-UP since the effect was most pronounced in the earliest years of production. Due to its more upright habit and good flower set close to the base of new growth, Sweet-N-Up was easy to train in all the canopy architecture studied, but was particularly straightforward in the SSA and DSSA systems, as the natural branch angles were appropriate for the two upright scaffolds in DSSA and facilitated setting fruit close to the leader.

Summary

This study's data on the early yields of planar high-density and multi-leader canopy training systems systems for peach emphasize their potential for improving yield while decreasing labor inputs associated with pruning excessive vegetative growth. Ease of pruning and training is also highly impacted by the genotype-dependent architecture of the variety, with upright branch angles and basal flower buds facilitating planar training. We did not observe consistent effects of training system on fruit quality, but fruit from all systems was generally of marketable quality. All planar orchard systems also demonstrated greater ease of harvest than the three-dimensional system, since

it was possible to harvest both sides of the upper canopy from a platform on one side of the tree, while the three-dimensional system required ladders, which had to be moved to harvest different leaders of the tree.

Acknowledgements

The authors would like to acknowledge Carla Redinger, Kathleen Rockwell, Andrew Scheil, Jack Sinnaeve, and the farm crew at Clarksville Research Station for their assistance with maintaining the research plot. The pruning, training, fruit thinning, and harvest measurements presented here would not have been possible without you. We would also like to acknowledge the many colleagues who assisted with harvest over the years, who are too numerous to name here.

Conflict of interests

The authors declare no conflict of interest.

REFERENCES

Anthony BM, Minas IS (2021) Optimizing peach tree canopy architecture for efficient light use, increased productivity and improved fruit quality. Agronomy **11(10)**: 1961

Cahn MB, Goedegebure J (1992) Economic aspects of apple production in relation to tree density. New Zealand Journal of Crop and Horticultural Science **20(3)**: 289–296

Dardick C, Callahan A, Horn R, Ruiz KB, Zhebentyayeva T, Hollender C, Whitaker M, Abbott A, Scorza R (2013) PpeTAC1 promotes the horizontal growth of branches in peach trees and is a member of a functionally conserved gene family found in diverse plants species. The Plant Journal **75(4)**: 618–630

Dejong TM, Negron CM, Favreau R, Day KR, Costes E, Lopez G, Guédon Y (2012) Using concepts of shoot growth and architecture to understand and predict responses of peach trees to pruning. Acta Horticulturae **962**: 225–232

DeJong TM, Tsuji W, Doyle JF, Grossman YL (1997) Do high density systems really pay? - Evaluation of high density systems for cling peaches. Acta Horticulturae **451**: 599-604

Eccher T, Granelli G (2006) Fruit quality and yield of different apple cultivars as affected by tree density. Acta Horticulturae **712**: 535–540

Giulivo C, Ramina A, Costa G (1984) Effects of planting density on peach and nectarine productivity. Journal of the American Society for Horticultural Science **109(3)**: 287–290

Grossman YL, DeJong TM (1998) Training and pruning system effects on vegetative growth potential, light interception, and cropping efficiency in peach trees. Journal of the American Society for Horticultural Science **123(6)**: 1058-1064

Hampson CR, Quamme HA, Kappel F, Brownlee RT (2004) Varying density with constant rectangularity: II. Effects on apple tree yield, fruit size, and fruit color development in three training systems over ten years. HortScience **39(3)**: 507–511

Hollender CA, Waite JM, Tabb A, Raines D, Chinnithambi S, Dardick C (2018) Alteration of *TAC1* expression in *Prunus* species leads to pleiotropic shoot phenotypes. Horticulture Research **5**: 26

Iglesias I, Echeverria G (2022) Current situation, trends and challenges for efficient and sustainable peach production. Scientia Horticulturae **296**: 110899

Iglesias I, Reighard G, Lang G (2023) Peach tree architecture: Training systems and pruning. *In* Peach. GB:CABI. pp. 17–53

Lang GA (2023) Innovation in tree fruit production system sustainability through horticultural engineering: Case studies. Acta Horticulturae **1366**: 195–202

Lauri PE, Costes E, Regnard JL, Brun L, Simon S, Monney P, Sinoquet H (2009) Does knowledge on fruit tree architecture and its implications for orchard management improve horticultural sustainability? An overview of recent advances in the apple. Acta Horticulturae **817**: 243–250

Loreti F, Massai R (2002) The high density peach planting system: Present status and perspectives. Acta Horticulturae **592**: 377–390

Parker M, Unrath CR, Safley C, Lockwood D (1998) High density apple orchard management. NC State Extension Publications, **AG-581** https://content.ces.ncsu.edu/high-density-apple-orchard-management

Phillips JHH, Weaver GM (1975) A high-density peach orchard. HortScience **10(6)**: 580–582

Platon IV (2007) Preliminary results on planting system and density trials in apple. Acta Horticulturae **732**: 471–474

Robinson T, Hoying S, Sazo MM, DeMarree A, Dominguez L (2013) A vision for apple orchard systems of the future. New York Fruit Quarterly **21(3)**: 11–16

Scorza R (2004a) Peach tree named 'Sweet-N-UP.' USPP15063P2

Scorza R (2004b) Peach tree named 'Crimson Rocket.' USPP15216P2

Scorza R, Bassi D, Rizzo M (1999) Developing new peach tree growth habits for higher density plantings. The Compact Fruit Tree **32(4)**: 18-20

Shane B (2011) Monitoring peach and nectarine ripening. MSU Extension, https://www.canr.msu.edu/news/monitoring_peach_and_nectarine_ripening

Sharma Y, Singh H, Singh S (2018) Effect of light interception and penetration at different levels of fruit tree canopy on quality of peach. Current Science **115(8)**: 1562–1566

Tustin DS, Van Hooijdonk BM, Breen KC (2018) The planar cordon – New planting systems concepts to improve light utilisation and physiological function to increase apple orchard yield potential. Acta Horticulturae **1228:** 1–12

United Nations (2008) Standard FFV-26.

Yu B, Lin Z, Li H, Li X, Li J, Wang Y, Zhang X, Zhu Z, Zhai W, Wang X, et al (2007) *TAC1*, a major quantitative trait locus controlling tiller angle in rice. The Plant Journal **52(5)**: 891–898